Load Transfer Characteristics Between Posterior Fusion Devices and the Lumbar Spine Under Shear Loading: an *in vitro* investigation

by

Angela Dorothy Melnyk

B.A.Sc., The University of British Columbia, 2008

A THESIS SUBMITTED IN PARTIAL FULFILLMENT OF
THE REQUIREMENTS FOR THE DEGREE OF

MASTER OF APPLIED SCIENCE

in

The Faculty of Graduate Studies

(Mechanical Engineering)

THE UNIVERSITY OF BRITISH COLUMBIA

(Vancouver)

February 2011

Abstract

Introduction: Clinical studies have demonstrated beneficial results of posterior arthrodesis for the treatment of degenerative spondylolisthesis (DS). The optimal stiffness of these fusion systems to enhance load-sharing and fusion rate while minimizing adjacent segment stresses is unknown. To our knowledge, posterior instrumentation for DS has not been tested under anterior shear loads, a highly relevant loading direction for DS.

Objectives: To determine the amount of shear load supported by posterior lumbar fusion devices of varying stiffness under shear loading.

Methods: The effect of implant stiffness and specimen condition on implant load was assessed in a biomechanical study. Fifteen human cadaveric lumbar functional spinal units were tested under a static 300 N axial compression load and a cyclic anterior shear load (5-250 N). Implants (High-Stiffness (HS): Ø 5.5 mm Titanium, Medium-Stiffness (MS): Ø 6.35 x 7.2 mm Oblong PEEK, Low-Stiffness (LS): Ø 5.5 mm Round PEEK, and Ultra-Low-Stiffness (ULS): Ø 5.5 mm Rod X), instrumented with strain gauges to measure loads, were tested in each of three specimen conditions simulating degenerative changes: intact, facet destabilization and disc destabilization.

Results: Transducers measured implant shear loads to within ±5 N. All implants supported significantly greater shear loads as the specimen was destabilized. The LS and ULS implants supported significantly less load than the HS and MS implants for all specimen conditions. Mean implant loads as a percent of the applied shear load in order of increasing specimen destabilization for the HS implant were: 43, 67 and 76%, for the MS implant were: 32, 56 and 77%, for the LS implant were: 18, 35 and 50%, and for the ULS implant were: 16, 39 and 42%. Standard errors were below 8%.

Discussion: An accurate shear load transducer was developed; the methodology is adaptable to many implant designs and materials. Implant shear stiffness significantly affected the shear load-sharing characteristics of the fusion devices. Low-stiffness implants transferred significantly greater loads to the spine, and may possibly enhance the transition to the adjacent, uninstrumented spine *in vivo*.

Preface

This thesis was written in its entirety by Angela Melnyk. Drs. Tom Oxland, Peter Cripton, and Marcel Dvorak provided guidance for the development of the testing methodologies and provided revisions for the writing of this thesis. Medtronic engineers, Philippe Pare, Joe Turner, and Vaneet Singh, provided guidance for the development of the testing methodologies and provided the posterior fusion devices for the testing presented in this thesis. Contributing work from other researchers for Chapters 2 and 3 are outlined below.

The loading rig used for the testing described in Chapters 2 and 3 was originally designed by Katie Beadon and JD Johnston and reported in a previous publication.[1] The original design was adapted by Dr. Qingan Zhu, Jason Chak and Angela Melnyk for the tests described in this thesis. A version of Chapter 2 will be submitted for publication. The testing and data analysis were completed by Angela Melnyk. Some of the testing was completed by Jason Chak. A version of Chapter 3 will be submitted for publication. All the surgical work was completed by visiting spine surgeon Dr. Tianlin Wen. The original development of the surgical model described in Chapter 3 was completed by Dr. Stephen Kingwell. Dr. Wen, Jason Chak and Angela Melnyk completed the specimen preparation and testing. Angela Melnyk performed the data analysis.

The specimen testing presented in Chapter 3 was approved by the UBC Ethics Committee (ethics certificate number H08-02587).

[1] Beadon K, Johnston JD, Siggers K, Itshayek E, Cripton PA. A repeatable ex vivo model of spondylolysis and spondylolisthesis. Spine 2008;33:2387-93.

Table of Contents

List of Tables

List of Figures

Glossary

Adjacent segment: the vertebra and disc directly above or below a fused vertebral segment.

Annulus fibrosus: (annular fibers) component of intervertebral disc; outer collagen ring surrounding layers of fibrocartilage; surrounds the nucleus pulposus.

Anterior column: vertebral bodies and intervertebral disc with associated ligaments (posterior and anterior longitudinal ligaments).

Corpectomy: removal of a vertebra or vertebra-disc unit. Often used as a spine model for *in vitro* testing in which no load-sharing is desired between the fusion instrumentation and the spine. This term is also applied to spine models that have a complete incision through the spine segment but the entire vertebra have not been removed. Clinically, after a corpectomy is performed an intervertebral cage is placed in the anterior column as a surrogate for the vertebral body (and disc).

Facet joint: also called zygapophysial joint is a synovial sliding joint in the spine allowing limited motion between a superior and inferior vertebra. A joint capsule surrounds the facet bones. There are two facet joints between two vertebrae, one on the left and right sides of the spinous process as viewed from the posterior. The anterior face of the facet joint is the posterior border of the intervertebral foramen through which a nerve passes.

High-stiffness implant: rigid metal fusion instrumentation, such as screw-rod or screw-plate systems.

Intervertebral disc: composed of annulus fibrosus surrounding the nucleus pulposus and is located between the vertebral bodies of adjacent vertebrae. The disc acts as a joint between each vertebra in the spine.

In vitro: literally "within glass"; in the context of this thesis *in vitro* refers to physical tests conducted on materials outside a living body (i.e. materials may be cadaveric tissue or non-biological materials such as plastic). Computer models are not considered *in vitro* testing.

In vivo: conducting experiments and recording signals from within the living body.

Lordosis: natural curvature of the lumbar spine. The lumbar lordosis is convex anteriorly. A loss of lordosis would be a decrease in the overall angle of the lumbar spine.

Low-stiffness implant: spinal implants that have a lower stiffness than traditional titanium/metal pedicle-screw plate/rod systems.

Moment (pure/impure): a moment is a quantity resulting from a force couple acting to rotate a body in a specific direction without causing other translations (pure). An impure moment causes a rotation in one direction with additional translations. An impure moment acting on a structure is composed of a pure moment combined with a force.

Mono-axial pedicle screw: original pedicle screw design in which the head of the screw is in a fixed and aligned orientation with the shaft of the screw.

Nucleus pulposus: component of intervertebral disc; gelatinous tissue in the middle of the intervertebral disc that is pressurized under compressive load.

Pedicle screw: bone screw used in spine surgery for insertion through the vertebral pedicles.

Poly-axial pedicle screw: new pedicle screw design in which the head of the screw can swivel and rotate with respect to the shaft of the screw. Once the longitudinal rod or plate member is inserted in the screw, the head is tightened to form a rigid connection between the screw head and shaft.

Posterior elements: the facet joints and associated joint capsule, lamina, spinous process, and associated posterior ligaments (ligamenta flava, supraspinous ligament, interspinous ligament) compose the posterior elements.

Posterior fusion device: any instrumentation including hooks, wires, screws, rods and plates surgically implanted into the posterior elements to assist the fusion process by supporting load in one or more directions.

Spine: column of vertebra-intervertebral disc units extending from the base of the skull along the posterior of the body to the pelvis; allows motion of the body including bending and twisting; houses and protects the spinal cord; supports body loads; attachment points for muscles.

Vertebra: Bone component of the spine. Articulates with adjacent superior and inferior vertebrae via the intervertebral disc and facet joints. Contains space for spinal cord and creates borders of intervertebral foramen through which a spinal nerve passes.

Acknowledgements

I would like to thank Dr. Tom Oxland for his guidance and support during this project. His calm disposition and steady motivation were encouraging. His focus on the big picture placed the various project hiccups in perspective. Thanks to Drs. Dvorak and Cripton for their contributions to this project. Dr. Dvorak reminded me of the clinical population we are trying to help and Dr. Cripton guided my understanding of the details of the results.

This project would not have been completed without the work of spine surgeon Dr. Wen and research engineer Jason Chak. The long testing days flew by with their support and positive outlook.

I would like to acknowledge my funding sources and collaborators: International Collaboration on Repair Discoveries, Natural Sciences and Engineering Research Council of Canada, Vancouver Coastal Health Research Institute, Medtronic Inc., and the University of British Columbia.

Thanks to my friends and lab mates who supported me on the hard days and congratulated me on the successes, especially Liz Arnott, Laurinda Cheng, Hannah Gustafson, Claire Jones, Laura Given, Emily McWalter, Robyn Newell and Carolyn Van Toen.

Finally, I would like to thank my family for their continuing support for whichever road in life I choose to travel. Thanks to my dad for encouraging me to get outside and stay in touch with the outside world. Thanks to my sister for sharing her graduate experience with me. And a special thanks to my mom for making me so many dinners - I would have starved if it was not for you!

To everyone affected by disease and searching for a cure

Chapter 1 Introduction

1.1 Overview

Degenerative spondylolisthesis (DS) is a debilitating form of spinal instability in which the upper vertebra slips forward with respect to the lower vertebra.[1] DS commonly occurs at the L4-5 vertebral level in the lumbar spine[2] and can result in severe neurological symptoms and pain.[3] Between 3% and 8% of the population suffers from DS,[4] a number that increases with age.[2,4] The current surgical treatment for DS is a lumbar spinal fusion[5] and the number of fusion surgeries performed has increased 220% from 1990 to 2001; the increase in surgery rate was greatest for people over the age of sixty.[6] Testing of a simulated DS spine instrumented with posterior fusion spinal devices is reported in this thesis.

Many fusion surgeries consist of implanting a posterior spinal device and laying bone graft between the two affected vertebrae. Ideally, as load is applied on the spine from the weight of the body and activities of daily living, the bone graft grows and fuses the two vertebrae together preventing further slippage and alleviating impingement of neural tissues. Loads applied on the spine are shared between the implant and the spine. If the implant bears too much load, the bone graft may not effectively develop due to stress shielding and fusion may not occur. Moreover, further spinal degeneration may occur at spinal segments adjacent to the fusion.[7] Conversely, if the implant takes too little load, the spine will continue to be unstable and motion between the vertebrae will prevent a fusion. The amount of load supported by the implant is dependent on the relative stiffness between the implant and spine. However, changing the normal vertebral loading pattern by implanting a fusion device may cause degeneration at the vertebral segment adjacent to the fusion.[8]

It has been reported that 43% of people with lumbar fusions have adjacent segment disease (ASD);[7] ASD is characterized by facet joint arthritis and degeneration of the disc adjacent to a fusion.[9] In response to the increasing number of lumbar fusions in the elderly population and ASD, medical device companies are designing novel implants with decreased stiffness to be used on degenerated spines that will presumably decrease the risk of ASD such as the Dynesys (Zimmer Inc., Warsaw, IN) and DSS (Paradigm Spine, New York, NY). Extensive biomechanical testing of these devices has not yet been reported, which is crucial to advance the design of these implants and assess implant performance.

In the following sections, I review the literature and discuss relevant study findings regarding DS, shear loads in the spine, spinal fusions, ASD and spinal implants. The conclusions from these sections lead to my thesis objectives, research questions and hypotheses.

1.2 Degenerative Spondylolisthesis

The etiology of DS is not well understood. Clinically, DS is characterized by degeneration of the intervertebral disc and facet joint with anterior slippage of the superior vertebra with respect to the inferior vertebra (Figure 1-1).[1] There are increasing severities of DS known as grades. The four grades are based on increasing amounts of anterior slippage measured on a sagittal lumbar radiograph. The anterior distance measured between the posterior edges of the superior and inferior vertebrae is divided by the anterior-posterior length of the superior vertebral body.[10] Grade I is 0-25%, Grade II is 26-50%, Grade III is 51-75%, and Grade IV is 76-100%.

Some researchers have concluded that disc degeneration alone is the cause of the anterior slippage, and any facet joint irregularities are due to remodeling and degeneration subsequent to the slippage.[11] Others argue that initial anatomic abnormalities in facet and lamina orientation[12] and preliminary joint arthritis[13] allow the slippage to occur when a disc is degenerated, predisposing people to DS. The elderly population is at a higher risk for DS than young people,[2,4] and the resulting spinal instability can cause spinal stenosis and severe pain.[3]

Biomechanical tests addressing DS and its treatment are sparse in the literature; there exist only two cadaveric models representing DS.[1,14] One research group created a Grade I DS in human cadaveric specimens by surgically destabilizing the disc and completely disrupting the facet joint.[1] The shear loads applied to the specimen were less than those estimated *in vivo*,[15] and no compressive load was applied. Applying a compressive load will increase the shear stiffness of the specimen. Therefore, anterior translations resulting from shear loading without a compressive load will be larger than those produced under shear without a compressive load. Since compressive loads due to body weight and muscle activity exist *in vivo* (Figure 1-2), a more accurate model of DS can be created under combined loading of shear and axial compression.

The second DS cadaveric model was developed in our lab as a preliminary study to the one presented in this thesis.[14] Lumbar functional spinal units were loaded with a dynamic shear force of -50 to 250 N combined with a static axial compressive force of 300 N. The magnitudes of the loads were representative of those estimated to exist *in vivo* at the L4-5 level.[15-17] The specimen was loaded in the intact state and at four other progressively destabilized conditions. The destabilized conditions were as follows: 2 mm facet gap, 4 mm facet gap, nucleotomy and annular fiber destabilization. Each destabilized condition was achieved with sequential surgeries. The 2 mm facet gap was created by disrupting the facet joint capsule and removing approximately 1 mm of bone from the facet joint surfaces of both the superior and inferior facet using a 2 mm burr tool. The gap was increased with a 4 mm burr tool for the second destabilization condition. The facet joint, although altered, remained

functional, as seen in the clinical case. A nucleotomy was performed by creating a small posterior window in the lamina and cutting into the posterior intervertebral disc; the nucleus tissue was removed. The final destabilization condition consisted of cutting the interior annular fibers with a scalpel to release the tension in this tissue. Care was taken not to cut through the entire annular wall. The surgical destabilization conditions were aimed to decrease the overall stability of the spine in anterior shear by altering the facet joint and intervertebral disc. The motion of the superior vertebra with respect to the inferior vertebra was recorded with an optoelectronic system. A mean anterior slip of approximately 3 mm was found which simulated a Grade 1 DS.

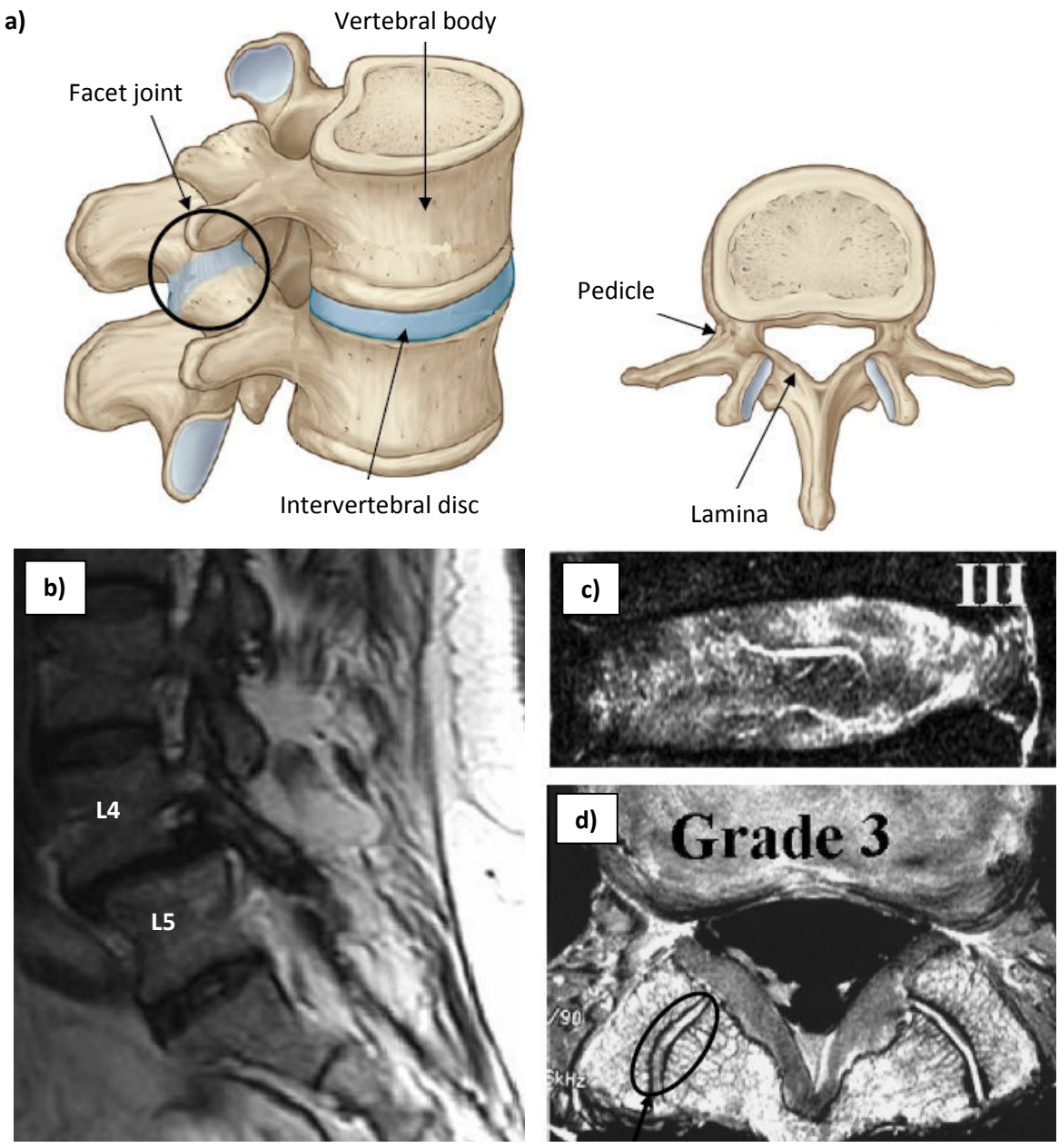

Figure 1-1: Anatomy of the spine and medical images of DS. (a) Drawing of a vertebra-disc-vertebra unit showing the anatomy of the lumbar spine[18] ©Elsevier Ltd., 2005. Reprinted from Drake et al., 2010 with permission from Elsevier (b) Computed tomography image of the lumbar spine in the sagittal plane showing anterolisthesis of L4 with respect to L5.[3] Reprinted from Sengupta and Herkowitz, 2005 with permission from Wolters Kluwer Health. (c) Magnetic resonance image of a Grade III degenerated disc and (d) Grade 3 cartilage degradation in the facet joint.[19] Reprinted from Fujiwara, et al., 2000 with permission from Wolters Kluwer Health.

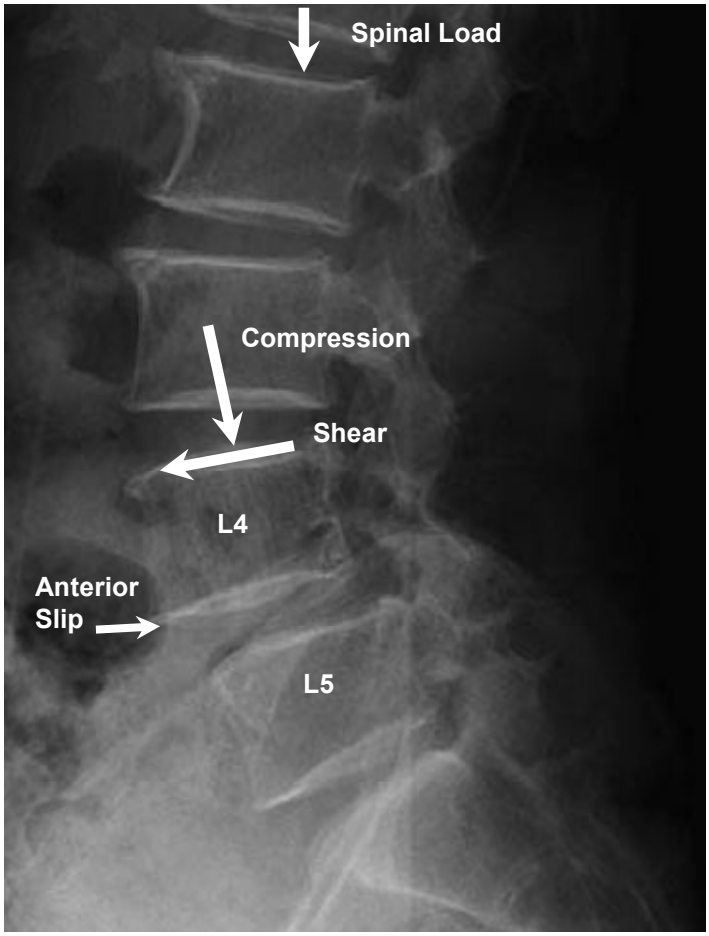

Figure 1-2: A radiograph showing a spine with DS at the L4-5 level.[20] The L4 vertebra has slipped forward with respect to the L5 vertebra. The spinal load due to the body weight and external loads from daily activities is composed of a shear and compressive load at the individual vertebral level. The shear load acts to push the L4 vertebra anterior with respect to the L5 vertebra. Reprinted from Lee DY et al., 2010 with permission from Georg Thieme Verlag.

Clinically relevant unstable spinal models need to be used in laboratory tests to determine the effects of treatment on specific spinal disorders. Many biomechanical researchers testing the lumbar spine to look at the effect of spinal instrumentation or surgical treatment on the kinematics or kinetics of the spine use intact cadaver spines.[21-24] The few studies that do surgically alter the spine before testing have not shown how that particular destabilization represents a clinical population.[25,26] Therefore, it is difficult to determine whether that instability would be managed by the treatment in a clinical setting.

The stiffness of the spine will affect how much load is supported by the fusion instrumentation. An unstable spine has a different stiffness than a stable spine[27] and surgical destabilizations simulating spine diseases or disorders may alter specimen stiffness in different directions.[14,25,28] Measuring the loads on fusion instrumentation implanted in intact spines may be an underestimation of the actual

loads that the device will support *in vivo* after implantation on a diseased spine. Therefore, implants should be tested under relevant loading directions on destabilized cadaveric spines. A clinically relevant model of DS can be used to test fusion devices designed to treat this condition.

1.3 Shear Loading in the Spine

It is not possible to directly measure the loads passing through a vertebra *in vivo*. This would require removing a vertebra and replacing it with a load sensing device, such as a load transducer. This is not safe in clinical practice, and further, inserting a foreign object into the spine would inherently change the way the spine functions at that level; the forces measured would not necessarily be the forces supported at that level by a normal spine. *In vivo* implant loads have previously been measured;[29] however, this is a measurement of load supported by the fusion device, not the spine. It would be useful to know the *in vivo* loads on the spine for the basic science of understanding spinal kinetics, for designing devices to support a portion of that load, and for appropriate loads to be applied in cadaveric experiments. Direct measurements of load supported by specific spinal structures as well as indirect estimates of total loads acting on the spine have been made.

1.3.1 Direct Measurements

Compressive loads supported by the anterior column during activities of daily life have been estimated using disc pressure measurements in the lumbar spine. Pressure transducers inserted in the intervertebral disc have been used to measure the *in vivo* and *in vitro* pressure in the disc.[30-32] Multiplying the pressure with the disc area, as measured in the axial plane, provides an approximation of axial force supported by the anterior column; an additional multiplier, dependent on the magnitude of the applied load, was used to increase the accuracy of this prediction.[33] Pressure measurements were recorded for various normal activities, such as standing, bending-over and twisting.[31] A compilation of the results of these disc pressure experiments showed that a maximal compressive force of 500 N occurred in the disc of the third lumbar vertebra when subjects were standing. Since the posterior elements support a relatively small percentage of load, compared to the anterior column,[33] 500 N is a reasonable approximation of the *in vivo* compression loads in the lumbar spine during standing.

The influence of shear loading on intradiscal pressure has been investigated *in vitro*.[33,34] While large increases in intradiscal pressure occurred due to increases in compression loads, disc pressure increases were small due to increases in anterior shear loads.[33] Under compression the pressure in the disc increases, whereas under shear the annular fibers of the disc support the load. Increases in load in the annular fibers are not reflected in pressure measurements. Overall lower disc pressures due to shear loading compared with compressive loading have been recorded for intact spines.[33,34] After removing

the posterior elements, which are composed of the facet joint, lamina and posterior ligaments, a significant increase in disc pressure occurred under shear loading;[33] the load originally supported by the posterior elements was transferred to the anterior column. Therefore, under shear loading, the main structures of the spine supporting the load are the annular fibers in tension, the posterior ligaments in tension, and the facet joint in compression.

In vivo disc pressures have not been converted to shear forces because the pressure due to shear would be confounded by the large pressures due to compression. Further, the shear load supported by the annular fibers would not be measured with pressure sensors. The aforementioned relative *in vitro* loading of the anterior column and posterior elements under anterior shear provides a qualitative relationship between these structures.

Degeneration of the disc and posterior elements in DS may cause a greater load transfer to a fusion device under shear loading compared with non-degenerated spines. The shear stiffness of cadaveric functional spinal units with either an incised intervertebral disc (Group 1) or removed posterior elements (Group 2) was compared.[35] In Group 1, the specimen shear stiffness decreased by 23% from the intact value, while in Group 2 stiffness decreased by 77%. This implies that under shear loading the posterior elements in a normal spine support a majority of the load and if those elements are damaged or degenerated, the load must be supported by another structure. For a degenerated spine with posterior fusion instrumentation, greater shear loads are likely supported by the implant than for a non-degenerated spine.

1.3.2 Indirect Estimates

Indirect methods have been used to estimate *in vivo* spine loads under various activities of daily living. The results from models used for indirect load estimates combined with the relationships developed from direct measurements can provide order-of-magnitude estimates of *in vivo* loads that can be used to guide *in vitro* experimental procedures. The two main methods of estimating *in vivo* loads are to use mathematical models or finite element models.[17,36]

There are two main mathematical model methods: ground-up[16] or top-down.[37,38] Ground-up mathematical models are based on representing the human body as rigid links and using inverse dynamics to calculate joint loads. Assumptions include frictionless pin joints for two-dimensional models for the joints such as the ankle, knee, or hip, anthropometric dimensions and body segment masses. Free body diagrams are constructed to analyze the joint loads at each rigid link starting with the foot to solve static equilibrium equations for joint forces and moments. The static equilibrium equations are applied to each subsequent segment in the body to determine all the joint forces and moments.[16] The

external forces and angles between segments are usually found using an experiment in which human motion is video recorded and external loads are recorded by force transducers or known dead-weights. Further, muscle activation may be recorded in these experiments to validate which muscles should be represented in the model.[39] In top-down, the model is solved by using the upper body as the weight on the lower body, and it does not take into account transient or impulse responses from ground forces during locomotion.[37]

To determine the loads on the lumbar spine, a transverse plane through the vertebra of interest divides the upper and lower body. The reaction forces at the spine and active muscle equivalent forces can be determined using the equations of motion. Limitations of the mathematical models include errors in anthropometric measurements, simplification of muscles to lines of action, and estimation of centroids of body segments. For example, a 20-35% reduction in predicted compressive forces were found by adjusting the moment arm and direction of line of action for a muscle equivalent.[40]

Finite element models are used to represent structures as deformable bodies, and generally, spine segments, not whole bodies, are modeled with finite elements. Rigid, whole body models were used in the aforementioned mathematical models. Finite element models of the lumbar spine have been developed to represent normal posture and loading environments expected during activities of daily life such as walking, bending over or standing.[17,41-43] Schmidt *et al*. developed a non-linear poroelastic model of the lumbar spine to determine the time-dependent response of the spine tissues to loading over the course of a day.[42] Authors found that the cyclic axial load of 1000 N caused a decrease in annular fiber stress magnitude over time. Kim and Kim created a finite element model of the lumbar spine with 117 pairs of trunk muscles simulating a neutral standing posture.[43] Optimization was used to determine which muscles were activated to maintain the posture. Rohlmann *et al*. loaded a validated finite element model of the lumbar spine in five modes of compression to determine the expected *in vivo* compression force.[17] They also loaded this model in six bending-compression modes to determine expected *in vivo* loads to simulate trunk bending.[41] Range of motion, disc pressures and facet joint contact loads were calculated by the model. Existing *in vivo* measurements of these parameters were compared with the finite element results and the loading mode that produced the best alignment with the *in vivo* data was defined as the most likely estimate of *in vivo* compression forces on the lumbar spine during standing[17] and compression-bending loads during trunk bending.[41]

In vivo compressive forces on the lumbar spine have been estimated using both rigid body models and finite element models. Compressive forces on the spine have been estimated, using mathematical models, to be between 470-2300 N during static bending and twisting postures,[39] 460-1670 N during level walking,[16,37,38] and 1000-3000 N under externally applied compressive and shear

loads.[44] Disc forces due to compressive loading predicted by a mathematical model were half the value reported in experiments using pressure transducers in the disc.[37] The author concluded that simplifications in the model including no stabilizing muscle activity account for the lower disc pressure. Predictions of range of motion, disc pressure and facet joint contact loads during standing from a finite element model matched experimental data well for an axial compressive load of 500 N.[17] Muscle activation maintaining a standing posture caused an axial compressive force on the L4 vertebra of approximately 600 N.[43]

In vivo shear loads during standing have been calculated by a finite element model with active muscles to be less than 100 N at the L4 vertebra.[43] Estimates of shear loads in mathematical models are smaller than compressive loads: 200 N during static bending and twisting postures,[39] 40-100 N during level walking,[16,38] and 50-200 N during applied compressive and shear loads.[44] The rigid body model predictions were based on a young, healthy, male population with non-pathological spines. A degenerated spine may have less ability to support the *in vivo* shear forces. Therefore, a spinal fusion device may support a greater percentage of the shear load than would be expected for a fusion device used on a non-degenerated spine.

1.4 Spinal Fusions

Spinal column injury from trauma, deformity or degeneration involving neurologic symptoms may be treated with fusion. Fusion is the bridging of two bony elements with bone graft to restrict motion between the elements. Under load, the bone graft grows into the elements forming a rigid connection. Fractures, bone diseases, and deformity in many parts of the body are treated with fusion, including the spine. The goal of spinal fusion is to immobilize the affected vertebral segments with a solid osteosynthesis.[45] An accompanying decompression surgery is intended to decompress nerve or spinal cord compression to alleviate neurological deficits.

1.4.1 Surgical Technique

The first surgical technique for spinal fusion was proposed by Hibbs in 1911.[46] He treated three people with Pott's disease by removing bone from the vertebrae and laying it across the spinous processes. Pott's disease is a type of tuberculosis that has spread into the spine. Over many decades, this surgical technique was adapted to incorporate instrumentation to improve the fusion. The instrumentation may consist of combinations of hooks, wires, screws, rods and plates to assist in stabilization of the vertebrae. One of the first techniques described that used screws to supplement a bone graft fusion was reported by King in 1948, who inserted screws through the facet joint.[47] Out of 44 patients, he had a fusion rate of 89%, and a satisfactory functional outcome of 91%. In 1976, Roy-

Camille described the technique that is used commonly today in instrumented fusions:[45] screws were inserted from the posterior into the vertebral body through the pedicles, and plates with holes to accommodate the screws lay on the posterolateral spine in the vertical direction across as many vertebrae as were used for the fixation (Figure 1-3).[45] Since this method was proposed, pedicle screws combined with plates or rods have become a common instrumentation system to supplement spinal fusion.

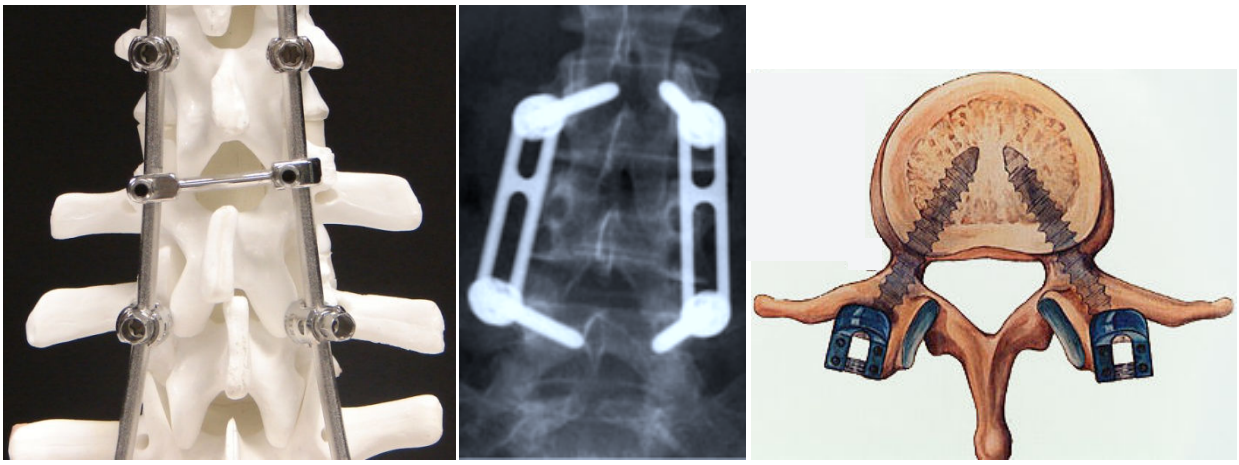

(a) (b) (c)

Figure 1-3: Posterior lumbar fusion instrumentation. (a) Posterior view of a pedicle screw-rod fixation system affixed to a spine model. (b) Posterior x-ray of pedicle screws connected to a plate system spanning two levels in the lumbar spine.[48] Reprinted from Rutherford et al., 2007 with permission from King, L and the Radiological Society of North America. (c) Axial view of a lumbar vertebra with pedicle screws inserted.[49] Reprinted from Foley et al., 2001 with permission from MedScape.com, 2010.

1.4.2 Fusion as a Treatment for DS

Treatment for DS includes non-operative, or conservative management, operative decompression, or operative decompression combined with fusion. A recent randomized control trial and prospective cohort study on 222 patients with DS was conducted to determine the effects of operative or non-operative treatments on listhesis, an increase in anterior slip, disc height and mobility.[50] Eighty-six percent of the population had a Grade I DS, while the rest a Grade II. The results of the study indicated that patients undergoing surgery improved more than the non-operative group. There are two main treatments for surgical intervention in the lumbar spine: the vertebrae may be decompressed only, or decompressed and fused. Decompression only resulted in a significantly greater amount of post-operative back and leg pain,[51] a greater proportion of unsatisfactory clinical results relating to patient-reported pain and function levels,[51,52] and increased post-operative listhesis.[51,53] Fusion surgery appears to be indicated for DS.

Fusion surgery performed with instrumentation significantly increased the rate of fusion in the lumbar spine compared with non-instrumented fusion surgeries.[52] Even when patients were stratified by diagnosis, those with DS treated with instrumented fusion surgery had fusion rates between 86% and 94%, higher than the fusion rates between 52% and 65% for fusion without instrumentation.[53-55] However, instrumented fusion does not necessarily correlate to patient satisfaction, defined as the amount of pain experienced by the patient, medication used by the patient, and employment status post-surgery.[54,55]

The effect of instrumented fusion on patient satisfaction has yielded mixed results. Lower clinical satisfaction rates compared with fusion rates have been reported for patients with degenerative lumbar spinal stenosis.[56] This finding is supported by the results of a meta-analysis specifically analyzing studies of fusion surgery for DS patients.[52] However, studies have also found higher rates of patient satisfaction compared to rates of solid fusion[54,55] with the implication that some patients with pseudarthrosis still have a satisfactory clinical outcome. Only one study comparing instrumented fusion surgeries to non-instrumented fusion surgeries was a randomized control trial, but the inclusion criteria for this study included many lumbar spine diagnoses, one of which was DS.[55] The effects on clinical outcome and patient satisfaction of confounding variables in non-randomized control trial studies and of including different diagnoses for surgical treatment are not well understood. However, the societal impact of poor clinical and patient outcomes still exists: some patients with an unsatisfactory outcome and continuing neurologic deficit will undergo a revision surgery and lower fusion rates for this second surgery have been reported.[55] Further, low-stiffness fusion devices have not been included in any of these epidemiological studies, and lower rates of revision surgery may result from using low-stiffness implants in the index fusion surgery.

Degenerative spinal conditions in the elderly are now being treated with spinal fusions. However, the early indications for fusion such as trauma and deformity did not include degenerative conditions. Reasons for expanding the indications for fusion to degenerative conditions include: advances in technology such as instrumentation systems that do not require intact facet joints or lamina, diagnostic equipment such as computed-tomography and magnetic resonance imaging that allow diagnosing spinal problems that previously could not be seen with plain x-ray, and improved post-operative care that allows elderly people with co-morbidities to be eligible for fusion surgery.[57] Elderly populations have the highest prevalence of DS in the population,[2,4] and they are now eligible for surgery. The influx in fusion surgeries on elderly patients has created a market for new spinal instrumentation. It is the rates of revision surgeries, pseudarthrosis, and unsatisfactory clinical outcomes that spinal implant companies aim to reduce by designing novel instrumentation for the degenerated spine.

1.5 Adjacent Segment Disease

1.5.1 Definition and Clinical Studies

Researchers have published numerous clinical and biomechanical studies addressing the controversial hypothesis that a posterior lumbar fusion causes ASD. ASD is characterized by degeneration of the mobile segment adjacent to a fusion.[9] It has been suggested that ASD is caused by changes in stress,[21,22] motion,[58] instability[59,60] and lordosis[61] at the adjacent segment to a fusion. Disc degeneration,[62] stenosis,[8,60] and poorer patient outcome[59,63] have been correlated with ASD, and the number of spinal levels fused is a risk factor in developing ASD.[7,59,62,64] Conversely, other researchers have proposed that ASD is a natural progressive degeneration of the spine, and its development is not caused by a fusion.

Studies have shown significant correlations between ASD and age[7,63,65,66] suggesting the elderly population is more at risk of ASD whether or not a fusion is present, although ASD would be diagnosed as degeneration if there is no adjacent fusion. Specifically, disc height and disc degeneration have been shown to change with age, not fusion length.[67,68] Further, sacral inclination[5] and menopause[69] have been correlated with ASD indicating that some persons may be predisposed. Radiographs of 42 fusion patients with an average of 23 years of follow up were assessed for ASD and compared to radiographs for age and gender matched control non-fusion patients with back pain.[70] The segment assessed for the control group was matched to the level of the fusion group's adjacent segment. No significant changes in the motion at the adjacent segment were found between the fusion group and control group. Further, there were no significant differences between the adjacent vertebra translation or disc height, or the incidence of developed DS for the two populations.

Still other researchers suggest that ASD is a natural progression of the spine that is *accelerated* by fusion.[65,71] One study included 101 patients with pedicle screw fusions with a preoperative diagnosis of DS and follow up at six years.[71] The effect of posterior spinal integrity on ASD was determined by separating the study group into subgroups composed of (1) a non-damaged group with an intact lamina and spinous process and (2) a damaged group with the whole spinous process of the upper or lower fused vertebra removed. They found an overall incidence of ASD of 23%, and that damaging the integrity of the posterior complex during the fusion operation increased the incidence of ASD from 6.5% in the non-damaged group to 24% in the damaged group, concluding that the surgical method may lead to acceleration of ASD.

These clinical studies have significant limitations. The populations studied were generally heterogeneous. Factors such as age, gender, fusion instrumentation, pre-operative diagnosis, pre-

operative spinal degeneration, living conditions, and work environment were usually not accounted for in the study.[62] Heterogeneous populations allow broad generalization of study results to populations, but more homogenous populations would lead to stronger relationships between the development of ASD and fusions.

A second limitation is the fusion group in the majority of these studies was not compared to a population of people without fusions;[5,7,8,61-67,71] some studies only included patients with ASD and did not compare them with people with a fusion without ASD.[8] This limitation is perhaps the reason why there is no conclusive evidence for or against the hypothesis that fusion causes ASD. Without a control group, it is impossible to prove whether ASD had a higher incidence in people with fusion than without or that the effects seen at the adjacent segment were not seen in an age-matched population. Perhaps this has been overlooked because the name ASD infers there must be a fusion to have an adjacent segment to become diseased. However, studies similar to Hambly *et al*. in which segment levels are matched between fusion groups and controls[70] are needed to determine if ASD is caused by, accelerated by, or unaffected by fusions. Possible accelerative effects of a fusion on ASD could not be assessed because measurements were made at only one follow-up time.[70] In addition, the control group had back pain and may have been predisposed to spinal degeneration;[70] back pain and associated muscle spasms may have resulted in a lower range of motion in this control population. Acceleration or causation of ASD from a fusion should also be determined with non-pathological and pain-free populations.

1.5.2 Biomechanical Studies

To increase the control in experiments and assess factors that would be otherwise impossible to characterize *in vivo*, cadaveric biomechanical experiments have been performed to determine the effect of fusion on adjacent segments. Contrary to many clinical studies, the results of the biomechanical studies showed effects of the fusion on adjacent segments. However, the method by which these studies were completed influenced the results.

1.5.2.1 Methodology of Biomechanical Studies

Generally, biomechanical *in vitro* studies performed to assess the effect of fusion instrumentation on the adjacent segment to the fusion use multi-segment spines tested with one of three methods: stiffness, flexibility or hybrid. The stiffness and flexibility protocols were defined by Panjabi to be used on multi-segment (two or more) spine specimens.[72] Stiffness testing involves applying a known displacement or rotation to a vertebra in a specific direction and measuring the resulting six forces and moments. However, by applying a rotation, the investigator is forcing the rotation axis to be in a particular location that may not represent the natural center of rotation of the spine. Further, if the

rotation is not about the physiologic axis, unknown constraints in other directions are created.[73] To eliminate these limitations the flexibility protocol can be employed. A known force or pure moment is applied to an unconstrained vertebra and the six translations and rotations are measured. A pure moment can be created with a force couple; no additional forces are created when a pure moment is applied to a structure. The resulting rotations and translations from a flexibility test are often acquired with an opto-electronic tracking system. Both stiffness and flexibility methods have significant limitations when used to assess effects of a fusion on adjacent segments to the fusion.

When assessing effects at the adjacent segment to a fusion, the stiffness and flexibility protocols directly influence the results. For example, if a flexion rotation is applied to a three-segment spine as per the stiffness protocol, the intervertebral rotations will sum to the applied rotation. If two segments are fused together, the total rotation will occur at the adjacent segment, creating an effect of fusion length and magnitude of applied rotation on the adjacent level range of motion (Figure 1-4a and b). Similarly, if a pure moment is applied as per the flexibility protocol, the same moment will exist at every level of the spine whether or not spinal instrumentation exists (Figure 1-4c and d). Therefore, an increase in range of motion at the adjacent level to a fusion will result from a stiffness protocol, while no change will be found with a flexibility protocol. Both stiffness[22,23,26] and flexibility[61,74-76] methodologies have been used in the biomechanical studies assessing adjacent segment effects. In addition to the rotation axis limitation in the stiffness protocol, moments combined with unknown forces causing were applied in some of the flexibility studies.[74,75]

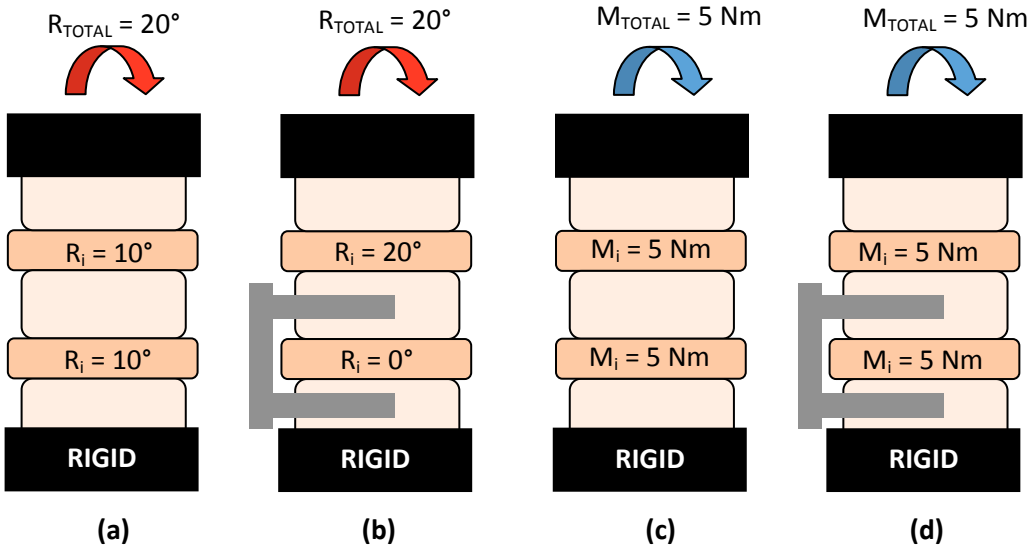

Figure 1-4: Schematics of three-vertebra spine segments tested with the (a) stiffness protocol in the intact state, (b) stiffness protocol with fusion instrumentation, (c) flexibility protocol in the intact state and (d) flexibility protocol with fusion instrumentation. In the stiffness protocol, the total rotation is spread across the length of the specimen in the intact state, while the total rotation must

exist at the only available segment after fusion. The flexibility testing causes a known pure moment to exist at every level of the spine, with or without fusion instrumentation.

To address the problems with flexibility and stiffness protocols, a hybrid method was developed by Panjabi.[77] This method specifically addressed the hypothesis that after a fusion, the remaining vertebral segments in a spinal region must adapt to accommodate normal activities of daily life, such as bending over to tie a shoelace. After a fusion surgery, people will bend over and achieve the same rotation as was achieved pre-surgery. Therefore, biomechanical studies must test long spine segments to measure the possible *in vivo* adaptation of a spinal region to a fusion. The hybrid method is composed of three steps:[77] (1) test the intact spine using the flexibility protocol and measure the overall range of motion of the spine segment (Figure 1-5a); (2) re-test the spine after fusion surgery and increase the pure moment until the range of motion from step 1 is reached (Figure 1-5b); and (3) analyze the desired output intervertebral data (i.e. range of motion, strain, load, etc.) from step 2 and compare and normalize with the intervertebral data from step 1. For the hybrid protocol, the intact rotation of the spinal region is maintained throughout testing, the rotation axis is not constrained, and the moment is increased from the intact to the instrumented test.

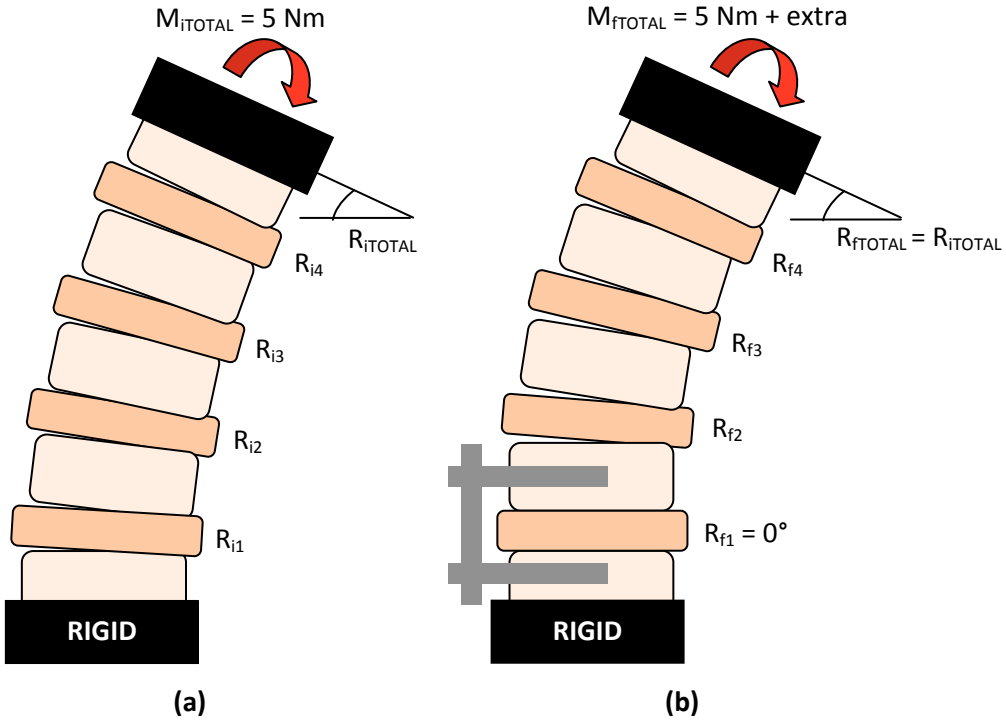

Figure 1-5: Schematic of a five-vertebra spine segment tested under the hybrid protocol[77] (a) in the intact state and (b) after fusion instrumentation. The pure moment is larger after fusion to maintain the same total segmental range of motion (R_{fTOTAL}) as in the intact state (R_{iTOTAL}). The intervertebral range of motions (R_{ij} and R_{fj}) sum to the total range of motion. After fusion, the total range of motion will be divided between three segments compared to four in the intact state.

1.5.2.2 Results of Biomechanical Studies

Some of the adjacent segment changes found from biomechanical studies comparing intact specimens to fused specimens are: increased motion,[21,22,26,74,75,78] shifts in the centers of rotation,[22] altered facet joint loading location,[22] increased disc pressure,[23,76] altered adjacent segment motion correlated to fusion length,[26] and increased strain on the posterior elements.[21,61,76] Results of one study did not show significant changes in disc pressure or increased motion at the adjacent segment after fusion but did find increased lamina strain and increased load across the fusion instrumentation when there was a loss of lordosis across the fused segment.[61] Lordosis is the natural curvature of the lumbar spine. A trend of decreasing lordosis was found at the fusion level due to fusion surgery in a patient population.[61] Authors concluded the altered mechanical loading due to fusion with a loss of lordosis at the adjacent segment may accelerate ASD. The results of the aforementioned studies are confounded by either the stiffness or flexibility testing methodology; none of the studies used the hybrid protocol, usually because it had not been developed at the time of the study.

One study from our lab assessed the effect of a posterior fusion device combined with rigid or flexible extension rods, to increase construct stability, on the kinematics of the adjacent segment using a modified hybrid testing protocol.[78] Thoracolumbar cadaveric specimens were tested in four conditions (Figure 1-6): (1) intact, (2) vertebral body spacer and rigid rod instrumentation, (3) distal rigid rod extension added to the rigid rod instrumentation, and (4) distal flexible rod extension added to the rigid rod instrumentation. Significant differences between using the rigid extension rods and flexible extension rods were found. Increases in range of motion at the adjacent, non-instrumented, segment compared to the intact condition with the addition of the extension rods were found. The flexible extension rod increased the range of motion by a smaller amount than the rigid extension rod. The authors of this study assumed that adjacent level motion caused by the fusion correlates to the risk of ASD. Therefore, the flexible extension rods may decrease the risk of ASD compared with the rigid extension rods.[78] The corpectomy level was instrumented by a traditional titanium posterior fusion device in all fusion conditions, and it is unknown what effect a flexible rod at the corpectomy level would have on the kinetics of the spine or kinematics of adjacent vertebrae.

As described previously, most of the biomechanical studies were limited by the use of the stiffness and flexibility protocols to test for adjacent level effects. Some of the studies also had limited clinical applicability. Few specimens were tested[21,23,61,74] making it difficult or impossible to reach levels of significance in the results. Some researchers did not destabilize the spine before testing the effects of a fusion,[21-23] thus the spine behavior did not represent the clinical situation in which the spine must initially have severe degeneration or deformity to warrant a fusion. A compressive follower load was not

applied to the specimens.[23,61,75,76] The muscles provide a stabilizing effect on the spine *in vivo*, and assessing kinematics, disc pressure, and posterior element strain *in vitro* without a follower load will alter the absolute values of these measurements. Although a follower load would not likely affect the general trends and comparisons made within a study, the absolute values may not accurately represent those existing *in vivo*.

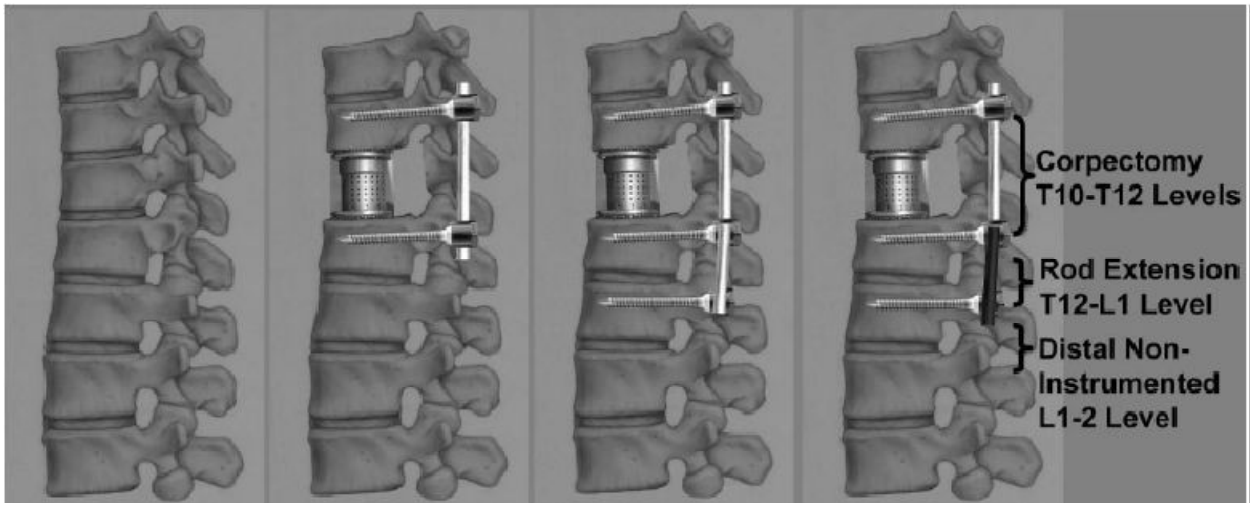

Figure 1-6: Schematics of long spine segments tested with the Hybrid protocol. The specimens were tested in each of the four conditions in flexion-extension, lateral bending and axial rotation under 5 Nm of applied moment.[78] (1) intact, (2) corpectomy model with interbody spacer and rigid rod instrumentation, (3) rigid extension rod in addition to rigid rod instrumentation and (4) flexible extension rod in addition to rigid rod instrumentation. Adjacent level effects were determined at the distal non-instrumented level. Reprinted from Tan et al., 2008 with permission from Wolters Kluwer Health.

1.5.3 The Cost of ASD

The incidence of ASD among people who have previously received a fusion has been reported as low as 13%[59] and as high as 46%,[5] with an annual rate of 4% after surgery.[62] The reported incidences were usually determined by assessment of radiographs or magnetic resonance images,[5,59,64,71,79] as opposed to incidence based on patient complaint of pain or neurological symptoms.[7,62] Reoperation rates for people with ASD have ranged from 22% to 100%.[62,64,71] From 1992 to 2003 the number of spinal fusions performed each year increased from 0.3 to 1.1 per 1000 people over the age of 65 in the United States, and lumbar fusion represented 47% of all back surgeries performed.[80] The total spent on surgeries in a year increased from $75 million in 1992 to $482 million by 2003. If only 22% of people with ASD after a lumbar fusion surgery have a revision surgery, and the rate of lumbar surgery remained at 1.1 per 1000, a conservative cost estimate in 2009 would be $34 million spent on revision surgeries for ASD.

In response to this economic burden on society, medical device companies have developed novel posterior spinal implants to prevent ASD. These implants are of two types: flexible implants designed for fusions and dynamic implants designed to restore the biofidelic behavior of the spine. The lower stiffness of these novel implants, compared to traditional titanium implants, is hypothesized to decrease the risk of ASD, or reduce accelerative effects of a fusion on ASD.[78,81] As a primary step, novel implants need to be compared to traditional titanium fusion devices to determine kinetic responses to loading to assure effectiveness of load transfer between the spine and implant and to determine if there are significant changes in implant loads when using a low-stiffness implant. An *in vitro* biomechanical study performed with a spine representing clinical degeneration warranting a fusion and fusion implants able to measure load can provide this information.

1.6 Spinal Implants

Spinal implants are designed to achieve clinical objectives of pain reduction, deformity correction and elimination of neurological symptoms in conditions due to trauma, deformity or degeneration. There are three biomechanical methods used to achieve these clinical objectives: immobilize the spine to induce fusion, re-create normal motion-patterns of the spine without fusion, or allow fusion without complete spinal immobilization. To assess how well an implant achieves these biomechanical goals, researchers conduct tests on implants to measure relevant mechanical parameters,[72] such as relative motion and stiffness, implant loading, fatigue and ultimate strength, and durability and wear. Clinical outcomes are assessed after the device has been implanted in humans through measurements on medical images to determine the amount of deformity correction and questionnaires regarding pain. The following subsections describe how different biomechanical goals affect implant design, how implants are tested to measure kinematic parameters such as spinal range of motion, and how implants are tested to measure kinetic parameters such as the amount of load supported by the implants.

1.6.1 Implant Design

Traditional, rigid, metal spinal implants were designed to assist in fusion, as described in section 1.4.1. Briefly, it was hypothesized that fusion of a spinal segment will decrease or eliminate any pain associated with the original spinal deformity, trauma or degeneration. Researchers found that the rate of fusion increased when a rigid device was implanted in the spine compared with non-rigid devices or when no device was implanted.[52-55] The goal of the rigid implant is to immobilize the spine. Low relative motions between adjacent vertebral segments and bone graft will allow healing of bone and a solid osteosynthesis.[45] Fusion implants need to be relatively stiff in all loading directions since minimal motion

between the vertebrae is required for bone growth.[82-84] The implants must support loads in all directions. A system of components capable of resisting or supporting loads in all directions without collapsing is defined as a structure.[85] Therefore, fusion devices used currently in surgery are designed to be structures. Once the bone mass has healed and fusion is complete, these devices theoretically support less load and are cycled at lower loads than prior to fusion. Therefore, fatigue and wear are less critical than strength and stiffness for traditional fusion implants. However, in practice the exact loading relationship between fusion implants and the spine over the course of bone growth is unknown; in some patients the implants may be loaded at a higher level for a longer time period. Thus, designs to prevent failures due to fatigue loading are relevant for traditional fusion implants.

Other spinal implants are designed to restore the motion of a destabilized spine to its intact, or normal, state; these devices are not designed for fusion and are referred to as dynamic devices.[24,86] Dynamic implants allow motion in particular directions and transfer greater loads to the spine. The yield strength of these devices may be lower than for fusion implants since greater load will be transferred to the spine. Wear particulate, fatigue strength, and motion patterns are the most important characteristics for dynamic implants. These implants will be cycled indefinitely and the amount of particulate due to wear may cause implant loosening, bone loss, and accumulation of particles in organs such as the liver and spleen.[87] The functional goal of motion-restoration must also be considered. One research group systematically varied the axial and bending stiffnesses of a generic posterior implant affixed to a finite element model of the lumbar spine.[88] The range of motion in flexion-extension was affected by the axial stiffness, but the range of motion was not affected by different values of bending stiffness. Based on this finding, the researchers recommended optimal dynamic implant stiffness values that were incorporated in the design of a new dynamic device aimed to restore a portion of the normal spinal motion.[89] Dynamic implants are sensitive to stiffness in particular directions, thus multi-directional stiffness similar to traditional fusion implants is an important characteristic to control for dynamic implants.

Finally, some devices are designed to assist fusion at an affected segment while allowing the spinal column loading to remain as close as possible to an uninstrumented, normal spine. The stiffness of this implant is lower than for traditional fusion implants so as to transfer greater loads to the spine.[28] Ahn *et al*. used a finite element model of a destabilized lumbar functional spinal unit to determine the axial load-sharing of two low-stiffness implants and a rigid implant.[90] The two low-stiffness implants supported 28% and 36% of the applied load compared to 67% for the rigid implant. The yield strength is an important parameter to consider during design of low-stiffness implants. Although there is little risk of traditional fusion implants yielding due to the high yield and ultimate strength of metals, low-stiffness

implants made of polymers may be loaded to the yield strength of the implant material. The design of low-stiffness implants involves a balance between stiffness and strength. Further, low-stiffness implants may result in larger relative motions between vertebrae compared to traditional fusion systems. This in turn may result in a longer time for healing which increases the risk of implant failure due to fatigue. However, in one study insignificant differences in the intervertebral range of motion were found when loading a spine instrumented with either a traditional or low-stiffness implant.[28]

Some dynamic and low-stiffness devices may also be affixed to the adjacent segment to a rigid fusion. This transitional implant may decrease the severity of the changes at that adjacent segment due to the fusion by preventing hypermobility while allowing some or all of the pre-fusion motion.[78] The risk of degeneration of the adjacent segment to the low-stiffness or dynamic implant would decrease since the kinematic and kinetic changes would be less than had a traditional fusion implant been used alone.

1.6.2 Implant Testing

Prior to use in humans, spinal implants are tested *in vitro*, using surrogate constructs to represent the spine (usually plastic) or cadaveric specimens (human or animal), and *in vivo* using animal models to determine the efficacy and safety of the device. As described by Panjabi, there are three main types of biomechanical tests conducted on implants: strength, fatigue and stability.[72] For strength tests, an implant is loaded in a particular direction of interest until failure of the implant or failure between the implant and the cadaveric spine occurs. Fatigue tests are long-term in which cyclic loads are applied to an implant until failure occurs. Many devices would be deemed safe for clinical use by researchers and companies after satisfactory results are observed in these first two tests. However, the results of the strength and fatigue tests do not relate to the function of the implant. The stability test indicates which implant achieves its main function of spinal immobilization (fusion) or spinal motion (non-fusion). None of these test types measure the kinetic behavior of the implant. Low-stiffness devices need to transfer loads to the spine to allow bony fusion to occur, restrict motion between the affected vertebrae, and prevent increased motion at the adjacent segments. Therefore, stability tests in which implant loads are measured need to be conducted.

Stability testing implies that the result of testing will indicate if the spine-implant construct is stable. There are two definitions of stability relating to a fundamental mechanical concept and a clinical concept. The mechanical definition of stability is defined as a structure having an optimal state of equilibrium.[91] For example, a ball on a hill is unstable because if it is perturbed, the ball will roll away from its initial position, whereas a ball in a valley is stable since it will return to its initial position if perturbed. In the clinical context, the definition of stability is not dichotomous (stable/unstable), but is

continuous (low to high) and is related to a structure's stiffness, or mobility. Increasing the stiffness of a structure increases the stability, while decreasing the stiffness decreases the stability. This definition is related to the amount of motion of the spine that is caused by an applied force. In this thesis the term stability was defined in the clinical context.

Fusion implants are designed to create a rigid connection between two adjacent vertebrae to stabilize that spinal segment. A stability test, or flexibility test, as first proposed by Panjabi,[72] can be used to determine the relative stiffness of different implant-spine constructs. A physiological load, defined as a pure moment or force applied about or along an axis from the orthogonal anatomical coordinate system with magnitude simulating that existing *in vivo*, is applied to the construct and the relative motion between the vertebrae is measured. The slope of the resulting load-deflection curve is the stiffness. The implant resulting in the maximum construct stiffness has best achieved the function of vertebral stabilization. As described in section 1.5.2.1, a stiffness test can also be used to test stability but is rarely used due to the associated limitations.

Since flexibility testing was first described,[72] numerous researchers have conducted flexibility tests on spinal implants using both experimental[28,86,92-94] and computer models.[88,89,95] In a study conducted by Panjabi *et al*. eight spinal fixation devices were affixed to cadaveric spine segments (T9-L3) and loaded with pure moments in flexion-extension, axial rotation and lateral bending.[93] Range of motion was measured and the relative flexibility of the spine-implant construct compared with the intact spine was calculated. All devices were posterior fusion devices except one that was an anterior fusion device. The anterior fusion device showed greater flexibility in flexion-extension.[93] Within posterior fusion devices, those secured to the spine with vertebral body screws or pedicle screws created greater stabilization in all directions (flexion-extension, axial rotation, lateral bending) compared with devices attached with hooks and wires only.[92]

The behaviour of low-stiffness implants has been compared to traditional rigid fusion devices. Evaluating pedicle-screw based implants, the range of motion between spines instrumented with posterior fusion rods made of titanium compared with rods made of polyether-ether-ketone (PEEK) was not significantly different, and both implants reduced the range of motion of the intact spine by three-fold.[28] No significant differences in range of motion were found when a rigid device was compared to a dynamic device, except for flexion-extension in which the spine immobilization was greater with the rigid device than the dynamic device.[86] Finite element analysis showed that the vertebral range of motion of a spine segment model instrumented with a generic posterior fusion rod of varying stiffness was affected by axial implant stiffness values less than 200 N/mm only[95] and was not significantly affected by implant bending stiffness values less than 500 N/mm.[88] With this information, an ideal low-

stiffness implant can be realized with an axial and bending stiffness such that a desired range of motion is achieved. However, if fusion is desired, load through the bone graft is required for healing; relative load through the spine and implant should be measured during stability tests to assess how loading through the spine is affected by different fusion implants.

1.6.3 Implant Loads

As long as the spine has some ability to support load, there will always be some load-sharing between an implant and the spine. Load-sharing in this thesis is defined as the proportion of applied load supported by one component in a multi-component structure.[96] Load-sharing of an implant refers to the percentage of the applied load to the spine-implant construct that the implant supports. For example, if an implant has 70% load-sharing in flexion, the implant supports 70% of the applied flexion moment and the spine supports the remaining 30%.

We can relate the amount of load supported by a component to its material and geometric properties for simple structures. For example, a composite structure is composed of two columns in parallel with different stiffness joined at the top and bottom by rigid members (Figure 1-7a). An axial compressive load is applied to the top rigid member and compresses the composite column by a distance ΔL. A horizontal cut through the composite column shows the forces in each column component due to the applied load (Figure 1-7b). This system can be represented schematically as a parallel spring system with two springs having different spring constants (Figure 1-7c).

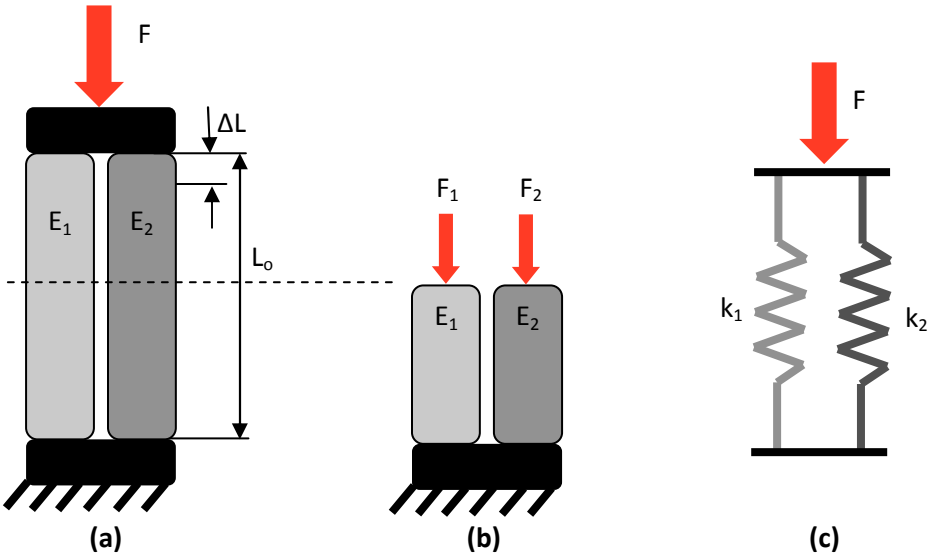

Figure 1-7: Load-sharing of a composite column. (a) The column is made of two materials with stiffness E_1 and E_2, respectively, and each with length L_o. The column is held rigidly at the top and bottom (black boxes). An axial compressive load, F, is applied to the column and compresses the column a distance of ΔL. (b) The composite column is cut at the location of the dashed line and the component forces, F_1 and F_2, due to F are shown. (c) An equivalent system of two parallel springs each with a spring constant, k_1 and k_2.

A mathematical derivation to find the load-sharing of each component in the column in Figure 1-7 is provided. Each column component has an equal strain since the original length and the compression are the same for components 1 and 2:

$$L_o = L_{o1} = L_{o2}$$

$$\Delta L = \Delta L_1 = \Delta L_2$$

$$\varepsilon = \varepsilon_1 = \varepsilon_2 = \frac{\Delta L}{L_o}$$

where L_o = original length of column, ΔL = amount of compression of the column, ε = strain

From first principles,

$$\sigma_1 = E_1 \varepsilon$$

$$\sigma_2 = E_2 \varepsilon$$

where σ = stress, E = Young's Modulus

Substituting our relationship for strain and the known relation between stress, force and cross sectional area (stress = force/area), yields:

$$\frac{F_1}{A_1} = E_1 \frac{\Delta L}{L_o} \qquad \frac{F_2}{A_2} = E_2 \frac{\Delta L}{L_o}$$

where F = applied force, A = cross-sectional area

We can isolate the forces supported by each component:

$$F_1 = E_1 A_1 \frac{\Delta L}{L_o} \qquad F_2 = E_2 A_2 \frac{\Delta L}{L_o}$$

From Figure 1-7a and b, we can see the component forces add to the applied force, F:

$$F = F_1 + F_2$$

$$F = E_1 A_1 \frac{\Delta L}{L_o} + E_2 A_2 \frac{\Delta L}{L_o}$$

The load-sharing (LS_i) of each component is the percentage of the applied load supported by the component:

$$LS_1 = \frac{F_1}{F} \qquad LS_2 = \frac{F_2}{F}$$

$$LS_1 = \frac{E_1 A_1 \frac{\Delta L}{L_o}}{E_1 A_1 \frac{\Delta L}{L_o} + E_2 A_2 \frac{\Delta L}{L_o}} \qquad LS_2 = \frac{E_2 A_2 \frac{\Delta L}{L_o}}{E_1 A_1 \frac{\Delta L}{L_o} + E_2 A_2 \frac{\Delta L}{L_o}}$$

Simplifying the above expression yields:

$$LS_1 = \frac{E_1 A_1}{E_1 A_1 + E_2 A_2} \qquad LS_2 = \frac{E_2 A_2}{E_1 A_1 + E_2 A_2}$$

The general solution for load-sharing for multi-component structures is:

$$LS_i = \frac{E_i A_i}{\sum_{j=1}^{n} E_j A_j}$$

where *i* = the component of interest, *j* = the index for the summation, *n* = the total number of components in the system

The general solution shows that the amount of load supported by a component in a structure is related to the stiffness and geometry of all the components within the structure. The load-sharing will depend on load direction because the cross-sectional area and stiffness may differ with different loading directions.

For the study described in this thesis (Chapter 3), load-sharing is the main parameter of interest. However, the spine-implant system is too complex to use a simple mathematical model to calculate load-sharing (Figure 1-8), especially when multiple loads are applied. The combined loading on the structure, complex geometry and unknown and potentially non-linear spine stiffness lead to the requirement of a direct measurement of load on the implant, as opposed to using a theoretical analysis. The amount of load supported by an implant may respond in a linear or non-linear manner under a linear load application and may differ between loading directions. And as shown by the previous load-sharing example, the stiffness of the implant and spine will affect the magnitude of implant load. Inferences from the results of stability studies testing corpectomy models indicate that a greater amount of load is transferred to the spine with more flexible implants.[92] However, other studies showed that dynamic and low-stiffness implants decrease the range of motion similarly to rigid implants.[28,86] It is unclear what effect a spine able to support a portion of the applied load will have on the loads supported by a fusion device.

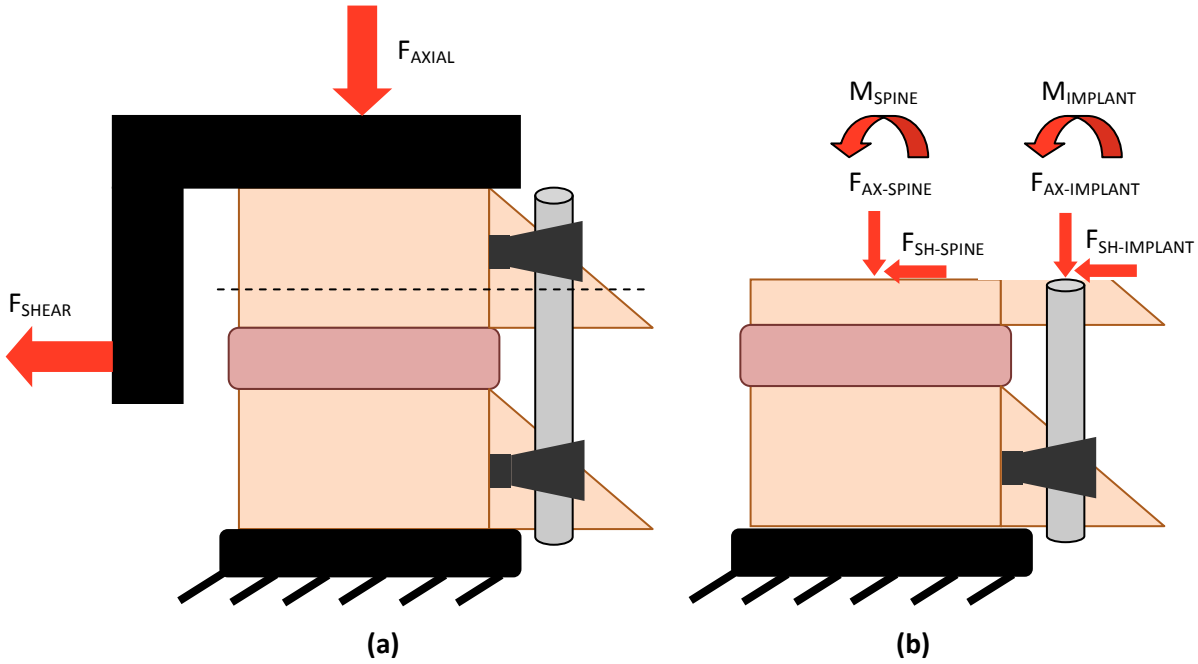

Figure 1-8: Free body diagram of a functional spinal unit with two applied loads. (a) The spine-implant construct supports the applied axial and shear loads. The implant rod is rigidly fixed to the spine via pedicle screws. (b) Forces and moments at the spine and implant due to the applied loads at the cut location marked by the horizontal dashed line are shown. Reaction forces at the rigid base are not shown.

In vitro implant loads as a percentage of an applied load are important to characterize because they can be used in conjunction with *in vivo* spinal loads to determine the load the implant will support *in vivo*. This information would greatly advance the ability of medical device companies to design new devices for specific spinal conditions. Directly inferring load-sharing from stiffness does not provide load-sharing magnitudes for specific implants, and it is erroneous to assume the spine and implant act in a linear manner; the basic assumption of the spine and implant as two parallel springs with static stiffness coefficients may be too simple to model the *in vivo* situation. Therefore, it is prudent that load-sharing be measured directly.

1.6.4 Load Measurement Methods

1.6.4.1 Types of Transducers

Direct measurements of implant load-sharing are required since indirect methods may be inaccurate. Several methods have been used to measure load on a spine-implant construct: electro-resistive sensors,[97,98] off-the-shelf load cells,[99] inductance transducers,[100] and strain gauges.[24,25,85,101-107] The strain gauge transducer is the most common sensor used in the spine-implant field because of the limitations of the former three sensors.

The electro-resistive sensors are arranged on a flat sheet that responds to pressure. Ideally, this sensor is compressed between two relatively smooth, large, flat surfaces. The accuracy of this sensor was low when inserted into small joints of the spine such as the facet joints.[108] Load cells from general transducer manufacturers are often too large to incorporate into a spinal implant and can rarely measure load in all six axes. A sub-miniature load cell was adapted with metal "endplates", mimicking the surface of vertebral endplates, to fit in the disc space to measure axial load in the anterior cervical column.[99] This method is currently restricted to measuring anterior column loads in the disc space due to the size of the load cell. The first *in vivo* loads measured on a spinal implant were measured by recording a change of inductance between two coils; this resulted in an axial load measurement through a scoliosis fusion rod.[100] This transducer only measured axial load and could not be adapted to other implant types since the actual rigid implant rod was replaced with the rigid transducer in the body. These limitations have led to extensive use of strain gauges to measure load (see Appendix A for details on the strain gauge).

Strain gauges are small resistive elements that can be affixed to different materials, surfaces, and shapes, and they respond to small deformations on the surface of a structure. Effects of a design change on an implant can be quantified by measuring the surface strain on select locations on the implant using strain gauges. Under compressive loading, poly-axial pedicle screws (head of screw can swivel on shaft of screw) were found to decrease the longitudinal rod strain compared to mono-axial pedicle screws.[104] This indicates that the poly-axial design change may be an improvement over the standard mono-axial head design.

Local strains can be converted into tensile stress[94] which is important for fatigue and strength tests. The tensile stress can be compared with the endurance limit or the yield stress. Stress levels below the endurance limit will not result in failure even if the device is cycled indefinitely. Metal stressed above its yield stress will plastically deform. In implant testing, strain gauges affixed to the root of pedicle screws have measured the stress in some implants to be greater than the endurance limit, indicating that those particular implants are at a higher failure risk than others with stress levels below the endurance limit.[94] If the gauges are affixed to high-risk locations on the structure such as the root of the pedicle screw, or other stress concentration locations, the results may show which fusion construct designs are at risk of failing. However, these stresses do not indicate how much load the implant supports.

Strains from combinations of gauges can be used to calculate forces and moments carried by the implant; this allows direct implant loads to be measured. There are two main methods of strain-force conversion: theoretical equations and calibration. Theoretical equations are determined by

analyzing the free body diagram of the construct and combining the geometric and material properties into standard mechanics of materials relationships. This method is ideal for common shapes like columns and cylinders made of a single material[109] but is difficult to apply to more complex designs involving multiple materials. This method is sensitive to gauge location and testing apparatus alignment. Errors from complex shape geometry, gauge alignment and testing apparatus alignment cannot easily be determined when only using theoretical equations.

The calibration method can be used for complex shapes and materials and does not require a high degree of accuracy when affixing the strain gauges to the implant. Calibration is a method in which a known input is related to a measured output. For example, to relate force and strain a known load is applied to an implant instrumented with strain gauges and the strain signal is recorded. As long as the relationship between the load input and strain output is linear, a relationship of $F = C \times S$ exists where F is the applied force, S is the recorded strain, and C is the constant relating these two signals. The construct is then used in an unknown load-sharing experiment, and the load is applied to the new structure composed of the implant and spine. The calibration constant is applied to the resulting strain measurement and the load supported by the implant is calculated. This method can incorporate the effect of as many load directions as are applied in the test by using the matrix method (see Appendix B).[110] The calibration method can be used alone or in combination with the theoretical method.

1.6.4.2 Load-Sharing with Strain Gauges

Pedicle screws instrumented with multiple strain gauges have been used to measure *in vitro* bending moments on spinal implants.[24,106,107,111,112] Strain signals from four gauges affixed to the hub of a screw were combined in theoretical equations to calculate moments on the screw.[106] Additionally, these transducers were calibrated before and after the experimental testing to assure the transducer errors were acceptably low. A compression-flexion load was applied to spine-implant constructs with increasing implant lengths. There was a three-fold increase in mean bending moment between an eight-screw intact construct spanning three vertebral levels, eight-screw corpectomy model and a four-screw corpectomy model spanning one vertebral level. Greater loads were supported by the implant spanning the least number of vertebral levels. However, the possibility of load-sharing was eliminated because a corpectomy model was tested in these experiments.

Cannulated pedicle screws were internally instrumented with strain gauges to determine the bending moments along the length of the screws.[111] These transducers were extensively calibrated and required accurate gauge placement. Seventy-five percent of the transducers failed the calibration and were discarded from use in experiments.[107] Bending moments showed a second order decline from the

hub of the screw towards the middle of the vertebral body.[111] This is expected since the moment arm of the compression force located over the vertebral body was smaller near the tip of the screws. These transducers were also used to assess the effect of pedicle screw insertion angle on the bending moments on the screw.[112] The intra-pedicular bending moments were 19% greater for screws angled superiorly than the moments measured on neutral screws, but screws angled inferiorly did not show significant differences compared with the neutral screw. The use of these transducers was limited to corpectomy models and the pedicle screws were connected with rigid fusion rods or plates.

More recently, simple pedicle screw transducers using two external strain gauges on the screw hub have been used to compare two dynamic spinal devices.[24] The simplicity of the transducer resulted in the measurement of a moment in a single plane that did not necessarily correspond to the maximum moment. Moments on the pedicle screws were measured under flexion-extension and lateral bending combined with an axial compressive load. The pedicle screws were calibrated in situ. Moments were significantly higher for one of the implants in both flexion-extension and lateral bending. Therefore, the load transfer to the spine was less for that implant compared with the other.[24] The designs of the two dynamic devices directly affected the load supporting capability of the implant as measured by pedicle screw transducers.

Unfortunately, pedicle screw transducers are not ideal for measuring shear loads, the relevant loading direction in a spine with DS, on a posterior fusion device (Figure 1-9). Pedicle screw transducers provide a method of quantifying the bending moment on the screw at a particular cross-section. However, these transducers are less sensitive to loads directed axially or transversely on the pedicle screw due to the low strain values in metals under pure tensile and shear loads. Further, the gauges are usually affixed as close to the screw head as possible and the effect of the poly-axial head orientation on the strain measurements and the load transfer between the screw and the implant is not clear. Gauges placed directly on the rods or plates connecting the pedicle screws could yield valuable implant load information not obtained by pedicle screw transducers, such as implant shear loads.

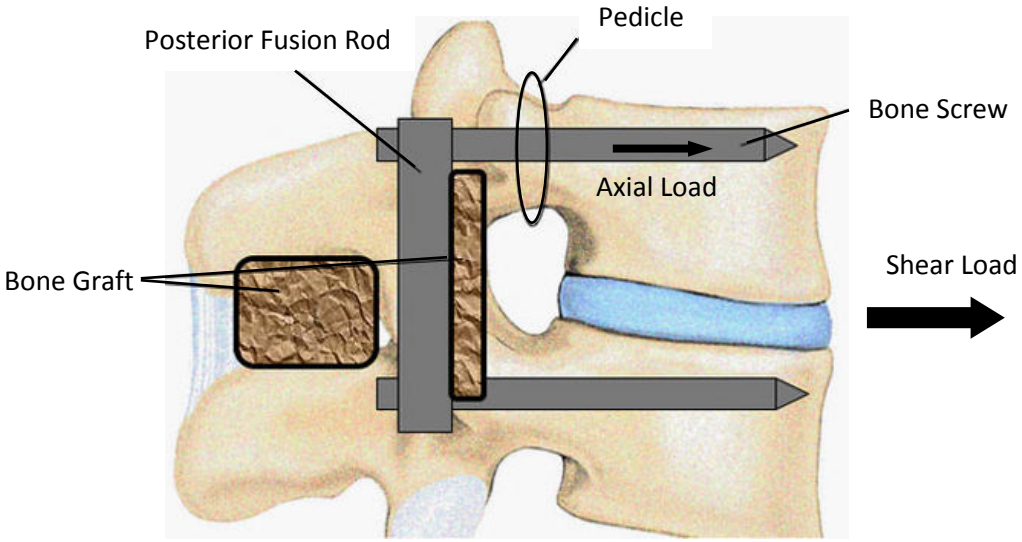

Figure 1-9: A drawing of a spinal segment fused with a posterior fusion device. The relevant loading direction for a DS spinal model is anterior shear which corresponds to an axial tensile load on the pedicle screws.[113] Reprinted from www.eurospine.org with permission from EuroSpine, the Spine Society of Europe.

Implant loads have been measured *in vivo* with a transducer designed to be implanted in humans. Rohlmann *et al*. (1994) developed a six-axis load transducer using strain gauges affixed to a rod that was encased to protect the gauges from the *in vivo* environment.[103] The rod was made to represent an AO fixator. Calibration and the matrix method were used to convert the strain output to the applied moments and loads. Implantation of this transducer in humans undergoing fusion surgery resulted in the first *in vivo* data. Measured implant forces during level walking showed compression forces of 100 to 200 N.[114] Unfortunately, implant load-sharing was not determined since global spine loads are unknown.

Low shear forces were measured in the fixator,[114] and it would not be expected that a metal rod would fail under shear loading. However, a low-stiffness device may support more load relative to its yield strength. Unfortunately, affixing a low-stiffness device with strain gauges for the *in vivo* environment is difficult since encapsulation of the device may increase the rigidity, and large strains on low-stiffness materials could result in gauge damage.

Implant transducers have been used *in vitro* to measure implant load and have provided complementary results to the *in vivo* work. The transducers have been created by affixing strain gauges to intervertebral cages[102] or the plates[85] and rods[25,105] connecting superior and inferior pedicle screws. A six-axis load transducer, created with strain gauges and a posterior fusion rod, was developed to measure load-sharing in surgically destabilized cadaveric lumbar functional spinal units.[25] The strains from the transducers were transformed via the matrix method to loads in an anatomical co-ordinate system.[115] The measurement error was less than 5% and the transducer was also validated under

combined loading environments prior to cadaveric testing. The load-sharing values for the fusion implant were applied to the *in vivo* loads measured previously,[29] and the overall load acting on the spine was predicted.[25] Both *in vivo* and *in vitro* studies simulated the AO fixator fusion device. However, the results are limited to metal fusion rods, and the surgical conditions created in the cadaveric test did not represent a degenerative spinal disorder.

The implant load-sharing measured in the aforementioned study was supported by a second study that measured the amount of axial force and bending moment supported by a metal fusion rod in an intact specimen.[105] Moments carried by the implant were approximately 15% of the applied flexion-extension moment.[105] Load-sharing is expected to be higher for degenerated spines and was found to be 1100% greater for a severe injury model, a spine with no posterior elements, compared to an intact specimen.[25]

A load transducer built as a surrogate intervertebral cage has been developed, but not yet tested in cadaveric experiments.[102] Four pillars instrumented with strain gauges are connected superiorly and inferiorly by flat parallel plates. The plates can be affixed to custom endplates that have the same surface finish and contour as clinically used interbody spacers. This load transducer will be used to measure load supported by the anterior column in the lumbar spine. Load-sharing between various anterior or posterior fusion devices could be determined using this transducer. However, the transducer must be inserted in the intervertebral space and only studies assessing spinal devices in combination with an intervertebral spacer will be performed.

1.6.4.3 Load-Sharing with Finite Element Models

Finite element models of the lumbar spine have been developed to investigate implant loads and to facilitate comparison of multiple implant devices.[88,90,95] These models are useful for assessing local strain and load, and for performing tests that are difficult to conduct in cadaveric experiments. A comparison of rigid and low-stiffness devices showed larger axial compressive forces on the rigid implant when the disc properties were adjusted to mimic a degenerative disc.[95] In another study, three rods of different axial stiffness supported different axial load magnitudes; implant load-sharing was 67% for a rigid metal rod, 28% for a polymer rod and 36% for an implant made of coiled Nitinol.[90] This study applied axial loads only, and since axial rod stiffness is different than shear rod stiffness, the shear load supported by each implant may be different.

Finite element models lack complete characterization of material properties and behaviour of biological tissues because these properties have not been fully characterized in a numerical form appropriate for use in finite element models. These finite element models are validated with kinematic

results such as range of motion from *in vitro* and *in vivo* experiments. It is important to verify computer model results with *in vitro* and *in vivo* implant load results.

1.7 Objectives

Numerous low-stiffness fusion implants have been designed and these implants must stabilize a degenerated spine appropriately to allow fusion to occur while supporting the shear forces in the lumbar spine. A scientific understanding of the effect of these implants on the shear load-sharing between the affected spine segment and the implant is needed. To date, shear load-sharing of low-stiffness implants has not been available for medical device companies during the design phase of their product development. To address this, a cadaveric model of a clinically relevant spinal disorder warranting a fusion with a novel posterior implant tested under shear loading is required. The research questions that I intend to answer are:

1. What is the percentage of applied load supported by a fusion implant affixed to the spine under shear loading?
2. What effect does implant stiffness have on the implant load?
3. How does a degenerative spinal disorder such as DS affect the implant load?

My specific hypotheses for this study are:

1. the proportion of shear force on the posterior implant increases with an increase in shear stiffness of the implant; and
2. the proportion of shear force on the posterior implant increases with decreasing integrity of the spine.

The overall objective of this study is to determine the load transfer characteristics between the spine and a posterior implant under shear loading, considering the effects of implant and spine stiffness. These load transfer characteristics are vital in estimating design loads in shear for novel implants designed for the degenerated spine. The following sections are divided into two manuscripts followed by an integrated discussion of the results of both manuscripts. The manuscripts will be submitted for publication with minor changes to the versions presented in this thesis. The first manuscript is a technical paper describing the accuracy of the load transducer developed to measure the implant loads in a cadaveric study. The second manuscript reports the measured implant loads found in a cadaveric experiment.

1.8 Scope

The project presented in this thesis is an *in vitro* biomechanical investigation testing the effect of four different posterior fusion devices on load-sharing between the spine and implant. The implants

were donated to our lab by our industrial collaborator, Medtronic Inc. The shear stiffness of the implants were 50 N/mm, 100 N/mm, 100 N/mm and 200 N/mm.

Fifteen human cadaveric lumbar functional spinal units were tested under combined anterior shear and axial compression loads. Two sequential surgical destabilizations were created in each specimen to achieve anterolisthesis of the upper vertebra with respect to the lower vertebra consistent with a Grade I DS. No attempt was made to obtain specimens from humans who had DS during life. Both L3-4 and L4-5 specimens were tested. The load magnitudes applied during testing were estimations of physiologic *in vivo* loads, however actual *in vivo* loads are unknown. A maximum anterior shear load of 250 N and axial compression load of 300 N were used to simulate expected loads during walking. Cyclic shear loading was applied, but fatigue testing was not completed.

Kinematic measurements at an adjacent segment to a fusion were not obtained because only two-vertebra spine segments were used in this study. Two vertebra segments were tested due to difficulties in applying a pure shear load to a multi-segment spine. Although the clinical occurrence of ASD motivated this study, adjacent level effects were not measured; a previous study in this lab addressed the effect of spinal implants on the adjacent level.[78] This study is a continuation of a larger research goal of characterizing spinal implant behaviour and the effect of implant stiffness on the loads on the spine.

Chapter 2 Development of Shear Load Transducers from Low-Stiffness Posterior Fusion Devices[2]

2.1 Introduction

Between 3% and 8% of the population suffers from DS.[4] DS is a degenerative disease that is characterized by the superior vertebra slipping forward with respect to the inferior vertebra.[1] This anterior slip is in the same direction as the shear loads in the lumbar spine, which may act to aggravate the slip. Lumbar spinal fusions are the current surgical treatment for DS[5] and the number of these performed has increased 220% from 1990 to 2001.[6]

In response to the increasing number of fusion surgeries for people with degenerative spinal conditions, medical device companies are designing novel instrumentation with decreased stiffness to be used for fusion of degenerated spines. Lower stiffness implants are thought to transfer greater loads to the spine, thereby assisting bony growth of the fusion mass and decreasing hypermobility at the adjacent segment[78] which may decrease the risk of further degeneration of the spine.[58] This load-sharing between the implant and the spine is a key mechanical parameter for determining the appropriate implant stiffness for fusion treatment for degenerative spinal conditions. A method of measuring implant shear load on these low-stiffness devices is needed.

Previously, *in vitro* and *in vivo* loads have been measured on spinal devices using custom load transducers. Loads supported by posterior fusion devices have been measured *in vivo* using mutual inductance coils[100] and strain gauges affixed to the spinal implants.[29,103] This work has advanced our understanding of realistic *in vivo* implant loads on rigid metal implants during tasks of daily living. Shear loads on these implants have been found to be relatively small *in vivo*.[114] However, *in vivo* load measurements have not yet been extended to low-stiffness implants and they have been limited to measurements of load on devices spanning more than one spinal segment.[100,103] Often only one vertebral level in a spine with DS is instrumented.[53]

In vitro implant loads have been determined with implants instrumented with strain gauges affixed to cadaveric spine segments.[24,25,105,106,111] The majority of implants tested were rigid.[25,105,106,111] One group that compared two dynamic spinal devices, designed to restore the motion of the spine, used pedicle screws instrumented with strain gauges to measure the bending moment on the screw under applied moments.[24] Posterior fusion rods have been instrumented with strain gauges to create load transducers; loads on the implants under applied bending moments were determined.[25] Some

[2] A version of this chapter will be submitted for publication. Melnyk, A., Chak, J., Cripton, P.A., Dvorak, M.F., and Oxland, T.R. (2011) Development of shear load transducers from low-stiffness posterior fusion devices.

researchers have reported extensive calibrations on their *in vivo* and *in vitro* transducers explicitly stating the transducer accuracy,[103,107,115] but some do not report the accuracy or sensitivity of the transducer to alignment in the spine. Shear loads were not applied to the implants in any of the *in vitro* studies. The load-sharing of low-stiffness implants designed for fusion of degenerated spines subjected to shear forces has not been investigated.

Limits of transducer accuracy, complexity of measuring loads in multiple directions, errors due to alignment within the spine, variability of cadaveric specimens, and advancement in finite element models have lead to the investigation of load-sharing using computational models. Under loads representative of those in standing, axial forces on a rigid implant were larger than those on a low-stiffness implant when the spine was simulated as intact, degenerated and distracted.[95] A second finite element study supported these results: axial implant load-sharing was found to increase from a low-stiffness device to a high-stiffness device when the functional spinal unit model was loaded in axial compression.[90] To validate the load predictions from these models an accurate and repeatable method of measuring *in vitro* implant loads is required.

In vitro characterization of load-sharing between the spine and low-stiffness implants under shear loading is needed to provide a basis for determining strength requirements for novel implant designs and to determine how different designs affect the load supported by these implants. A method of creating and calibrating a transducer to measure shear loads must be adaptable to current low-stiffness implants. Further, calibration of these transducers should account for the positioning of the implant in each specimen thus taking into account inter-specimen variability. The objectives of this study were to (1) develop shear load transducers from current posterior spinal fusion rods and develop a specimen-specific calibration method; (2) determine the accuracy and repeatability of the load transducers; and (3) determine the reliability and sensitivity of the calibration.

2.2 Methods

2.2.1 Transducers

Four types of posterior fusion rods of varying stiffness were converted into shear load transducers. Each rod-pair was considered one transducer: High-Stiffness Transducer (HST), Medium-Stiffness Transducer (MST), Low-Stiffness Transducer (LST), and Ultra-Low-Stiffness Transducer (ULST). The implant names were based on the relative axial stiffness values of the implants as provided by the manufacturer (Medtronic Inc., Minneapolis, MN). However, the shear stiffness values did not result in the same relative relationships. The shear stiffness values are approximately: 200 N/mm for HST, 100 N/mm for MST, 100 N/mm for ULST and 50 N/mm for LST. The shear stiffness of each rod-pair was

determined by applying a shear load of 150 N to the rod-pair affixed to plastic blocks that were secured to a materials testing machine. The load from the materials testing machine load cell and the displacement of the materials testing machine actuator was recorded at 50 Hz. The slope of the least squares linear curve fit to the load-deflection data was defined as the shear stiffness. The test was repeated three times for each transducer type and the stiffness was averaged.

All rods had a similar radius of curvature of 157 mm and length of 50 mm (Ø5.5 mm Titanium, 7.2 x 6.35 mm Oblong PEEK, Ø5.5 mm Round PEEK, Ø5.5 mm Rod X; Medtronic Inc., Minneapolis, MN). The Titanium (HST), Round PEEK (LST) and Rod X (ULST) had circular cross-sections, while the Oblong PEEK (MST) had an elliptical cross-section. The HST was manufactured from titanium, the MST and LST were manufactured from PEEK, and Rod X was manufactured from multiple components including a titanium shell, a metal cable and a polymer bumper.

Six uniaxial foil strain gauges with a nominal resistance of 120 Ω (EA-06-015DJ-120; Vishay Intertechnology Inc., Malvern, PA) were affixed to the outside surface of each rod for the HST, LST and ULST, while four gauges were attached to each of the rods for the MST (Figure 2-1). Gauge location was determined for the curved rods by adapting previously described methods for measuring moments and axial load on a cylinder with strain gauges.[109] The MST did not use six gauges because the method described by Tuttle does not apply to a beam with an elliptical cross-section.[109] Therefore, four gauges two each on the convex and concave surfaces were affixed to each MST rod. From the results of initial transducer testing, the force was not accurately calculated from the strain signals using the method described by Tuttle; the approximation of the curved rods as straight rods resulted in unacceptably high errors. Therefore, a direct, physical calibration was required to relate the strain output to load input. Each strain gauge was wired in a three-wire 1/4-bridge Wheatstone circuit (Appendix A) and the voltage signal was collected at 20 Hz with a data acquisition unit (National Instruments Co., Austin, TX). A custom software program (LabView 9.0.1, National Instruments Co., Austin, TX) was used to convert the voltage to strain (Appendix A).

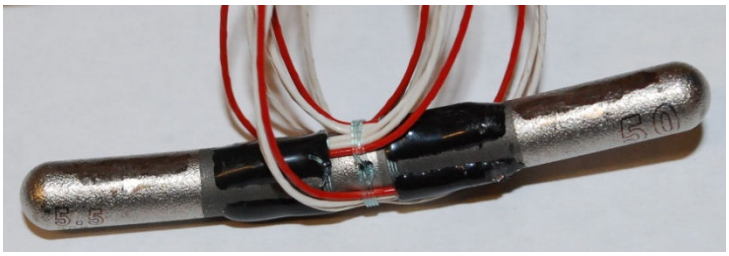

Figure 2-1: Image of an example HST posterior fusion rod with strain gauges affixed to the surface. The black rectangles are a surface coating to protect the gauges from moisture. Each gauge has three exiting wires: high and low voltage and ground. Six gauges are affixed to the HST in two arrays each of three gauges around the circumference of the rod. All gauges are oriented longitudinally along the length of the rod.

2.2.2 Calibration

Calibration relates a known applied load to the strain output from the transducers. Five each of the HSTs, MSTs and LSTs and four ULSTs were calibrated to measure shear load. Each rod pair was connected to ultra-high-molecular-weight-polyethylene blocks representing the superior and inferior vertebrae of a cadaveric functional spinal unit via pedicle screws (Figure 2-2). Each vertebral calibration block is made of two adjacent blocks; one block contains one screw. The medial-lateral, anterior-posterior and superior-inferior location of the pedicle screw head in each block was matched to a cadaveric specimen. The locations of four pedicle screws that had previously been inserted in a lumbar spine specimen were measured with calipers (Figure 2-2b). The angles of the pedicle screws in the specimen were not matched to the calibration blocks; the screws in the calibration blocks were parallel to the mid-sagittal plane, whereas the pedicle screws in the specimen were angled towards the mid-sagittal plane. A HST was tested in calibration blocks with angled or parallel screws and loaded under anterior shear. The error between the applied load and the transducer-predicted shear load for the two screw conditions was less than 5.2 N. From preliminary pilot work the accuracy of the transducer was expected to be around 10 N, thus it was assumed the angle of the pedicle screws would not affect the study results.

The four plastic blocks represented a specific specimen. The rods were inserted into the pedicle screws in the calibration blocks and each set screw clamping the rod to the pedicle screw was torqued to within 2% of 8 Nm with a digital torque wrench. A gap separating the superior and inferior blocks allowed the applied load to be completely supported by the implants (Figure 2-3). The calibration block construct was mounted in a materials testing machine (Instron 8874, Instron, Norwood, MA) (Figure 2-3). The inferior block was mounted rigidly to the Instron base, and the calibration loads were applied to the superior block. A counterbalance affixed to the superior block at the center of gravity removed the weight of the superior calibration block and loading plate from the transducer.

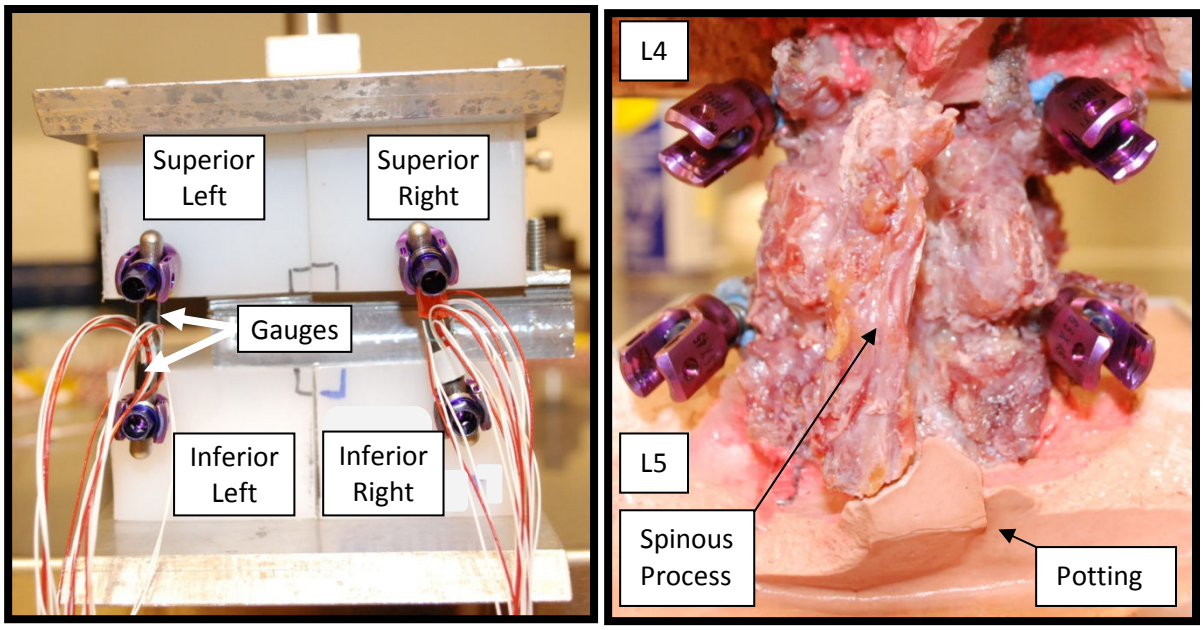

(a) (b)

Figure 2-2: Posterior view of calibration blocks and a specimen. (a) Superior and inferior calibration blocks representing a cadaveric functional spinal unit with the HST clamped to the pedicle screws with set screws. The gauges measuring the strain on the rods are indicated. Each calibration block is custom machined to match the screw location to the associated specimen. (b) Posterior view of an L4-5 cadaveric specimen with four pedicle screws cemented into the pedicles. The location of these screws are matched to the calibration blocks shown on the left.

a)

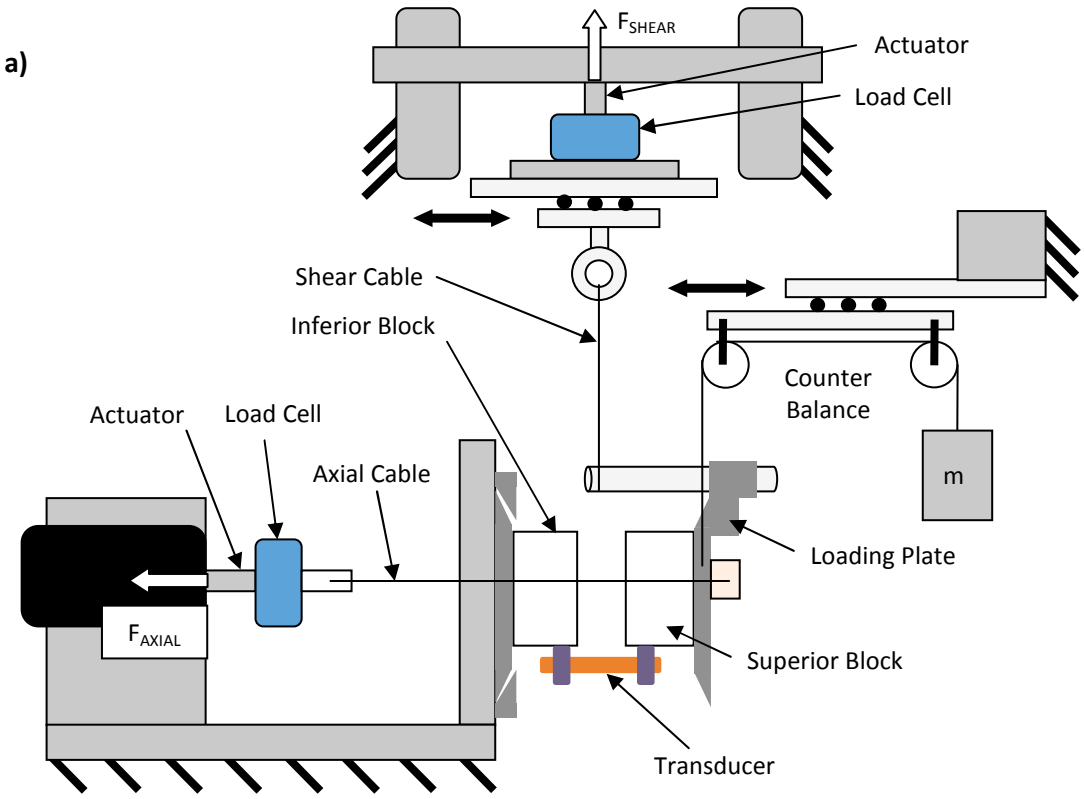

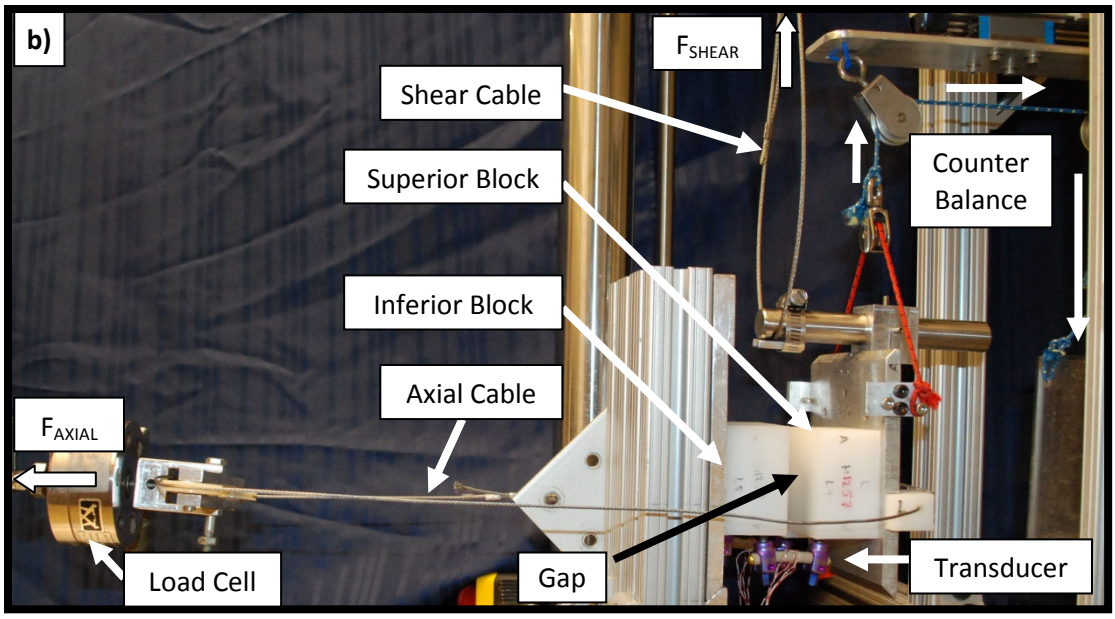

Figure 2-3: The loading rig. (a) Schematic of the loading rig shows the two actuators at 90° that applied the axial compression and anterior shear loads through cables to the calibration block representing the superior vertebra. The counterbalance system removed the weight of the superior calibration block and loading plate from the transducer. Linear guides in the counterbalance system and shear actuator maintained unconstrained motion in the sagittal plane. (b) Image of the loading rig with an MST mounted in the calibration blocks. The shear actuator is not shown, but the cable applying the shear load to the superior calibration blocks is indicated (more rig images in Appendix D).

The calibration process consisted of three tests: isolated shear loading, isolated axial loading and a combined test with both axial and shear loading. In the isolated shear test an anterior shear load was applied, through a steel cable by the Instron actuator, to the block construct at the location of the center of the disc as measured from the cadaveric specimen. The maximum applied shear load varied depending on the transducer being calibrated: 250 N for HST and 150 N for MST, LST and ULST. The maximum load was less for the MST, LST and ULST to keep the strain signal within the working range of the strain gauge (30 000 με).

In the isolated axial load test, a second hydraulic actuator (Model A591-4, Instron, Norwood, MA) oriented at 90° to the shear actuator was used to apply an axial compression load at the neutral line measured from the cadaveric specimen; the specimen does not flex or extend when compressed at the neutral location. Maximum loads were 150 N for HST, 50 N for MST, 25 N for LST and 15 N for ULST. These loads were applied to the MST and LST to keep the strain within the working strain range. The ULST had low axial stiffness and this load was applied to prevent the superior block from touching the inferior calibration block due to rod bending. For both isolated load tests, three load-control triangular waveform cycles were applied at 0.05 Hz.

A third combined loading test was performed in which a constant axial load was applied with a cyclic shear load. The maximum loads were the same as for the isolated load tests. The combined test was used to determine the accuracy of the transducer to predict shear load in a combined loading environment. Three load-control triangular waveform cycles of shear load were applied at 0.05 Hz. Data from the third loading cycle for all test types were analyzed. The construct was not moved between the isolated shear, isolated axial and combined loading tests.

Testing was repeated to incorporate the effect of variability between tests in the load application and orientation of the calibration construct in the loading rig on the transducer accuracy. The three tests described above (isolated shear, isolated axial and combined test) represented a single calibration trial. Three trials were completed with the construct removed between each trial and the transducer removed and reinserted into the construct to replicate slight changes in transducer behavior due to reinsertion.

The strain signals from the transducers were converted, using a mechanics of materials equation for curved rods (Appendix C), into axial and shear implant forces. The strain signals were converted to both axial and shear forces for each of the three test types. For example, during the isolated shear test, the strain signals were combined into a shear force and an axial force, even though the applied axial load was zero. A direct calibration constant relating the applied shear load and predicted shear force, and a coupling calibration constant relating the applied shear load and predicted axial force were determined as the slopes of least-squares linear curves fit to the force data (Figure 2-4a and b). An axial calibration constant and coupling constant were found in the same manner from the isolated axial test (Figure 2-4c and d). The calibration data were analyzed using the matrix method (Equation 1; Appendix B).[110]

$$\begin{bmatrix} F_1 \\ F_2 \end{bmatrix} = \begin{bmatrix} C_{D1} & C_{C2} \\ C_{C1} & C_{D2} \end{bmatrix} \begin{bmatrix} S_1 \\ S_2 \end{bmatrix} \qquad \text{Equation 1}$$

where F_i is the applied shear or axial load, C_{Di} and C_{Ci} are direct and coupling calibration constants, respectively, and S_i is the prediction of shear or axial force found from the strain gauge data.

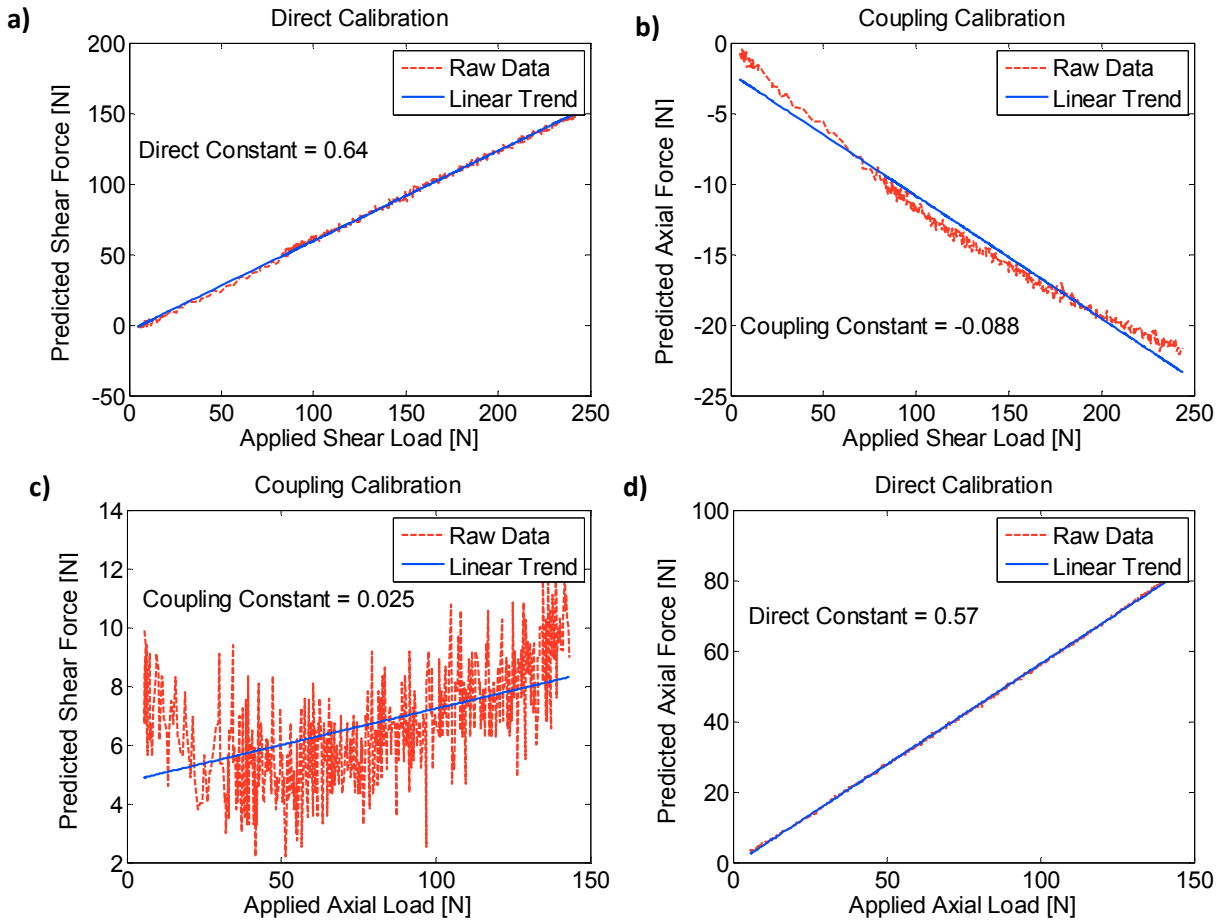

Figure 2-4: Example isolated load test calibration curves for the third calibration trial for the HST. The known applied shear load is linearly related to the (a) predicted shear force and (b) predicted axial force. The applied axial load is linearly related to the (c) predicted shear force and (d) predicted axial force. The calibration constants represent a direct relation between applied shear load and predicted shear force and a coupling effect of applied shear load and predicted axial force. The same relationships were derived for the isolated axial calibration.

The average calibration matrix found from the three isolated axial and shear load tests was applied to the strain from each of the three combined loading tests to determine the shear load on the transducer. Variability in the application of loads between trials and between isolated load tests and the combined test resulted in a constant offset between the known applied shear load, as measured by the Instron load cell, and the transducer-predicted shear load, calculated from the transducer strain signals during the combined loading test and the calibration matrix. The average offset from the three trials was then applied to the combined loading data to yield the final transducer error in the calibration process (Appendix B).

The transducer error was defined as the difference between the known applied load and the calibrated load (Figure 2-5). A shear error was calculated for the isolated shear test, an axial error for the isolated axial test and a shear error for the combined test. The error was generally positive or

negative for the loading cycle, but occasionally had both positive and negative error values over the range of loading. The absolute value of the errors over 5-95% of this range of data were averaged. The error from each of the three trials for each test was averaged to yield the final error for that transducer. The transducer error was averaged across the five transducers for each implant type (four for ULST). The mean error reported in the results is positive due to taking an absolute value of the error over the loading range so as to assume the worst-case; simply averaging the positive and negative error values would dilute the magnitude of the errors associated with each transducer. It is assumed that the transducer will have an equal error above and below zero. The transducer accuracy was accepted if the error was within 10 N of the applied load.

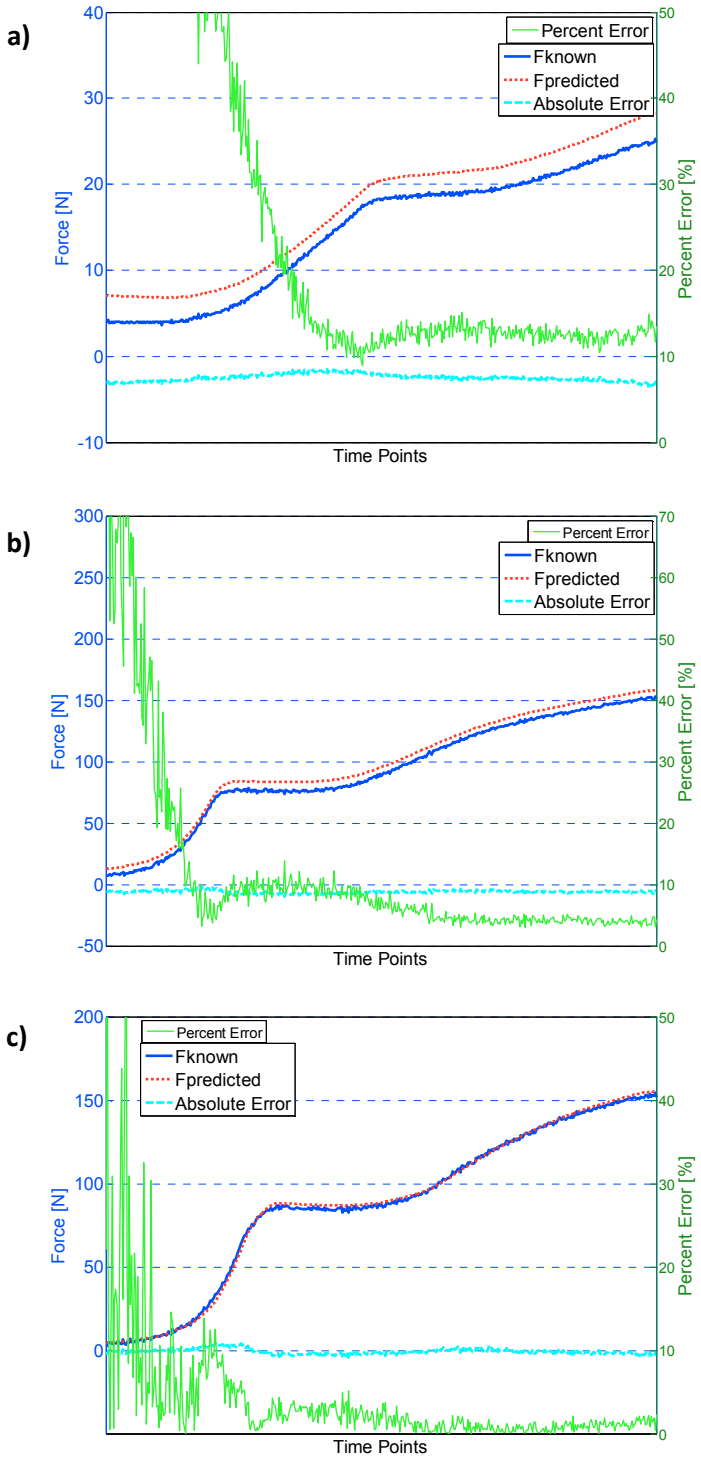

Figure 2-5: Example data for a single calibration trial for the LST. (a) Isolated axial test, (b) isolated shear test and (c) combined loading test show the applied load (blue), the predicted force from the calibration constants and strain gauge output (red), and the absolute error (cyan), or difference between these loads. The percent difference between the loads (green) is shown on the secondary vertical axis. The third loading cycle is shown for each test with time on the horizontal axis.

The repeatability of the transducer was determined by calculating the standard deviation of the error for one transducer for 15 trials for each of HST, MST and LST. The 15 trials were completed for the

sensitivity analysis (described below) and were not completed for the ULST. The repeatability for the ULST was estimated as the standard deviation of the error for the three trials used to calculate the transducer accuracy as previously described. Data were analyzed using custom software programs (Matlab v. R2009b, MathWorks, Natick, MA).

2.2.3 Reliability Test

The transducer reliability was assessed by comparing the predicted shear load supported by the implant during cadaveric testing using calibration matrices and offsets from calibration tests conducted before and after cadaveric specimen testing. The cadaveric testing is fully described elsewhere (Chapter 3). Briefly, shear and axial loads were applied to the specimen-implant construct. Strains from the transducers were converted to load via the calibration matrix and offset values found during the pre-test calibration. The amount of implant load-sharing, defined as the percent of applied shear load supported by the implant, was calculated. Calibration tests as previously described were then repeated after specimen testing and this matrix and offset were used as a second prediction of the shear load supported by the implant during cadaveric testing. The difference between the two predictions of load-sharing was used as a measure of transducer reliability. A Bland-Altman plot was created for each transducer type and the transducer was accepted as reliable if the bias between the pre- and post-values of implant load-sharing was less than 10%. A Wilcoxon Matched Pairs test was used to compare the pre- and post-values of implant load-sharing, and a P-value less than 0.05 was considered significant.

2.2.4 Sensitivity Test

The sensitivity of the transducer to measurement errors of the screw location between the cadaveric specimen and the calibration blocks was determined by creating known measurement errors in the location of one of the pedicle screws in its calibration block. One specimen-specific set of calibration blocks was used as the known condition, and four additional right-inferior blocks (Figure 2-2) were machined as the misaligned conditions: 3 mm medial translation, 3 mm inferior translation, 4 mm anterior translation, and all three previous translations combined. Magnitudes of translation were estimated as reasonable values of two screws being misaligned (i.e. each screw being misaligned up to 1.5 or 2 mm).

Three calibration trials were completed for each of the five conditions with one transducer of each of three implant types: HST, MST and LST; ULST was not tested in the sensitivity test. The matrix and offset found from testing the transducer in each misaligned condition were applied to the transducer strains in the known condition. For the combined tests in the known condition the error

between the known applied shear load and calibrated shear load was determined. The data analysis for the sensitivity test differed from the previously described accuracy test. All implant loads and errors were calculated with the strains from the combined test for the known condition and matrices found from isolated tests for the misaligned conditions. A Friedman's analysis of variance was used to test if the dependent variable, shear error, changed significantly with the independent factor, misalignment condition. For a significant analysis of variance ($P<0.05$), multiple comparisons were conducted between the misalignment conditions and the known condition using Dunnett's test modified for non-parametric analysis.

2.3 Results

The accuracy of the transducer to measure shear load in a combined loading environment was within ±5 N for all the transducers with the largest errors for ULST (Figure 2-6; additional results in Appendix E). The shear errors for the isolated shear tests were larger than the axial errors for the isolated axial tests and the shear errors for the combined tests. The combined test did not reflect the large shear errors because of the incorporation of the offset. The repeatability of each transducer to measure shear load is 1.5 N for HST, 1.2 N for MST, 1.5 N for LST and 2.8 N for ULST.

The Wilcoxon Matched Pairs test showed no significant differences between the implant load as predicted by the pre-test calibration and by the post-test calibration for all transducer types ($P=0.5$ for HST, $P=0.2$ for MST, $P=0.1$ for LST and $P=0.5$ for ULST). Bland-Altman plots for each transducer show a small positive bias for MST, LST and ULST implants (Figure 2-7; additional results in Appendix E). There is an increase in spread of the bias for larger averages between the pre- and post-implant loads that is visualized on the Bland-Altman plots. However, all paired-comparisons were less than 6% for each transducer type, therefore, each transducer reliably measured the implant load.

The median shear errors from the combined tests for the sensitivity analysis were within ±5 N for the MST and LST for all conditions (Figure 2-8). The maximum median shear error was 25 N for the HST for the anterior misalignment condition. The errors are displayed as positive values in Figures 2-6 and 2-8 due to the data processing described in the methods in which the absolute value of error was obtained, representing the worst-case for the transducer accuracy. It was assumed each transducer would over- and under-predict the shear load equally. The Friedman analysis of variance performed on the sensitivity errors was significant (HST $P=0.022$, MST $P=0.017$, LST $P=0.017$). However, given that the median errors were within the transducer accuracy of 5 N for the LST, a multiple comparisons test was not performed for this transducer. Significant differences between the median shear error of the

combined tests for the known condition compared with the misalignment anterior and combined conditions for both HST and MST were found using the Dunnett's test ($P<0.05$).

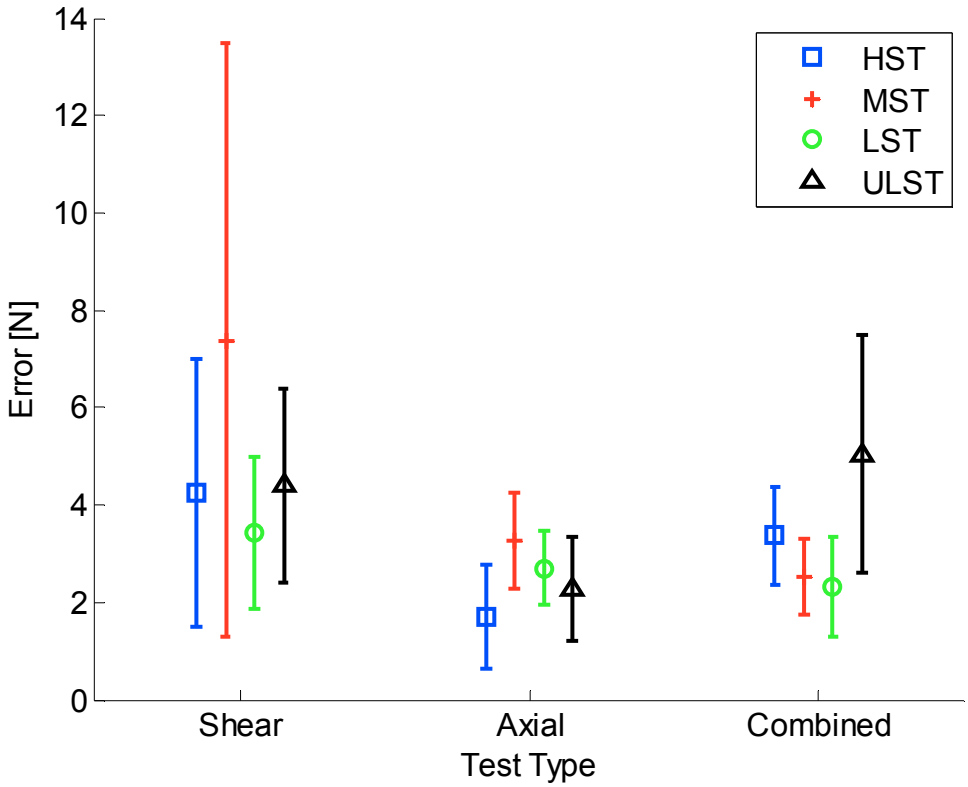

Figure 2-6: The mean transducer error (±1 standard deviation) for each test type in the calibration. For the shear test, the error is the difference between the applied shear load and the calculated shear load. For the axial test, the error is the difference between the applied axial load and the calculated axial load. For the combined test, the error is the difference between the applied shear load and the calculated shear load.

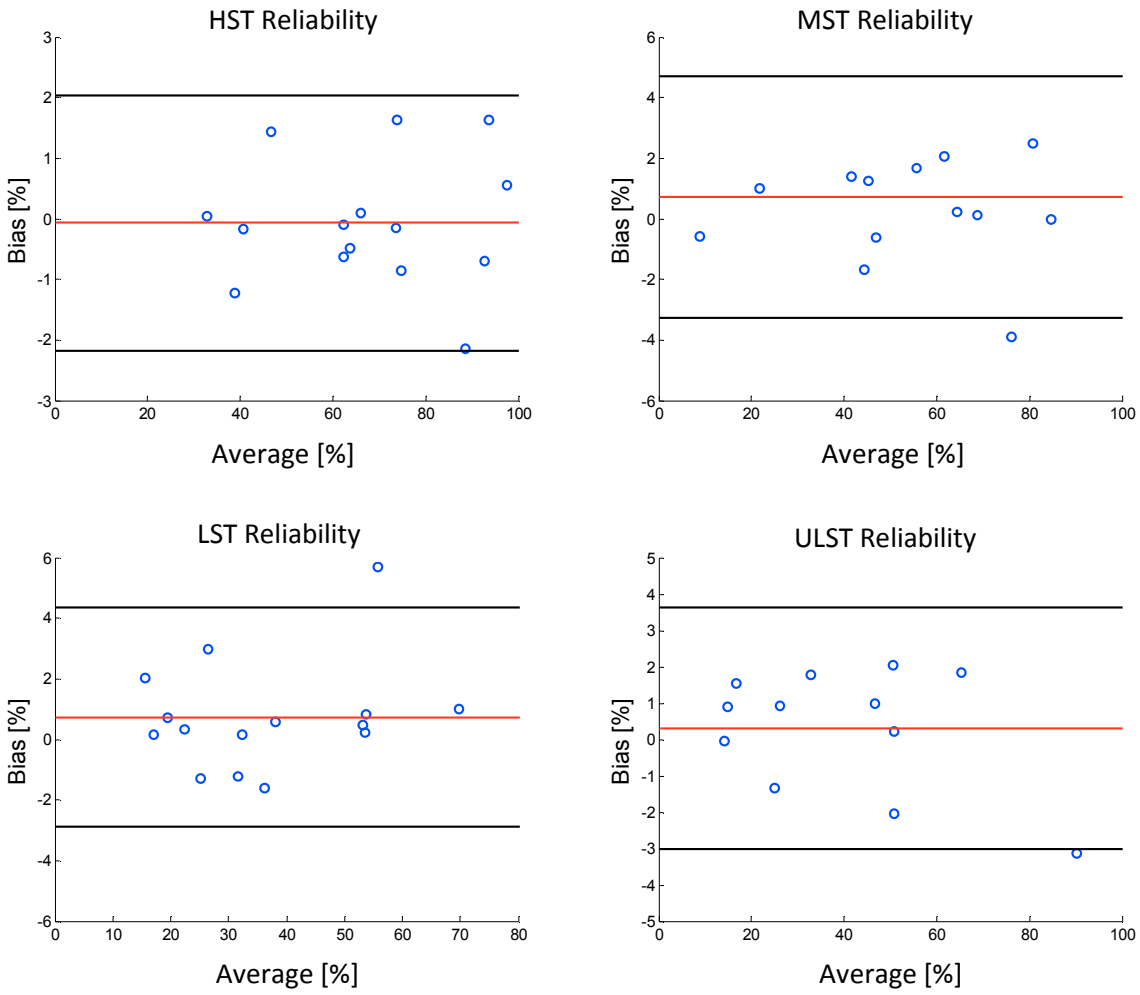

Figure 2-7: The transducer reliability results displayed on Bland-Altman plots for each transducer type. The difference in implant shear load-sharing calculated using the matrices and offsets from the pre- and post-test calibrations is the bias (vertical axis), and the horizontal axis is the average of the two load-sharing measurements. The red horizontal line is the mean bias; a value of zero would indicate no systematic difference between the two measurements. The black horizontal lines are the mean bias ±2 standard deviations. Each point is a result from a cadaveric test using one of the five (four) transducers for HST, MST or LST (ULST) to measure implant load. Three specimen tests were performed for each transducer for HST, LST and ULST. There were two missing tests for the MST transducer (i.e. there are 13 points on the plot instead of 15).

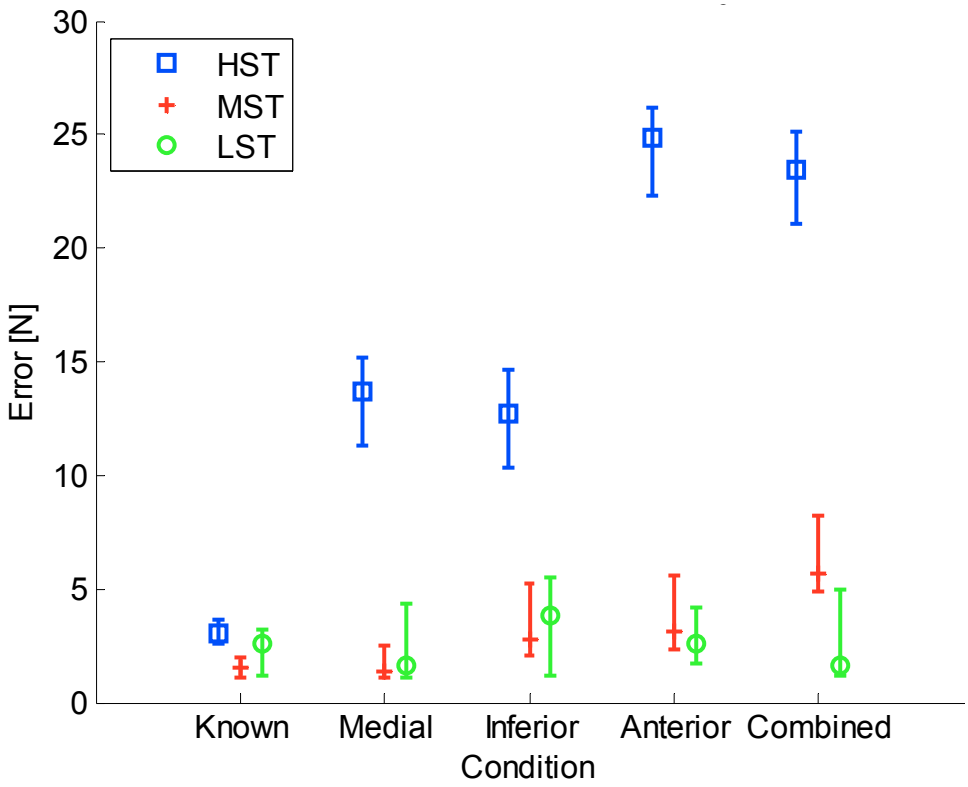

Figure 2-8: The transducer sensitivity results displayed as the median shear error (range) for the combined loading test in the known condition for three of the transducer types (HST, MST and LST). The errors are separated by the type of misalignment matrix that was applied to the strain data for the known condition. A single transducer of each type was tested.

2.4 Discussion

Four posterior fusion devices were converted into shear load transducers by affixing strain gauges to the surface of each device and using a specimen-specific calibration method to relate the strain output to a load input. The range of mean error across all four transducer types to measure the applied shear load under a combined loading environment was from 2.3 to 5.0 N and each transducer type was repeatable to within ±3 N. The shear load supported by the implants during specimen testing was reliably calculated using calibration matrices found from pre- and post-test calibrations. Both the HST and MST were more sensitive than the LST to misalignment between pedicle screw locations in the specimen and calibration blocks.

The errors associated with the transducers are likely due to the estimation of the coupled motion by a linear relationship when a relatively high noise to signal ratio existed (Figure 2-4), especially for the isolated axial calibration. This error may be reduced by changing the orientation of the gauges on each posterior fusion rod. However, in spite of this linear approximation of the coupled relationship, the error of the transducer in measuring shear load in a combined loading environment was less than 10 N and the transducer was deemed accurate.

The errors of the transducers were an average of 2.4 N larger for the isolated shear calibration test compared to the axial test, possibly because the isolated axial calibration test was less affected by slight misalignments of the load line of action. The strain gauges responded directly to the axial load and indirectly to a bending moment due to the axial load eccentricity in the axial test, whereas for the shear test, the gauges only responded to an indirect bending moment that was dependent on the shear load. A shift in the load line of action did not affect the direct axial load, only the indirect bending moments for both axial and shear calibrations, causing a smaller percent change of strain in the axial tests. Minimizing differences in the location of the shear load line between trials and between the calibration and specimen testing was critical for maintaining small absolute shear errors. However, the shear error from the combined test, of interest since it is representative of real-world loading, was smaller than the isolated shear error, possibly due to the application of the offset to the combined loading data.

For the reliability test, the largest difference between implant loads predicted by the pre- and post-test calibrations was 6% for a single test for the LST (Figure 2-7). During the post-test calibration for this particular test, the wires from a strain gauge were accidentally severed and were soldered together again. This could have altered the resistance of the wire which then influenced the magnitude of strain measurements and caused the large bias.

The sensitivity evaluation of the HST to pedicle screw misalignment resulted in the highest shear errors of all the transducers for predicting the associated shear loads under combined loading. This specific HST was not used after the sensitivity test for any specimen tests. It is possible that this transducer's function was compromised at the time of sensitivity testing which may have caused the high sensitivity. Based on the performances of the other HSTs in the accuracy and reliability studies, and comparing those to the performances of the LST and MST, there was no indication that the HST was more sensitive to misalignment conditions. Although there was a significant increase in error from the anterior and combined misalignment conditions compared to the known condition for MST, the magnitude of the median errors were all within ±6 N, comparable to the errors found in the accuracy test for the MST of ±3 N.

Implant loads have been measured on rigid metal fusion devices; however, to the author's knowledge, polymer fusion devices have not been converted into load transducers until now. Cripton *et al*. modified titanium rods and instrumented them with strain gauges to create six-axis load transducers.[25] This transducer was calibrated under known loads and was further validated under combined loading tests;[115] errors of 5% were reported.[25] A rigid fusion device developed for *in vivo* load measurement has been extensively calibrated in six-axes using the matrix method and errors between 2 and 5% of the applied load were reported.[103] A pedicle screw transducer developed to measure bending

moments at the hub of the screw was calibrated with a known moment in both the direction of interest and in the transverse direction.[107] Errors less than 10% of the applied load due to the transverse loading were accepted. The reported accuracies of the aforementioned transducers of 5%[25,103] and 10%[107] are similar to the accuracies found in this study. However, one of the previous studies did not test the transducer under a combined loading environment during calibration,[103] and it is not obvious if the reported accuracy reflects the total error when multiple loads were applied to the transducer during the *in vivo* test.

Reliability is infrequently reported for transducers. One transducer was reported to be functional with a high accuracy for 10 to 25 tests,[107] and a second transducer was reported to be calibrated before and after testing, although quantitative results were not provided.[106] The measure of reliability in the current study validates the function of each transducer during specimen testing.

The specimen-specific calibration method used in the current study accounted for anatomical differences between specimens in the calculation of shear load from the transducer output. Previously, rigid, metal implant transducers had been calibrated in six-axes but specimen-specific calibrations were not used.[25,103] Misalignments between the implant and anatomical coordinate systems were accounted for in only one of these studies.[25] Specimen-specific calibrations were conducted on a pedicle screw transducer measuring sagittal plane moments for two dynamic spinal implants.[24] This calibration method was adaptable for any spinal device affixed to the spine via pedicle screws, but the transducers were limited to measuring bending moments on the screws; shear loads through the implants were not measured.

The accuracies of four different implants for measuring shear load in a combined load environment were determined in the current study. Previous *in vitro* studies have tested one or two implants[24,25,99,105] and only a few finite element studies of the lumbar spine have reported results for more than two implants.[88,90] It is difficult to compare results across studies due to differences in methodologies and outcome measurements. Therefore, a single study comparing three low-stiffness implants with a traditional rigid implant will provide a comprehensive comparison of the response of these implants to load.

There were several limitations in this study. The angles of the pedicle screws in the specimen were not matched to the angles of the pedicle screws in the calibration blocks. Clinically, pedicle screws are angled towards the mid-sagittal plane in a vertebra. However, the pedicle screws inserted in the calibration blocks were parallel to the mid-sagittal plane. During specimen testing (Chapter 3), the poly-axial head of a pedicle screw in the specimen was angled to maintain alignment of the posterior aspect of the implant with the posterior aspect of the specimen. During calibration, the implant and calibration

blocks were aligned without angling the poly-axial head of the pedicle screw. It was assumed that the angle of the poly-axial head had a minimal effect on the loading of the implants as long as the posterior aspect of the implant was aligned with the posterior aspect of the specimen and calibration blocks.

The available surface area to place strain gauges on the implant rods limited the gauge size, which also limited the maximum strain capacity of the gauge. On the polymer implants (MST and LST) the gauges operated in their upper range, and 57 gauges failed throughout testing due to over strain or mechanical damage. Higher rated gauges that are slightly larger may decrease the rate of gauge failures and the costs associated with gauge replacement. Some of the gauges were redundant and could be removed to allow larger gauges to be affixed. Gauge failure did not affect the results since gauges that failed were not included in the data processing.

The calibration trials did not yield an accurate prediction of axial load on the implant during combined loading. Since both isolated shear and axial calibrations were performed on the transducers, load on the implant in either of these directions can theoretically be calculated. The axial offset found from the calibration was not applied to the combined loading data to predict the axial load because the offset for the axial data changed over the range of load application. Therefore, an average value would not be representative of the overall error. This limitation does not affect the accuracy, repeatability, reliability or sensitivity of the shear load transducers.

Shear load transducers were developed from clinically relevant lumbar spine fixation implants used to treat degenerative spinal disorders. Three of these transducers are the first low-stiffness spinal implants able to measure shear loads. These transducers can be used in biomechanical studies to determine the load-sharing characteristics of the spinal implants.

Chapter 3 Load Transfer Characteristics Between Posterior Fusion Devices and the Lumbar Spine Under Shear Loading: an *in vitro* study[3]

3.1 Introduction

Three to eight percent of the population has DS,[4] a prevalence which increases with age.[2,4] In people with DS, neurological deficit and pain may accompany radiographic evidence of anterior slip of the superior vertebra with respect to the inferior vertebra, a degenerated intervertebral disc, and degenerated facet joints.[1] The most commonly affected joint is the L4-5 vertebral level.[2]

DS may be treated with fusion surgery at the affected vertebral level and the number of lumbar fusion surgeries has increased 220% over ten years.[6] Posterior instrumented lumbar spinal fusion surgeries have been found to result in high rates of solid bony fusion in patients with degenerative spinal conditions.[52,53,55,56] Specifically, fusion surgeries for DS have been found to have a 93% rate of bony fusion when rigid pedicle screw instrumentation is used.[52]

However, researchers postulate that commonly used rigid metal instrumentation for fusions accelerate ASD[65,71] possibly by causing increased mobility[58] or instability[59,60] at the adjacent intervertebral joint. ASD is characterized by increased degeneration at the vertebral segment adjacent to a fusion.[9] Surgical revision rates for ASD after a fusion surgery have been reported to be between 5 and 27%.[62,71] In one *in vitro* study from out lab testing the effects of instrumentation stiffness on adjacent level mobility, rigid spinal fixation devices were extended an extra vertebral level with either rigid or flexible instrumentation.[78] The flexible instrumentation resulted in a smaller increase in motion at the adjacent level as compared to the rigid instrumentation. Flexible, or low-stiffness, fixation devices may decrease the rate of ASD by preventing excessive motion at the adjacent level to the fusion.

In response to the possible acceleration of ASD caused by rigid fusion devices and the subsequent revision surgeries, implant companies have developed novel, low-stiffness fusion devices. The goals of these devices are to decrease adjacent segment motion while providing stability to a degenerated spinal segment. However, it is not known what effect these low-stiffness devices will have on the amount of load supported by the fusion instrumentation.

An important loading direction in a spine with DS is anterior shear. The slip of the superior vertebra with respect to the inferior vertebra, characteristic of DS, is in the anterior direction, and the larger disc inclination at the L4-5 level compared with the thoracic levels[116] allows for a greater

[3] A version of this chapter will be submitted for publication. Melnyk, A., Wen, T., Kingwell, S., Chak, J., Cripton, P.A., Dvorak, M.F., Oxland, T.R. (2011) Load transfer characteristics between posterior fusion devices and the lumbar spine under shear loading: an *in vitro* study.

percentage of the total spinal load to be composed of an anterior shear force at the L4-5 level. Furthermore, the facet joints have been shown to support the majority of applied load in anterior shear.[35] Degenerated facet joints in a spine with DS may not be able to support the same amount of load as a facet joint without degeneration.

There has been one previous cadaveric model of DS reported in the literature.[1] The facet joints were completely disrupted in this model to achieve adequate anterolisthesis of the upper vertebra. A more recent model of DS was developed as a pilot study to the current study.[14] A cyclic shear load (-50 to 250 N) was applied to cadaveric functional spinal units; stages of destabilization including a facet gap and a nucleotomy were performed surgically. A Grade I anterolisthesis was achieved.

Previous *in vivo* shear loads were measured on rigid posterior fusion instrumentation implanted in the lumbar spine.[114] The shear loads were lower than compressive loads, and the indications for fusion surgery were not solely DS. The overall load on the spine cannot be determined from these experiments. Studies using inverse dynamics and mathematical models have predicted *in vivo* anterior shear loads on the lumbar spine of 40 to 200 N in a variety of activities including static bends and twists,[39] level walking,[16,38] and when external compressive and shear loads were directly applied to people.[44] These studies did not calculate loads on fusion instrumentation. The relationship between spine loads, implant loads and implant stiffness has not been determined from *in vivo* or inverse dynamics studies. It is not known which low-stiffness devices will sufficiently support the anterior shear loads in the lumbar spine.

Applied load to a spine-implant construct is supported by both the spine and implant components, a concept known as load-sharing. The relative stiffness of the spine and implant will dictate how much load is supported by each component. Measuring the load supported by an implant and knowing the applied load allows the load-sharing of the implant to be calculated. Pedicle-screw transducers, capable of measuring bending moments, were used to determine implant load-sharing of two spinal devices loaded under flexion-extension and lateral bending moments.[24] Strain gauges affixed to implant rods[25,105] and anterior plates[99] have been used to measure the load-sharing of these posterior and anterior fusion devices, respectively. Implant load-sharing has also been determined using finite element models of the lumbar spine loaded under bending moments and axial compression.[90,95] Some of these studies only measured loads on rigid implants.[25,105] Those that tested low-stiffness implants found that greater loads are transferred to the spine compared with a rigid implant;[90,95,99] however, these studies only applied an axial load to the spine-implant construct. The amount of load supported by an implant differs depending on the loading direction,[25,29,105] and an implant may have varying stiffness values depending on the direction of applied load. For example, the amount of load supported by an

implant in anterior shear is likely to differ from the amount of load supported by that implant in axial compression.

Limitations of previous studies have resulted in a knowledge gap of the performance of low-stiffness fusion devices. Validated spinal models that represent clinical presentations that would warrant a fusion have not been used in prior experiments.[24,25,90,99,105] It is difficult to assess whether the implant has been subjected to forces that are representative of those in a pathological spine for which fusion is indicated in these previous studies. Moreover, the instabilities that have been created in previous models are not representative of degenerative spines.[21,35,39] The loading in previous *in vitro* or finite element studies has been limited to compressive loads[90,99] and bending moments from flexion-extension, axial rotation or lateral bending.[24,25,105] Implant load-sharing in a degenerative spinal model tested under anterior shear loading has not been studied.

The purpose of this study was to determine the load-sharing characteristics of four posterior fusion devices of increasing stiffness with the spine under shear loading. A biomechanical *in vitro* study was used to assess the effect of implant stiffness and simulated DS on load-sharing. The hypotheses for this study were: (1) the proportion of shear force on the implant increases with increasing implant stiffness and (2) the proportion of shear force on the implant increases with decreasing stability of the spine.

3.2 Methods

3.2.1 Transducers

Four types of posterior fusion rods (Ø5.5 mm Titanium, 7.2 x 6.35 mm Oblong PEEK, Ø5.5 mm Round PEEK, Ø5.5 mm Rod X; Medtronic Inc., Minneapolis, MN) were instrumented with 120 Ω nominal resistance strain gauges (EA-06-015DJ-120; Vishay Intertechnology Inc., Malvern, PA) to create shear load transducers. All rods were designed to affix to the spine via poly-axial pedicle screws (Ø6.5 mm titanium bone screw; Medtronic Inc., Minneapolis, MN). Each rod-pair represented a single transducer with each rod in the pair being affixed with four or six strain gauges. One transducer type had only four gauges on each rod because its cross-sectional shape differed from the other three transducer types; the cross-section was elliptical while the other rods all had circular cross-sections. Gauges were positioned 180° apart on the long axis of the ellipse for transducer. The transducers varied in stiffness based on the material and shape of the rods: HST, MST, LST and ULST. The rods were designed for fusion surgeries and were not physically altered by the affixation of strain gauges. The HST and MST rods are used clinically, while the LST and ULST are in the development phase.

3.2.2 Calibration

The transducers were calibrated in axial compression and anterior shear loading before and after testing of each cadaveric specimen. The calibration process and transducer performance characteristics are reported elsewhere (Chapter 2). The calibration procedure has been summarized in a flow chart (Figure 3-1). Briefly, a calibration trial consisted of three tests: an isolated shear load test, an isolated axial load test and a combined shear and axial load test. Three trials were performed for each transducer type for each specimen. The transducer was secured via poly-axial pedicle screws to plastic blocks representing the cadaveric specimen to be tested. The calibration was specimen-specific; measurements of the screw location were taken from the associated cadaveric specimen and used to position the pedicle screws in the plastic calibration blocks.

For the isolated tests, an isolated shear or axial load was applied to each transducer by an actuator (shear: Instron 8874, Instron, Norwood, MA; axial: Model A591-4, Instron, Norwood, MA) and the resulting strains were related to the applied loads with calibration constants. Coupling effects from the shear and axial loads were accounted for with the matrix method.[110] The combined load test consisted of a constant axial compressive load and a cyclic shear load. The average calibration matrix found from the three isolated shear and axial tests was applied to the strains from the three combined loading tests. An offset between the transducer-predicted shear load and the known applied shear load was determined for the combined loading tests. This offset was generally constant across the range of applied shear load. An average of this offset was determined for each combined test. These average offsets were further averaged across the three repeated combined tests. Finally, the average calibration matrix and average offset were applied to the strains from the three combined loading tests. The accuracy of the transducer was the average shear error between the known applied shear load and the shear load predicted with the transducer. The accuracy of the transducer to predict the shear load during the combined loading tests was within ±5 N for all the transducer types (Chapter 2).

The average matrix and offset values found from the calibration were applied to the strains from the cadaveric test to calculate the shear load supported by the implant. This load was divided by the maximum applied shear load to determine the implant load-sharing. The calibration procedure was repeated after the cadaveric testing and both pre- and post-test calibrations were used to calculate the shear load-sharing of the implant. The difference between the calculated implant load-sharing using the pre- and post-test calibration matrices was defined as the transducer reliability and was less than 2% for HST, 4% for MST, 6% for LST and 4% for ULST (Chapter 2).

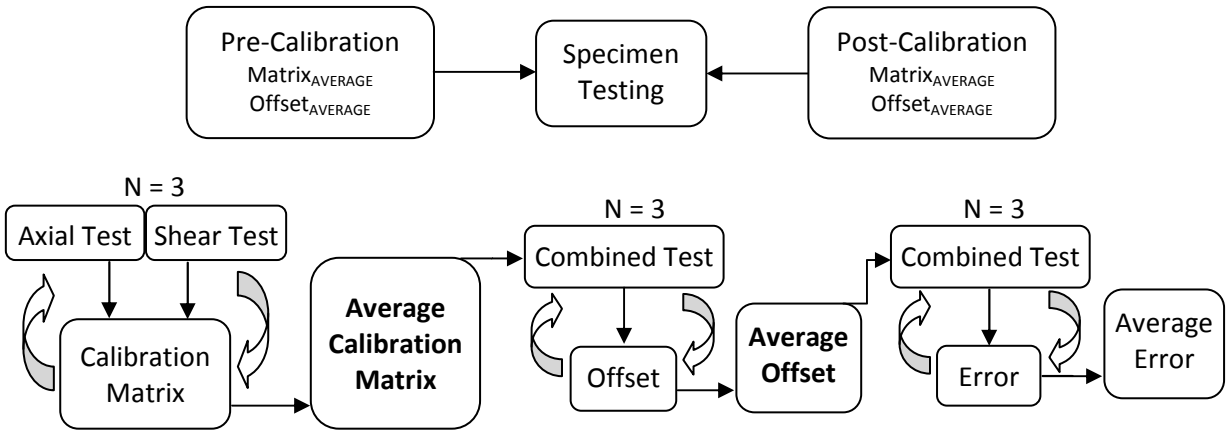

Figure 3-1: Flow diagram of the calibration procedure. Calibration on each transducer type was performed before and after the cadaveric testing (upper flow diagram). Isolated axial, shear and combined load tests were repeated three times (lower flow diagram). The average calibration matrix and average offset (bold) were applied to the transducer strains during specimen testing. The transducer accuracy (Average Error) was the final output of each calibration and is reported elsewhere (Chapter 2).

3.2.3 Specimens

Fifteen human cadaveric lumbar functional spinal units were used in this study (thirteen L4-5 and two L3-4). Musculature and soft tissue were removed from the functional spinal units while preserving the ligaments and disc. Donor ages ranged from 51 to 89 years (mean 73.7 years; standard deviation 11.1 years), and there were five females, nine males, and one unknown. Anterior-posterior and lateral x-rays were used to screen for exclusion criteria including tumors, missing facet joints or evidence of previous spinal surgery. Each specimen was fixated in gypsum potting material (Tru-Stone, Modern Materials Heraeus, South Bend, IN) in custom-made aluminum potting boxes. Wood screws and wires secured to the vertebral body provided stronger fixation between the vertebral endplate and dental stone. The transverse plane at the intervertebral disc midline was aligned parallel to the top and bottom of the potting boxes. A custom aluminum plate was affixed to each end of the potting boxes and the inferior plate was rigidly secured to the testing apparatus. Holes for the four poly-axial pedicle screws were under tapped, as is done clinically to prevent screw loosening, before screw insertion. The screws were cemented into the pedicles and vertebral bodies with poly-methyl-methacrylate (PMMA; Bosworth Co., Skokie, IL) to remove any confounding effects of possible screw loosening as a result of the repeated testing as described below.

3.2.4 Testing

The specimen was loaded in shear combined with axial compression, representing the compressive loads due to the weight of the body and musculature on the spine,[16,37] in a custom rig

designed for use with the Instron materials testing machine (Figure 3-2). The inferior potting block was rigidly attached to the base frame of the loading rig and the superior potting block was attached to the loading actuators. Sagittal plane motion of the specimen was unrestricted through a loading cable and linear slider. A counterbalance system was designed to remove the weight of the superior potting block and loading plate from the specimen (Figure 3-2b). This system prevented the mass of the superior potting block from applying an initial load on the specimen and implant transducer due to gravity.

The Instron actuator applied a 0.1 Hz cyclic shear load (5-250 N) for 25 cycles to simulate walking while a second actuator oriented perpendicular to the first actuator applied a constant 300 N axial compression load to the superior potting block. The loads were applied through steel cables and the lines of action of the loads were adjusted such that the shear load was applied through the center of the disc and the axial load was applied to achieve a neutral compression without visible flexion or extension. Applied load measured by the load cells on the actuators and strain signals from the implant transducers were collected at 50 Hz by a personal computer and data acquisition system (National Instruments Co., Austin, TX).

Each specimen was tested in three states of stability and with four fusion device types; a total of fifteen tests were performed on each specimen. The specimen was tested without a fusion device and then four subsequent times with the randomly ordered fusion devices combined with the current specimen condition (Table 3-1). The testing order of the fusion devices was randomized for each specimen using a random number table. The three tests without instrumentation (row 1 of Table 3-1) were always performed after the instrumentation tests to prevent possible specimen damage from affecting the instrumented tests.

The three specimen conditions, based on a pilot study in our lab,[14] were tested sequentially and were of progressively decreasing stability: intact, facet joint destabilization, and intervertebral disc destabilization. The facet joint destabilization consisted of disrupting the facet joint capsule and removing approximately 2 mm of bone from both the superior and inferior facet surface using a 4 mm burr tool. The surgeon visually aligned the burr tool to the natural angle of the facet joint. The resulting 4 mm gap represented the existing, but degenerated, facet joints of DS (Figure 3-3a). The disc destabilization consisted of removing the ligamentum flavum and creating a small posterior window in the lamina of the superior and inferior vertebra using a pair of rongeurs to remove the bone, performing a nucleotomy, and cutting the interior annular fibers with a scalpel from inside the disc space, without cutting through the outermost fibers (Figure 3-3b). This surgical condition represents degeneration of the disc allowing anterior slippage of the superior vertebra with respect to the inferior vertebra

consistent with a Grade I anterolisthesis[10] while maintaining partial integrity of both the disc and facet joints, characteristic of DS.[1]

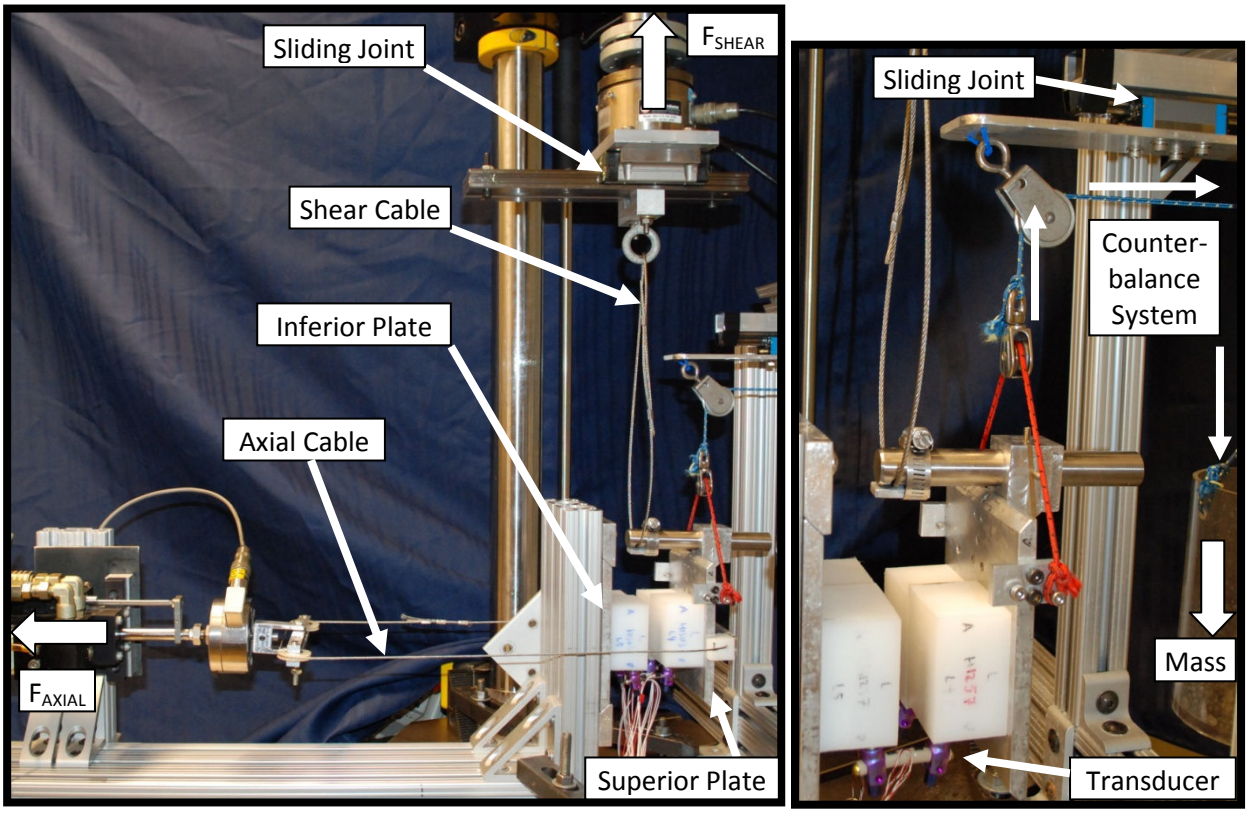

(a) (b)

Figure 3-2: The loading rig attached to the materials testing machine. (a) The calibration blocks are shown in this image but the specimen and potting blocks were located in the same location and orientation. The inferior plate is rigidly secured to the base of the loading rig and the shear and axial loads are applied to the superior plate through cables. The loading rig has a sliding joint to allow pure shear loads to be applied in the sagittal plane at the center of the disc; the cylindrical beam on the superior potting block can be adjusted in the anatomical superior-inferior direction to align the shear force line of action with the center of the disc. For a schematic drawing of the loading rig see Appendix D. (b) The counterbalance system removes the weight of half the specimen, superior potting block and loading plate from the transducer; this prevents initial strain on the transducer due to gravity.

Table 3-1: The testing plan for a repeated measures design with two factors: specimen condition (columns) and instrumentation stiffness (rows). Additionally, the specimen was tested without instrumentation (first row). Each of the 15 specimens were tested in all of the 15 cell conditions shown in the table. The order of instrumentation tested was randomized, but the specimen conditions were tested sequentially.

Experimental Design			Integrity of Specimen		
			Intact	Surgical Cond. 1 (4mm facet gap)	Surgical Cond. 2 (disc destabilization)
Instrumentation Conditions	none		n=15	▬▬▬▬▬▬▶	
	Implant Shear Stiffness	HST	Randomized testing order of implant stiffness		
		MST			
		LST			
		ULST			

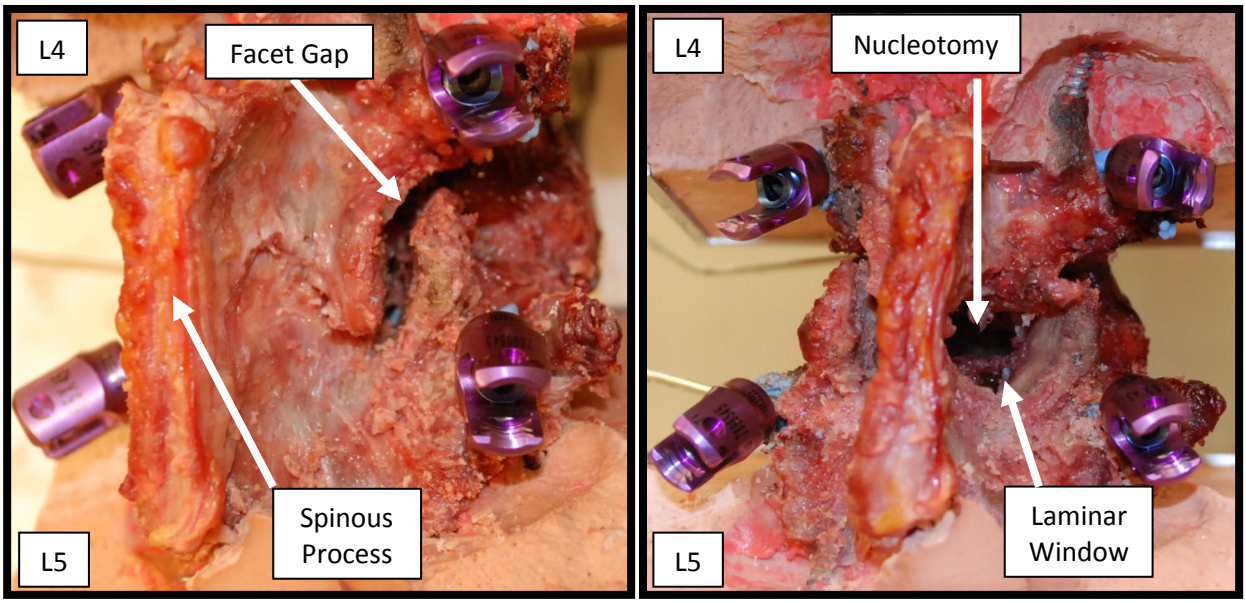

(a) **(b)**

Figure 3-3: Surgical changes to an example specimen to create (a) a facet joint destabilization defined as a 4 mm gap created with a burr tool and (b) a disc destabilization defined as a posterior nucleotomy through a laminar window combined with cutting anterior and lateral interior annular fibers.

3.2.5 Data Analysis

The strain and load data were processed with custom software programs (Matlab v. R2009b, MathWorks, Natick, MA). The strain was converted into load supported by the implant using the average calibration matrix and offset from each of the pre- and post-test calibrations. Results found

from applying the post-test calibration matrix and offset values to the specimen data are presented in this paper, except for one specimen in which the post-test calibration was performed incorrectly, the pre-test calibration matrix and offset were used. The percent load-sharing of the implant was calculated by dividing the amount of shear load supported by the implant by the known maximum applied shear load measured from the Instron load cell (nominally 250 N).

3.2.6 Statistics

A two-way repeated measures analysis of variance was performed on the load-sharing results using statistics software (Statistica v9, StatSoft Inc.,Tulsa, OK). The independent variables, or factors, were the specimen condition and the fusion device type. The dependent variable was the value of load-sharing. For a significant analysis of variance, a multiple comparison Student-Newman-Keuls test was performed to determine significant differences between specific cases. A P-value less than 0.05 was considered significant.

Load-sharing results for five of the fifteen specimens contained missing data. Missing data were due to an insufficient number of working strain gauges on the transducers. To account for the missing data the data were analyzed with a two-way repeated measures analysis of variance twice: once with complete data sets from ten specimens and a second time with data from fifteen specimens. For the fifteen specimen analysis, the missing data were replaced by the average implant load for that particular transducer type and specimen condition. The HST had no missing data, the MST had missing data for five specimens, and both the LST and ULST each had missing data for one specimen.

3.3 Results

Example strain data from a specimen tested in the disc destabilization condition instrumented with the LST are shown in Figure 3-4a. Strain gauges on the left and right posterior fusion rods that were not working were not used to calculate the implant load (indicated by DNU in the plot legends). The strain data were converted into the implant shear force by applying the matrix and offset found from the calibration. The value of implant load-sharing at an applied shear load of 250 N was obtained for each specimen (Figure 3-4b) at every combination of implant type and specimen condition as outlined in Table 3-1.

The compiled load-sharing data for all 15 specimens shows the amount of shear load supported by the implant (Figure 3-5); the spine supports 100% less the implant load. For example, in Figure 3-5c HST supports approximately 40% of the applied shear load in the intact condition, and the spine load is 60%. The statistical results for the 10 specimen analysis are presented here; the 15 specimen analysis supported these findings and is presented in Appendix E. The two-way repeated measures analysis of

variance was significant for specimen condition ($P<0.0001$; Figure 3-5a), fusion device type ($P<0.0001$; Figure 3-5b) and the interaction of these factors ($P<0.0027$; Figure 3-5c).

The average implant load supported by the LST and ULST increased approximately linearly by 16% for each progressive specimen condition: intact, facet joint destabilization and disc destabilization (Figure 3-5c). The average load supported by the MST also increased approximately linearly by 22%, whereas the load supported by the HST increased non-linearly: a 24% increase between the intact state and the facet destabilization followed by an 8% increase to the subsequent disc destabilization.

The multiple comparison Student-Newman-Keuls test found the individual comparisons between implant load-sharing values to all be significantly different except for six (bold values in Table 3-2). LST and ULST supported a similar load across all conditions, HST and MST supported a similar load for condition 3, and MST in the intact specimen condition supported a similar load to both LST and ULST in the facet destabilization specimen condition.

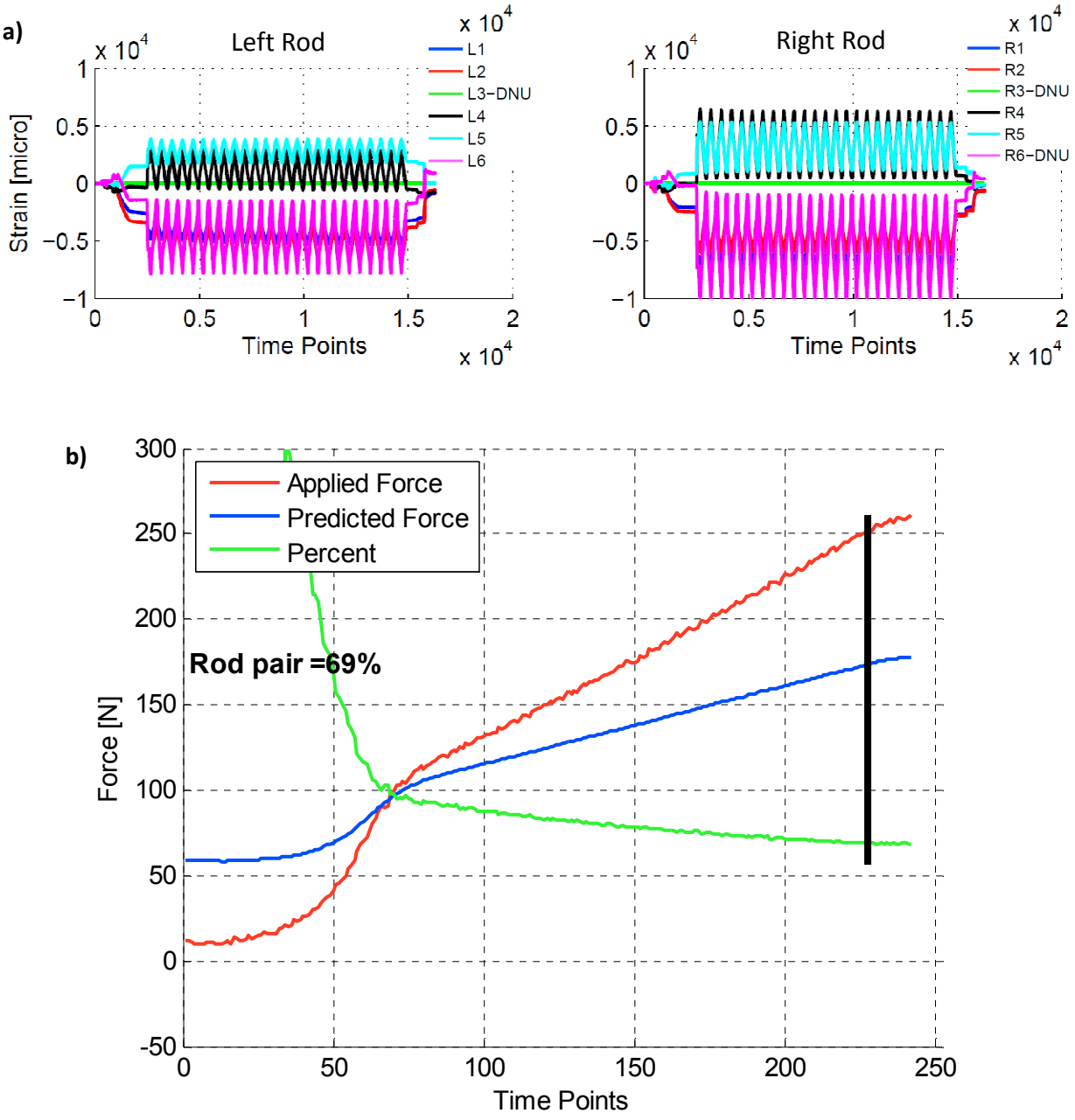

Figure 3-4: Example strain and load data from a single specimen test. (a) Strain data for specimen 2 for the LST tested for 25 cycles in the disc destabilization condition. Six strain gauges were affixed to each of the left and right posterior fusion rods. The gauges that were not used during processing due to damage are indicated by DNU (did not use) in the legend. (b) The applied shear load (red) for the 25th loading cycle plotted against time. The implant load calculated with the strain data and post-test calibration matrix and offset (blue) and the implant load-sharing (green) are also plotted. The load-sharing scale [%] is the same as the force scale [N] on the vertical axis. The load-sharing value of 69% occurs at 250 N of applied shear load as indicated by the vertical black line.

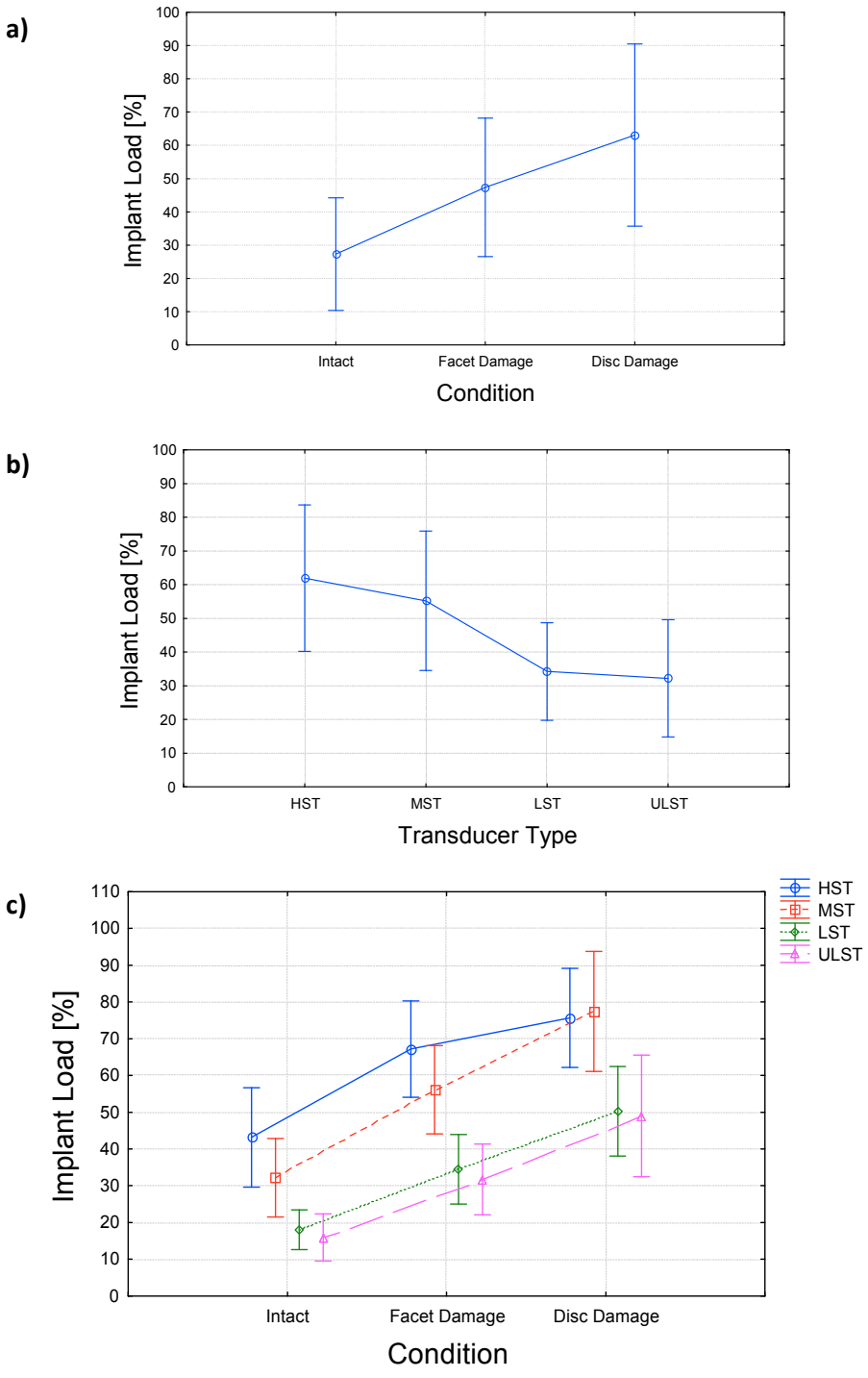

Figure 3-5: Mean implant shear load-sharing with 95% confident intervals (vertical bars) for a significant analysis of variance for (a) the specimen condition factor, (b) the implant type factor, and (c) the interaction between specimen condition and implant type. Load on the fusion device increased as the specimen stability decreased (specimen condition increased). Implant load decreased with decreasing implant stiffness. The amount of load supported by a specific fusion type was dependent on the specimen condition (HST, disc destabilization condition).

Table 3-2: The results of the multiple comparison Student-Newman-Keuls test showed significant differences between all implant load-sharing comparisons except six (bold). P-values were rounded to the nearest 0.0001. Implant type is listed with specimen condition: 1=intact, 2=facet joint destabilization, and 3=disc destabilization.

		HST			MST			LST			ULST		
		1	2	3	1	2	3	1	2	3	1	2	3
HST	1		0.0001	0.0001	0.0007	0.0003	0.0001	0.0001	0.0030	0.0355	0.0001	0.0009	0.0405
	2			0.0036	0.0001	0.0003	0.0016	0.0001	0.0001	0.0001	0.0001	0.0001	0.0002
	3				0.0001	0.0001	**0.5255**	0.0001	0.0001	0.0002	0.0002	0.0001	0.0001
MST	1					0.0001	0.0001	0.0001	**0.4041**	0.0001	0.0002	**0.8772**	0.0002
	2						0.0002	0.0001	0.0001	0.0383	0.0001	0.0001	0.0334
	3							0.0002	0.0001	0.0001	0.0001	0.0001	0.0001
LST	1								0.0002	0.0001	**0.4505**	0.0001	0.0001
	2									0.0002	0.0001	**0.5823**	0.0001
	3										0.0001	0.0001	**0.6509**
ULST	1											0.0001	0.0001
	2												0.0001
	3												

3.4 Discussion

A biomechanical investigation was undertaken to determine the effect of specimen destabilization and posterior fusion device stiffness on the amount of shear load supported by the fusion device. As specimen destabilization increased, the amount of shear load supported by the fusion devices increased (Figure 3-5a). For a given specimen destabilization condition, the two lower stiffness devices (LST and ULST) supported less load than the two higher stiffness devices (HST and MST; Figure 3-5b).

If the simple linear model of load-sharing described in Chapter 1 accurately described the spine-implant relationship tested in the current study, it would be expected that within each specimen condition the load-sharing for each of the different implant types would be approximately proportional to their stiffness. For example, the load-sharing for the MST would be approximately double that of the LST since the shear stiffness of the MST is twice that of the LST. Likewise, the load-sharing of the HST would be approximately four times that of the LST since the shear stiffness of the HST is four times that of the LST. However, the data presented in Figure 3-5c do not follow these relationships which implies the load-sharing model based on a constant stiffness, or linear force-displacement behaviour, is not adequate to describe the results found in the current study. The results of the pilot study, in which the surgical model of DS was developed, showed non-linear specimen stiffness, especially for the facet and disc destabilization conditions and variability of the stiffness between specimens.[14] These two factors

likely influenced the variability in the load-sharing measurement from the current study. Therefore, it would be inaccurate to simplify a non-linear load-sharing system with a linear mathematical model; an *in vitro* test system with direct load measurements is required.

In addition to the implant stiffness, implant design affects the load characteristics of fusion devices. The ULST, which has the same shear stiffness as the MST, supported similar loads to the LST. The shear stiffness of each device was determined prior to the cadaveric testing by loading each implant, secured to polymer blocks with pedicle screws, with a materials testing machine; the stiffness was found from the slope of the linear trend line relating the applied shear load to the actuator displacement. The HST, MST and LST are all made of solid materials, whereas the ULST is made up of multiple materials and multiple components, each of which can shift or twist with respect to each other. The axial stiffness of the ULST is less than that for the MST and LST. It is possible that the constant axial compression during the cadaveric testing caused the steel cable component in the ULST to slacken, causing the shear stiffness of the ULST to decrease to the level of the LST. This would not occur for the LST, MST or HST since these devices do not have a cable component in their designs.

Implant load-sharing has been measured using *in vitro* and finite element studies that tested a variety of implant designs. However, only moments and axial compression were applied to the spine-implant constructs. Large implant loads and strains were measured on rigid, metal fusion devices when the implants were tested on cadaveric specimens that were maximally destabilized;[25,75] the initial, less-severe destabilization procedures did not result in large implant load differences when compared to the intact state. Under flexion-extension, load-sharing on a posterior fusion device was less than 10% of the applied moment in the intact state, but increased to almost 100% at the most severe destabilization.[25] In the cervical spine, the anterior column axial load-sharing, measured with a custom load cell altered to mimic an interbody spacer, showed significantly greater load supported by a metal fusion plate but not a polymer plate, compared to the interbody spacer alone.[99] The low-stiffness polymer plate supported less load and transferred more to the spine, similar to the results in the current study. The axial load supported by the fusion implants increased by approximately 20% from the interbody spacer alone to the metal plate,[99] while the mean implant shear load in the current study increased by approximately 30% from the low-stiffness to the high-stiffness implants.

In a finite element study, a normal and slightly degenerated lumbar spinal segment were simulated, each instrumented with a low and high-stiffness spinal implant.[95] An axial force was applied to the spine-implant construct to simulate standing conditions and the axial load on the implant was calculated. For each of the low- and high-stiffness implants, the axial implant force was the same for both the intact and degenerated specimen simulations. Distraction of the degenerated spine model

resulted in larger forces on both implant types. Across all specimen conditions, the forces in the rigid implant were larger than those in the low-stiffness implant, with the largest difference for the distracted model.

In another finite element model of a lumbar functional spinal unit with a discectomy, axial compressive implant forces were also found to increase with increasing implant stiffness.[90] Posterior fusion rods made of PEEK, Nitinol or titanium-alloy stabilized the discectomy model; two of the implants in the finite element model simulated two of the implants tested in this study. The implant shear load-sharing found in the current study was greater than the axial load-sharing found in the finite element study: 50% for LST compared with 27% for PEEK, and 76% for HST compared with 67% for titanium-alloy. These findings indicate that load-sharing in one direction is not equivalent to load-sharing in other directions; there was greater implant load-sharing under shear load compared to axial compression.

It is important to assess the function of fusion implants on a clinically relevant spine model tested with physiologic loads; this will most closely simulate the *in vivo* environment in which fusions are used to treat degenerated and destabilized spines. The DS model used in the current study was developed with applied shear loads of -50 to 250 N to simulate *in vivo* loads during walking.[15,16,37] Similar or larger loads were applied to cadaveric specimens in previous studies testing the lumbar spine under shear loading.[34,35,117] In the development of a previous DS model, shear loads of only ±50 N were applied to the specimen,[1,118] below the expected *in vivo* loads and three times smaller than anterior shear loads applied to cadaveric lumbar spines in a study characterizing the kinematic response of the normal spine.[119]

To the author's knowledge, this is the first biomechanical study in which implant shear loads in a DS spinal model were measured. The previously developed DS spinal model[1] was used to determine the effect of interbody cages, bone dowels and pedicle screws and rods on the kinematic response of the spine;[118] loads on the implants were not measured. *In vivo* shear loads less than 65 N on rigid fusion implants have been recorded during level walking,[114,120] while shear loads near 100 N were found in a rigid implant connected to a finite element model of a degenerated lumbar spine during static flexion.[95] Dividing the *in vivo* shear implant loads with the percent load values from the current study for the HST using the facet destabilization condition yields estimates of global *in vivo* spinal loads between 100 and 150 N; for example, (*in vivo* implant load of 100 N)/(*in vitro* implant load-sharing of 67%) = global spine load of 150 N.

Sequential destabilization of specimens for biomechanical testing is important for determining how different spinal conditions, treated clinically by fusion, are affected by a specific implant. Few studies have assessed implant performance on a sequentially destabilized spine.[25,75,99] One study

measured moments on a rigid implant affixed to an intact spine that was subsequently altered by removal of the posterior elements followed by complete discectomy.[25] There was a large increase in moment supported by the implant for the final specimen condition. However, it is not obvious that the destabilizations were representative of a clinical condition or surgical model. The current study tested a clinically relevant destabilized cadaveric model that resulted in anterior slips expected in DS. The magnitude of the anterior slippage of approximately 3 mm under shear load was found during a pilot study in our lab.

In another study, range of motion of a vertebra adjacent to a rigid fusion implant and implant strain were measured under flexion and extension of the lumbar spine.[75] The specimen was destabilized with medial facet, total facet, and discectomy surgeries; these destabilizations are closest to the current study, but represent a surgical model, as opposed to a clinical model. There were no differences in implant strain between the intact and facet destabilization procedures but there were significantly larger strains after the partial discectomy. In the current study, significant differences in implant load were found between all surgical conditions.

Although adjacent segment effects were not measured in the current study, inferences can be made from the results of previous studies. One study testing destabilized cadaveric spine specimens instrumented with different fusion constructs found the increase in range of motion compared to the intact condition at the adjacent segment was largest for the most destabilized spinal condition when instrumented with the stiffest fusion construct, posterior rods and an interbody cage.[75] The smallest increase in range of motion at the adjacent segment was for the same destabilization, but with the least stiff fusion construct made of posterior rods without an interbody cage. The range of motion at the adjacent segment to low-stiffness rods extending from a fusion construct was found to increase by a lesser amount than when the fusion construct was extended with high-stiffness rods.[78] Extending these results to the current study, the low-stiffness constructs tested in shear would likely correspond to a smaller increase in range of motion at an adjacent segment compared to the high-stiffness constructs. Therefore, low-stiffness implants may act to mitigate adjacent level effects such as hyper-mobility.

The methodology used in the current study strengthened the findings. The repeated measures study design increased the ability of finding significance in the data because each specimen acted as its own control, limiting the effect of inter-specimen variability on the results. The same surgeon performed both destabilization surgeries on all the specimens, maintaining the consistency of the surgeries between specimens. The effects of the two factors of interest, specimen condition and implant type, on load-sharing were not confounded by loosening of pedicle screws, a common problem in an osteoporotic vertebra, because the screws were cemented into the vertebral body and pedicles.

There were several limitations in this study. Although the repeated measures design decreased the effect of inter-specimen variability on the results, the repeated testing on each cadaveric specimen increased the risk of damage to the specimen throughout the testing procedure. The order of fusion devices tested was randomized to mitigate the effect of specimen damage. There was also a possibility of specimen dehydration from the nine-hour testing period for each specimen. The specimen was sprayed with saline throughout the test day and wrapped with saline-soaked gauze during rest periods to maintain specimen hydration.[121] Differences in implant loads were highly significant (P-values less than 0.0001); any damage or dehydration that occurred likely had a small effect on the specimen stiffness and did not affect the conclusions.

The Instron actuator applied an anterior shear load through a cable, but did not apply a posterior shear load (Figure 3-2). As a result, the specimen was not loaded through its neutral zone and the force-displacement curves could not be appropriately aligned using the neutral zone to compare different conditions.[72] The specimen shear stiffness for each of the surgical conditions would have provided an additional parameter to compare with the load-sharing results. However, the average shear stiffness at 250 N of applied shear load of lumbar functional spinal units destabilized to represent DS was determined in the initial pilot study.[14]

One or more pedicle screws for five of the fifteen specimens were inserted in a non-clinical location within the pedicle due to anatomical limitations. Clinically, pedicle screws are centered in the superior-inferior direction within the pedicles. However, on specimens with smaller heights, the pedicle screws had to be placed farther apart to prevent damage to the implant transducer. The pedicle screws were visually inspected and in each test the screws remained within the pedicle. Specimens with a vertebral height that was too small for this technique were excluded from the study; the majority of these specimens were female. This selection bias of larger, male specimens would not likely affect the general trends of the results, especially since each specimen acted as its own control. However, had the implant transducers been smaller, allowing the excluded specimens to be tested, the average load-sharing values may have differed from those reported in the current study. Caution should be taken in equating the average implant loads found in the current study to those that would exist in implants affixed to specimens with small vertebral heights.

The shear loading direction is highly relevant for the DS spinal instability. Novel low-stiffness fusion devices are designed to treat degenerative spinal conditions while minimizing changes at the adjacent segment to the fusion. The low stiffness of these implants becomes increasingly important to their load supporting capability. Shear loading on the implant is affected by implant and specimen stiffness. Combining this information with estimated *in vivo* spinal loads may lead to optimal implant

strength and stiffness. Further, future tests to characterize the effect of these low-stiffness devices on adjacent segment behaviour will help to guide implant design and ultimately reduce the incidence of pseudarthrosis and revision surgery for adjacent segment degeneration.

Chapter 4 Conclusion

4.1 Summary of Thesis

Four clinically relevant posterior lumbar spinal fusion devices, consisting of a pair of longitudinal rods affixed to the spine via four poly-axial pedicle screws, were converted into shear load transducers. Implant loads were measured on sequentially destabilized human cadaveric lumbar functional spinal units (n=15), representing stages of DS, that were tested under physiologic anterior shear loads. All transducer types measured shear loads accurately to within ±5 N of a known shear load and were repeatable to within ±3 N under a combined static axial compressive load and cyclic anterior shear load. One transducer of each implant type was calibrated before and after each specimen test by loading the implant in a polymer-block construct representative of the specific specimen that was tested. Calibration parameters from the pre- and post-test calibrations were applied to the transducer output during specimen testing and reliably predicted the implant shear load. Implant shear load-sharing was found for each implant type and specimen condition. Implant loads increased with increasing implant stiffness and as the specimen was destabilized from an intact state.

4.2 Explanation of Discrepancies in Results

4.2.1 Transducer Error

Transducer errors were low for all implant types. The error was defined as the difference between the predicted shear force and applied shear load in the combined loading test of the calibration trials. The transducer error in measuring an isolated applied load was determined as the difference between the applied isolated load and predicted force. The error from the isolated shear test was larger than the error from the isolated axial test (Figure 2-6), possibly because the shear calibration configuration has a greater sensitivity to misalignments of the load line of action than the isolated axial compression configuration (Figure 4-1). Simplifying the curved implant rods tested in the current study by straight rods and solving equations relating local stress to the applied loads and rod geometry illustrates the effect of changing the shear and axial load lines of action (d_A and d_S) from an ideal location 1 to location 2, shifted by 1 mm, on the stress (or strain). The normal stress due to an axial load is dependent on a direct load as well as an indirect bending moment, whereas the normal stress due to a shear load is dependent on an indirect bending moment only (Equation 1, Figure 4-1). The change in stress due to shifting the load line by 1 mm is dependent on the indirect moments only for both shear and axial loads (Equation 4, Figure 4-1). The percent change in stress due to the shifting load line is

greater for shear loading compared with axial loading (Equation 6, Figure 4-1). Therefore, slight misalignments in the shear load line will have a greater effect on the predicted shear force from the isolated shear load test, which was reflected in the larger error (lower accuracy) for this test compared with the isolated axial load test. Care was taken to align the shear load line in the same location between trials, however given that the linear slider and cable were not rigidly attached to the loading rig (Figure 2-3), identical loading lines of action between tests were likely not achieved.

The MST had the greatest error of all the transducer types in the isolated shear and axial loading tests (Figure 2-6). Any sensitivity to the load line location was likely compounded by the design of this implant. The MST had an elliptical cross-section that plastically deformed causing an increase in the medial-lateral diameter and a decrease in the anterior-posterior diameter upon initial clamping within the pedicle screw. The transducer is designed to deform under initial clamping. However, since the transducers were re-used for multiple specimens and multiple calibrations, the repeated plastic deformation made it difficult to orient the transducer in the ideal alignment for that particular test. This non-ideal alignment likely caused the larger errors for the MST.

The ULST had the largest combined error compared to its isolated loading errors and compared to the combined loading errors for all other transducers (Figure 2-6). This is likely due to the low strain signals on the ULST compared to the other transducers in response to the applied loads (sometimes less than 100 με), as well as the low applied axial load. Only 15 N of axial compression were applied in the calibration tests for ULST due to its low axial stiffness. A linear relationship between the strain and applied load was approximated by the slope of a least-squares line fit to the raw data, but it is possible that had the load been higher and the strain signal been larger, the slope might be different than that found in the current study. Applying this slope to the combined loading may have resulted in higher error for the ULST than for the other transducers that had larger strain signals compared to the applied load.

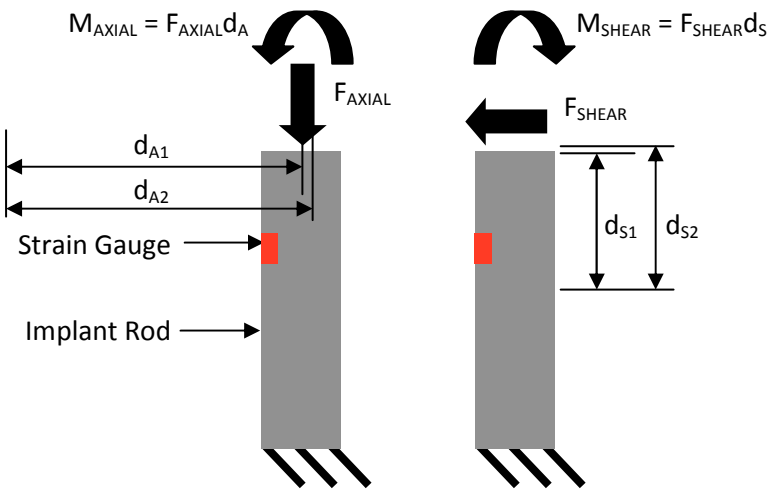

$$\sigma_A = \frac{F_{AXIAL}}{A} + \frac{M_{AXIAL}c}{I} \qquad \sigma_S = \frac{M_{SHEAR}c}{I} \tag{1}$$

$$\sigma_{A1} = \frac{F_{AXIAL}}{A} + \frac{F_{AXIAL}d_{A1}c}{I} \qquad \sigma_{S1} = \frac{F_{SHEAR}d_{S1}c}{I} \tag{2}$$

$$\sigma_{A2} = \frac{F_{AXIAL}}{A} + \frac{F_{AXIAL}d_{A2}c}{I} \qquad \sigma_{S2} = \frac{F_{SHEAR}d_{S2}c}{I} \tag{3}$$

$$\Delta\sigma_A = \sigma_{A1} - \sigma_{A2} = \frac{F_{AXIAL}c(d_{A1}-d_{A2})}{I} \qquad \Delta\sigma_S = \sigma_{S1} - \sigma_{S2} = \frac{F_{SHEAR}c(d_{S1}-d_{S2})}{I} \tag{4}$$

$$\frac{\Delta\sigma_A}{\sigma_{A1}} = \frac{\frac{F_{AXIAL}c(d_{A1}-d_{A2})}{I}}{\frac{F_{AXIAL}}{A}+\frac{F_{AXIAL}d_{A1}c}{I}} \qquad \frac{\Delta\sigma_S}{\sigma_{S1}} = \frac{\frac{F_{SHEAR}c(d_{S1}-d_{S2})}{I}}{\frac{F_{SHEAR}d_{S1}c}{I}} \tag{5}$$

$$\frac{\Delta\sigma_A}{\sigma_{A1}} = \frac{d_{A1}-d_{A2}}{\frac{I}{Ac}+d_{A1}} \qquad \frac{\Delta\sigma_S}{\sigma_{S1}} = \frac{d_{S1}-d_{S2}}{d_{S1}} \tag{6}$$

d_{A2} - d_{A1} = 1 mm; d_{S2} - d_{S1} = 1 mm;

In this study, $d_{A1} > d_{S1}$ but the conclusions are true even if $d_{A1} = d_{S1}$

Then, $\frac{\Delta\sigma_A}{\sigma_{A1}} < \frac{\Delta\sigma_S}{\sigma_{S1}}$

where σ = stress at the surface of the rod, F = force, M = moment, d = moment arm, I = second moment of area, A = cross-sectional area, and c = distance from center of rod to surface of rod (radius)

Figure 4-1: The posterior fusion rods used in the current study were approximated by straight slender beams with circular cross-section. To analyze the stress on the implant the loads applied to the spine-implant construct were transferred to the free body diagram of the rods. The reaction forces at the bottom of the rod are not shown. Shifting the eccentric axial load by a distance d_A to the center of the beam (~40 mm) caused a moment on the beam (left rod), and shifting the shear load by a distance d_S (~25 mm) to the top of the beam also caused a moment (right rod). Equations 1 to 6 show the effect of shifting the load line application for the shear and axial loads by 1 mm on the stress measurement.

4.2.2 Transducer Reliability

A measure of transducer reliability was displayed as the bias in Bland-Altman plots (Figure 2-7). The bias showed some dispersion for the HST, MST and ULST as the average implant load-sharing increased. The greater absolute bias corresponds to the implant loads during the third specimen condition (disc destabilization). The percent of applied shear load supported by the implants at this final testing condition was approximately 80% for the HST and MST and 50% for the ULST (Figure 3-6c) corresponding to implant load values of 200 N and 125 N, respectively.

The implants supported loads in the final specimen condition that were in the upper range of their calibrations. The maximum shear load applied in the calibrations was 250 N for the HST and 150 N for the MST and ULST. The maximum axial load applied in the calibrations was 150 N for HST, 50 N for MST and 15 N for ULST. However, during specimen testing an axial load of 300 N was applied to the spine-implant construct. Given that the largest shear load on the implant occurred during testing in the final specimen condition, it can be assumed that the largest axial load on the implant will also occur during this test. The coupling effect of the axial load with the shear load on the transducer may not be as accurately represented by the calibration matrix for the larger axial implant loads applied during the disc destabilization condition. A lower maximum load was applied in the axial calibration tests compared to the axial load applied in the cadaveric tests. Extrapolation of the shear-axial coupling calibration matrix value to strains from an axial implant load larger than that applied during calibration may account for the larger bias between the pre- and post-test calibrations for the disc destabilization condition.

4.2.3 Load-sharing

The shear load supported by the implants was determined by applying the calibration matrix to the strain data collected during specimen testing. The implant load-sharing was calculated by dividing the implant shear load by the applied shear load of 250 N (Figure 3-4). The general trends in the results were expected: implant load increased with specimen destabilization and with increasing implant stiffness. However, the increase in implant load on the HST between the facet and disc destabilization conditions was smaller than the increase between the intact and facet destabilization conditions. This result was not found for the other implant types.

To investigate this discrepancy, the specimens were divided into male (N=9) and female (N=5) groups and the data were re-processed; specimens with missing data points were included in this analysis since the HST, not the MST, showed the smaller increase in implant load between the last two specimen conditions. This smaller load increase was found for the female specimens, but not the male

specimens (Figure 4-2). This finding was most pronounced for the HST, but was also evident for the MST and LST; the ULST did not reflect this change.

Greater stability in female specimens, transferring less load to the implant, may be attributed to the fact that approximately 67% less nucleus was removed from the female specimens compared to the male specimens, as estimated from photos of the removed nucleus following the disc destabilization surgery. The lower quantity of nucleus may be due to a smaller disc height in female specimens.[122] The cadaveric model of DS in this study seems to provide an approximately linear transfer of load to the implant across specimen conditions for male specimens. However, the load-sharing results for female specimens may indicate that the DS model was not appropriately created for the final condition. The confidence intervals in the plots are relatively large for the female group (Figure 4-2b), and more specimens would be required to verify this hypothesis.

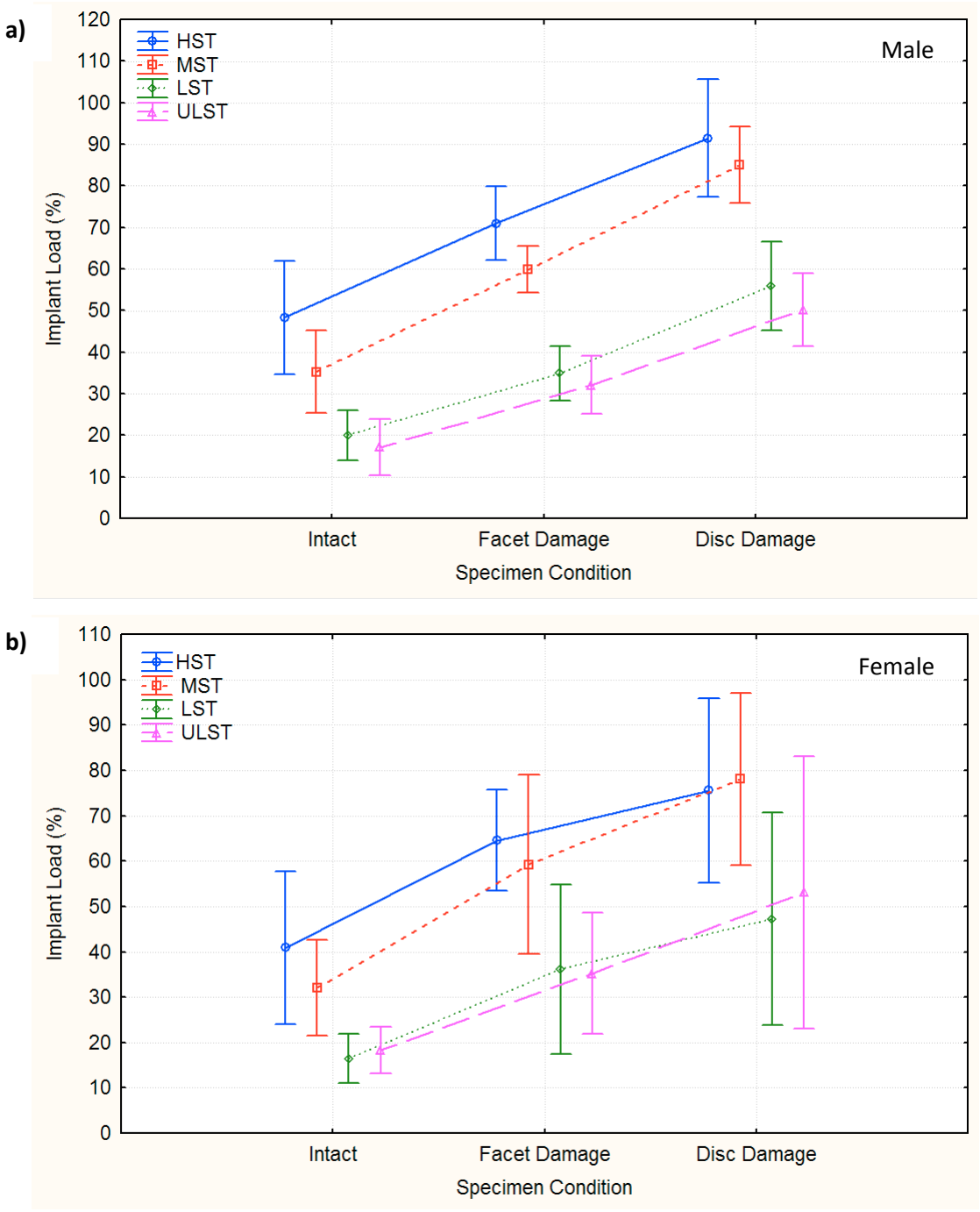

Figure 4-2: Average implant shear load-sharing across the three specimen conditions with 95% confidence intervals (vertical bars) for (a) male and (b) female specimens. The confidence intervals are larger for the female group because there are only five specimens, whereas there are nine for the male group (one unknown).

4.3 Compare Study Methodology to Literature

4.3.1 Transducer Type: the strain gauge

To develop the shear load transducers, foil strain gauges were affixed to the posterior fusion rods of the implant. Strain is the most common parameter to measure on spinal implants to determine load.[24,25,103,105-107] Other measurement techniques such as inductance[100] and pressure transducers[97] have limited use in measuring spine and implant loads, except for intervertebral disc pressure measurements.[31] The advantages of the strain gauge make it ideal for measuring implant loads. The strain gauge is small and flexible and is adaptable to many materials and implant designs. Using strain gauges does not generally require physical changes to be made to the implant. Strain data can be compared with output from finite element models. Strain gauges have large strain ranges and they respond linearly to a linear load application. The accuracies of previous spinal implant transducers that used strain gauges were high[102,103,107,115] and compared well with the accuracy of the transducers used in the current study, whereas the accuracy of a pressure transducer was reported to be low.[108]

4.3.2 Study Design: *in vitro* testing

Studies investigating spine implant performance and function can be divided into three types: *in vitro*, *in vivo* and finite element models. Each methodology has advantages and disadvantages for generating data and producing results that guide implant design or relate to actual implant behaviour in humans. *In vivo* implant loads have previously been measured on rigid posterior fusion rods.[29,100,114] However, the global loads acting on the spine cannot be determined from *in vivo* implant load measurements. Therefore, the percent of total load supported by the implant cannot be deduced. It is difficult to obtain ethical approval for human studies in which transducers are surgically implanted in patients, and this type of testing is not feasible for implants in the design and development phase. The confounding factors associated with each individual participating in an *in vivo* study, including anthropometry, diet and mobility, may result in large ranges of data across subjects but will increase the applicability of the results to a broad population. One of the main limitations of the previous *in vivo* studies is the limited number of patients within the same pre-operative diagnosis group.[29] The effect of initial spine condition on implant response is not well understood from *in vivo* studies.

Finite element models calculate strain values over the entire surface of the spine model and implant. The strains can illuminate specific areas of weakness in an implant design or in the spine due to a specific specimen condition. However, usually the models are used to compare the effect of two implants, that differ by a single parameter such as stiffness, on implant load or range of motion.[88,90,95] Computational models are useful for performing experiments that are difficult or impossible to conduct

in a lab. However, model geometry is based on a specific individual or a generic population, such as the 50th percentile male; it is not possible to determine population variation with a model, unless model parameters are systematically altered for each experiment. Validation of finite element models is difficult as all spine tissue material properties have not been fully characterized. A model may be validated for a particular loading direction[90] and results from testing that model in other configurations may not be accurate. Validation of a model is performed by comparing model output to results from *in vivo* and *in vitro* studies. Once a model is developed and validations have been performed, experiments can be conducted relatively quickly compared to *in vivo* or *in vitro* studies.

The results of *in vitro* studies are necessary to validate finite element models, and they capture the variability of a population. Study designs can be used to decrease the effect of specimen variability on the ability to detect significance, such as the repeated measures design used in the current study. *In vitro* studies can be used to measure implant load-sharing by directly measuring both the applied load and implant load.[24,25,105] Just as output from finite element models needs to be validated for all directions of interest, the sensitivity of the load measurement method must be characterized for the coupled motions that may exist in the experiment. Reports of some transducers account for loads in all directions of interest,[25,99,107] while others do not.[24] The transducers in the current study are directly calibrated for each specimen and account for the specific shear and axial loads applied in each experiment. Unlike *in vivo* studies, the effect of specimen destabilization on load-sharing can be determined; surgical changes in the specimen act to represent *in vivo* conditions. Ideally, large *in vivo* studies for a specific pre-diagnosis would generate valuable implant load data that are not currently reported in the literature. However, the expense will likely prevent this type of study from being conducted. Therefore, a clinical condition such as DS represented by surgical destabilization in this study is the best surrogate available to measure the effect of specimen degeneration on load-sharing.

4.4 Compare Results to Literature: how will implant stiffness affect fusion of degenerated spines and ASD?

It is well documented in clinical studies that rigid fusion devices result in high rates of fusion in the lumbar spine for treatment of degenerative conditions.[52-56] Preventing acceleration of degeneration of the adjacent vertebral segment to the fusion has resulted in the development of low-stiffness fusion devices. Low-stiffness posterior fusion rods may decrease the magnitude of mechanical changes at the adjacent segment to a fusion[78] while stabilizing the spine as effectively as traditional rigid devices.[28] Therefore, low-stiffness devices will also likely result in high fusion rates, maintaining low rates of

pseudarthrosis. However, if these low-stiffness devices behave identically to rigid devices, acceleration of ASD will not be mitigated.

Fusion devices that transfer a greater load to the spine compared to traditional rigid devices may act to reduce the progression of ASD. As found in the current study and previous finite element studies,[90,95] low-stiffness devices do transfer greater loads to the spine in shear and axial compression; the original loading of the spine is better maintained by low-stiffness devices. The magnitude of implant stiffness that affects implant load-sharing differs from that affecting the ability of the implant to stabilize the spine. Posterior fusion rods with an axial stiffness less than 200 N/mm increased the range of motion of the instrumented segment compared to rigid implants.[88] The stiffness of the two fusion devices tested in a finite element model that were most similar to the LST and HST implants tested in the current study had axial stiffness values of 1800 N/mm and 64 500 N/mm, respectively.[90] Both stiffness values are well above the axial stiffness cut-off. Although range of motion at the level of the fusion may be maintained by the LST, the implant loads were significantly reduced compared to the HST.

It appears that low-stiffness devices have the desired effect of stabilization and load-transfer to the spine. Unfortunately, an exact value for the change in range of motion at the adjacent segment that is acceptable is unknown. The LST tested in the current study transfers a substantial proportion of load to the spine while maintaining stability at the instrumented level.[28] However, to the author's knowledge, the range of motion at the adjacent segment to this particular implant has not been reported. A study measuring both load-sharing of low-stiffness fusion devices and range of motion at the adjacent segment would elucidate the relationship between these two parameters.

4.5 Study Strengths and Limitations

4.5.1 Strengths

A human cadaveric model of DS was developed[14] and used in the current study. Previously, Panjabi recommended that spinal implants be tested on reproducible cadaveric models representing conditions that would warrant stabilization with that implant.[72] The DS model used in the current study was reproducible[14] and highly relevant to the aging spine as a condition for which fusion is indicated. Implants have been tested on various *in vitro* spinal models including: intact,[24,101] corpectomy,[94,106] spinal transection,[92,93] posterior, translaminar or anterior interbody fusion,[28,105] discectomy,[99] facet and disc injury,[75,123] and posterior and anterior column injury.[25,118] Only one of these models was specifically designed to represent a degenerative spine.[1,118] As the population ages, degenerative spinal instability conditions are being surgically treated more frequently and cadaveric models need to represent this

population. The low-stiffness fusion implants tested in the current study are specifically designed for treating the degenerated spine.

Measuring implant load-sharing using a cadaveric injury model likely provided more accurate results compared to using an intact specimen. Comparing the approximate average load-sharing results for the LST and HST for the intact specimen condition shows load-sharing of 20% and 40%, respectively; whereas, for the third specimen condition the load-sharing was 50% and 80% for the LST and HST, respectively. Significantly greater load-sharing occurred for the destabilized specimen, and this likely mimicked *in vivo* instability, degeneration, deformity and muscle weakness better than the intact specimen. The results of the current study showed that different injury models produced different amounts of load-sharing (the facet destabilization condition compared to the disc destabilization condition). Therefore, it is vital for researchers to test implants on destabilized specimens and for *in vitro* specimen destabilizations to simulate *in vivo* spinal instabilities.

The implants tested in the current study are clinically relevant; some are currently used in humans and others are in the development phase. Previous studies have physically altered rigid implants to adapt them for load measurement.[25,103] Changes to the implants did not likely affect the study results since the stiffness of the implants was high. However, physically altering low-stiffness implants may affect the implant response to load. Finite element studies used models of generic implant design to measure the effect of changing the implant stiffness, as opposed to the effect of design, on implant response.[88,90,95] As shown in the current study, the design, in addition to the stiffness, affected the load-sharing of the ULST.

To the author's knowledge, the shear loading direction has not been studied with respect to load-sharing of spinal fusion implants. Shear loading has been used to study DS[1,118] and isthmic spondylolisthesis[117] in biomechanical studies. General cadaveric spine behaviour including range of motion and disc pressure under shear loading has also been studied.[33-35] Only one study tested a DS spinal model with stabilizing implants[118] but did not measure loads supported by the implants. Implant loads have been measured under applied moments and axial compression[24,25,90,95,99,105,106] but not anterior shear. The results from the current study contribute new information to the implant load-sharing field.

The study design used in the current study incorporated a repeated measure of implant load across three specimen conditions each tested with four implant types. The repeated testing allowed each specimen to act as its own control minimizing the effect of specimen variability on the results. Highly significant comparisons of implant load between the conditions were found with only ten specimens and confirmed with an additional five specimens. A one-way repeated measures design has

been used previously in which multiple treatments (implants) are tested on a single specimen.[75,99,106] A two-way repeated measures design, such as that used in this study, allows the effect of an additional factor to be assessed; a greater amount of information can be retrieved using this study design, but it has been implemented sparingly in the load-sharing literature.[24]

4.5.2 Limitations

The limitations of this study can be separated into three groups: cost, methodology and results. The cost of the testing is high due to strain gauge failures and repairs, the use of cadaveric specimens, and the time required to test each specimen, and the testing reported in the current study may not be feasible for small medical device design companies to complete in-house. The methodology has limitations with respect to the calibration, implants and specimens. The results are limited by the accuracy of the load predictions and the available data for statistical analysis.

4.5.2.1 Cost

The gauges on the MST and LST operated in their upper strain range and failed relatively frequently; a few gauges failed during testing for each specimen. The failed gauges were not used in the data analysis and did not affect the results, but the repairs were costly and caused time delays during testing. A gauge with a larger strain range was not used because available surface area on the implant was limited. However, to reduce the number of failures, future transducers should be made with larger strain gauges with a higher range, possibly by changing the location of the gauges since this was not found to have a large influence on the strain-force relationship.

Testing with cadavers is more expensive than using an already developed computer model, or testing the implant with plastic blocks, commonly used for fatigue analysis. The use of cadavers requires appropriate safety and biohazard precautions and requires an anatomy lab with appropriate surgical instrumentation and storage facilities. This is costly for small companies designing implants, but sub-contracting cadaver tests to universities or private biomechanical labs eliminates the overhead cost of installing an anatomy lab and acquiring required equipment.

Finally, testing a single specimen required 40 person-hours. The specimen-specific calibration testing required an additional 20 person-hours because the tests were performed before and after each specimen was tested. Since the transducers were proven to be reliable for the 15 specimens presented in this thesis, future tests could be conducted with only the post-test calibration to reduce the number of required person-hours.

4.5.2.2 Methodology

The angles of the pedicle screws in the coronal plane in the specimen were not matched to the pedicle screw angles in the calibration blocks. The pedicle screws in the specimens were always angled towards the midline plane, whereas in the calibration blocks, the pedicle screws were parallel to the midline plane. The posterior surface of the implant was aligned with the posterior of the specimen by swiveling the poly-axial head of the pedicle screws. The posterior of the implant was aligned with the posterior of the calibration construct without swiveling the poly-axial heads because the screw shaft was already directed to the posterior.

It was assumed that posterior alignment of the implant and specimen and implant and calibration blocks was important for strain measurement, but the angle of the shaft of the pedicle screw would not affect these measurements. This assumption was supported by the results from testing a HST fixed in calibration blocks with angled or parallel screws. Three calibration trials for both screw conditions were conducted. The difference between the errors for predicting the shear load in the combined test for the two screw conditions was less than 5.2 N across the six trials. This verification test was not performed for the other transducer types, but given the similar accuracy, repeatability, and reliability results for all transducer types (Chapter 2), it is assumed that the screw angle had a minimal effect on the study results.

The plastic deformation of the MST after clamping into the pedicle screws sometimes prevented posterior alignment of the implant with the posterior of the specimen. Further, the position of the internal components of the swiveled poly-axial head of the angled pedicle screw would sometimes cause an axial rotation of the MST prior to clamping in the screw. In the pre-test calibration the posterior of the transducer was visually aligned with the posterior of the calibration construct when clamped with the non-swiveled straight pedicle screws. Misalignment of the implant in the pedicle screws affixed to the specimen was minimized as much as possible; large misalignments for a specimen test were noted and rods were slightly rotated for the post-test calibration in an attempt to mimic the specimen test.

The implant loads presented in Chapter 3 were calculated based on the post-test calibration matrices for all but one specimen because the pre-test calibration was generally less accurate than the post-test calibration. For the pre-test calibration, the axial compression load line was estimated from the potted specimen as the location in which compression of the functional spinal unit would not result in any visible flexion or extension rotations. However, physical compression of the specimen was not performed until the test-day which occurred after the pre-test calibration. Once the specimen was mounted in the loading rig for testing, the estimated location of the axial load line was visually verified.

One specimen had visible rotation and the load line was adjusted. The load line for the post-test calibration was also adjusted to reflect the specimen testing, and the pre-test calibration matrix did not correctly predict the implant load. The estimate of the location of the axial load line prior to specimen testing was not as accurate as if the specimen had been mounted in the rig for testing; the post-test calibration more accurately predicted the implant load compared to the pre-test calibration.

The linear relationship that was approximated between the strain signal and applied load for the ULST during calibration may not have been as accurate as the approximations for the other transducer types. During calibration, the axial load applied to the implant-block construct was low compared to the applied shear load for all transducer types. The axial stiffness of the implants was much lower than the shear stiffness: 5 times lower for HST, 10 times lower for MST, 13 times lower for LST and 90 times lower for ULST. Even for the low axial loads, the strain signal was relatively high for the MST and LST because the PEEK material that these rods are made from has a low modulus of elasticity. However, the ULST has a titanium shell upon which the strain gauges were placed, and the signal was extremely low for the low applied axial loads. The ULST had a different construction and design than all the other implants (multi-component versus solid material) which may have influenced the ability of this transducer to accurately measure the axial load. Each implant component could move relative to the other components and it is not obvious if different initial positions of the components affected the response of the implant. Using semiconductor strain gauges on the ULST, which are more sensitive to load than foil gauges, may result in a more accurate strain response to the low applied axial loads.

For some specimens, the strain gauge array on the implant closest to the inferior vertebra was approximately aligned with the shear load line and responded to the applied shear loads with very low strain signals. For each transducer, two gauge arrays were affixed on either side of the middle of the rod towards the inferior or superior vertebra because it was thought that the shear load line would be positioned between these arrays. However, as viewed in the sagittal plane, the center of the intervertebral disc, which is the location of the shear load line, was lower than the middle of the implant, and on some specimens the disc was centered near the lower strain gauge array. In these cases, the load line passing through the array should ideally cause zero strain given that the load is in the transverse direction compared to the strain gauges. However, the strain gauges do not read exactly zero under transverse loads. Only the HST and ULST responded with these low strains; the MST and LST responded with relatively high linear strains even with the load line near the array, likely due to the small non-zero moment arm from the load line to the gauge location. The magnitude of the transverse errors may have been on the same order of magnitude as the strain response from a small moment on the HST and ULST.

The specimens were imaged prior to testing for further analysis into the effect of disc degeneration on implant load-sharing for a future study beyond the scope of this thesis. Plain x-rays, dual x-ray absorptiometry scans and magnetic resonance images were obtained for each specimen. The specimens were thawed and re-frozen between imaging scans, potting, testing and dissection. Freezing has been shown to have an insignificant effect on human cadaveric functional spinal unit behaviour,[124] and freeze-thaw cycles have been shown to have an insignificant effect on porcine cadaveric functional spinal unit behaviour.[125] Assuming results from the porcine testing can be extended to human cadaveric tissue, the freeze-thaw cycles for the specimens tested for this study did not likely affect the results.

Specimens that were too short for the implant size used in this study were excluded (five female and two male) creating a selection bias of larger, male specimens. Although it is impossible to know what load would be supported by the implants on the excluded specimens, a division of the current data set into male and female groups shows minimal differences between the mean and standard deviation of implant load (Figure 4-3), indicating a relatively homogeneous group of specimens. The largest difference is for HST at the disc damage condition in which the male specimens support an average of 16% more shear load than the female specimens.

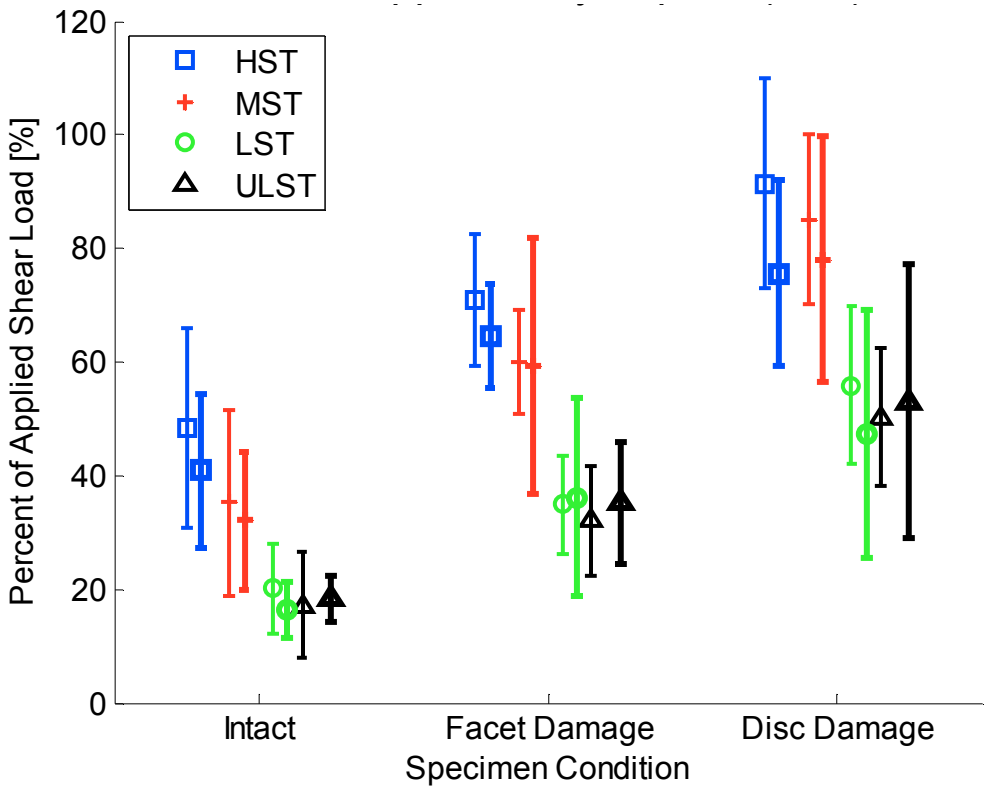

Figure 4-3: Average implant load-sharing (standard deviation) for each specimen condition for male (light line) and female (heavy line) specimens.

Both L3-4 and L4-5 specimens were tested in the present study (two L3-4 and thirteen L4-5). DS most commonly affects the L4-5 segment. After separating the L3-4 from the L4-5 results, implant load-sharing for all but one implant type and specimen condition for both L3-4 specimens fell within the standard deviation of the implant load-sharing of the L4-5 specimens (Figure 4-4). The one outlier datum (MST, facet destabilization) indicates that this L3-4 specimen supported a greater amount of load, by transferring less to the MST, than the L4-5 specimens for the facet destabilization.

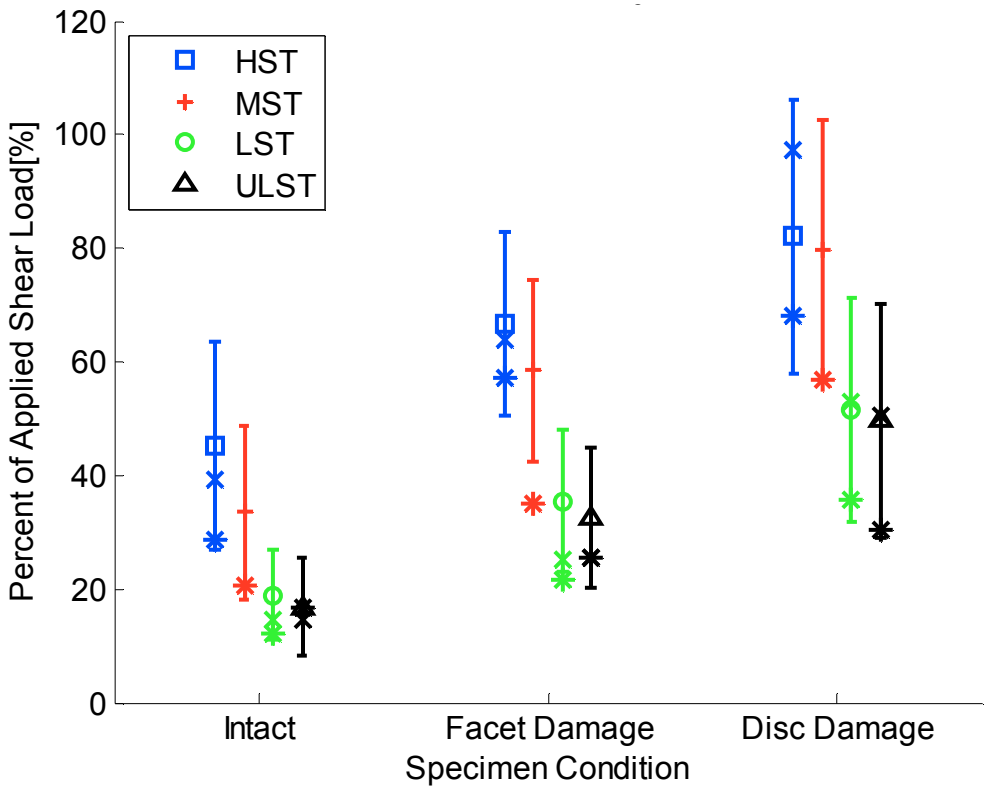

Figure 4-4: Average implant load-sharing (standard deviation) for each specimen condition for the L4-5 specimens. The x and * symbols are the value of implant load for the two L3-4 specimens included in this study. The specimen marked with x was not tested with the MST transducer.

4.5.2.3 Results

The axial load on the implant during combined loading was not predicted accurately. Although this does not affect the answers to the study questions posed in this thesis, it does limit an analysis of how axial loads on the implant may have affected the shear results. Both isolated shear and axial loading calibrations were performed on the transducers. Therefore, the load on the implant in either of these directions can theoretically be determined.

A shear offset found from the calibration was applied to the combined loading data to increase the accuracy of the shear load prediction. However, the axial offset found from the calibration was not applied to the combined loading data because the offset was not constant across the loading range;

averaging the offset across the data range, as was done for the shear offset, would not represent the error accurately. One dataset was re-analyzed with an axial offset applied (Figure 4-5). Although the error of the predicted axial load in the combined test decreased, the absolute error was still larger than for the shear error, especially for the low-stiffness implant types. The transducer axial load measurement was not accepted as accurate. However, this error did not affect the shear load results.

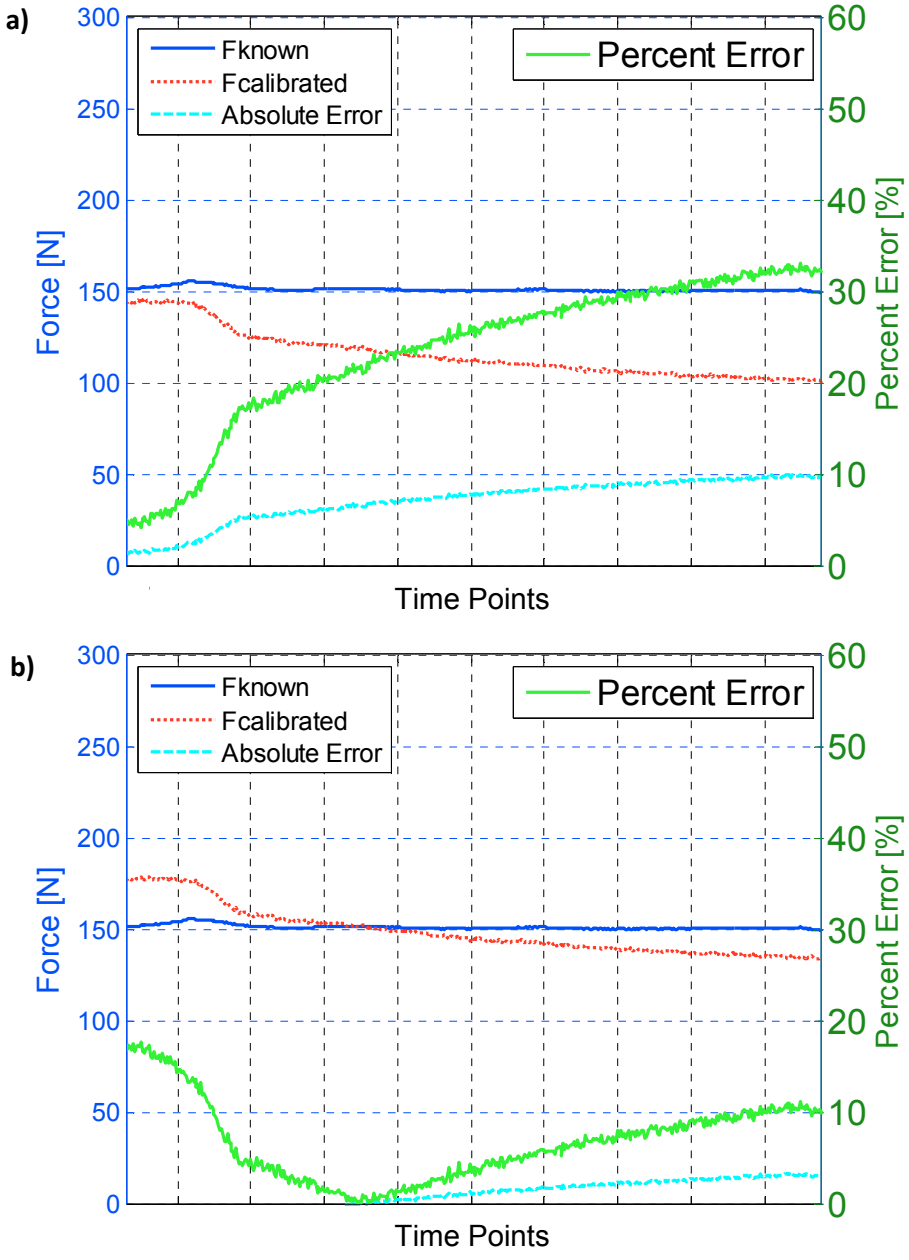

Figure 4-5: Example force-time traces from one combined loading calibration test for the HST for specimen 2. Predicted axial error with (a) no axial offset applied to the data and (b) an axial offset applied to the data. The percent error values (green) are on the right vertical axis. The values for the known applied force (blue), the predicted axial force from the calibration matrix (red) and the difference between these loads (cyan) are shown on the left vertical axis. The absolute error for the first third of the lower graph is negative and not shown.

Five of the 15 specimens were tested with faulty MSTs. The required strain gauge combinations for this transducer had not been determined at the time of these tests, and it was assumed that two working strain gauges was sufficient to measure the shear load. Unfortunately, post-analysis showed these pairs of gauges to be inadequate to accurately measure shear load. These five specimens were removed from statistical analysis in Chapter 3. The missing data for MST were replaced with an average implant load from the available 10 specimens. Re-analyzing the data for all implant types did not change the significant results from the statistical analysis (Appendix E). This indicates that these five specimens behaved in a similar manner to the other 10 specimens when instrumented with the HST, LST and ULST. It is assumed that the five specimens behaved in a similar manner to the other 10 when affixed with the MST.

4.6 Future Work

This study will be extended to evaluate the shear load-sharing of a fifth fusion device type with 15 more specimens, to determine the effect of disc degeneration on implant load-sharing, and to determine the effect of disc degeneration on specimen stiffness. Further, measurements were taken for the 15 specimens that were not reported in this thesis but will be combined with the results for the next 15 specimens: instrumented and non-instrumented specimen motion was recorded with an optoelectronic system and magnetic resonance images of the specimen were obtained to grade the level of disc degeneration.

One question still unanswered is how low-stiffness implants affect the behaviour of the adjacent segment to the fusion. Studies have measured range of motion of the adjacent segment to a rigid fusion device.[21,22,26,74,75] Two rigid fusion devices with different stiffness resulted in no significant differences in disc pressure or lamina strain of the adjacent segment compared to the intact specimen.[76] In one study, a rigid fusion was extended with a rigid or flexible rod and the range of motion at the adjacent segment increased from the non-instrumented case by a lesser amount with the flexible rod.[78] These adjacent segment biomechanical studies have not tested current low-stiffness fusion devices nor assessed the effects of both specimen condition and fusion device on adjacent level effects. A similar study as presented in Chapter 3 could be used to address this issue. Specimens with more vertebral segments than those used in the current study would need to be tested with the Hybrid protocol to address adjacent segment behaviour (Hybrid protocol was described in section 1.5.2.1).

References

1. Crawford NR, Cagli S, Sonntag VK, Dickman CA. Biomechanics of grade I degenerative lumbar spondylolisthesis. Part 1: in vitro model. J Neurosurg 2001;94:45-50.

2. Kalichman L, Kim DH, Li L, Guermazi A, Berkin V, Hunter DJ. Spondylolysis and spondylolisthesis: prevalence and association with low back pain in the adult community-based population. Spine 2009;34:199-205.

3. Sengupta DK, Herkowitz HN. Degenerative spondylolisthesis: review of current trends and controversies. Spine (Phila Pa 1976) 2005;30:S71-81.

4. Jacobsen S, Sonne-Holm S, Rovsing H, Monrad H, Gebuhr P. Degenerative lumbar spondylolisthesis: an epidemiological perspective: the Copenhagen Osteoarthritis Study. Spine 2007;32:120-5.

5. Disch AC, Schmoelz W, Matziolis G, Schneider SV, Knop C, Putzier M. Higher risk of adjacent segment degeneration after floating fusions: long-term outcome after low lumbar spine fusions. J Spinal Disord Tech 2008;21:79-85.

6. Deyo RA, Gray DT, Kreuter W, Mirza S, Martin BI. United States trends in lumbar fusion surgery for degenerative conditions. Spine 2005;30:1441-5; discussion 6-7.

7. Cheh G, Bridwell KH, Lenke LG, et al. Adjacent segment disease followinglumbar/thoracolumbar fusion with pedicle screw instrumentation: a minimum 5-year follow-up. Spine 2007;32:2253-7.

8. Lee CK. Accelerated degeneration of the segment adjacent to a lumbar fusion. Spine 1988;13:375-7.

9. Park P, Garton HJ, Gala VC, Hoff JT, McGillicuddy JE. Adjacent segment disease after lumbar or lumbosacral fusion: review of the literature. Spine 2004;29:1938-44.

10. Meyerding H. Spondylolisthesis: surgical treatment and results. Surgery, gynecology and obstetrics; an international magazine 1932;54:371-7.

11. Matsunaga S, Sakou T, Morizono Y, Masuda A, Demirtas AM. Natural history of degenerative spondylolisthesis. Pathogenesis and natural course of the slippage. Spine 1990;15:1204-10.

12. Nagaosa Y, Kikuchi S, Hasue M, Sato S. Pathoanatomic mechanisms of degenerative spondylolisthesis. A radiographic study. Spine 1998;23:1447-51.

13. Grobler LJ, Robertson PA, Novotny JE, Pope MH. Etiology of spondylolisthesis. Assessment of the role played by lumbar facet joint morphology. Spine 1993;18:80-91.

14. Kingwell S, Melnyk AD, Zhu QA, Oxland TR, Dvorak MF. An in vitro model of degenerative spondylolisthesis. In. Vancouver: University of British Columbia; 2010:(unpublished work).

15. 3D Static Strength Prediction Program. In. 5.0.4 ed. Ann Arbor, MI: University of Michigan; 2005.

16. Callaghan JP, Patla AE, McGill SM. Low back three-dimensional joint forces, kinematics, and kinetics during walking. Clin Biomech (Bristol, Avon) 1999;14:203-16.

17. Rohlmann A, Zander T, Rao M, Bergmann G. Applying a follower load delivers realistic results for simulating standing. J Biomech 2009.

18. Drake RL, Vogl AW, Mitchell AWM. Gray's Anatomy for Students. 2nd ed. Philadelphia, PA: Churchill Livingstone Elsevier; 2010.

19. Fujiwara A, Lim TH, An HS, et al. The effect of disc degeneration and facet joint osteoarthritis on the segmental flexibility of the lumbar spine. Spine 2000;25:3036-44.

20. Lee DY, Lee SH, Shim CS, Lee HY. Decompression and interspinous dynamic stabilization using the locker for lumbar canal stenosis associated with low-grade degenerative spondylolisthesis. Minim Invasive Neurosurg 2010;53:117-21.

21. Ha KY, Schendel MJ, Lewis JL, Ogilvie JW. Effect of immobilization and configuration on lumbar adjacent-segment biomechanics. J Spinal Disord 1993;6:99-105.

22. Lee CK, Langrana NA. Lumbosacral spinal fusion. A biomechanical study. Spine 1984;9:574-81.

23. Weinhoffer SL, Guyer RD, Herbert M, Griffith SL. Intradiscal pressure measurements above an instrumented fusion. A cadaveric study. Spine 1995;20:526-31.

24. Meyers K, Tauber M, Sudin Y, et al. Use of instrumented pedicle screws to evaluate load sharing in posterior dynamic stabilization systems. Spine J 2008;8:926-32.

25. Cripton PA, Jain GM, Wittenberg RH, Nolte LP. Load-sharing characteristics of stabilized lumbar spine segments. Spine 2000;25:170-9.

26. Shono Y, Kaneda K, Abumi K, McAfee PC, Cunningham BW. Stability of posterior spinal instrumentation and its effects on adjacent motion segments in the lumbosacral spine. Spine (Phila Pa 1976) 1998;23:1550-8.

27. Hasegewa K, Kitahara K, Hara T, Takano K, Shimoda H. Biomechanical evaluation of segmental instability in degenerative lumbar spondylolisthesis. Eur Spine J 2009;18:465-70.

28. Ponnappan RK, Serhan H, Zarda B, Patel R, Albert T, Vaccaro AR. Biomechanical evaluation and comparison of polyetheretherketone rod system to traditional titanium rod fixation. Spine J 2009;9:263-7.

29. Rohlmann A, Bergmann G, Graichen F. Loads on internal spinal fixators measured in different body positions. Eur Spine J 1999;8:354-9.

30. Nachemson A. The load on lumbar disks in different positions of the body. Clin Orthop Relat Res 1966;45:107-22.

31. Nachemson AL. Disc pressure measurements. Spine (Phila Pa 1976) 1981;6:93-7.

32. Andersson GB, Ortengren R, Nachemson A. Intradiskal pressure, intra-abdominal pressure and myoelectric back muscle activity related to posture and loading. Clin Orthop Relat Res 1977:156-64.

33. Berkson MH, Nachemson A, Schultz AB. Mechanical-Properties of Human Lumbar Spine Motion Segments .2. Responses in Compression and Shear - Influence of Gross Morphology. J Biomech Eng-T Asme 1979;101:53-7.

34. Frei H, Oxland TR, Nolte LP. Thoracolumbar spine mechanics contrasted under compression and shear loading. J Orthop Res 2002;20:1333-8.

35. Lu WW, Luk KD, Holmes AD, Cheung KM, Leong JC. Pure shear properties of lumbar spinal joints and the effect of tissue sectioning on load sharing. Spine (Phila Pa 1976) 2005;30:E204-9.

36. Schultz AB, Andersson GB. Analysis of loads on the lumbar spine. Spine (Phila Pa 1976) 1981;6:76-82.

37. Cappozzo A. Compressive loads in the lumbar vertebral column during normal level walking. J Orthop Res 1984;1:292-301.

38. Cappozzo A. The forces and couples in the human trunk during level walking. J Biomech 1983;16:265-77.

39. Schultz AB, Andersson GB, Haderspeck K, Ortengren R, Nordin M, Bjork R. Analysis and measurement of lumbar trunk loads in tasks involving bends and twists. J Biomech 1982;15:669-75.

40. McGill SM, Norman RW. Effects of an anatomically detailed erector spinae model on L4/L5 disc compression and shear. J Biomech 1987;20:591-600.

41. Rohlmann A, Zander T, Rao M, Bergmann G. Realistic loading conditions for upper body bending. J Biomech 2009;42:884-90.

42. Schmidt H, Shirazi-Adl A, Galbusera F, Wilke HJ. Response analysis of the lumbar spine during regular daily activities--a finite element analysis. J Biomech 2010;43:1849-56.

43. Kim K, Kim YH. Role of trunk muscles in generating follower load in the lumbar spine of neutral standing posture. J Biomech Eng 2008;130:041005.

44. Callaghan JP, McGill SM. Muscle activity and low back loads under external shear and compressive loading. Spine (Phila Pa 1976) 1995;20:992-8.

45. Roy-Camille R, Saillant G, Berteaux D, Salgado V. Osteosynthesis of thoraco-lumbar spine fractures with metal plates screwed through the vertebral pedicles. Reconstr Surg Traumatol 1976;15:2-16.

46. Hibbs RA. An operation for progressive spinal deformities - A preliminary report of three cases from the service of the orthopaedic hospital. Clin Orthop Relat R 2007:17-20.

47. King D. Internal fixation for lumbosacral fusion. J Bone Joint Surg Am 1948;30A:560-5.

48. Rutherford EE, Tarplett LJ, Davies EM, Harley JM, King LJ. Lumbar Spine Fusion and Stabilization: Hardware, Techniques, and Imaging Appearances. RadioGraphics 2007;27:1737-49.

49. Foley KT, Gupta SK, Justis JR, Sherman MC. Percutaneous pedicle screw fixation of the lumbar spine. Neurosurg Focus 2001;10:E10.

50. Pearson AM, Lurie JD, Blood EA, et al. Spine patient outcomes research trial: radiographic predictors of clinical outcomes after operative or nonoperative treatment of degenerative spondylolisthesis. Spine (Phila Pa 1976) 2008;33:2759-66.

51. Herkowitz HN, Kurz LT. Degenerative lumbar spondylolisthesis with spinal stenosis. A prospective study comparing decompression with decompression and intertransverse process arthrodesis. J Bone Joint Surg Am 1991;73:802-8.

52. Mardjetko SM, Connolly PJ, Shott S. Degenerative lumbar spondylolisthesis. A meta-analysis of literature 1970-1993. Spine (Phila Pa 1976) 1994;19:2256S-65S.

53. Bridwell KH, Sedgewick TA, O'Brien MF, Lenke LG, Baldus C. The role of fusion and instrumentation in the treatment of degenerative spondylolisthesis with spinal stenosis. J Spinal Disord 1993;6:461-72.

54. Schwab FJ, Nazarian DG, Mahmud F, Michelsen CB. Effects of spinal instrumentation on fusion of the lumbosacral spine. Spine (Phila Pa 1976) 1995;20:2023-8.

55. Zdeblick TA. A prospective, randomized study of lumbar fusion. Preliminary results. Spine (Phila Pa 1976) 1993;18:983-91.

56. Gu Y, Chen L, Yang HL, et al. Efficacy of surgery and type of fusion in patients with degenerative lumbar spinal stenosis. J Clin Neurosci 2009;16:1291-5.

57. Katz JN, Spratt KF, Andersson GB, et al. Epidemiology introduction. 1995 Focus Issue Meeting on Fusion. Spine (Phila Pa 1976) 1995;20:76S-7S.

58. Axelsson P, Johnsson R, Stromqvist B. The spondylolytic vertebra and its adjacent segment. Mobility measured before and after posterolateral fusion. Spine (Phila Pa 1976) 1997;22:414-7.

59. Yang JY, Lee JK, Song HS. The impact of adjacent segment degeneration on the clinical outcome after lumbar spinal fusion. Spine 2008;33:503-7.

60. Lehmann TR, Spratt KF, Tozzi JE, et al. Long-term follow-up of lower lumbar fusion patients. Spine 1987;12:97-104.

61. Umehara S, Zindrick MR, Patwardhan AG, et al. The biomechanical effect of postoperative hypolordosis in instrumented lumbar fusion on instrumented and adjacent spinal segments. Spine 2000;25:1617-24.

62. Ghiselli G, Wang JC, Bhatia NN, Hsu WK, Dawson EG. Adjacent segment degeneration in the lumbar spine. J Bone Joint Surg Am 2004;86-A:1497-503.

63. Rahm MD, Hall BB. Adjacent-segment degeneration after lumbar fusion with instrumentation: a retrospective study. J Spinal Disord 1996;9:392-400.

64. Gillet P. The fate of the adjacent motion segments after lumbar fusion. J Spinal Disord Tech 2003;16:338-45.

65. Aota Y, Kumano K, Hirabayashi S. Postfusion instability at the adjacent segments after rigid pedicle screw fixation for degenerative lumbar spinal disorders. J Spinal Disord 1995;8:464-73.

66. Wiltse LL, Radecki SE, Biel HM, et al. Comparative study of the incidence and severity of degenerative change in the transition zones after instrumented versus noninstrumented fusions of the lumbar spine. J Spinal Disord 1999;12:27-33.

67. Pellise F, Hernandez A, Vidal X, Minguell J, Martinez C, Villanueva C. Radiologic assessment of all unfused lumbar segments 7.5 years after instrumented posterior spinal fusion. Spine 2007;32:574-9.

68. Wai EK, Santos ER, Morcom RA, Fraser RD. Magnetic resonance imaging 20 years after anterior lumbar interbody fusion. Spine 2006;31:1952-6.

69. Etebar S, Cahill DW. Risk factors for adjacent-segment failure following lumbar fixation with rigid instrumentation for degenerative instability. J Neurosurg 1999;90:163-9.

70. Hambly MF, Wiltse LL, Raghavan N, Schneiderman G, Koenig C. The transition zone above a lumbosacral fusion. Spine (Phila Pa 1976) 1998;23:1785-92.

71. Lai PL, Chen LH, Niu CC, Fu TS, Chen WJ. Relation between laminectomy and development of adjacent segment instability after lumbar fusion with pedicle fixation. Spine (Phila Pa 1976) 2004;29:2527-32; discussion 32.

72. Panjabi MM. Biomechanical evaluation of spinal fixation devices: I. A conceptual framework. Spine (Phila Pa 1976) 1988;13:1129-34.

73. Grassmann S, Oxland TR, Gerich U, Nolte LP. Constrained testing conditions affect the axial rotation response of lumbar functional spinal units. Spine (Phila Pa 1976) 1998;23:1155-62.

74. Akamaru T, Kawahara N, Tim Yoon S, et al. Adjacent segment motion after a simulated lumbar fusion in different sagittal alignments: a biomechanical analysis. Spine (Phila Pa 1976) 2003;28:1560-6.

75. Oda I, Abumi K, Yu BS, Sudo H, Minami A. Types of spinal instability that require interbody support in posterior lumbar reconstruction: an in vitro biomechanical investigation. Spine (Phila Pa 1976) 2003;28:1573-80.

76. Sudo H, Oda I, Abumi K, Ito M, Kotani Y, Minami A. Biomechanical study on the effect of five different lumbar reconstruction techniques on adjacent-level intradiscal pressure and lamina strain. J Neurosurg Spine 2006;5:150-5.

77. Panjabi MM. Hybrid multidirectional test method to evaluate spinal adjacent-level effects. Clin Biomech (Bristol, Avon) 2007;22:257-65.

78. Tan JS, Singh S, Zhu QA, Dvorak MF, Fisher CG, Oxland TR. The effect of cement augmentation and extension of posterior instrumentation on stabilization and adjacent level effects in the elderly spine. Spine 2008;33:2728-40.

79. Greiner-Perth R, Boehm H, Allam Y, Elsaghir H, Franke J. Reoperation rate after instrumented posterior lumbar interbody fusion: a report on 1680 cases. Spine 2004;29:2516-20.

80. Weinstein JN, Lurie JD, Olson PR, Bronner KK, Fisher ES. United States' trends and regional variations in lumbar spine surgery: 1992-2003. Spine (Phila Pa 1976) 2006;31:2707-14.

81. Turner JL, Paller DJ, Murrell CB. The mechanical effect of commercially pure titanium and polyetheretherketone rods on spinal implants at the operative and adjacent levels. Spine (Phila Pa 1976) 2010;35:E1076-82.

82. Kaufman HH, Jones E. The principles of bony spinal fusion. Neurosurgery 1989;24:264-70.

83. Zdeblick TA, Shirado O, McAfee PC, deGroot H, Warden KE. Anterior spinal fixation after lumbar corpectomy. A study in dogs. J Bone Joint Surg Am 1991;73:527-34.

84. McAfee PC, Farey ID, Sutterlin CE, Gurr KR, Warden KE, Cunningham BW. 1989 Volvo Award in basic science. Device-related osteoporosis with spinal instrumentation. Spine (Phila Pa 1976) 1989;14:919-26.

85. Carson WL, Duffield RC, Arendt M, Ridgely BJ, Gaines RW, Jr. Internal forces and moments in transpedicular spine instrumentation. The effect of pedicle screw angle and transfixation--the 4R-4bar linkage concept. Spine (Phila Pa 1976) 1990;15:893-901.

86. Xu HZ, Wang XY, Chi YL, et al. Biomechanical evaluation of a dynamic pedicle screw fixation device. Clin Biomech (Bristol, Avon) 2006;21:330-6.

87. Jacobs JJ, Hallab NJ, Urban RM, Wimmer MA. Wear particles. J Bone Joint Surg Am 2006;88 Suppl 2:99-102.

88. Schmidt H, Heuer F, Wilke HJ. Which axial and bending stiffnesses of posterior implants are required to design a flexible lumbar stabilization system? J Biomech 2009;42:48-54.

89. Wilke HJ, Heuer F, Schmidt H. Prospective design delineation and subsequent in vitro evaluation of a new posterior dynamic stabilization system. Spine (Phila Pa 1976) 2009;34:255-61.

90. Ahn YH, Chen WM, Lee KY, Park KW, Lee SJ. Comparison of the load-sharing characteristics between pedicle-based dynamic and rigid rod devices. Biomed Mater 2008;3:44101.

91. Pope MH, Panjabi M. Biomechanical definitions of spinal instability. Spine (Phila Pa 1976) 1985;10:255-6.

92. Gaines RW, Jr., Carson WL, Satterlee CC, Groh GI. Experimental evaluation of seven different spinal fracture internal fixation devices using nonfailure stability testing. The load-sharing and unstable-mechanism concepts. Spine (Phila Pa 1976) 1991;16:902-9.

93. Panjabi MM, Abumi K, Duranceau J, Crisco JJ. Biomechanical evaluation of spinal fixation devices: II. Stability provided by eight internal fixation devices. Spine (Phila Pa 1976) 1988;13:1135-40.

94. Ashman RB, Galpin RD, Corin JD, Johnston CE, 2nd. Biomechanical analysis of pedicle screw instrumentation systems in a corpectomy model. Spine (Phila Pa 1976) 1989;14:1398-405.

95. Rohlmann A, Burra NK, Zander T, Bergmann G. Comparison of the effects of bilateral posterior dynamic and rigid fixation devices on the loads in the lumbar spine: a finite element analysis. Eur Spine J 2007;16:1223-31.

96. Beer FP, Johnston ER, DeWolf JT. Mechanics of Materials. 3rd ed. New York: McGraw-Hill; 2001.

97. Niosi CA, Wilson DC, Zhu Q, Keynan O, Wilson DR, Oxland TR. The effect of dynamic posterior stabilization on facet joint contact forces: an in vitro investigation. Spine (Phila Pa 1976) 2008;33:19-26.

98. Brodke DS, Gollogly S, Bachus KN, Alexander Mohr R, Nguyen BK. Anterior thoracolumbar instrumentation: stiffness and load sharing characteristics of plate and rod systems. Spine (Phila Pa 1976) 2003;28:1794-801.

99. Cheng BC, Burns P, Pirris S, Welch WC. Load sharing and stabilization effects of anterior cervical devices. J Spinal Disord Tech 2009;22:571-7.

100. Nachemson A, Elfstrom G. Intravital wireless telemetry of axial forces in Harrington distraction rods in patients with idiopathic scoliosis. J Bone Joint Surg Am 1971;53:445-65.

101. Ashman RB, Birch JG, Bone LB, et al. Mechanical testing of spinal instrumentation. Clin Orthop Relat Res 1988;227:113-25.

102. Demetropoulos CK, Morgan CR, Sengupta DK, Herkowitz HN. Development of a 4-axis load cell used for lumbar interbody load measurements. Med Eng Phys 2009;31:846-51.

103. Rohlmann A, Bergmann G, Graichen F. A spinal fixation device for in vivo load measurement. J Biomech 1994;27:961-7.

104. Chen SH, Mo Lin R, Chen HH, Tsai KJ. Biomechanical effects of polyaxial pedicle screw fixation on the lumbosacral segments with an anterior interbody cage support. BMC Musculoskelet Disord 2007;8:28.

105. Kettler A, Niemeyer T, Issler L, et al. In vitro fixator rod loading after transforaminal compared to anterior lumbar interbody fusion. Clin Biomech (Bristol, Avon) 2006;21:435-42.

106. Kostuik JP, Munting E, Valdevit A. Biomechanical analysis of screw load sharing in pedicle fixation of the lumbar spine. J Spinal Disord 1994;7:394-401.

107. Smith TS, Yerby SA, McLain RF, McKinley TO. A device for the measurement of pedicle screw moments by means of internal strain gauges. J Biomech Eng 1996;118:423-5.

108. Wilson DC, Niosi CA, Zhu QA, Oxland TR, Wilson DR. Accuracy and repeatability of a new method for measuring facet loads in the lumbar spine. J Biomech 2006;39:348-53.

109. Tuttle ME. Load measurement in a cylindrical column or beam using three strain gages. Experimental Techniques 1981;5:19-20.

110. Bergmann JS, Rohlmann A, RKolbel R. Measurement of spatial forces by the 'matrix method'. In: Proceedings of V/VI of the 9th World Congress IMECO; 1982; 1982. p. 395-404.

111. Yerby SA, Ehteshami JR, McLain RF. Loading of Pedicle Screws Within the Vertebra. J Biomech 1996;30:951-4.

112. Youssef JA, McKinley TO, Yerby SA, McLain RF. Characteristics of pedicle screw loading. Effect of sagittal insertion angle on intrapedicular bending moments. Spine 1999;24:1077-81.

113. Lumbar Spine. EuroSpine, 2007. (Accessed Oct. 28, 2010, at http://www.eurospine.org/cm_data/LumbarSpine_Fig13_en.jpg.)

114. Rohlmann A, Bergmann G, Graichen F. Loads on an internal spinal fixation device during walking. J Biomech 1997;30:41-7.

115. Jain GM. Load-sharing characteristics of instrumented lumbar spine fusions [Master of Science]. Detroit, MI: Wayne State University; 1993.

116. Bernhardt M, Bridwell KH. Segmental analysis of the sagittal plane alignment of the normal thoracic and lumbar spines and thoracolumbar junction. Spine (Phila Pa 1976) 1989;14:717-21.

117. Beadon K, Johnston JD, Siggers K, Itshayek E, Cripton PA. A repeatable ex vivo model of spondylolysis and spondylolisthesis. Spine 2008;33:2387-93.

118. Cagli S, Crawford NR, Sonntag VK, Dickman CA. Biomechanics of grade I degenerative lumbar spondylolisthesis. Part 2: treatment with threaded interbody cages/dowels and pedicle screws. J Neurosurg 2001;94:51-60.

119. Cripton PA, Berleman U, Visarius H, Begeman PC, Nolte LP. Response of the lumbar spine due to shear loading. Society of Automotive Engineers SP-1077 1995;Paper#950662:111-26.

120. OrthoLoad. Charite - Universitaetsmedizin Berlin, 2008. (Accessed Nov. 8, 2010, at http://www.OrthoLoad.com.)

121. Wilke HJ, Jungkunz B, Wenger K, Claes LE. Spinal segment range of motion as a function of in vitro test conditions: effects of exposure period, accumulated cycles, angular-deformation rate, and moisture condition. Anat Rec 1998;251:15-9.

122. Frobin W, Brinckmann P, Biggemann M, Tillotson M, Burton K. Precision measurement of disc height, vertebral height and sagittal plane displacement from lateral radiographic views of the lumbar spine. Clin Biomech (Bristol, Avon) 1997;12 Suppl 1:S1-S63.

123. Niosi CA, Zhu QA, Wilson DC, Keynan O, Wilson DR, Oxland TR. Biomechanical characterization of the three-dimensional kinematic behaviour of the Dynesys dynamic stabilization system: an in vitro study. Eur Spine J 2006;15:913-22.

124. Panjabi MM, Krag M, Summers D, Videman T. Biomechanical time-tolerance of fresh cadaveric human spine specimens. J Orthop Res 1985;3:292-300.

125. Hongo M, Gay RE, Hsu JT, et al. Effect of multiple freeze-thaw cycles on intervertebral dynamic motion characteristics in the porcine lumbar spine. J Biomech 2008;41:916-20.

Appendix A Strain Gauge Theory and Wheatstone Bridge Circuit

A.1 Strain Gauge Theory

A foil strain gauge is a device consisting of a grid of wire that when adhered to a surface will stretch and deform with the surface under an applied load (Figure A-1). Deforming a wire changes its resistance. When a voltage is applied across the strain gauge, the change in resistance can be measured as a change in the voltage output (voltage = current x resistance). Therefore, a strain gauge affixed to a body subjected to an externally applied load can be used to measure the surface strain at the gauge location. Relationships between strain and force can be used to then determine the force on a component of interest. The following illustrations and equations show the relationship between wire deformation, resistivity and strain.[4]

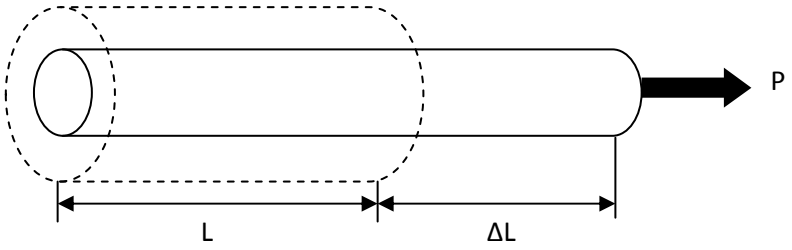

Figure A-1: The deformation of a wire under a load. A length of wire L is stretched due to a load P to a length L+ΔL. The original diameter has decreased according to Poisson's effect.

The resistance of a wire (R) is proportional to its resistivity (ρ), length (L) and inversely proportional to its cross-sectional area (A) (Equation 1).

$$R = \rho \frac{L}{A} \qquad \text{Equation 1}$$

A small change in resistance can be found by taking the derivative of both sides of Equation 1.

$$dR = d\left(\rho \frac{L}{A}\right) \qquad \text{Equation 2}$$

Taking the natural logarithm of each side within the derivative yields Equation 3:

$$d(\ln R) = d(\ln \rho) + d(\ln L) - d(\ln A) \qquad \text{Equation 3}$$

With the known relationship,

$$d(\ln x) = \frac{dx}{x}$$

Equation 3 can be re-written as:

[4] Electrical Resistance Strain Gage Circuits. (Accessed November 11, 2010, at http://www.ae.gatech.edu/people/jcraig/classes/ae3145/Lab2/strain-gages.pdf.)

$$\frac{dR}{R} = \frac{d\rho}{\rho} + \frac{dL}{L} - \frac{dA}{A} \qquad \text{Equation 4}$$

The last term in Equation 4 can be replaced with the differential area of a circle:

$$\frac{dA}{A} = \frac{2\pi r dr}{\pi r^2} = 2\frac{dr}{r} \qquad \text{Equation 5}$$

The longitudinal strain (ε) and tangential strain (ε_T) relate to the change in length of the wire and change in diameter of the wire, respectively, and can be related to each other using Poisson's Ratio (ν).

$$\frac{dL}{L} = \varepsilon \qquad \frac{dr}{r} = \varepsilon_T \qquad \varepsilon_T = -\upsilon\varepsilon$$

Using the above relationships, the following equation is found:

$$\frac{dR}{R} = \frac{d\rho}{\rho} + \varepsilon - 2\varepsilon_T$$

$$\frac{dR}{R} = \frac{d\rho}{\rho} + \varepsilon - 2(-\nu\varepsilon)$$

$$\frac{dR}{R} = \frac{d\rho}{\rho} + \varepsilon(1 + 2\nu) \qquad \text{Equation 6}$$

The change in resistance is dependent on the inherent resistivity of the material (1st term) and on the strain (2nd term). For a strain gauge, a constant called the gauge factor (GF) is defined as:*

$$GF = \frac{dR/R}{\varepsilon} = \frac{d\rho}{\rho\varepsilon} + 1 + 2\nu \qquad \text{Equation 7}$$

*As long as there is no change in resistivity of the material under strain, GF is a constant dependent on Poisson's Ratio. In practice the gauge factor is not always constant and is dependent on what type of material is used for the gauge.

A.2 Wheatstone Bridge Circuit

A circuit is required to detect the small resistance changes associated with strain gauges (usually microstrain is the unit of measure for strain). The Wheatstone bridge is one of the commonly used bridges for strain gauges (Figure A-2). There are many bridge designs for various numbers of gauges, but the following description is for a three-wire 1/4-bridge circuit since this is the bridge type used in the experiments presented in this thesis. A 1/4-bridge circuit has a strain gauge in only one arm of the bridge, while the other three arms are resistors, usually internal to the data acquisition unit (Figure A-3).

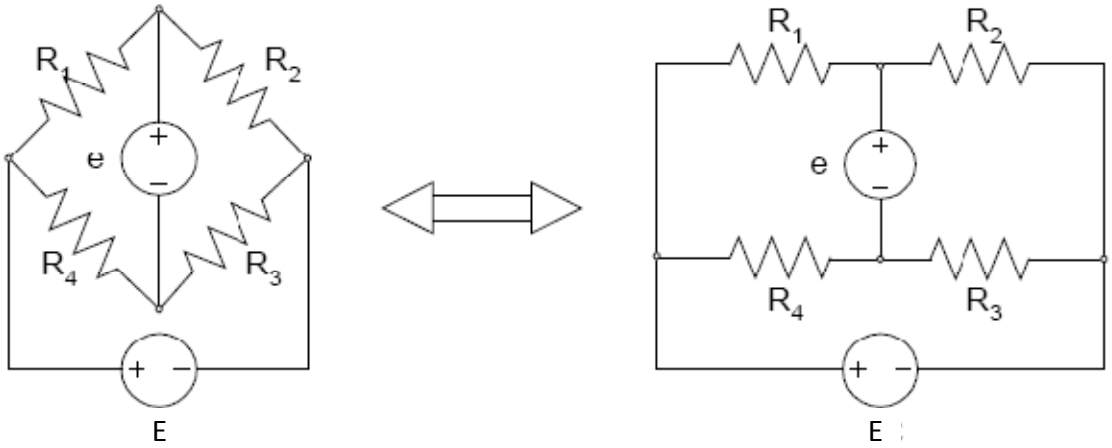

Figure A-2: A Wheatstone bridge circuit drawn (a) in the traditional diamond configuration and (b) in a square configuration to highlight the voltage dividers creating the bridge. The output voltage (e) spans two opposite corners of the bridge, while the input voltage (E) spans the other two corners. Usually, the resistors, or strain gauges, have the same resistance rating. Reprinted from www.ae.gatech.edu/people/jcraig/classes/ae3145/Lab2/strain-gages.pdf with permission from Professor J. Craig.

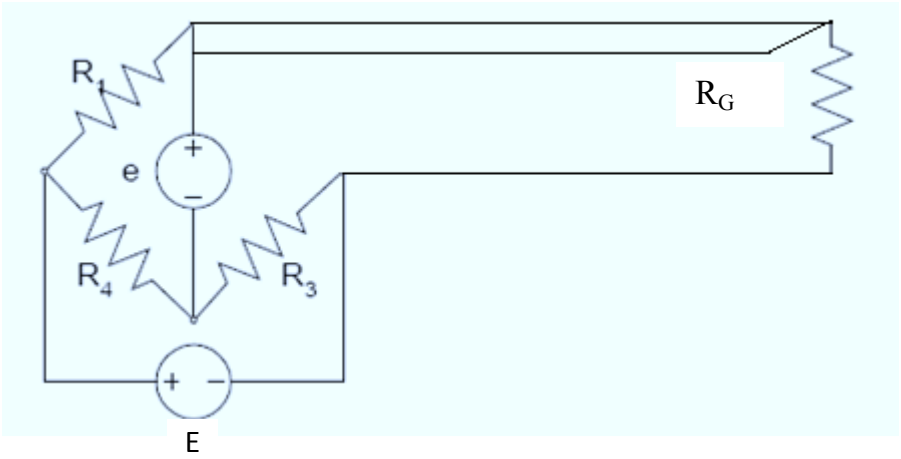

Figure A-3: A three-wire 1/4-bridge circuit showing resistor R_2 replaced with a strain gauge with resistance R_G. The third wire connected directly to the output voltage compensates for errors associated with losses due to resistance and temperature changes over the length of the wire that extends to the gauge. However, this circuit does not allow for complete temperature compensation since only one gauge is active (i.e. temperature fluctuations affecting the active gauge cannot be separated from strain due to applied loads). This circuit was used in a constant temperature environment, and accuracy of 10 microstrain is acceptable for this thesis.[5]

[5] Electrical Resistance Strain Gage Circuits. (Accessed November 11, 2010, at http://www.ae.gatech.edu/people/jcraig/classes/ae3145/Lab2/strain-gages.pdf.)

A relationship exists between the input and output voltage. Circuit analysis is used to determine this relationship. From nodal analysis the output voltage is the difference between the voltage at the top and bottom nodes (Figure A-2a).

$$e = V_1 - V_4 \qquad \text{Equation 8}$$

Using the relations for the two voltage dividers seen in Figure A-2b, the nodal voltages can be expressed in terms of the resistors and the input voltage.

$$V_4 = \frac{R_3}{R_4+R_3}E \qquad \text{Equation 9}$$

$$V_1 = \frac{R_2}{R_1+R_2}E \qquad \text{Equation 10}$$

$$e = V_1 - V_4 = \left(\frac{R_2}{R_1+R_2} - \frac{R_3}{R_4+R_3}\right)E \qquad \text{Equation 11}$$

This is the basic equation relating the input and output voltages through the resistors in a Wheatstone Bridge. One of the properties of this bridge type is that when there is no change in the resistance, the bridge balances (i.e. the output voltage is zero). Let us assume that $R_1 = R_2 = R_3 = R_4 = R$, then

$$\frac{e}{E} = \frac{R}{2R} - \frac{R}{2R} = 0$$

We would like to relate the output voltage that we measure directly to strain. First, we assume that R_1 and R_2 both equal R_G (although only R_2 is an active gauge) and R_3 and R_4 both equal R. Equation 10 becomes:

$$\frac{e}{E} = \frac{R}{2R} - \frac{R_G+\Delta R_G}{R_G+R_G+\Delta R_G}$$

$$\frac{e}{E} = \frac{1}{2} - \frac{R_G+\Delta R_G}{2R_G+\Delta R_G}$$

$$\frac{e}{E}(2R_G + \Delta R_G) = -\frac{\Delta R_G}{2}$$

$$\frac{e}{E}\left(2 + \frac{\Delta R_G}{R_G}\right) = -\frac{\Delta R_G}{2R_G} \qquad \text{Equation 12}$$

Substituting the relation for gauge factor into Equation 12 yields:

$$\frac{e}{E}(2 + \varepsilon GF) = -\frac{1}{2}\varepsilon GF$$

$$\frac{e}{E} = -\frac{1}{2}\varepsilon GF\ \left(\frac{1}{2+\varepsilon GF}\right)$$

$$\frac{e}{E} = -\frac{GF}{4}\varepsilon\ \left(\frac{1}{1+\frac{\varepsilon}{2}GF}\right) \qquad \text{Equation 13}$$

For large strains there is a non-linear relationship between voltage and strain (Equation 13). However, for small strains the (1+ε/2*GF) factor in Equation 13 will be approximately 1. Since strain gauges can only measure small strains before plastic deformation of the gauge wire (or the matrix and glue used to adhere the gauge wire to the surface) will occur, this approximation is valid for the majority of applications and for the majority of strain gauges. Other factors such as temperature will have a larger non-linearity effect on the output from the gauge. Incorporating the previous assumption, the final equation relating the known input and output voltages, gauge factor and strain from the active gauge is:

$$\frac{e}{E} = -\frac{GF}{4}\varepsilon \qquad \text{Equation 14}$$

Appendix B Matrix Method

The strain gauge signal from the implant transducer was converted to load using the matrix method.[6] For the study in this thesis two loads were applied to the implant: anterior shear and axial compression, but only shear load on the implant was reported (Chapter 3). Strain responses to the forces were linear, and a relationship exists as follows:

$$\begin{bmatrix} S_S \\ S_A \end{bmatrix} = \begin{bmatrix} C_{11} & C_{12} \\ C_{21} & C_{22} \end{bmatrix} \begin{bmatrix} F_{SHEAR} \\ F_{AXIAL} \end{bmatrix} \qquad \text{Equation 1}$$

where S_S and S_A are measured strains,*
F_{SHEAR} and F_{AXIAL} are known applied forces,
and C_{ij} are unknown calibration constants

*Each of the working strain signals on each implant rod were incorporated into an estimate of the shear and axial force using two "curved rod" equations developed from a mechanics of materials text book (Appendix C). Each strain signal yielded an estimated shear or axial force. The force was then averaged across the number of working gauges to yield S_S and S_A. Therefore, S_S and S_A are strain predictions of shear and axial force, respectively. Simplifications and assumptions in the theoretical equations required a physical calibration.

To determine the calibration constants, isolated shear and axial loads were applied to the transducer in the calibration loading rig (Chapter 2, Appendix D). The loads and strains were recorded and the four matrix constants were calculated (Equations 2 to 5). Two of the matrix constants were direct calibration constants (i.e. the constants related the applied shear load to the shear force prediction or applied axial load to the axial force prediction) and the other two constants were coupling constants (i.e. the constants related the applied shear load to the axial force prediction or the applied axial load to the shear force prediction).

$S_{SS} = C_{11} \times F_{SHEAR} + C_{12} \times 0$ yields C_{11} (direct) Equation 2

$S_{AS} = C_{21} \times F_{SHEAR} + C_{22} \times 0$ yields C_{21} (coupling) Equation 3

$S_{SA} = C_{11} \times 0 + C_{12} \times F_{AXIAL}$ yields C_{12} (coupling) Equation 4

$S_{AA} = C_{21} \times 0 + C_{22} \times F_{AXIAL}$ yields C_{22} (direct) Equation 5

Using the calibration matrix, shear loads supported by the transducer were determined. After the strains from the combined shear and axial loading test were converted into shear and axial force predictions (Appendix C) these forces were multiplied by the inverted calibration matrix to determine

[6] Bergmann JS, Rohlmann A, RKolbel R. Measurement of spatial forces by the 'matrix method'. In: Proceedings of V/VI of the 9th World Congress IMECO; 1982; 1982. p. 395-404.

the shear loads supported by the implant (Equations 6 to 9). This combined load test was not a load-sharing test (i.e. all applied shear load was supported by the implant). Therefore, the error between the calculated shear load and the known applied shear load was determined (Chapter 2).

$$[S] = [C][F] \quad \text{Equation 6}$$

$$[C]^{-1}[S] = [C][C]^{-1}[F] \quad \text{Equation 7}$$

$$[D] = [C]^{-1} = inv(C)\ and\ [C][C]^{-1} = 1 \quad \text{Equation 8}$$

$$[F] = [D][S] \quad \text{Equation 9}$$

Theoretically, Equation 9 yields perfect prediction of applied loads. However, errors between the calculated shear load and known applied shear load resulted. The difference between the known and calculated shear forces, or the absolute error, found in the calibrations was usually constant across the range of applied load and is referred to as an offset. If the average offset from the three calibration trials was applied to the data from the combined loading test, the average error was reduced (Figure B-1 and Table B-1). In Figure B-1, the dashed light blue line, or absolute error, is positive. For other tests on the same implant type this may have been negative (Table B-2). This error appears to be random because there is no trend in the positivitity of the offset values across the specimens. However, within a calibration for a specific specimen, some of the offsets were the same sign for the three repeated combined loading tests (Table B-3).

There is a possibility that some aspect of the calibration process caused a biased error. The re-clamping of the rod within the pedicle screws between the three trials combined with drift of the Instron load cell and strain gauge signals may have contributed to this biased offset. It is also possible, that if this test was repeated 100 times, the average offset would be zero indicating a random, not biased error; the random sample of three trials may give a false impression of biased error. To further explore this concept, re-analysis of all the data must be performed without applying the offset (i.e. only the calibration matrix is applied as shown in Equation 9). This is outside the scope of this thesis.

The maximum average offset for each implant type (12 N for HST, -11 N for MST, -8 N for LST and 9 N for ULST, Table B-2) is well below the applied shear load of 250 N. Removing this maximum average offset would not have a large effect on the overall trends seen in the implant load results (Chapter 3). Specifically, removing the maximum offset values from the mean implant loads provides an estimate of the worst-case effect of this offset (Table B-4). The trend of increasing implant load for increasing specimen destabilization remains the same. The inter-rod relationships show some differences between the LST and ULST loads. The maximum offsets were in opposite directions for these two rods which explains the change in mean load-sharing between these two implants. However, this

maximum average offset is for one specimen and the other smaller average offsets for the other 14 specimens would tend to decrease this difference between LST and ULST (and between the other implant types). Therefore, the values in Table B-4 represent the maximum possible deviation from the results reported in Chapter 3 due to removing the offset from the analysis.

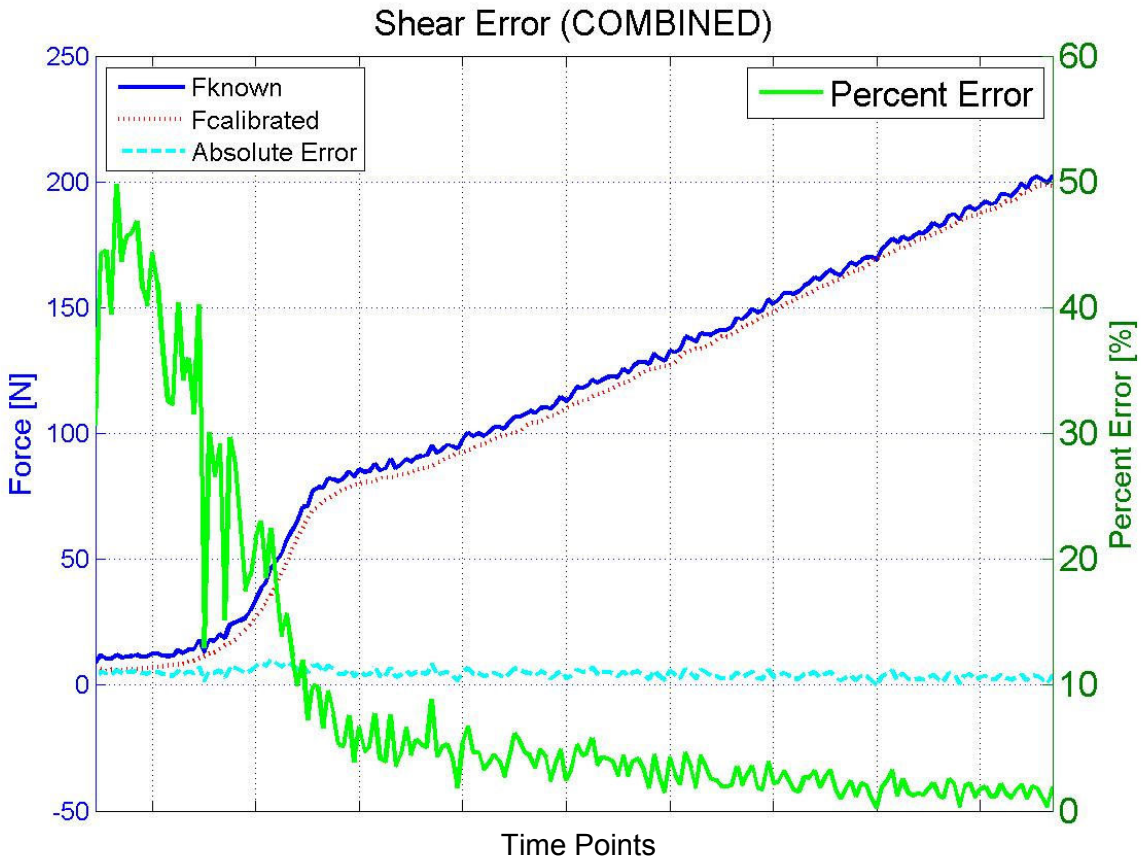

Figure B-1: Example data from one of the combined loading calibration tests with a HST. The applied shear load (solid blue) and calculated shear load from the matrix equation (dotted red) show an increasing ramp from 0 to 200 N. The difference between the known and calculated shear load is the absolute error (dashed light blue) and represents the offset from a trial. The percent error (green, secondary vertical axis) between the known and calculated shear loads is below 10% for the majority of the data.

Table B-1: Offset values found from four combined loading tests with the construct removed from the loading apparatus and reinserted between trials 1 and 2, and between 3 and 4. The average offset of 11.35 N was applied to the data and the final error (Error column) for this testing sequence was found.

Test	Average Shear Error [N]	Error [N]
1	11.5	0.18
2	14.4	3
3	10	-1.15
4	13	1.41
Average Offset	**11.4**	

Table B-2: Average offset values for each specimen and each implant type. The empty cells occur for specimens in which that specific implant type did not have a sufficient number of working strain gauges to be calibrated. The maximum average offset for each implant type is bold.

Specimen #	HST	MST	LST	ULST
1	-4.5	3.7	-4.4	7
2	-2	3.7	-0.3	-0.7
3	2.3	5.6	1.8	3.6
4	1.8	-3.5	-1.3	0.6
5	-7.3	1.4	-5.2	-4.3
6	-4.9	**-11**	1.9	-0.4
7	-0.2	-1.6	0.5	0.8
8	9.9		-2.6	8.8
9	**12**		-7.1	-0.1
10	-1.2			1.1
11	10		3.3	**9.4**
12	3		**-8**	
13	-2	1.9	-1.7	4
14	2.7	-9.2	-3.5	2.9
15	3.6	-6.7	-6	3.9

Table B-3: Offset values for each of the three combined trials completed during post-calibration for each implant type for each specimen. The specimens were tested chronologically in decreasing numerical order (15 to 1). The bold values indicate the calibration trials with the offset in the same direction (all positive or all negative).

Specimen #	HST			MST			LST			ULST		
	Trial 1	Trial 2	Trial 3	Trial 1	Trial 2	Trial 3	Trial 1	Trial 2	Trial 3	Trial 1	Trial 2	Trial 3
1	9	-9	-14	-4	6	9	**-7**		**-2**	**6**	**7**	**8**
2	10	-8	-8	**2**	**5**	**4**	1	-1	-1	0.5	-4	1
3	-1	4	4	**6**	**6**	**4**	0.1	5	-0.1	3	-0.5	8
4	**2**	**1**	**2**	**-6**	**-3**	**-1**	-1	0.1	-3	0.3	-0.05	1
5	**-6**	**-6.5**	**-9**	0.2	-0.2	4.2	**-4**	**-6**	**-5**	-2	4	-15
6	1	-11	-5	-18	-8	-7	**1**	**2**	**3**	-6	3	2
7	-0.2	4	-5	-4	0.5	-1	1	-2	3	-2	0.2	5
8	**13**	**6**	**11**				-4	-5	1	-1	11	17
9	**12**	**10**	**14**				-4	-9	-8	-6	-4	10
10	4	-1	-7							-0.02	-5	9
11	**16**	**5**					**3**	**3**	**3**		**9**	**10**
12		-1.5	7				**-10**	**-6**	**-8**			
13	**-3**	**-2**	**-1**	-2	4	4	-5	-2	1	-2	6	8
14	**1**	**5**	**2**	**-12**	**-10**	**-6**	-4	4	-10	**2**	**1**	**5**
15	**2**	**3**	**5**	**-4**	**-6**	**-9**	**-2**	**-12**	**-5**	**2**	**2**	**8**

Table B-4: Comparison of the original mean values of implant shear load-sharing [%] for each of the three specimen conditions from the results section in Chapter 3 (for which the average offsets in Table B-2 were applied) and those implant loads adjusted by removal of the maximum average offset for each transducer type to provide the worst-case effect of the offset on the implant load values.

		Implant Type							
		HST		MST		LST		ULST	
		Original	No Offset	Original	No Offset	Original	No Offset	Original	No offset
Condition	1	43	38	32	36	18	21	16	12
	2	67	62	56	60	35	38	32	28
	3	76	71	77	81	50	53	49	45

Appendix C Gauge Location on Rods and Strain Equations

Equations for the theoretical strain at the locations marked on the rod drawings were derived.[7] A brief derivation is shown here highlighting the geometric relationships needed for a curved rod. A derivation for straight rods in reported elsewhere.[8] It is assumed the reader is familiar with stress (σ) and strain (ε) equations for straight, slender beams:

$\sigma = E\varepsilon$ General stress-strain relationship where *E* is the modulus of elasticity Equation 1

$\sigma = \frac{P}{A} + \frac{My}{I}$ Equation relating stress to an external force (*P*) and moment (*M*) Equation 2

where *A* is the perpendicular cross-sectional area of the beam,
y is the distance between the location of interest and the neutral axis,
and *I* is the second moment of area of the cross-section

A curved rod with known dimensions and material properties is shown below (Figure C-1). The rod is subjected to an axial compressive load and shear load applied at points above the rod in the figure. The loads are applied to rigid blocks (not shown) that are rigidly attached to the rods at each end (P_1 and P_2). The block attached at P_2 is rigidly affixed to the superior vertebra, while the block attached at P_1 is rigidly affixed to the inferior vertebra. Each load was analyzed individually to determine the strain at the gauge location during the isolated calibration tests. Geometric relationships and free body diagrams will be used to determine the loads, moments and constants to substitute into Equation 2 to find strain at each gauge location.

[7] Beer FP, Johnston ER, DeWolf JT. Mechanics of Materials. 3rd ed. New York: McGraw-Hill; 2001.

[8] Tuttle ME. Load measurement in a cylindrical column or beam using three strain gages. Experimental Techniques 1981;5:19-20.

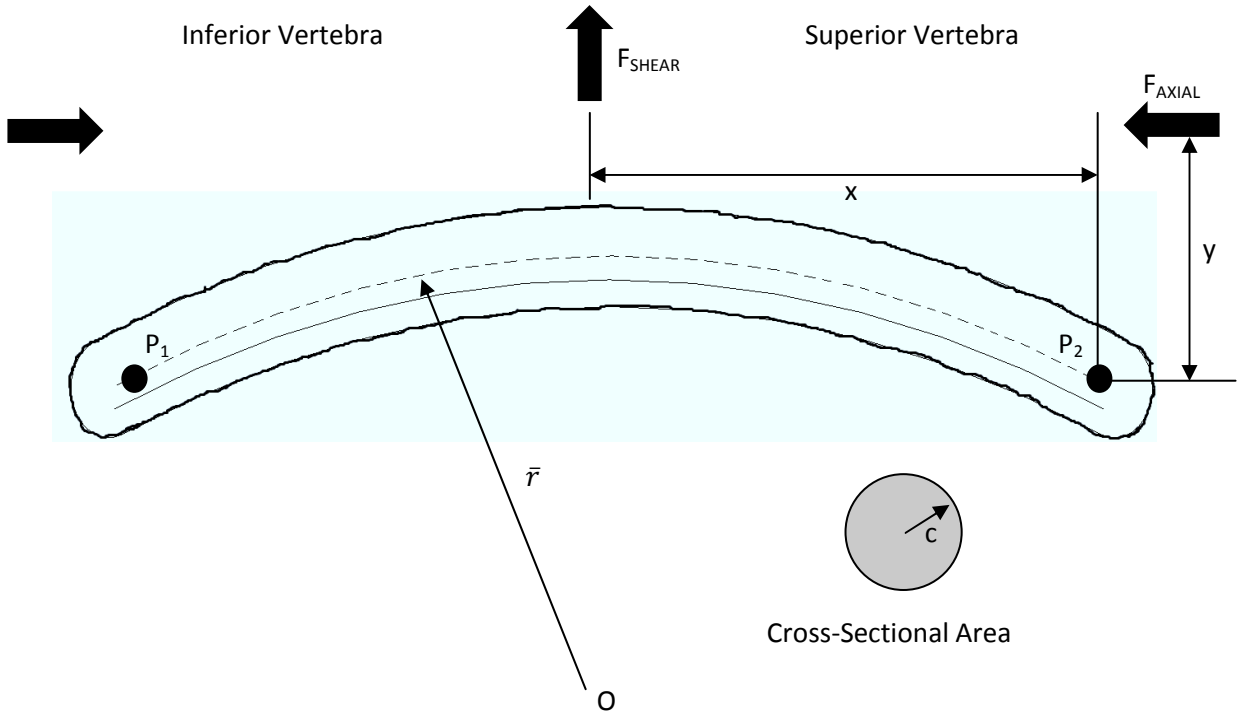

Figure C-1: Diagram of a curved rod with an external axial compressive and shear load applied at indicated distances (x, y) from the rod. The curved rod has a circular cross-section. The radius of curvature of the rod is indicated ($\bar{r}$) with the origin at point O. The geometric center of the rod is dashed and the neutral axis is solid.

C.1 Axial Compression

The rod is clamped rigidly at P_1 and P_2 (Figure C-2). The applied forces and moments are shown as shaded arrows (superior vertebra end) and reaction forces and moments are shown as open arrows (inferior vertebra end). Relevant dimensions and measurements for the analysis are shown in the figure. For a curved member, a neutral axis exists such that under pure bending, strains along this curvature would be zero. The neutral axis is found from the radius of curvature ($\bar{r}$) and the radius of the rod (c):*

$$R = \frac{1}{2}\left(\bar{r} + \sqrt{\bar{r}^2 - c^2}\right) \qquad \text{Equation 3}$$

*R is calculated differently for the MST because its cross-section is not circular.

$$R = \frac{\pi\left(\frac{d_1}{2}\right)\left(\frac{d_2}{2}\right)}{2\pi\left(\frac{d_2}{d_1}\right)\left(\bar{r} - \sqrt{\bar{r}^2 - \left(\frac{d_1}{2}\right)^2}\right)}$$

where d_1 and d_2 are the large and small diameters of the MST cross-section, respectively

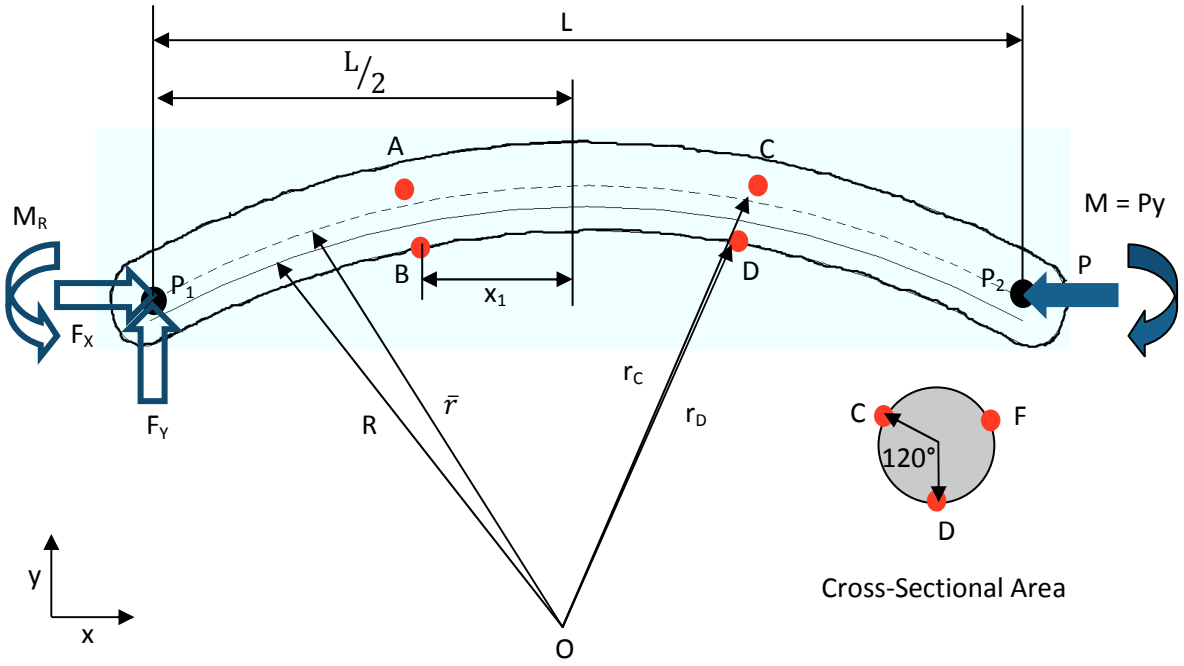

Figure C-2: Diagram of a curved rod with an applied axial compressive load P and a moment M=Py (shaded arrows) due to moving the load P a distance y to the point P_2. Reaction forces M_R, F_X and F_Y are shown at P_1 (open arrows). The red dots indicate the location of the strain gauges on the rods with circular cross-sectional areas. There are six gauges in total: one each at 0°, 120°, and 240° on the left and right ends of the rod. The gauges on the concave surface are at a known distance x_1 from the rod centerline and the overall length of the rod (L) is known. The radius of curvature ($\bar{r}$), distance to the neutral axis (R), and distances to the gauges (r_C and r_D) are shown and are all scalar quantities.

The eccentricity of the neutral axis is a scalar distance of how much this axis (solid line in Figure C-2) deviates from the geometric curvature of the rod (dashed line in Figure C-2) and is denoted by *e*:

$$e = \bar{r} - R \qquad \text{Equation 4}$$

The distance to the gauges is as follows:*

$$r_D = r_B = \bar{r} - c \qquad \text{Equation 5}$$

$$r_C = r_F = r_A = \bar{r} + c\cos\tfrac{120^\circ}{2} \qquad \text{Equation 6}$$

*The distance to the gauges is calculated differently for the MST because of its cross-section and because the gauges are located in slightly different places than for the other rod types.

$$r_B = r_D = \bar{r} - \left(\frac{d_1}{2}\right)$$

$$r_A = r_C = \bar{r} + \left(\frac{d_1}{2}\right)$$

The normal component of the force at the gauge location can be found using a free body diagram (Figure C-3a), equations of static equilibrium (Figure C-2), and geometry (Figures C-2 and C-3b).

Equations of static equilibrium from Figure D-2:

$$\sum F_x = F_X - P = 0 \qquad F_X = P \qquad \text{Equation 7}$$

$$\sum F_y = F_Y = 0 \qquad F_Y = 0 \qquad \text{Equation 8}$$

$$\sum M = M_R - M = 0 \qquad M_R = M = Py \qquad \text{Equation 9}$$

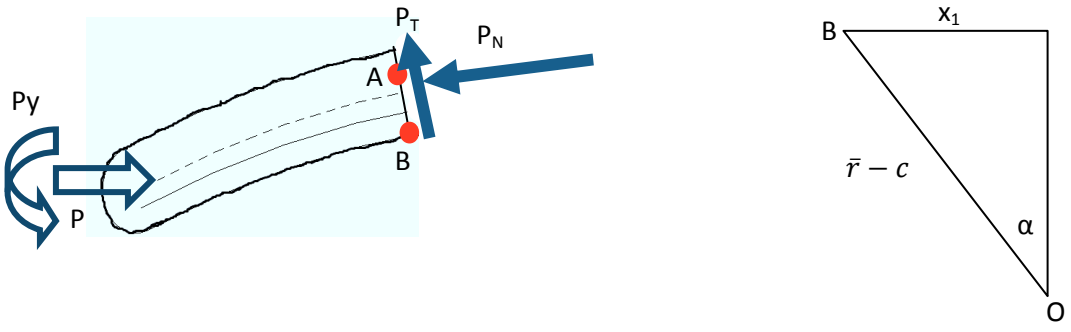

Figure C-3: (a) Free body diagram of the left side of the curved rod cut at the plane of the gauges A, B and C (not shown). The reaction forces and moments were found from Equations 7 to 9. The normal and tangential component of the axial force on the gauge plane are shown in the image. The normal force is required for solving Equation 2. (b) The angle of the normal force with the horizontal is found from simple trigonometry where two sides of the triangle are known and the angle is found using the sine relationship.

The angle for the normal force can be determined using a right angle triangle with two known dimensions (Figure C-3b).

$$\alpha = \sin^{-1}\frac{x_1}{\bar{r}-c} \qquad \text{Equation 10}$$

where x_1 is the horizontal distance between the center of the rod and the gauge location

The normal force can now be found (Figure C-3a):

$$P_N = P\cos\alpha \qquad \text{Equation 11}$$

The general equation for strain due to an eccentric axial load on a curved rod is found from the following equation (Equation 12), slightly altered from the bending equation for a straight member (Equation 2). The negative signs indicate a compressive axial force and a counterclockwise moment.

$$\varepsilon E = -\frac{P_N}{A} - \frac{M(r_i - R)}{Aer_i}$$ Equation 12

where P_N is the normal force,
r_i is the radial distance to the strain location of interest (i.e. the gauge location),
and A is the perpendicular cross-sectional area of the curved rod

Substituting in the equations for the normal force and moment yields the final equation for strain due to an eccentric axial compressive load (Equation 13).

$$\varepsilon_i E = -\frac{P\cos\alpha}{A} - \frac{Py(r_i - R)}{Aer_i}$$ Equation 13

C.2 Anterior Shear

The equation for strain at specific locations for a curved rod under shear load is similar to that for an axial load with the axial load P replaced with the shear load S. The free body diagram and corresponding equations of static equilibrium (Equations 14 to 16) show how the axial component of the shear force and the moment were determined at the gauge locations (Figures C-4 and C-5).

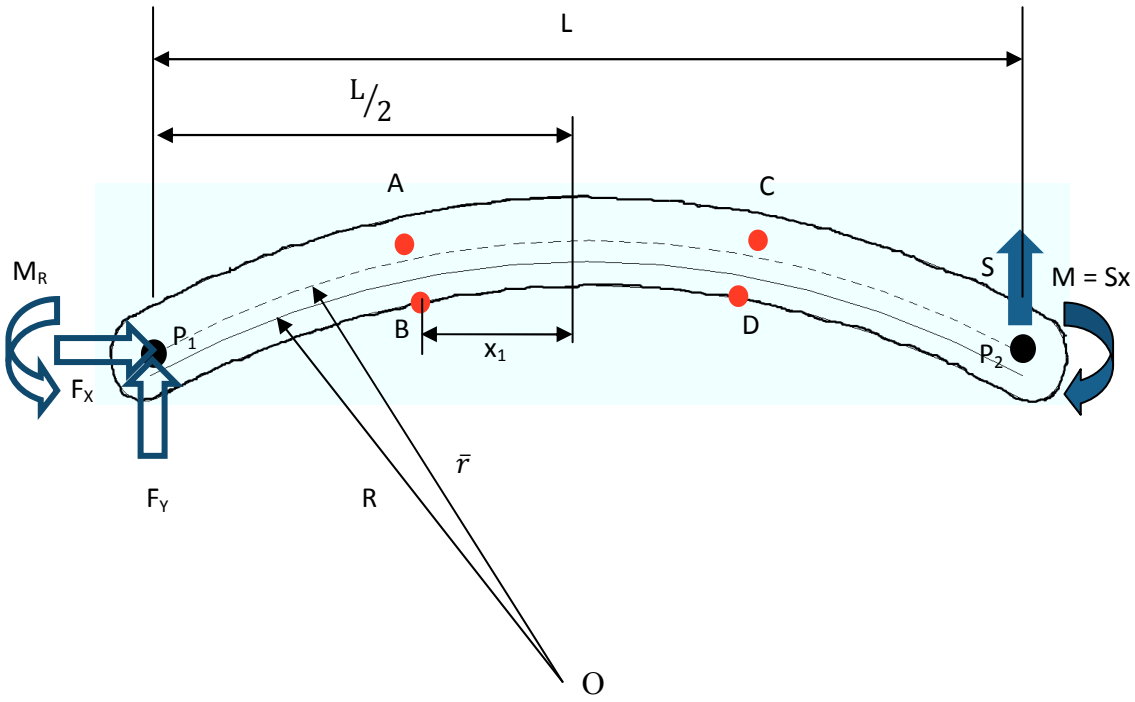

Figure C-4: Diagram of a curved rod with an applied shear load S and a moment M=Sx due to moving the load S a distance x to the point P_2. Reaction forces M_R, F_X and F_Y are shown at P_1. The red dots indicate the location of the strain gauges on the rods with circular cross-sectional areas. There are six gauges in total: one each at 0°, 120°, and 240° on each of the ends of the rod corresponding to the superior and inferior vertebrae. The gauges on the concave surface are at a known distance x_1 from the rod centerline and the overall length of the rod (L) is known. The radius of curvature ($\bar{r}$) and distance to the neutral axis (R) are shown.

Equations of static equilibrium:

$$\sum F_x = F_X - 0 = 0 \qquad F_X = 0 \qquad \text{Equation 14}$$

$$\sum F_y = F_Y + S = 0 \qquad F_Y = -S \qquad \text{Equation 15}$$

$$\sum M = M_R - M = 0 \qquad M_R = M = Sx \qquad \text{Equation 16}$$

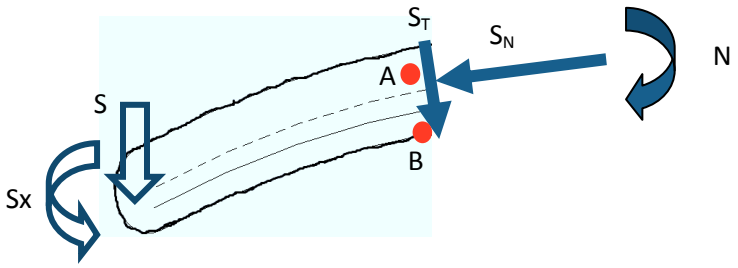

Figure C-5: Free body diagram of the left side of the curved rod cut at the plane of the gauges A, B and C (not shown). The reaction forces and moments were found from Equations 14 to 16. The normal and tangential component of the shear force on the gauge plane are shown in the image, as well as the moment, N. The normal force is required for solving Equation 2. The angle of the normal force with the horizontal is found from simple trigonometry where two sides of the triangle are known and the angle is found using the sine relationship (for image see Figure C-3b).

The normal component of the shear force is:

$$S_N = S \sin \alpha$$

Substituting the force and moment relations into the general strain equation yields:

$$\varepsilon_i E = -\frac{S \sin \alpha}{A} - \frac{Sx(r_i - R)}{Aer_i}$$

where α, r_i, e and R are the same as previously defined for the axial compression case

The strain signals from each gauge were converted into force using the equations in this appendix. The forces were averaged to use in the matrix calculation (S_S and S_A in Appendix B).

Appendix D Loading Rig

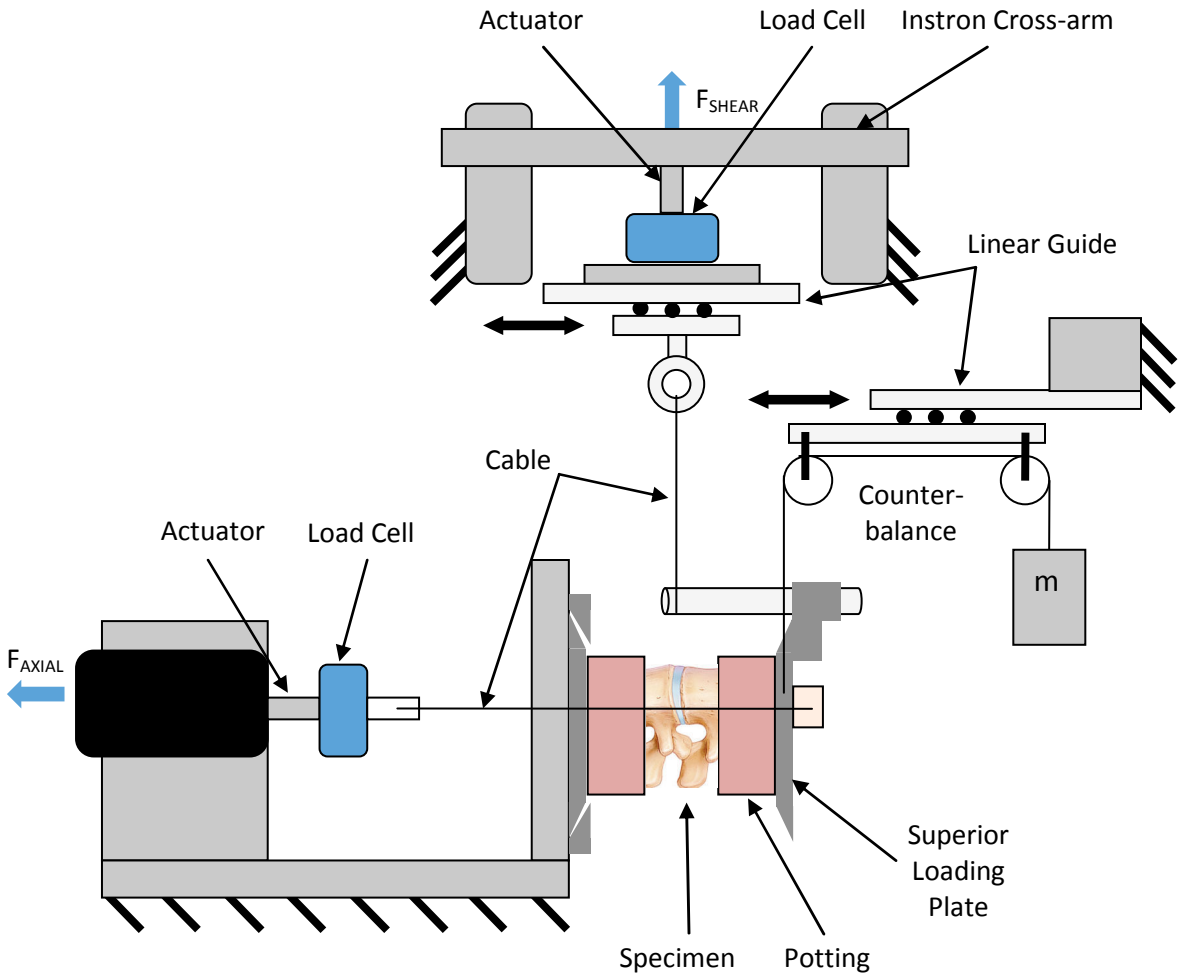

Figure D-1: Schematic of loading rig with a specimen in potting. The superior vertebra is on the right. The anterior of the specimen is towards the top of the schematic. Shear and axial forces were applied to the superior vertebra through cables attached to the superior loading plate. The counter-balance removes half the weight of the specimen, potting and superior loading plate from the specimen-implant system. The linear guides allow unconstrained motion in the sagittal plane.

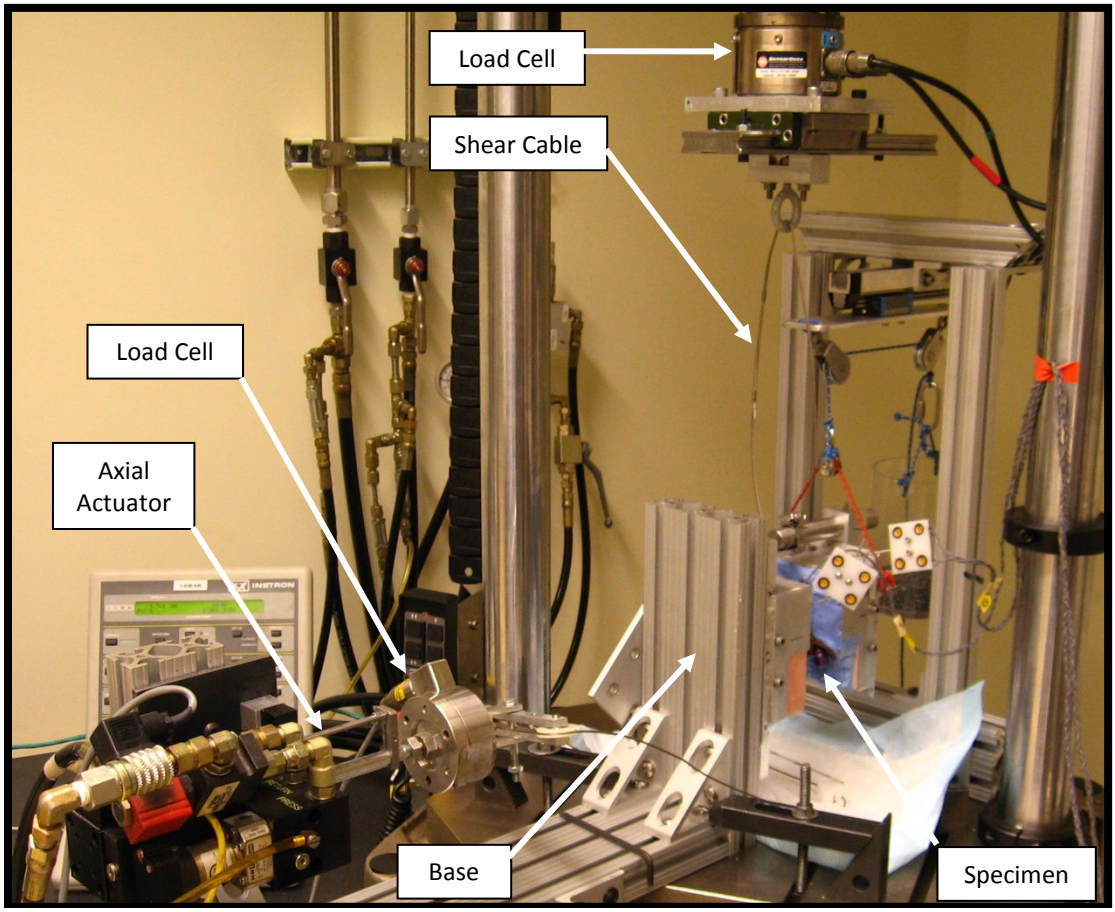

Figure D-2: Image of the loading rig with the specimen attached to the base. Infrared markers are attached to the superior and inferior vertebral bodies. The counter-balance system is behind the base.

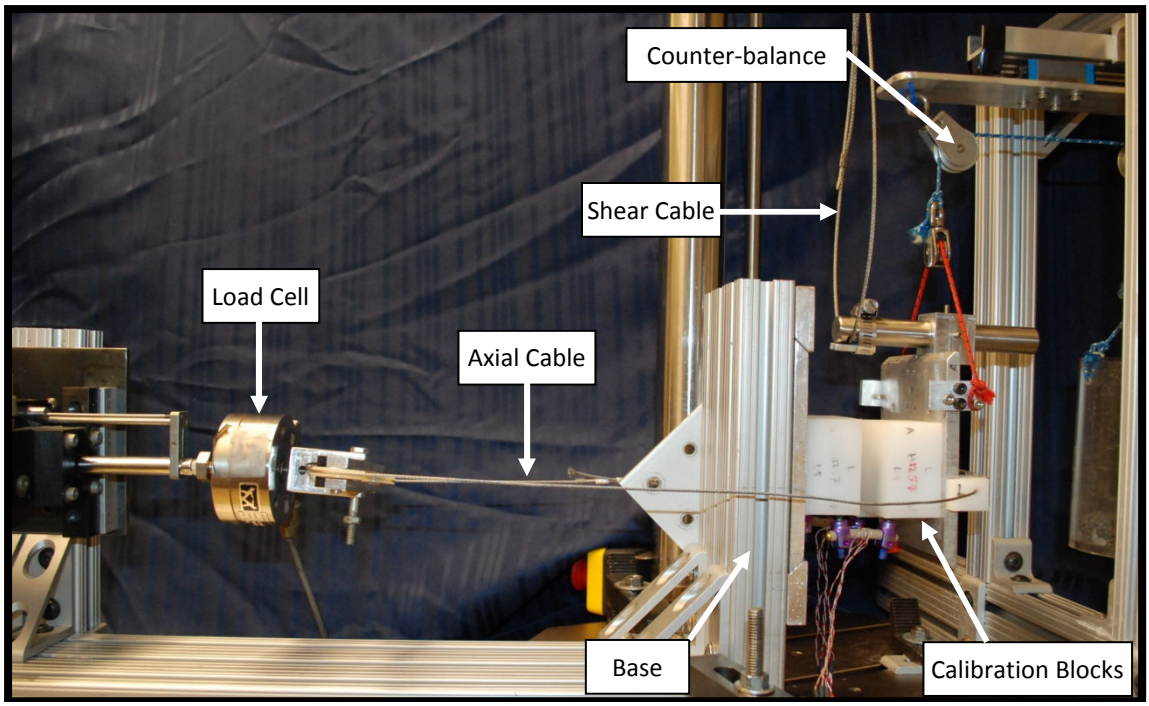

Figure D-3: Image of the loading rig with calibration blocks attached to the base.

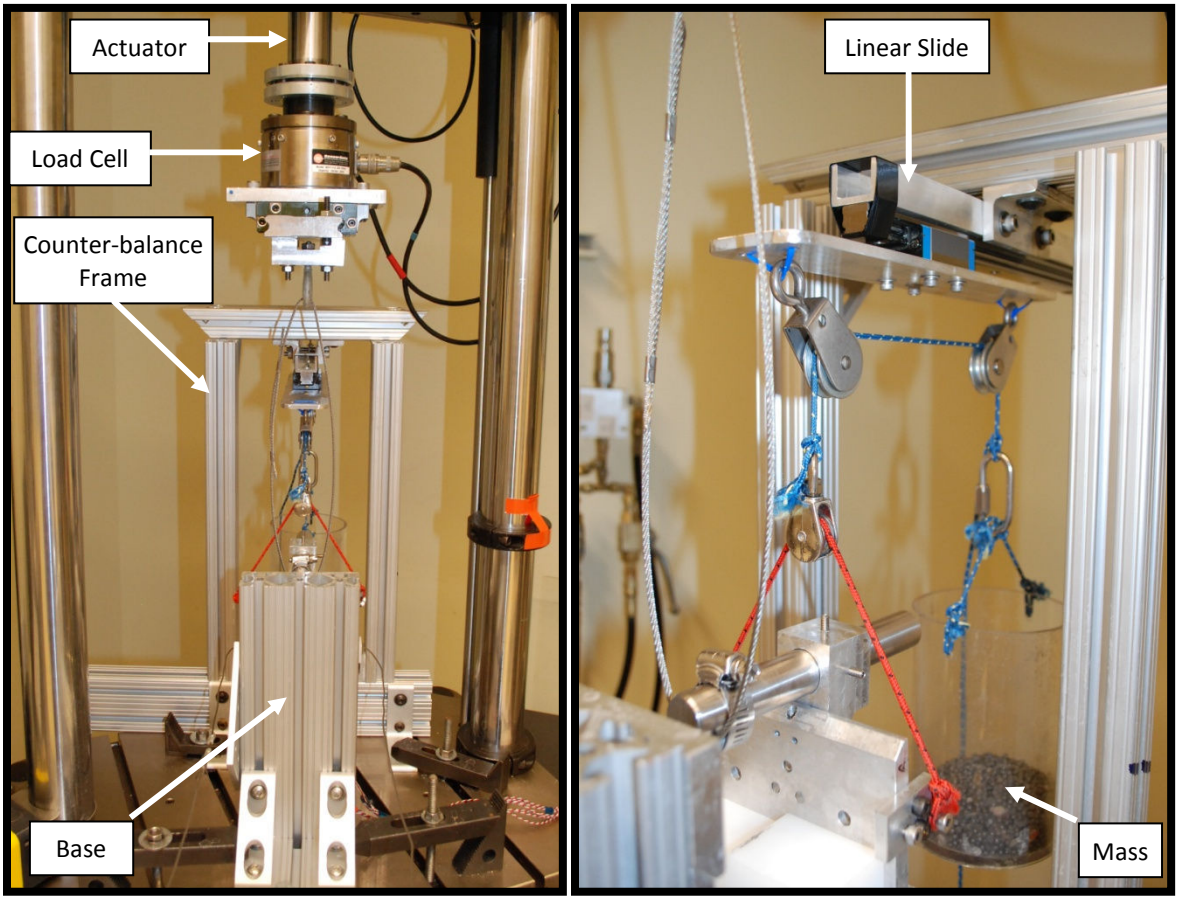

(a) **(b)**

Figure D-4: Front view of the loading rig and counter-balance system. (a) The Instron actuator and load cell apply shear load to the specimen through the steel cable. The frame for the counter-balance system is shown behind the rig base. (b) An angled view of the counter-balance system that removed the weight of half the calibration blocks/specimen and loading plate from the transducer.

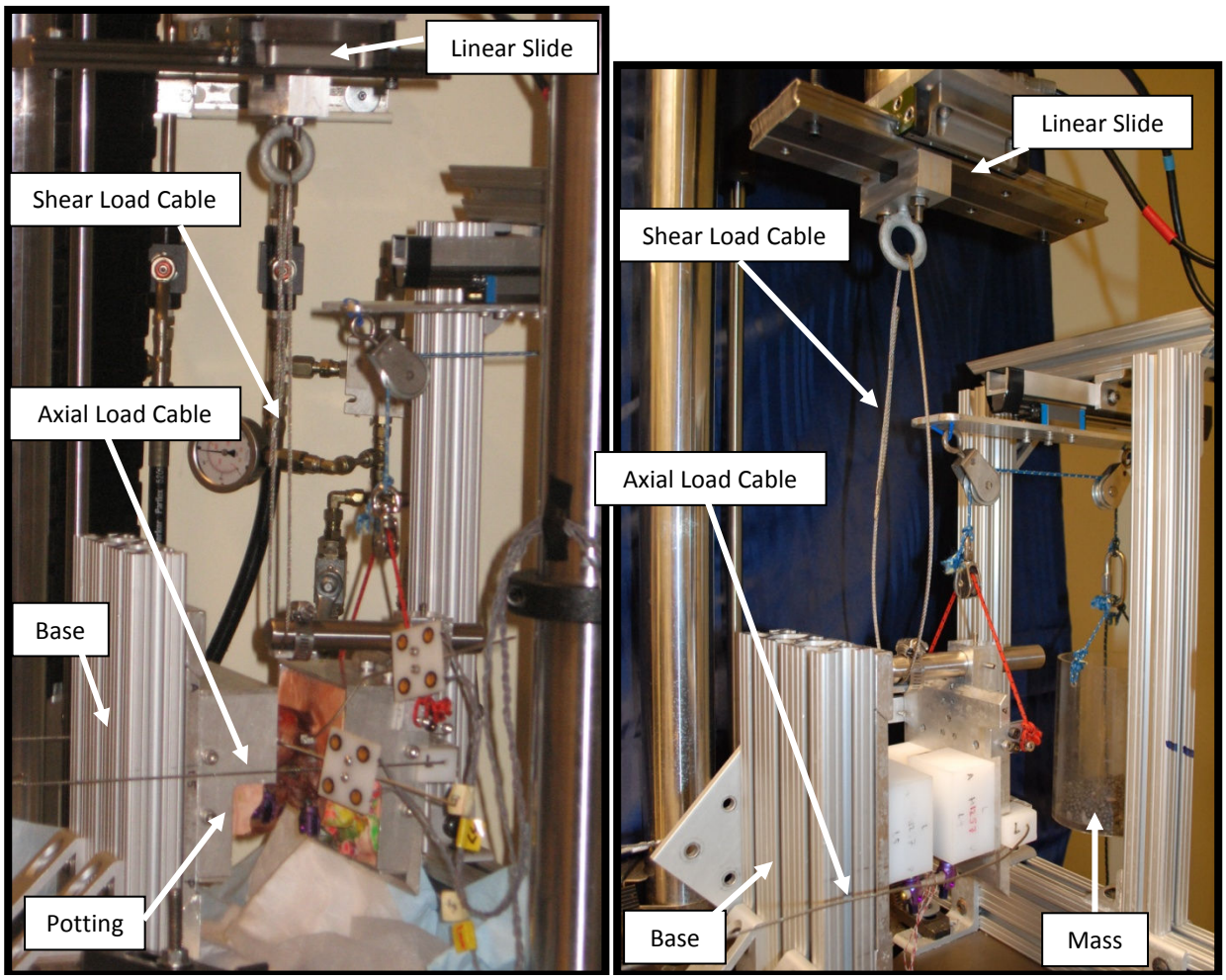

(a) (b)

Figure D-5: Images of the loading rig from the side view with (a) a specimen secured to the rig base and (b) the calibration blocks secured to the rig base.

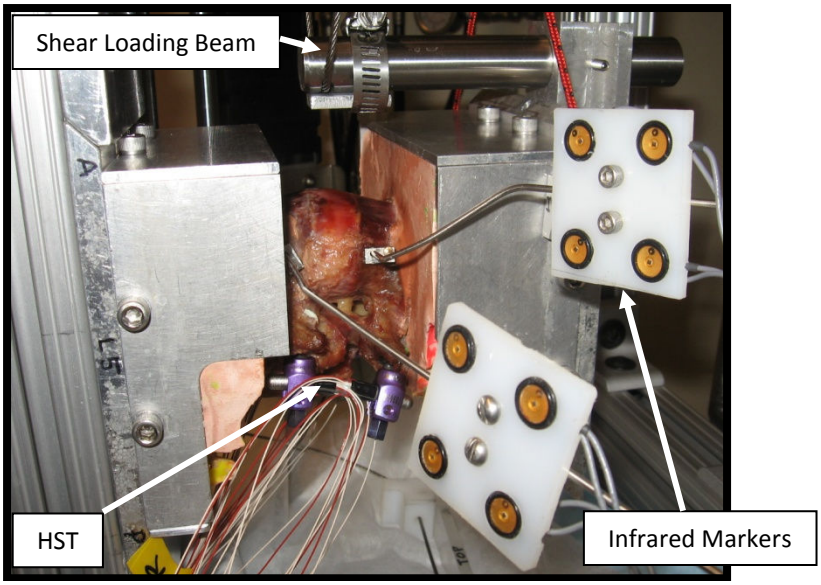

Figure D-6: Close-up view of a specimen in the loading rig with infrared markers. HST is affixed to the specimen. The anterior of the specimen is upwards and the superior vertebra is to the right.

Appendix E Additional Results

E.1 Additional Results for Chapter 2

The transducer error and reliability results presented in Chapter 2 were from an analysis of five unique transducers (four for ULST). These analyses were repeated with all available data for 15 specimens. Certain combinations of rod pairs were repeated for multiple specimens. These data are presented in this appendix for completeness.

The mean transducer error is within ±5 N for all the transducer types under the combined loading test with the largest error for the ULST (Table E-1). The errors for the isolated shear tests were larger than the errors for the other test types. The combined test did not reflect the large shear errors because of the incorporation of the offset.

The Wilcoxon Matched Pairs test showed no significant differences between the implant load as predicted by the pre-test calibration and by the post-test calibration for HST, MST and ULST (Table E-1). A significant difference was found for LST, but the difference between load-sharing values from pre- and post-test calibrations were less than 6%, below the reliability cut-off of 10%. The Bland-Altman plots for each transducer show a small positive bias for MST, LST and ULST implants (Figure E-1).

Table E-1: Numerical results of the transducer error and reliability. The mean implant errors are displayed in the first three rows for all transducer types. The P-values from the Wilcoxon Matched Pairs test are displayed in the fourth row for all transducer types (red value indicates significance).

Measure	Data Type	Transducer type			
		HST	MST	LST	ULST
Transducer Error [N] Mean (standard deviation)	Shear	4.02 (3.10)	9.06 (6.87)	6.57 (5.42)	4.94 (3.63)
	Axial	3.58 (5.44)	3.00 (1.73)	2.91 (1.76)	2.16 (1.69)
	Combined	3.79 (2.20)	3.34 (1.64)	2.77 (1.48)	4.38 (2.52)
Reliability (P-value)	Pre-Post	0.501	0.886	0.00573	0.116

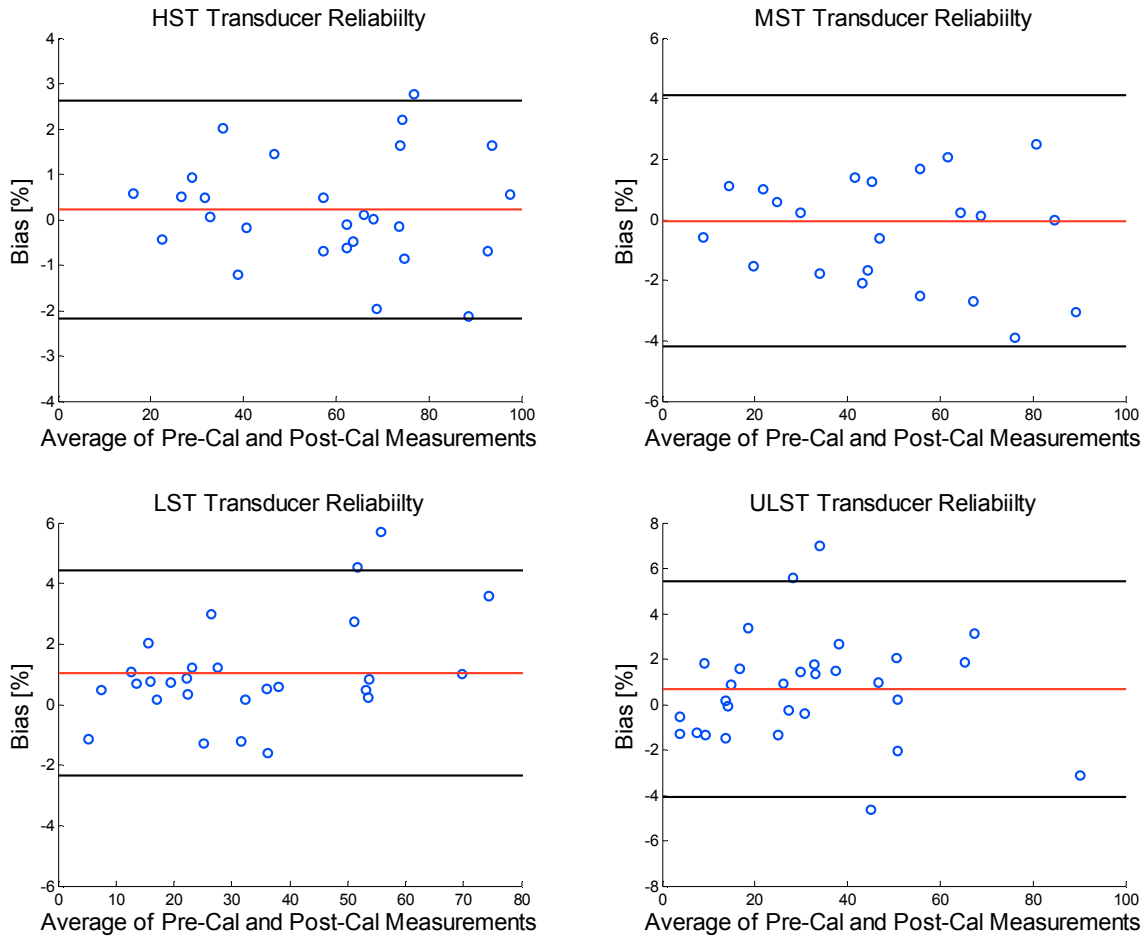

Figure E-1: Transducer reliability results displayed on Bland-Altman plots for each transducer type. The difference in implant shear load-sharing calculated using the pre-test and post-test calibrations is the bias (vertical axis), while the horizontal axis is the average of the two load-sharing measurements. The red horizontal line is the mean bias; a value of zero would indicate no systematic difference between the two measurements. The black horizontal lines are the mean bias ±2 standard deviations.

E.2 Additional Results for Chapter 3

The statistical results presented in Chapter 3 of this thesis were from an analysis of 10 specimens. The two-way repeated measures analysis of variance was also repeated with 15 specimens in which the missing data were replaced by the average of the implant load for that particular transducer type for that specimen. Both the 10 and 15 specimen analyses found similar results. One comparison from the Student-Newman-Keuls test showed significance in the 10 specimen analysis that was not found in the 15 specimen analysis. The 15 specimen analysis is presented in this appendix for completeness.

The two-way repeated measures analysis of variance was significant for both factors, specimen condition ($P<0.0001$; Figure E-2a) and fusion device type ($P<0.0001$; Figure E-2b), and the interaction of these factors ($P<0.007$; Figure E-2c, Table E-2).

The Student-Newman-Keuls test found the individual comparisons of implant load-sharing values to all be significant except for seven comparisons (bold values in Table E-3). The results indicate that LST and ULST supported a similar load across all conditions, HST and MST supported a similar load for condition 3, and MST in condition 1 supported a similar load to both LST and ULST in condition 2. The insignificant relationship that was not found in the 10 specimen analysis that was found in the 15 specimen analysis was the HST in condition 1 supported a similar load to the ULST in condition 3; however, the P-values were relatively close in both analyses, straddling the 0.05 level ($P=0.0405$ in the 10 specimen analysis and $P=0.08$ in the 15 specimen analysis). Comparisons between different implants across different specimen conditions are not clinically relevant but are provided here for completeness.

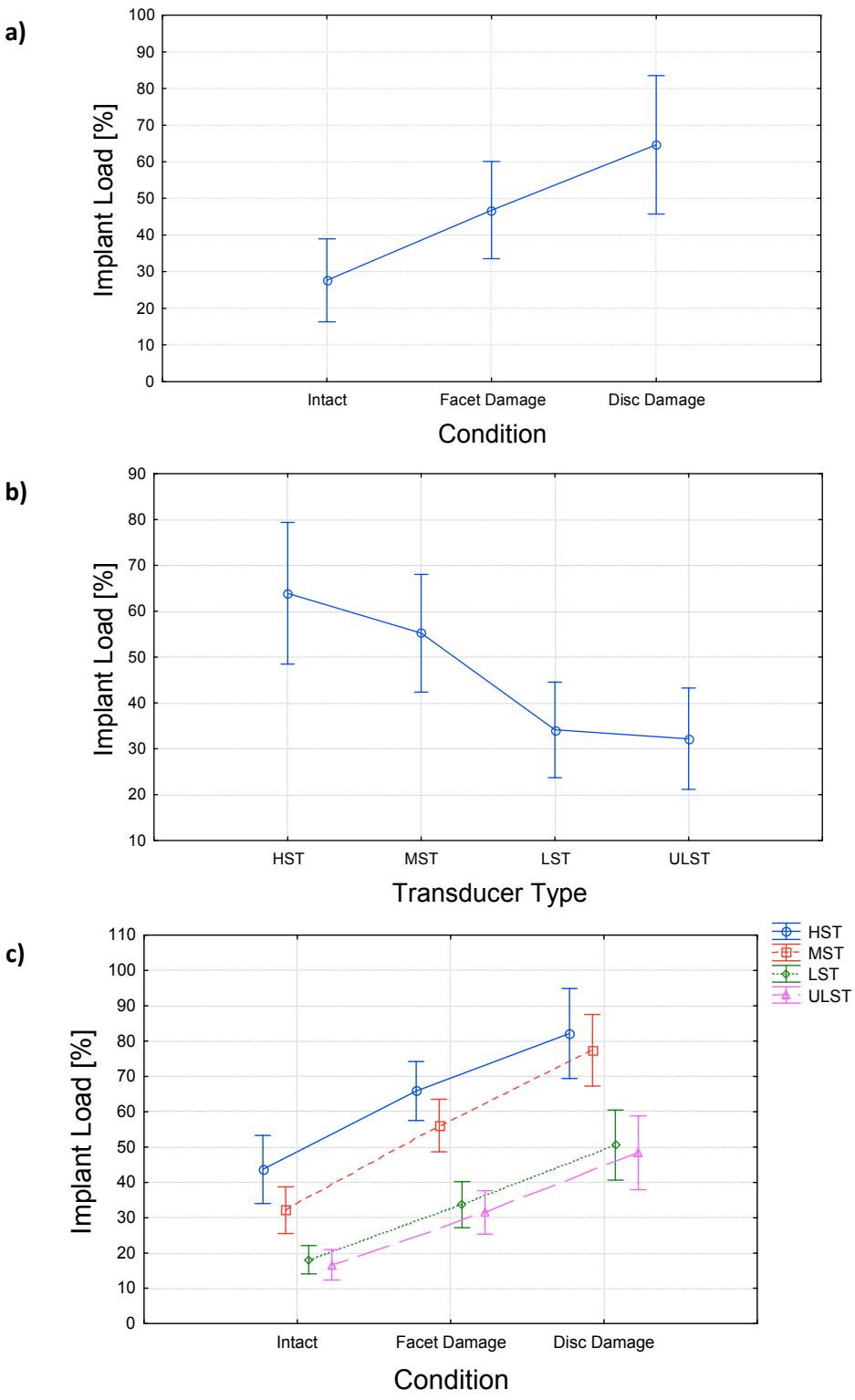

Figure E-2: Mean implant load-sharing with 95% confident intervals (vertical bars) for a significant analysis of variance for (a) the specimen condition factor, (b) the implant type factor, and (c) the interaction between specimen condition and implant type. Load on the fusion device increased as the specimen stability decreased (specimen condition increased). Implant load decreased with decreasing implant stiffness. The amount of load supported by a specific fusion type was dependent on the specimen condition (HST, disc destabilization condition).

Table E-2: Numerical results for the mean implant load-sharing. Specimen condition 1=intact, 2=facet joint destabilization, and 3=disc destabilization. Values presented as mean [%] (standard error; -95% confidence interval; +95% confidence interval)

		Implant Type			
		HST	MST	LST	ULST
Condition	1	43.7 (4.50;34.1;53.3)	32.2 (3.09;25.5;38.8)	18.1 (1.87;14.1;22.1)	16.7 (2.00;12.4;21.0)
	2	65.9 (3.90;57.5;74.2)	56.1 (3.48;48.7;63.6)	33.7 (3.05;27.2;40.3)	31.5 (2.87;25.4;37.7)
	3	82.2 (5.94;69.4;94.9)	77.4 (4.72;67.3;87.5)	50.6 (4.63;40.6;60.5)	48.4 (4.87;38.0;58.8)

Table E-3: Results of the multiple comparison Student-Newman-Keuls test showed significance for all comparisons except seven (bold). P-values have been rounded to the nearest 0.0001. Implant type is listed with specimen condition: 1=intact, 2= facet joint destabilization, and 3=disc destabilization.

		HST			MST			LST			ULST		
		1	2	3	1	2	3	1	2	3	1	2	3
HST	1		0.00012	0.0001	0.0002	0.0002	0.0001	0.0001	0.0004	0.0279	0.0001	0.0002	**0.0759**
	2			0.0001	0.0001	0.0005	0.0001	0.0001	0.0001	0.0001	0.0002	0.0001	0.0001
	3				0.0001	0.0001	**0.0730**	0.0002	0.0001	0.0001	0.0001	0.0002	0.0001
MST	1					0.0001	0.0001	0.0001	**0.5509**	0.0001	0.0001	**0.8065**	0.0001
	2						0.0001	0.0001	0.0001	0.0363	0.0001	0.0001	0.0114
	3							0.0002	0.0001	0.0001	0.0002	0.0001	0.0001
LST	1								0.0001	0.0001	**0.5881**	0.0001	0.0001
	2									0.0001	0.0001	**0.6764**	0.0001
	3										0.0001	0.0001	**0.4131**
ULST	1											0.0001	0.0001
	2												0.0001
	3												

Appendix F Example and Raw Data

Example data processed for the transducer analysis presented in Chapter 2 of this thesis are presented in this appendix. Load-sharing data from all specimens used for the results presented in Chapter 3 and Appendix E are also presented in this appendix.

F.1 Example Data for Chapter 2

The transducer error presented in Chapter 2 was found by analyzing the results from each calibration trial (Figure F-1). Three trials for each transducer type were repeated before and after specimen testing, pre- and post-test calibration. The average of 5-95% of the absolute error from the combined loading test (dashed cyan in Figure F-1c) was used to determine the transducer accuracy and repeatability presented in Chapter 2.

Bar plots show the shear load-sharing of the implant when a shear load of 250 N was applied to the specimen during testing (Figure F-2). The implant load was calculated using matrices and offset values from the pre- and post-test calibrations. The difference between the load-sharing predications for each specimen for each transducer type represented a measure of transducer reliability presented in Chapter 2.

Example plots of one combined loading test for each of the conditions of the sensitivity analysis presented in Chapter 2 are shown (Figure F-3). A plot for each of the testing conditions is presented: known and the four misalignment conditions anterior translation, medial translation, inferior translation and combined translations. The error was calculated as the absolute difference between the known applied shear load and predicted shear load for the known condition. Each of the matrices from the misaligned conditions were applied to the combined load test data for the known condition. For example, the error presented in Chapter 2 for the Medial Translation misalignment condition is the error between the predicted and applied shear loads of the Known test condition after the matrix from the misalignment condition was applied to the Known condition strain data. The statistical results to determine if the errors using the misaligned calibration blocks were larger than the known calibration block is presented in Chapter 2.

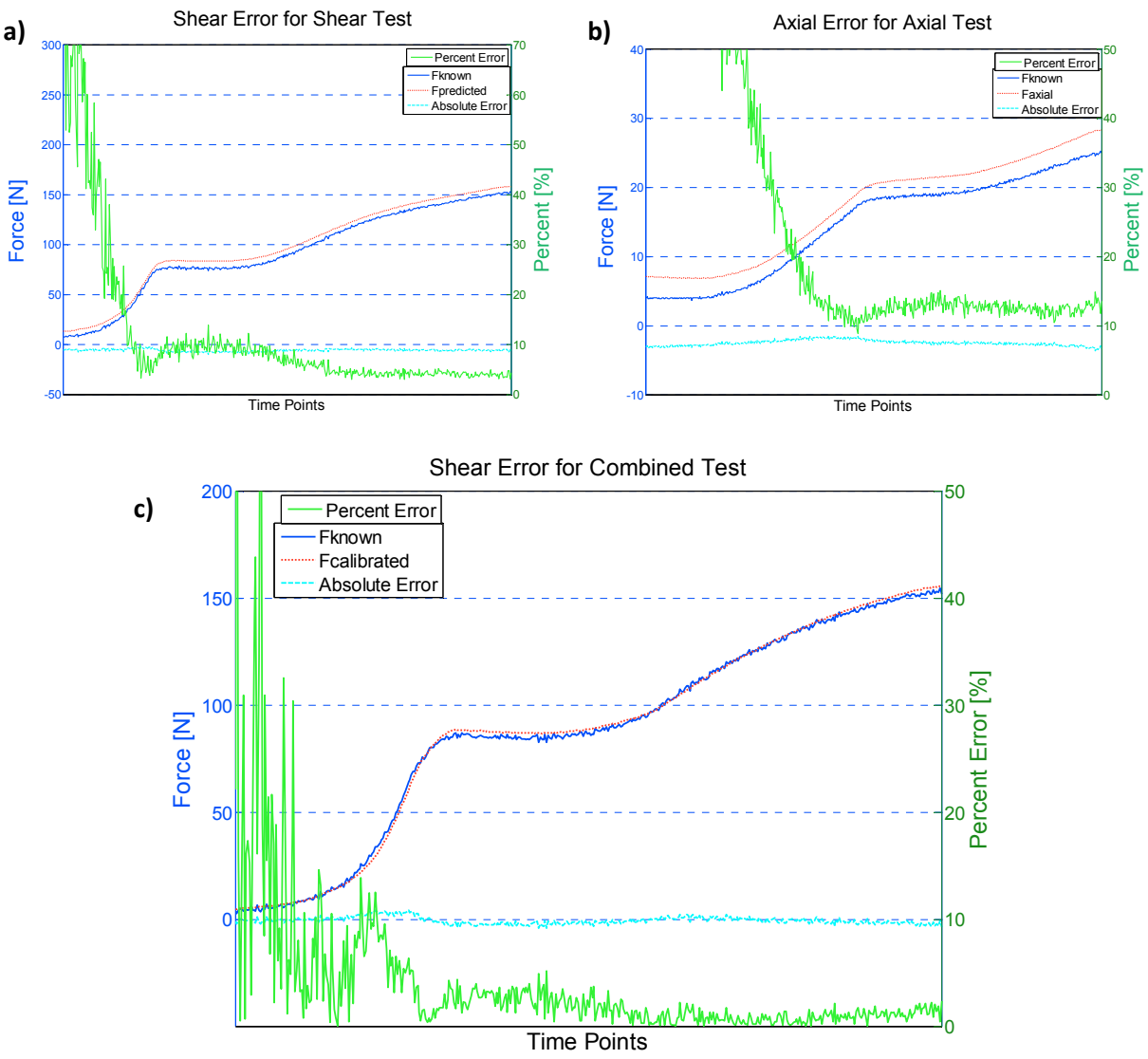

Figure F-1: Example post-calibration data from one specimen used to calculate the transducer accuracy (Specimen 2; transducer LST). Each test type, isolated shear and axial and combined, was repeated three times and the error averaged across the three trials. The absolute value of the error (light blue dashed line) shown in each of the plots for each test type was averaged over a range of 5 to 95% of the data. The combined loading error is the relevant transducer error which represents the error of the transducer in measuring shear load under a combined shear and axial load. The errors are averaged across the three repeated trials for each specimen. Results of errors for five unique transducers for each transducer type are presented in Chapter 2, and the error results for all the available transducer data were presented earlier in Appendix E.

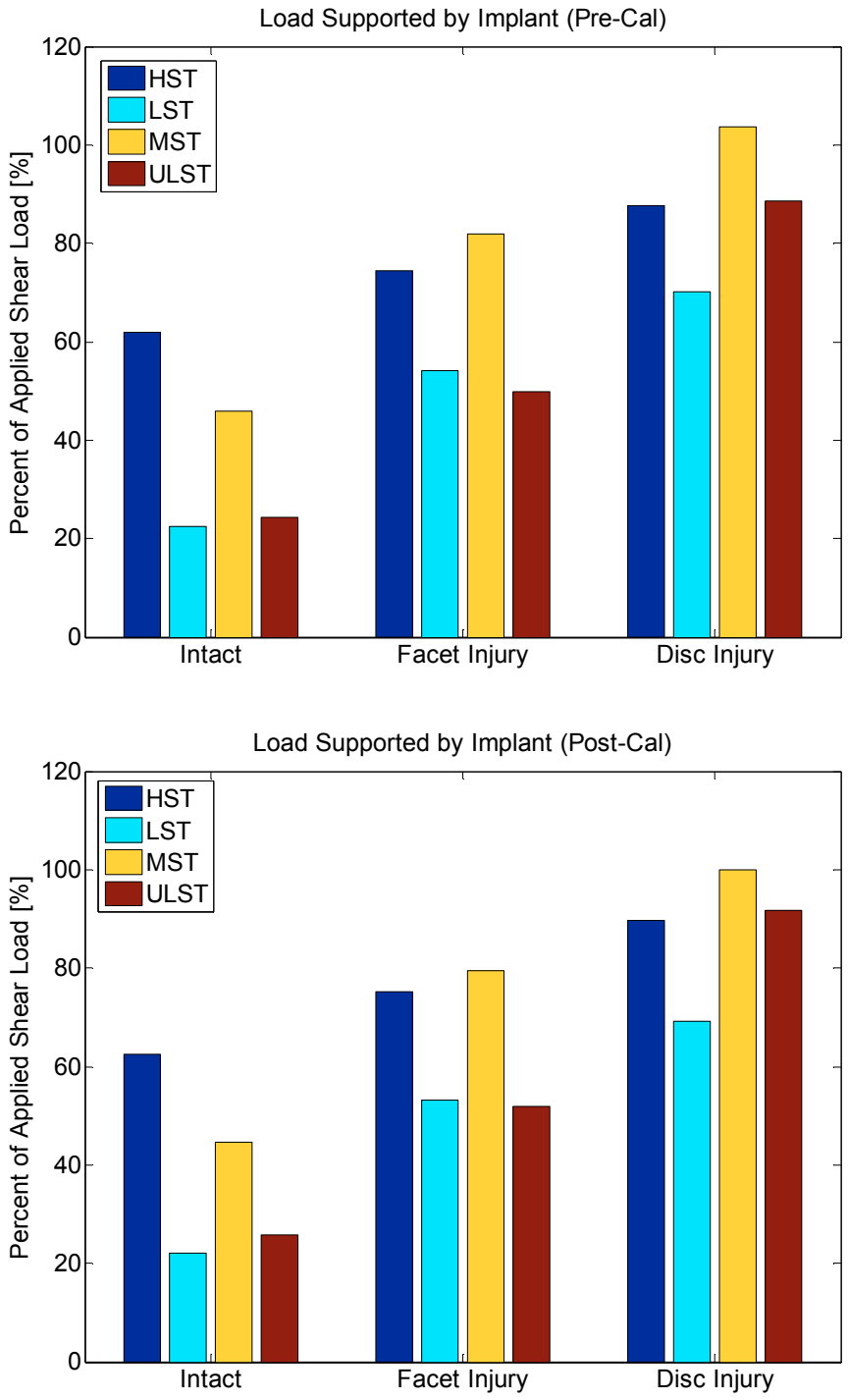

Figure F-2: Example implant load-sharing results for specimen 2. (a) Pre- and (b) Post-test calibration matrices and offsets were used to calculate the shear load supported by the implants. The difference between the pre- and post-implant load values were used to determine the transducer reliability. The difference between the pre- and post-values is called the bias and was plotted on the vertical axis of the Bland-Altman plots (Chapter 2) and the average of the two values was plotted on the horizontal axis of the Bland-Altman plots.

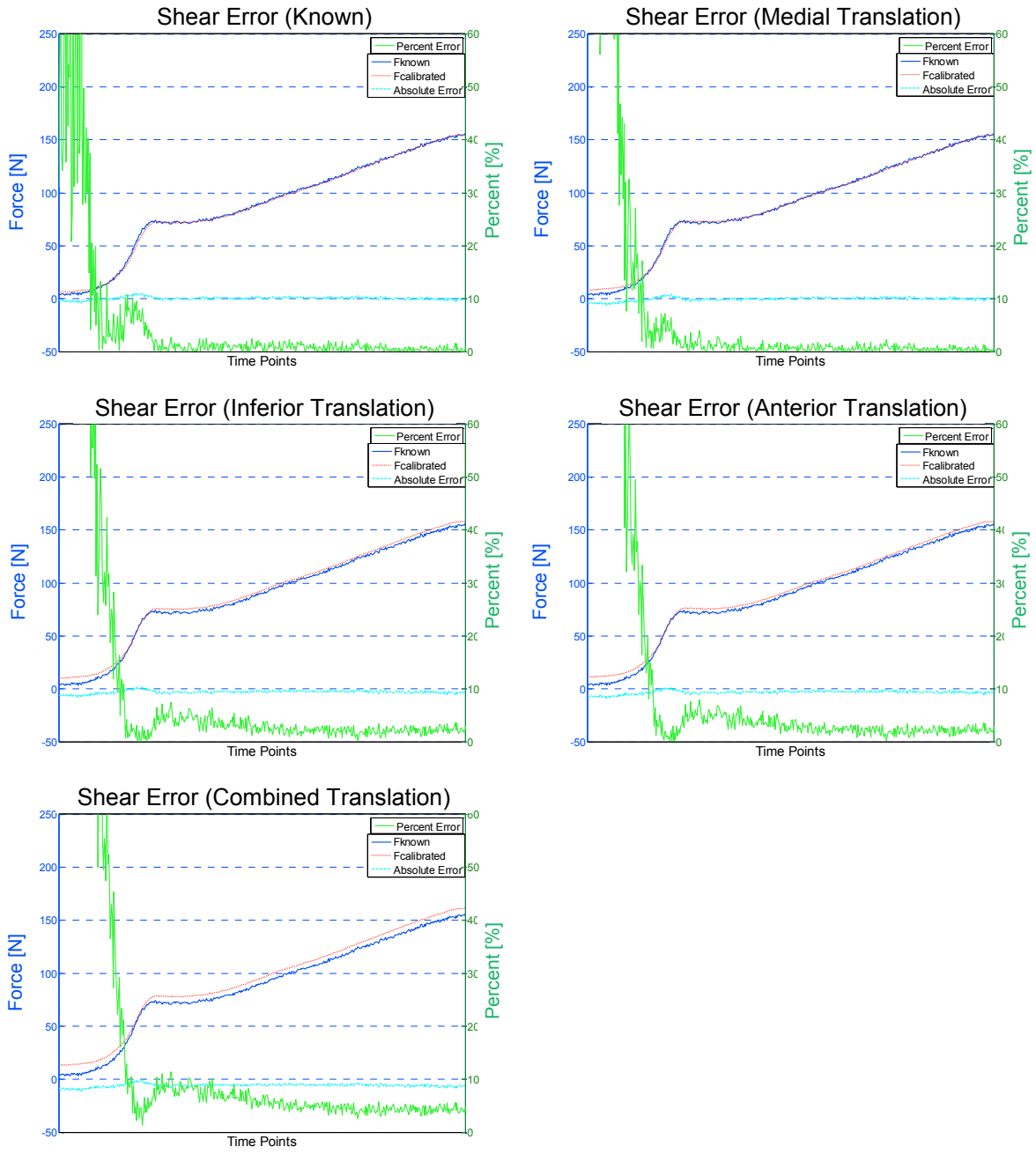

Figure F-3: Example data for each test condition from one of the three sensitivity trials for the MST. The combined loading tests are shown here; the isolated shear and axial tests are not shown.

F.2 Raw Data for Chapter 3

The implant load as a percentage of applied shear load, used for statistical analysis (Chapter 3), was found from individual specimen analysis (Table F-1). The plots of this percent implant load for all specimens over all conditions are compiled in this appendix (pages 127 to 182).

The plots show the percent of implant load for the 25th loading cycle. The vertical axis is both force [N] and percent difference [%] on the same scale. The applied force from the Instron (red) and predicted force (blue) as measured by the transducer are displayed. The percent difference between these two measurements is shown in green. The percent displayed as text on each plot is the implant load as a percentage of 250 N of applied load ("Rod pair = X%"); this value is reported in Table F-1. The implant load as calculated using the matrix and offset values from the pre- and post-calibrations are shown in the left and right columns, respectively. The specimen conditions are divided into three rows: C1=intact, C2=facet joint destabilization and C3=disc destabilization. The order of force plots are as follows: HST, MST, LST and ULST with results for each transducer type on a separate page. Some transducers did not record strain for some of the specimens (missing data as described previously in this thesis) and load was not calculated for these cases. Cases in which the pre- or post-calibration was completed incorrectly are shown, but are listed below. These "incorrect" cases were not used for the results in either Chapter 2 or 3 of this thesis.

1. Specimen 4: the pre-test calibration for all transducer types is incorrect
2. Specimen 8: the pre-test calibration for all transducer types is incorrect
3. Specimen 11: the first pre- and post-test calibrations for all transducer types were incorrect. A third calibration (post-cadaveric testing) was completed and labeled as "true" in this appendix
4. Specimen 12: the post-test calibration for all transducer types is incorrect
5. Specimen 14: the pre-test calibration for all transducer types is incorrect
6. Specimen 15: the pre-test calibration for HST is incorrect

Table F-1: Implant shear load-sharing [%] for 15 specimens. Missing data in empty cells was due to insufficient working strain gauges on the implant. For the 15 specimen analysis, the missing data was replaced by the mean of the load sharing for the transducer under the specific specimen condition. For the 10 specimen analysis, the specimens with missing data were removed (specimen # 8, 9, 10, 11, 12).

	HST			MST			LST			ULST		
	Condition			Condition			Condition			Condition		
Specimen	**1**	**2**	**3**	**1**	**2**	**3**	**1**	**2**	**3**	**1**	**2**	**3**
1	28.53	57.04	68.12	20.51	34.90	56.92	12.00	21.78	35.80	16.80	25.40	30.58
2	62.58	75.27	89.76	44.59	79.41	100.1	22.16	53.28	69.18	25.72	51.88	91.73
3	40.67	62.28	73.65	40.98	54.89	60.63	25.86	32.13	37.05	13.70	27.34	30.91
4	77.06	78.13	99.25	48.90	57.45	90.35	25.08	33.39	55.02	26.39	35.47	54.17
5	45.96	73.07	92.85	44.16	68.49	90.84	16.89	32.19	53.43	8.13	32.45	36.69
6	15.92	26.30	31.35	13.85	24.48	29.73	7.26	13.15	15.47	4.46	8.15	10.01
7	34.48	75.41	73.14	21.19	64.39	84.67	19.16	37.69	52.94	14.13	46.15	64.50
8	35.57	53.99	52.97				12.38	20.61	22.55	16.68	27.71	35.93
9	39.38	64.01	97.33				14.49	25.00	52.87	14.46	25.61	50.64
10	32.77	65.86	93.05							15.99	31.98	49.50
11	72.06	69.37	105.7				31.14	44.05	46.61	27.17	38.61	51.77
12	44.09	63.06	127.2				15.15	37.58	83.34			
13	22.72	57.55	69.74	9.10	45.21	78.17	5.90	22.51	49.51	4.13	14.40	47.42
14	44.99	70.89	73.94	31.10	63.32	77.28	19.10	48.95	61.44	16.59	39.34	57.84
15	58.60	95.79	84.68	47.14	68.72	105.6	26.88	49.78	72.52	29.15	36.63	65.89
Average	43.69	65.87	82.18	32.15	56.13	77.42	18.10	33.72	50.55	16.68	31.51	48.40
Standard Deviation	17.41	15.10	22.99	14.93	16.83	22.81	7.51	12.26	18.59	8.05	11.52	19.56

Specimen 1

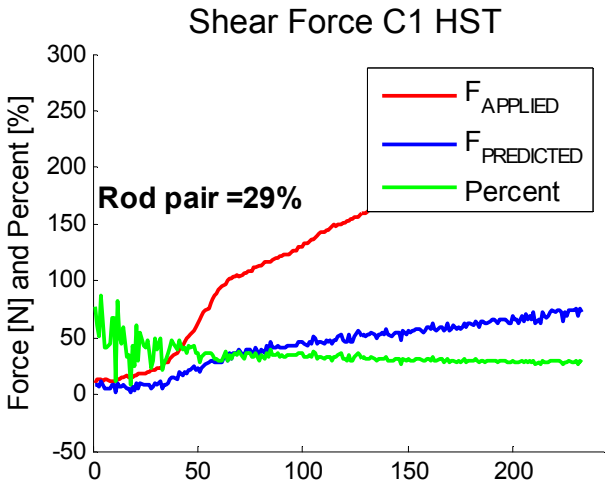
Shear Force C1 HST
F APPLIED
F PREDICTED
Percent
Rod pair =29%
Force [N] and Percent [%]

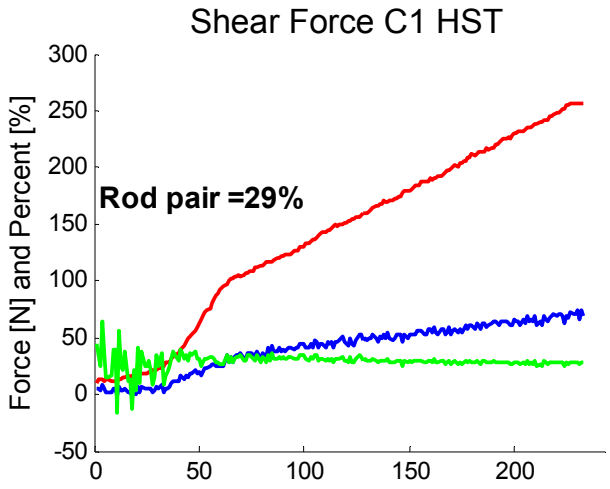
Shear Force C1 HST
Rod pair =29%
Force [N] and Percent [%]

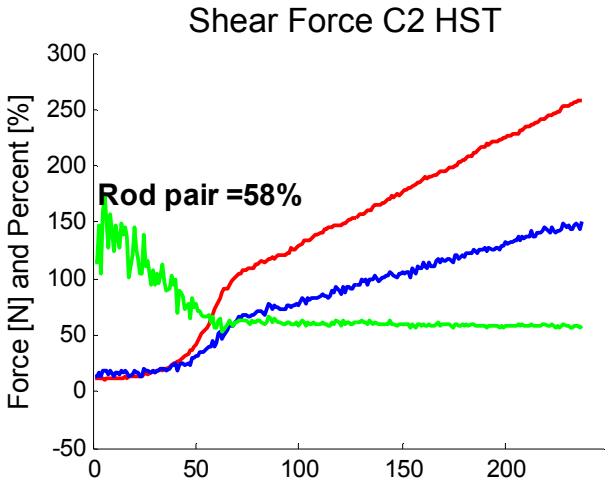
Shear Force C2 HST
Rod pair =58%
Force [N] and Percent [%]

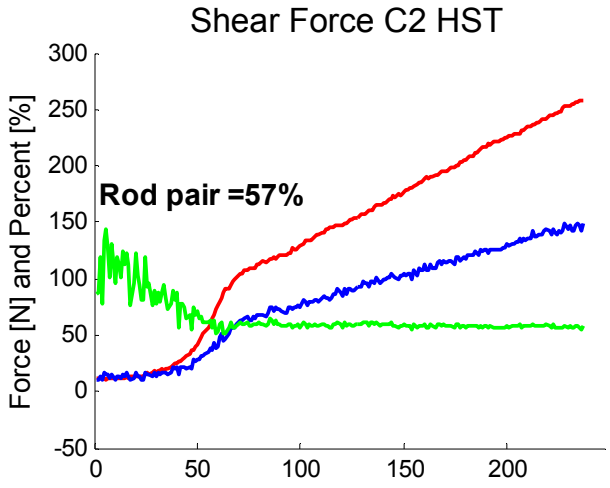
Shear Force C2 HST
Rod pair =57%
Force [N] and Percent [%]

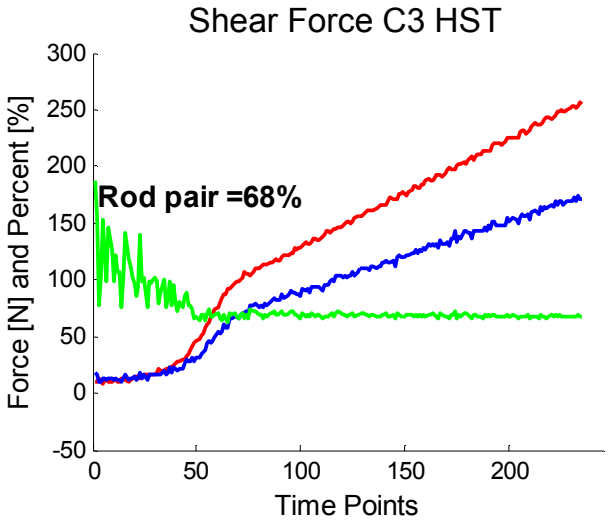
Shear Force C3 HST
Rod pair =68%
Force [N] and Percent [%]
Time Points

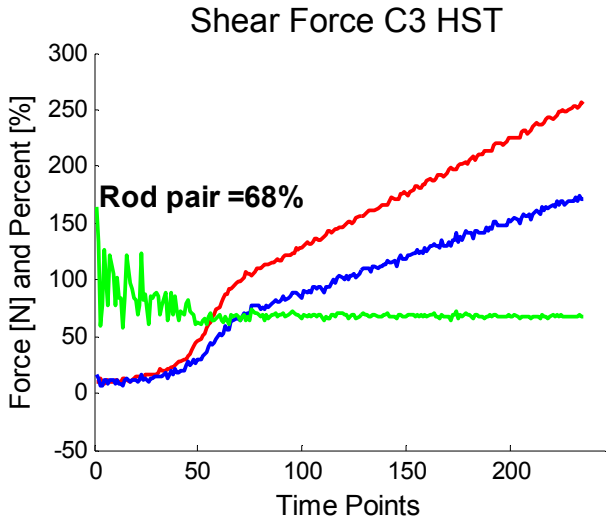
Shear Force C3 HST
Rod pair =68%
Force [N] and Percent [%]
Time Points

Specimen 1

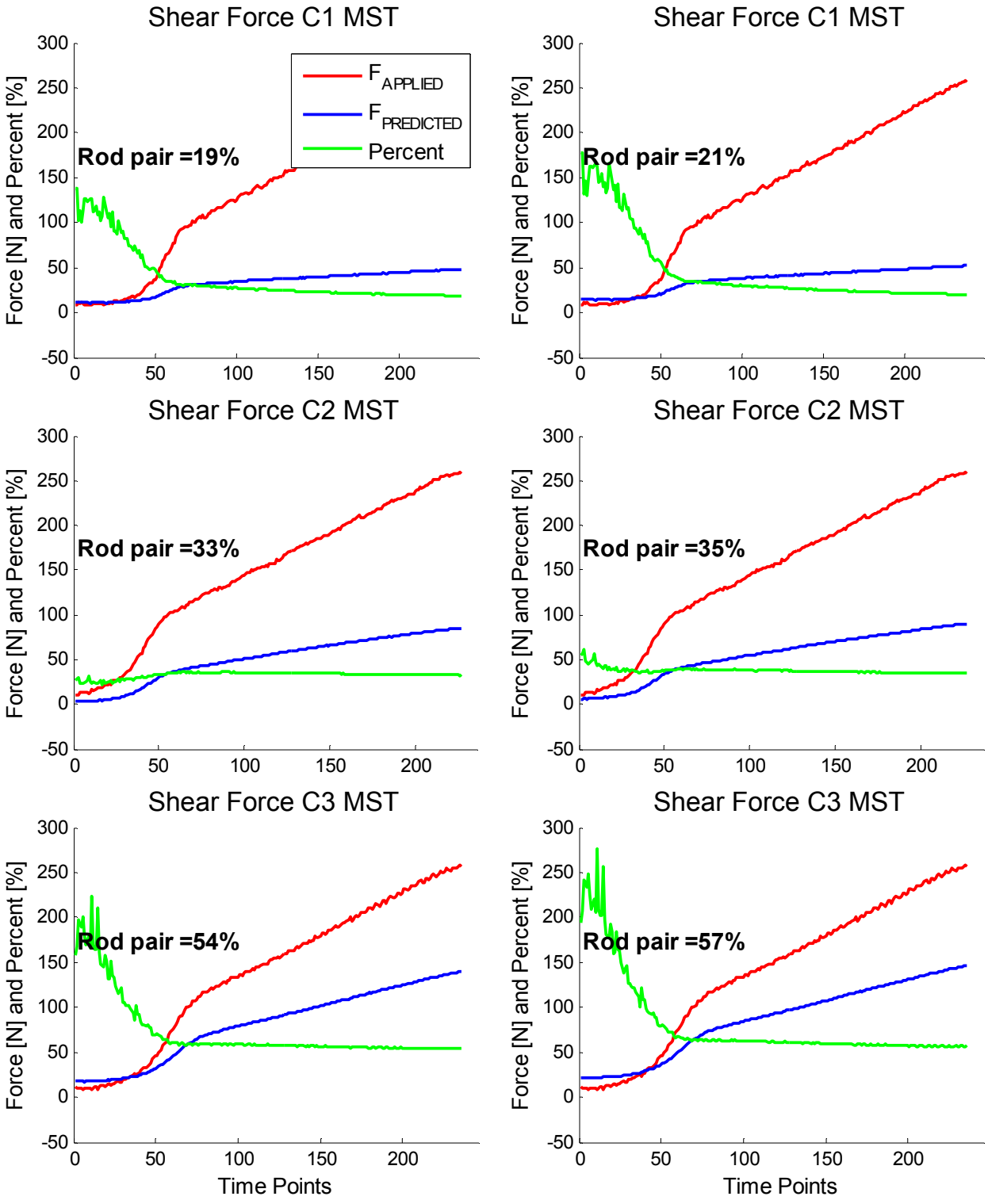
Shear Force C1 MST
Force [N] and Percent [%]
F APPLIED
F PREDICTED
Percent
Rod pair =19%
Shear Force C1 MST
Force [N] and Percent [%]
Rod pair =21%
Shear Force C2 MST
Force [N] and Percent [%]
Rod pair =33%
Shear Force C2 MST
Force [N] and Percent [%]
Rod pair =35%
Shear Force C3 MST
Force [N] and Percent [%]
Rod pair =54%
Time Points
Shear Force C3 MST
Force [N] and Percent [%]
Rod pair =57%
Time Points

Specimen 1

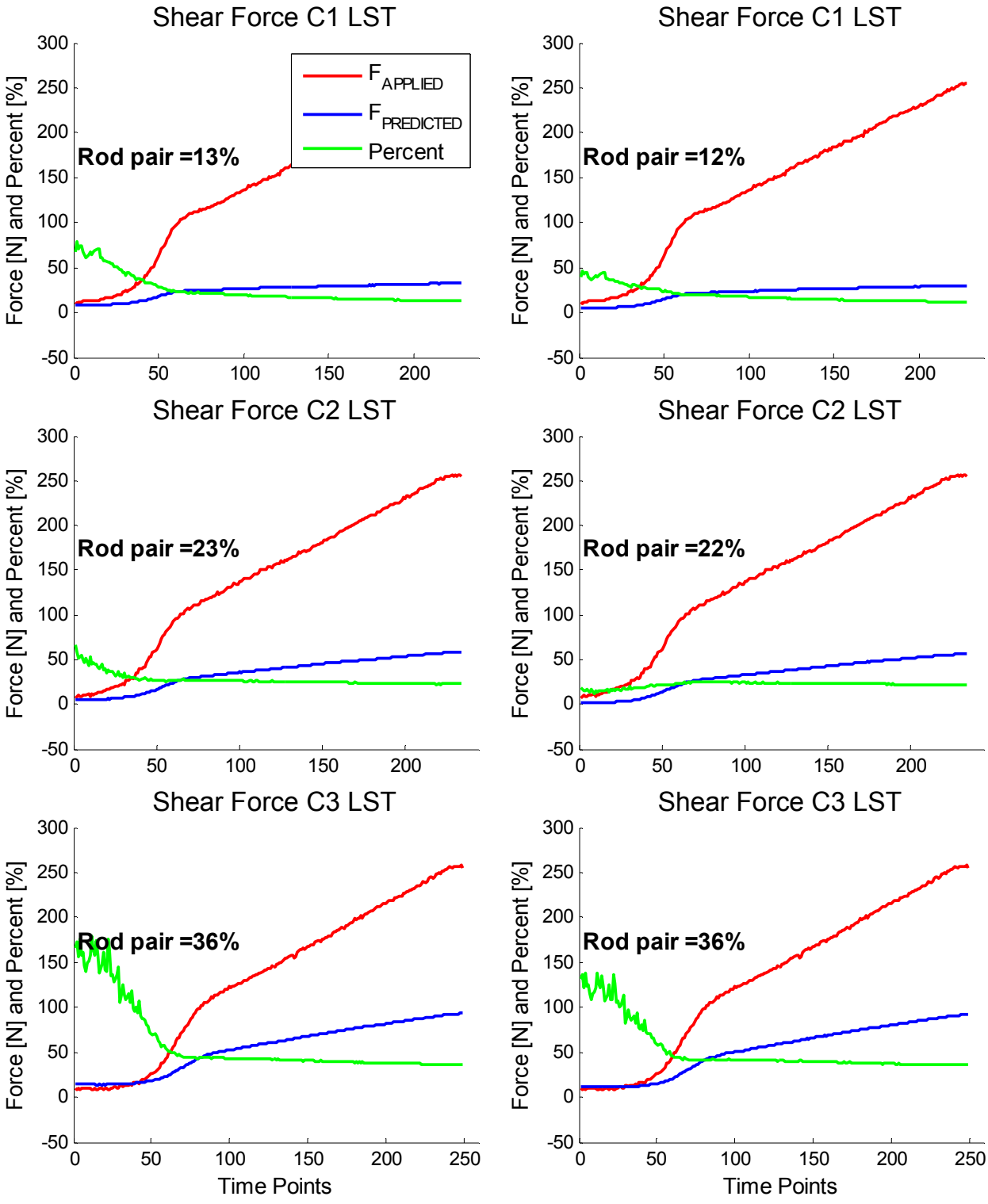
Shear Force C1 LST
Force [N] and Percent [%]
F APPLIED
F PREDICTED
Percent
Rod pair =13%
Shear Force C1 LST
Force [N] and Percent [%]
Rod pair =12%
Shear Force C2 LST
Force [N] and Percent [%]
Rod pair =23%
Shear Force C2 LST
Force [N] and Percent [%]
Rod pair =22%
Shear Force C3 LST
Force [N] and Percent [%]
Rod pair =36%
Time Points
Shear Force C3 LST
Force [N] and Percent [%]
Rod pair =36%
Time Points

Specimen 1

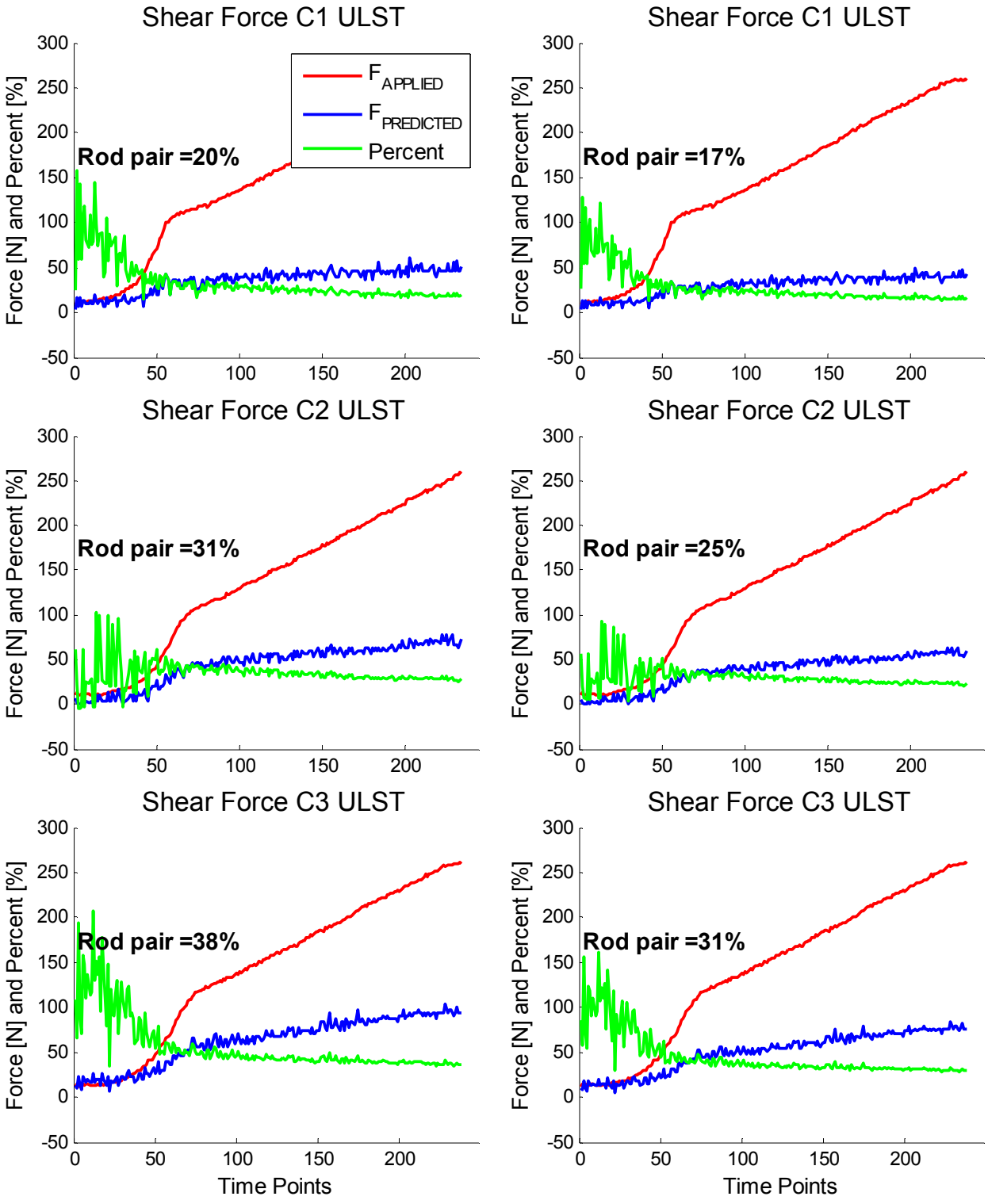
Shear Force C1 ULST
Force [N] and Percent [%]
F APPLIED
F PREDICTED
Percent
Rod pair =20%
Shear Force C1 ULST
Force [N] and Percent [%]
Rod pair =17%
Shear Force C2 ULST
Force [N] and Percent [%]
Rod pair =31%
Shear Force C2 ULST
Force [N] and Percent [%]
Rod pair =25%
Shear Force C3 ULST
Force [N] and Percent [%]
Rod pair =38%
Time Points
Shear Force C3 ULST
Force [N] and Percent [%]
Rod pair =31%
Time Points

Specimen 2

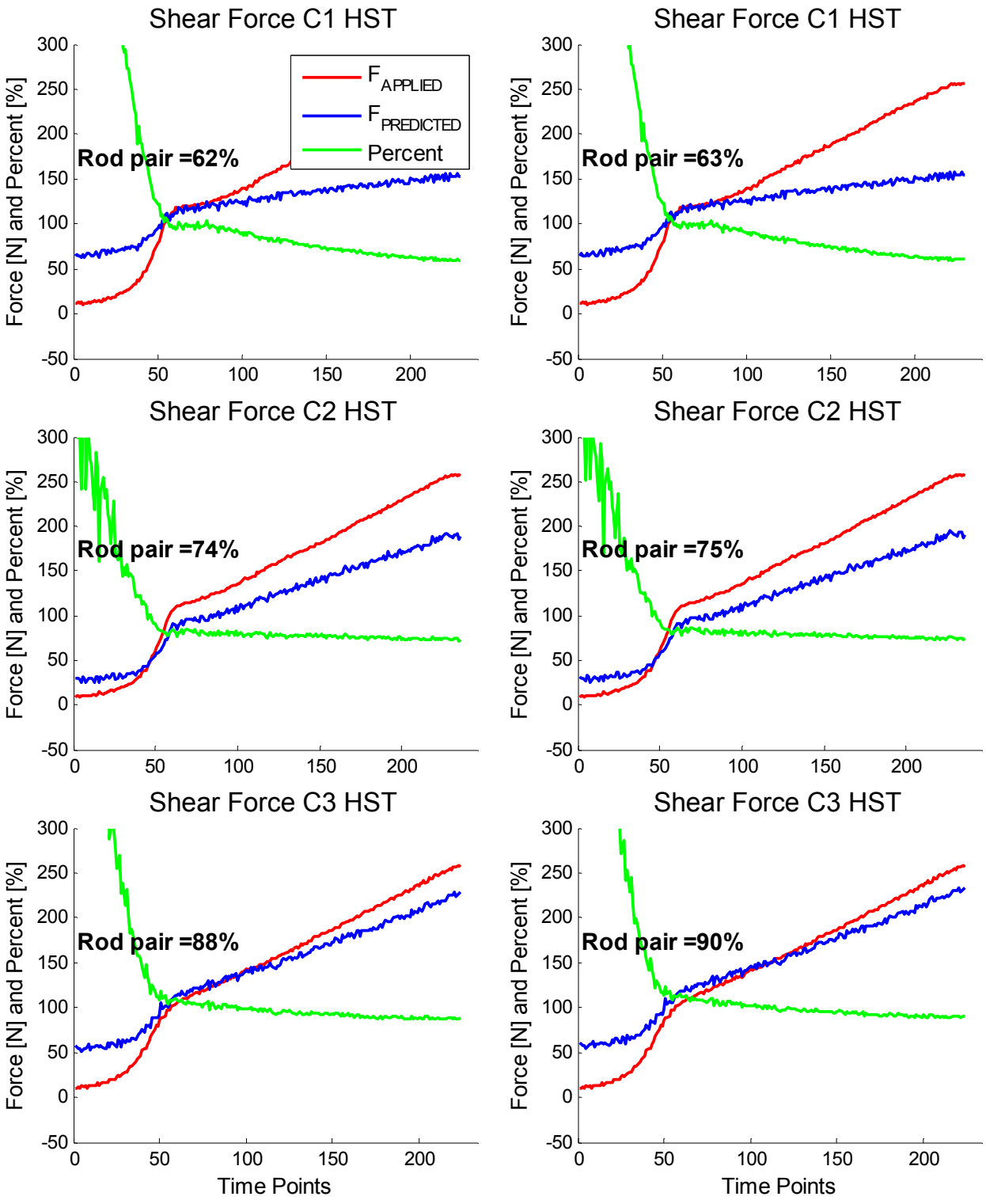
Shear Force C1 HST
Force [N] and Percent [%]
F APPLIED
F PREDICTED
Percent
Rod pair =62%
Shear Force C1 HST
Rod pair =63%
Shear Force C2 HST
Rod pair =74%
Shear Force C2 HST
Rod pair =75%
Shear Force C3 HST
Rod pair =88%
Shear Force C3 HST
Rod pair =90%
Time Points
Time Points

Specimen 2

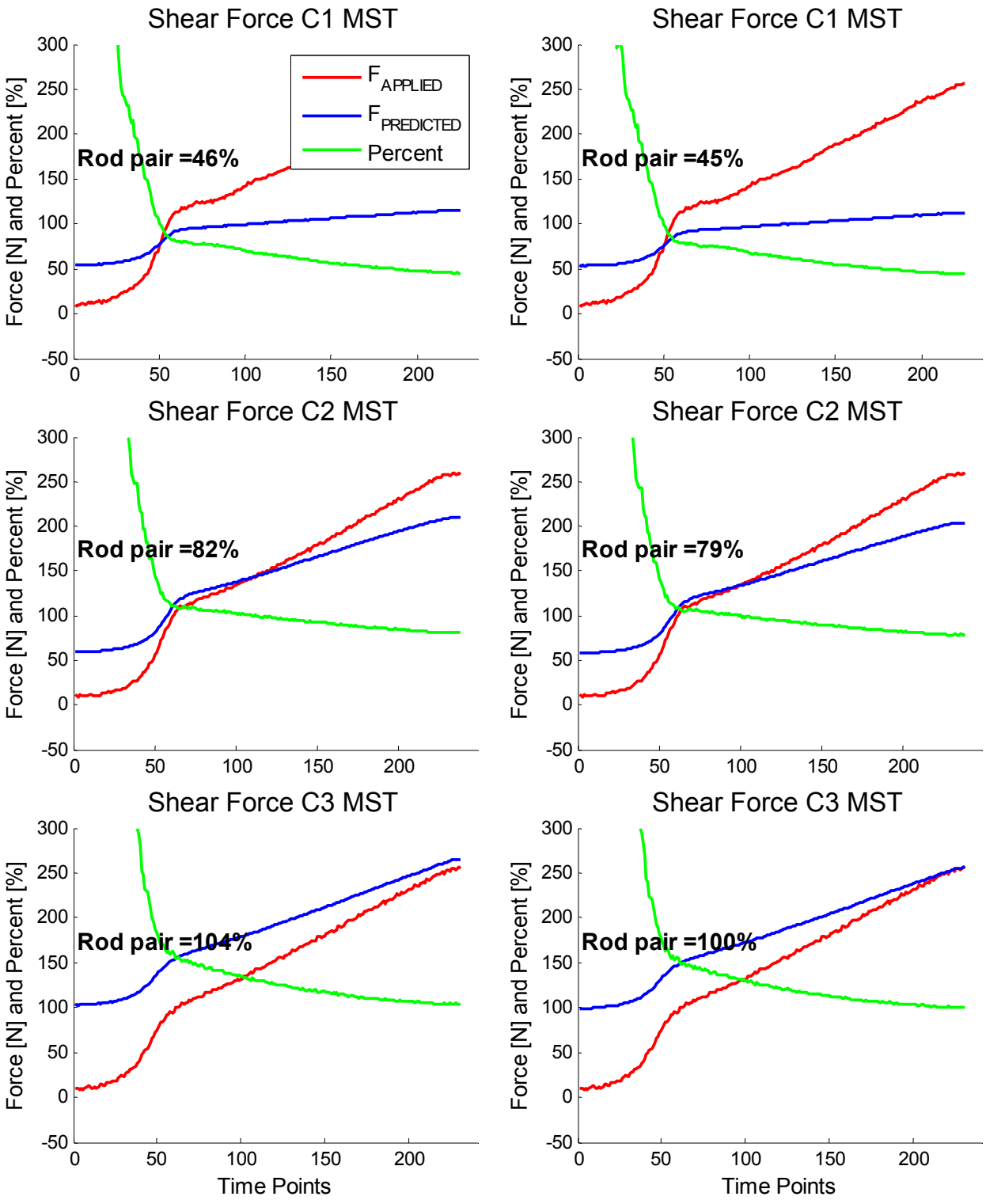
Shear Force C1 MST
Force [N] and Percent [%]
F APPLIED
F PREDICTED
Percent
Rod pair =46%
Shear Force C1 MST
Rod pair =45%
Shear Force C2 MST
Rod pair =82%
Shear Force C2 MST
Rod pair =79%
Shear Force C3 MST
Rod pair =104%
Shear Force C3 MST
Rod pair =100%
Time Points
Time Points

Specimen 2

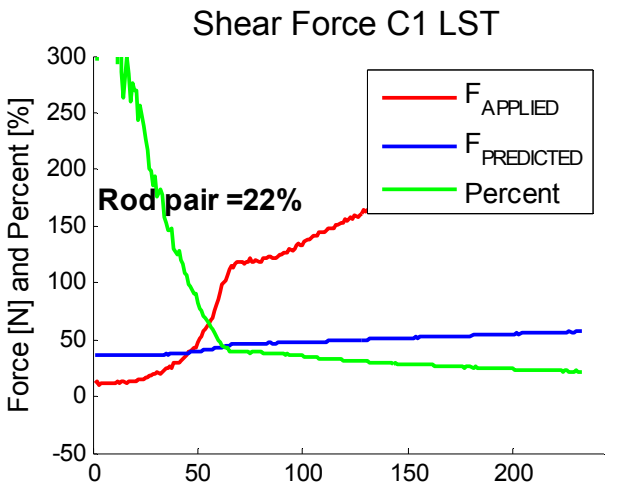
Shear Force C1 LST
F APPLIED
F PREDICTED
Percent
Rod pair =22%
Force [N] and Percent [%]

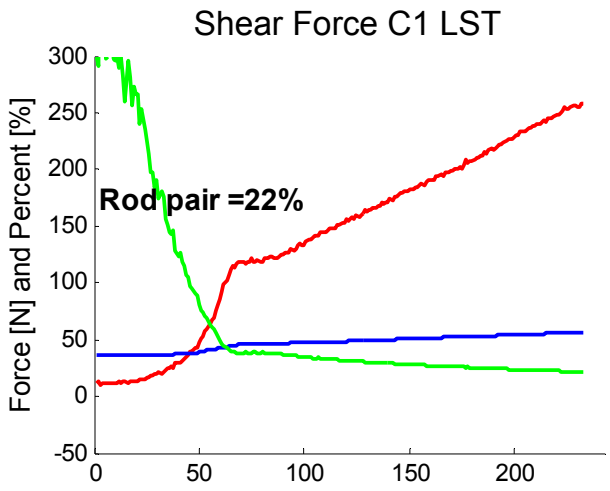
Shear Force C1 LST
Rod pair =22%
Force [N] and Percent [%]

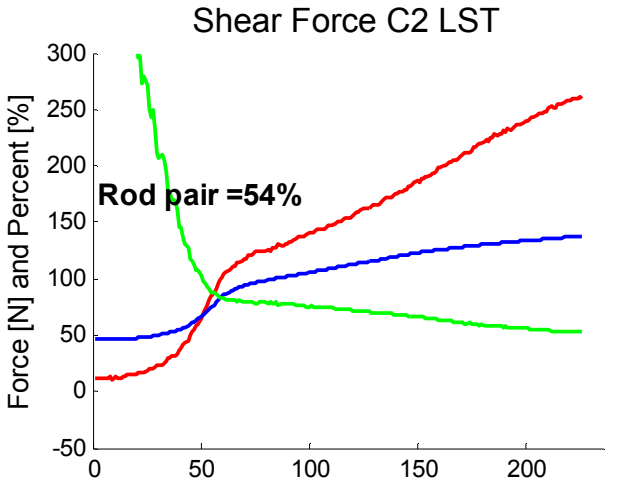
Shear Force C2 LST
Rod pair =54%
Force [N] and Percent [%]

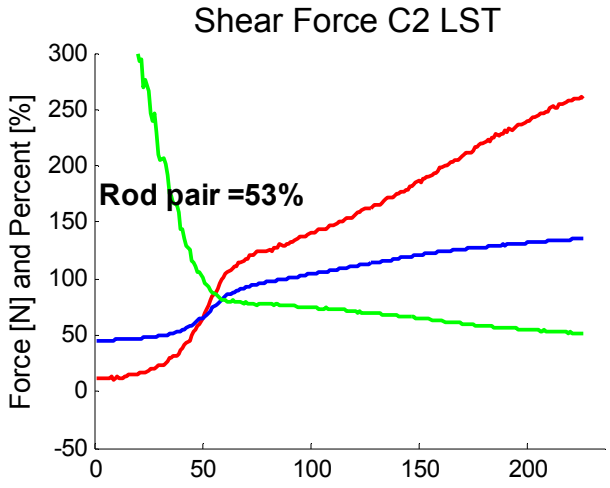
Shear Force C2 LST
Rod pair =53%
Force [N] and Percent [%]

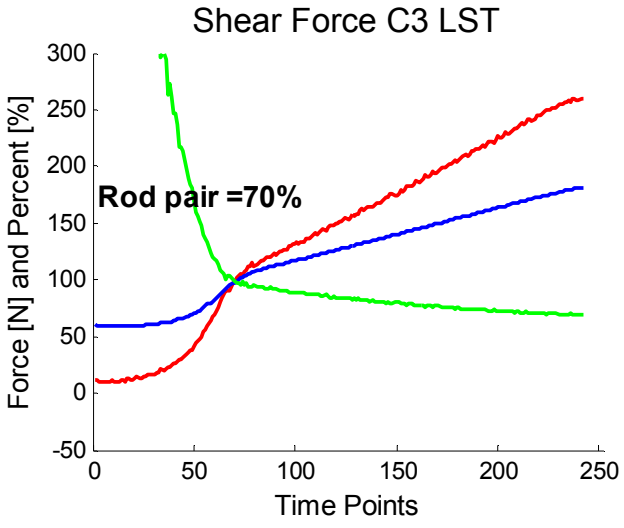
Shear Force C3 LST
Rod pair =70%
Force [N] and Percent [%]
Time Points

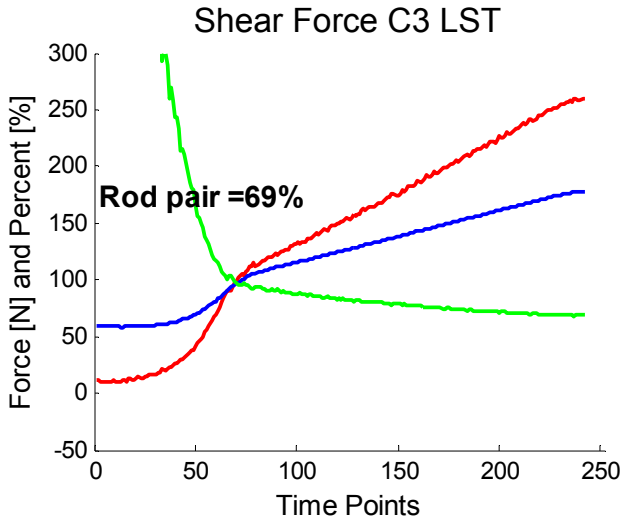
Shear Force C3 LST
Rod pair =69%
Force [N] and Percent [%]
Time Points

Specimen 2

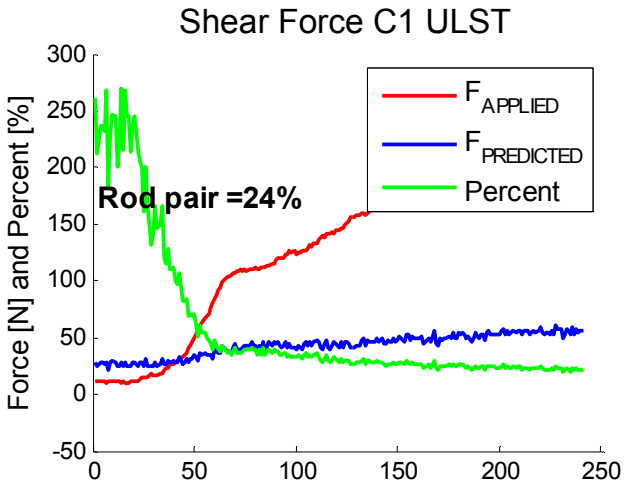
Shear Force C1 ULST
F APPLIED
F PREDICTED
Percent
Rod pair =24%
Force [N] and Percent [%]

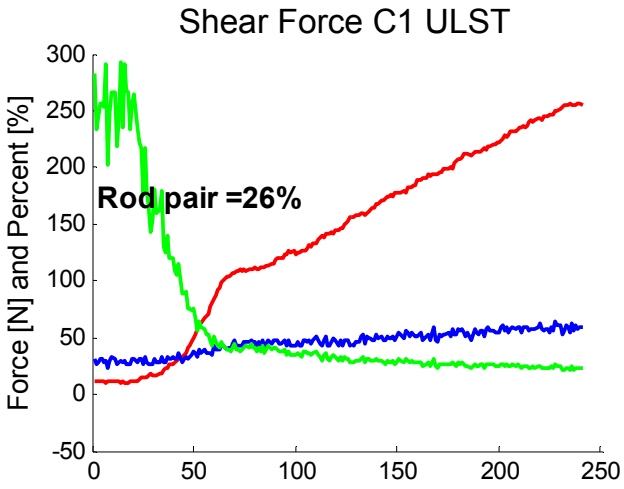
Shear Force C1 ULST
Rod pair =26%
Force [N] and Percent [%]

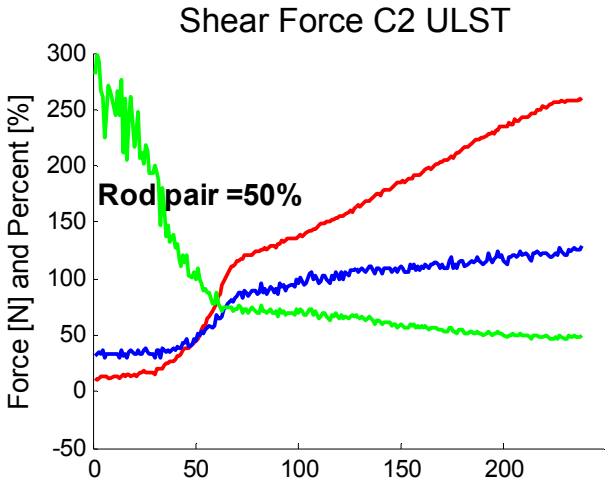
Shear Force C2 ULST
Rod pair =50%
Force [N] and Percent [%]

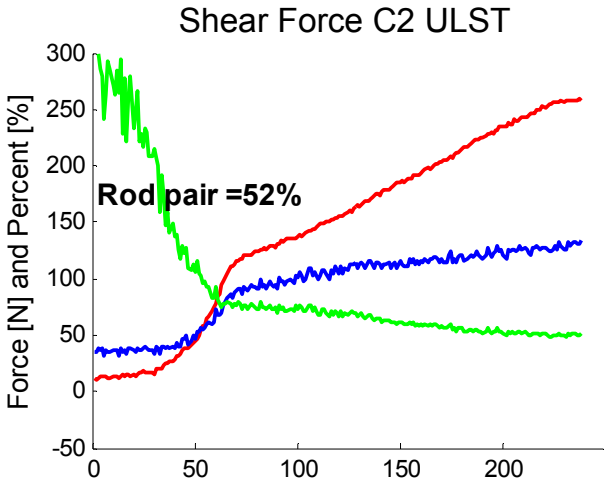
Shear Force C2 ULST
Rod pair =52%
Force [N] and Percent [%]

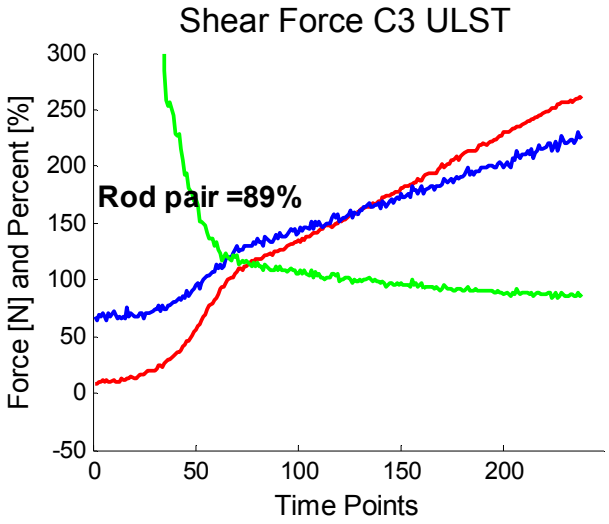
Shear Force C3 ULST
Rod pair =89%
Force [N] and Percent [%]
Time Points

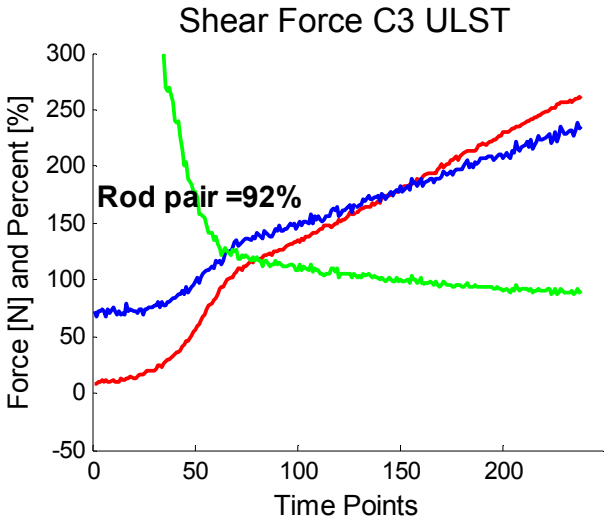
Shear Force C3 ULST
Rod pair =92%
Force [N] and Percent [%]
Time Points

Specimen 3

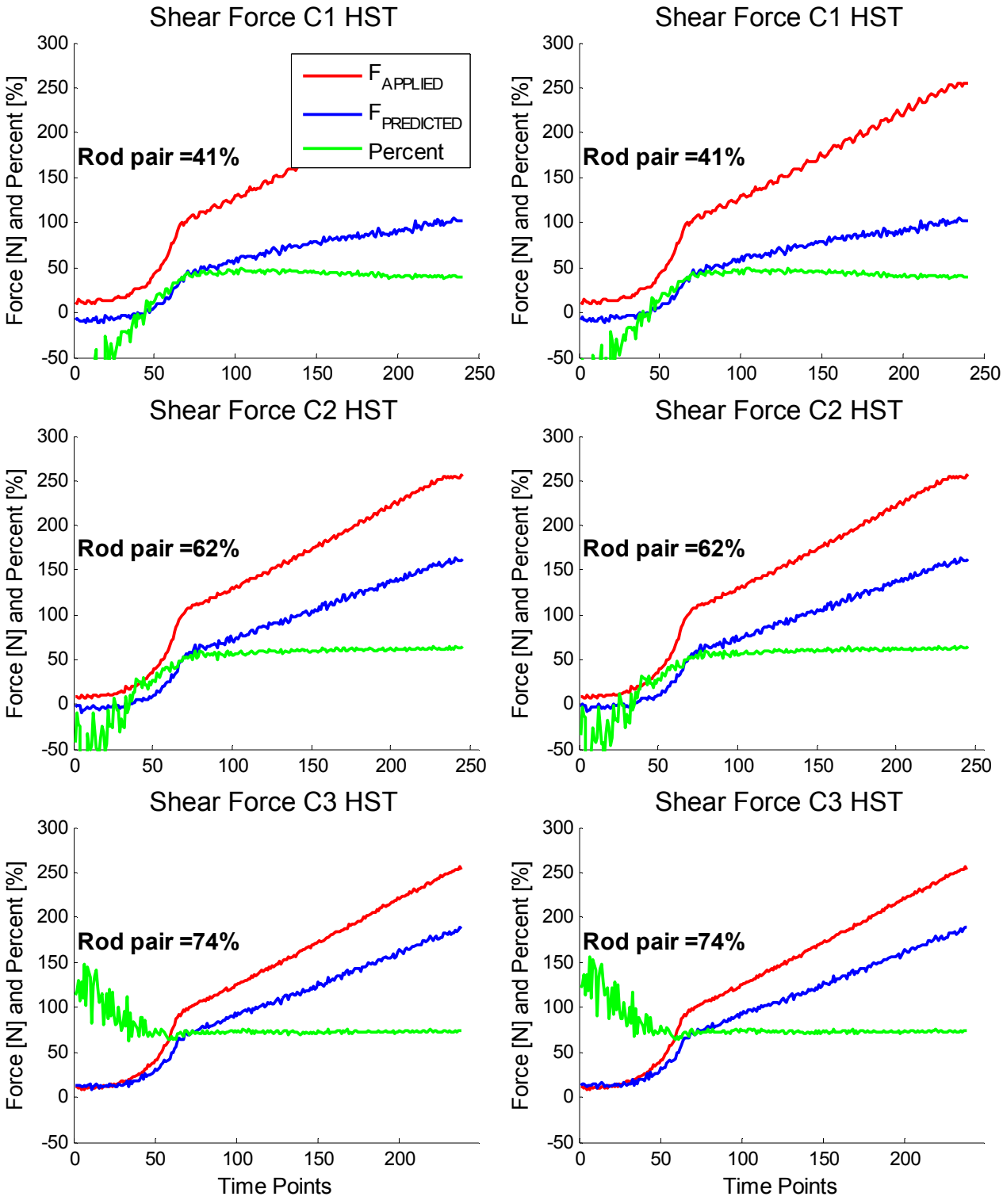
Shear Force C1 HST
Rod pair =41%
F APPLIED
F PREDICTED
Percent
Force [N] and Percent [%]
Shear Force C2 HST
Rod pair =62%
Shear Force C3 HST
Rod pair =74%
Time Points

Specimen 3

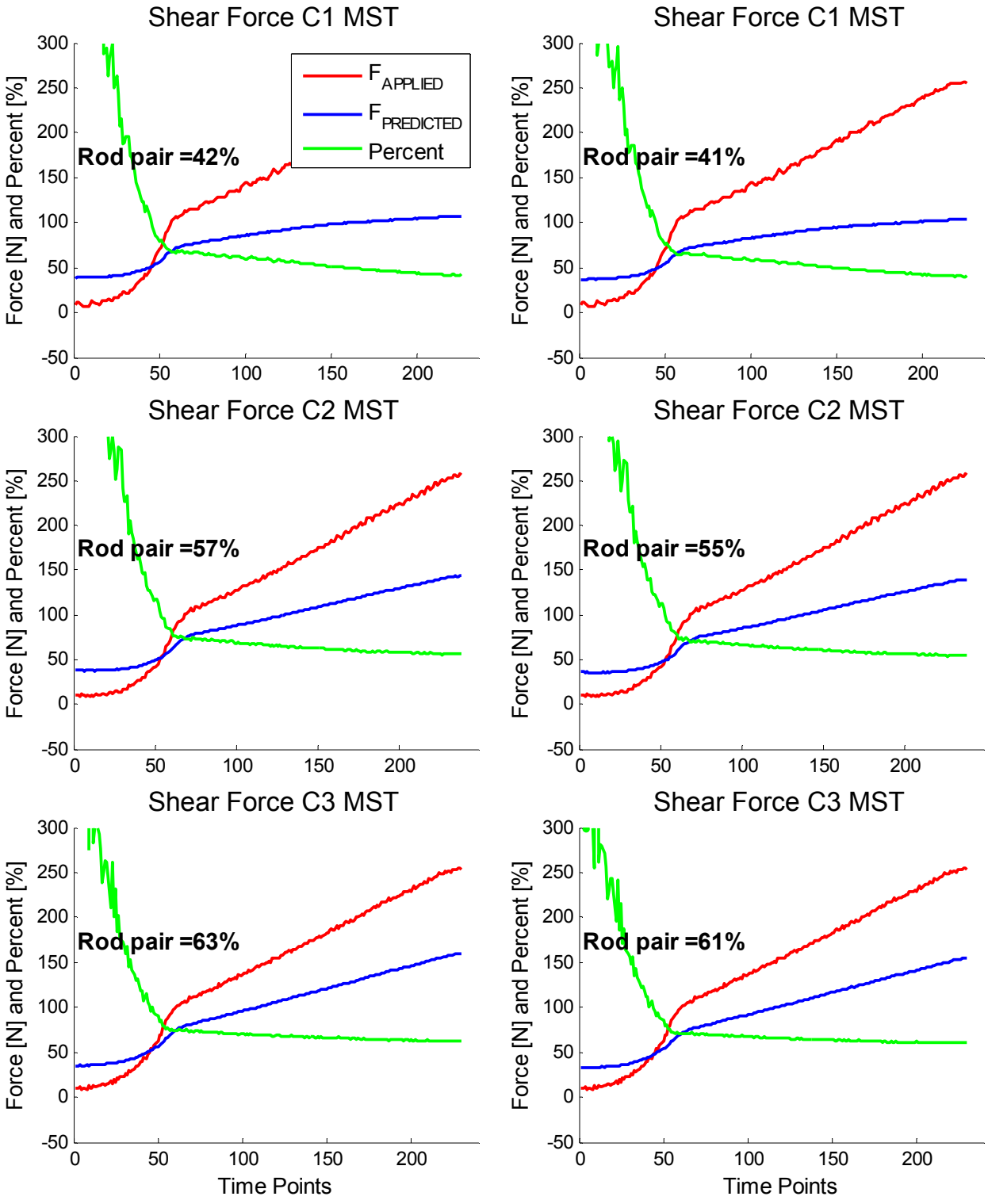
Shear Force C1 MST
Force [N] and Percent [%]
F APPLIED
F PREDICTED
Percent
Rod pair =42%
Shear Force C1 MST
Rod pair =41%
Shear Force C2 MST
Rod pair =57%
Shear Force C2 MST
Rod pair =55%
Shear Force C3 MST
Rod pair =63%
Shear Force C3 MST
Rod pair =61%
Time Points
Time Points

Specimen 3

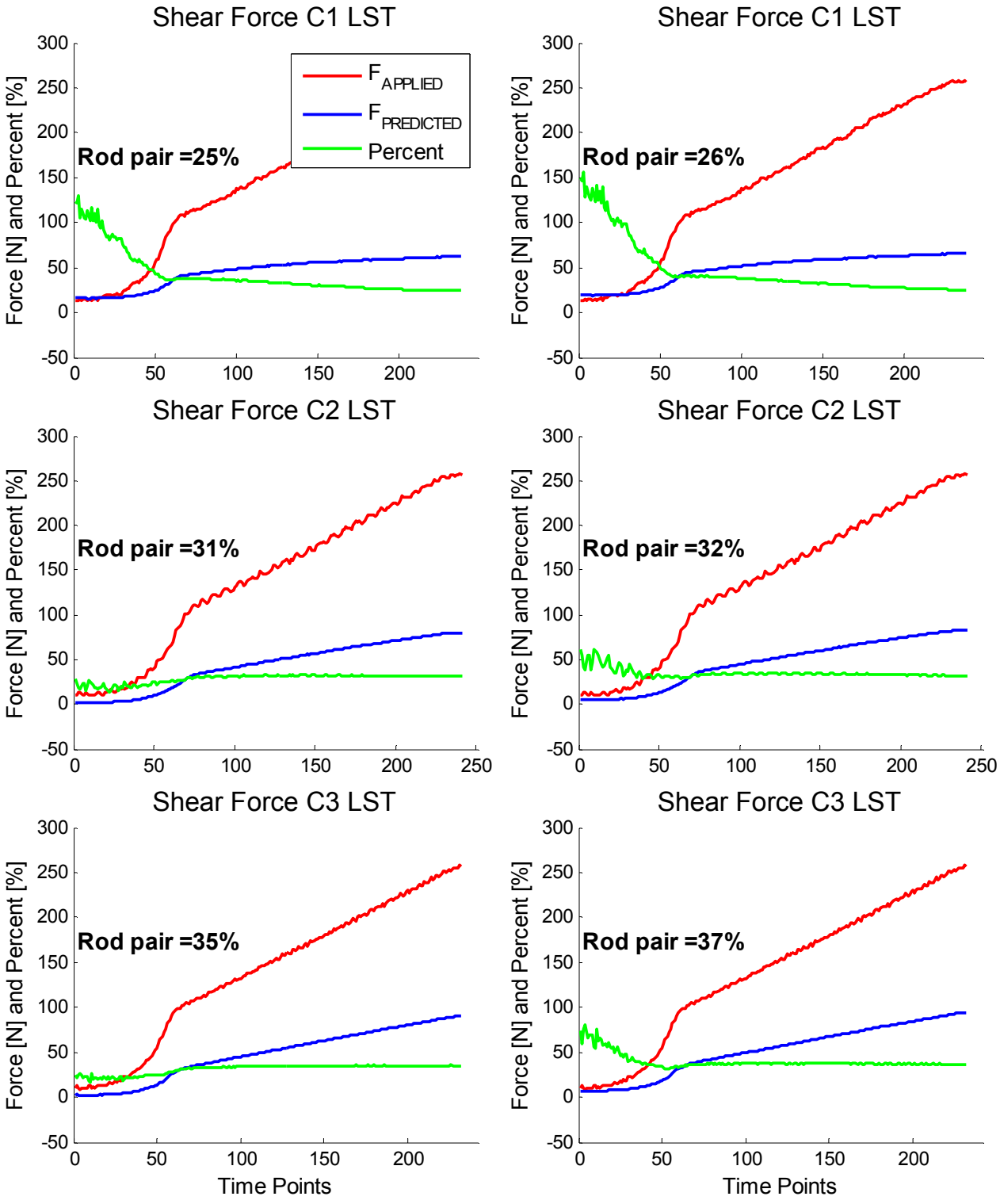
Shear Force C1 LST
Force [N] and Percent [%]
F APPLIED
F PREDICTED
Percent
Rod pair =25%
Shear Force C1 LST
Rod pair =26%
Shear Force C2 LST
Rod pair =31%
Shear Force C2 LST
Rod pair =32%
Shear Force C3 LST
Rod pair =35%
Shear Force C3 LST
Rod pair =37%
Time Points
Time Points

Specimen 3

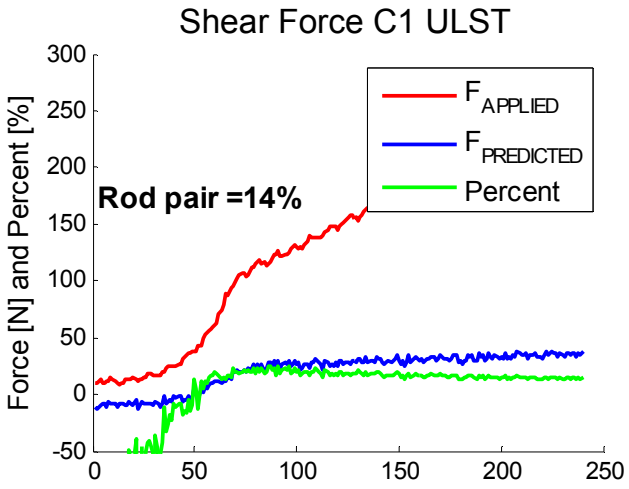
Shear Force C1 ULST
F APPLIED
F PREDICTED
Percent
Rod pair =14%
Force [N] and Percent [%]

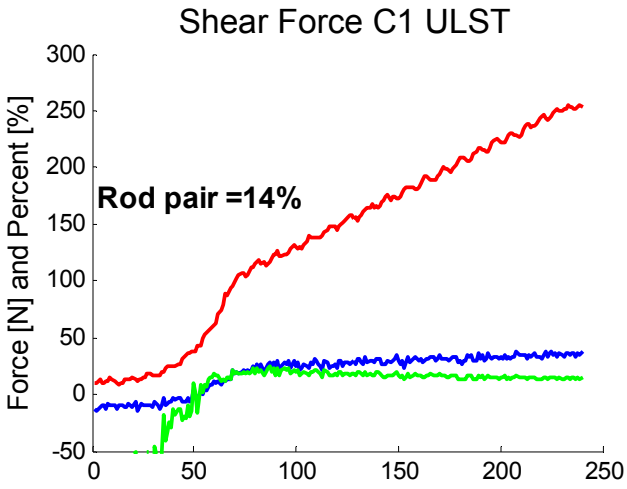
Shear Force C1 ULST
Rod pair =14%
Force [N] and Percent [%]

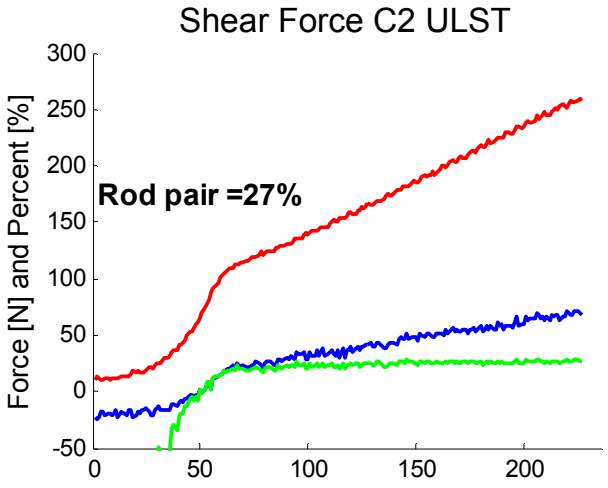
Shear Force C2 ULST
Rod pair =27%
Force [N] and Percent [%]

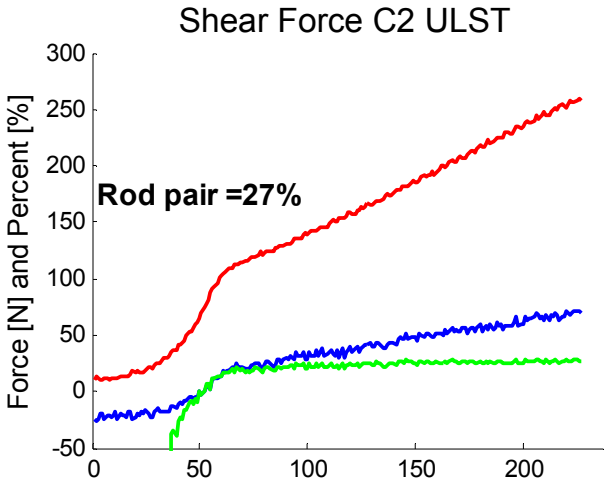
Shear Force C2 ULST
Rod pair =27%
Force [N] and Percent [%]

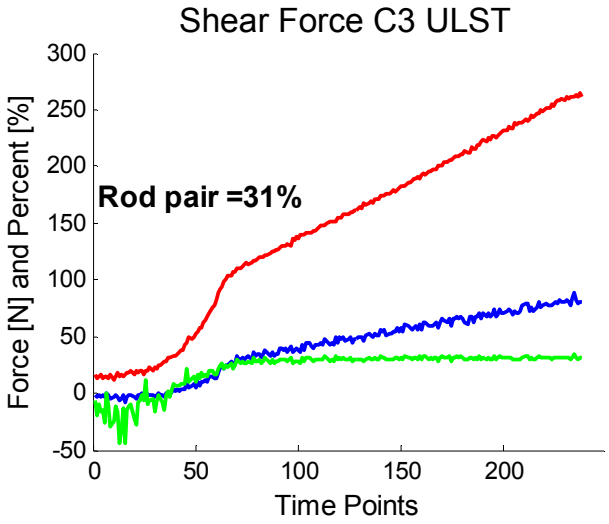
Shear Force C3 ULST
Rod pair =31%
Force [N] and Percent [%]
Time Points

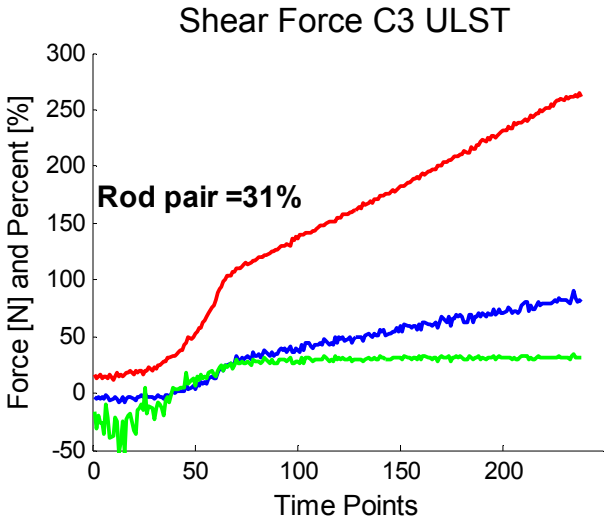
Shear Force C3 ULST
Rod pair =31%
Force [N] and Percent [%]
Time Points

Specimen 4

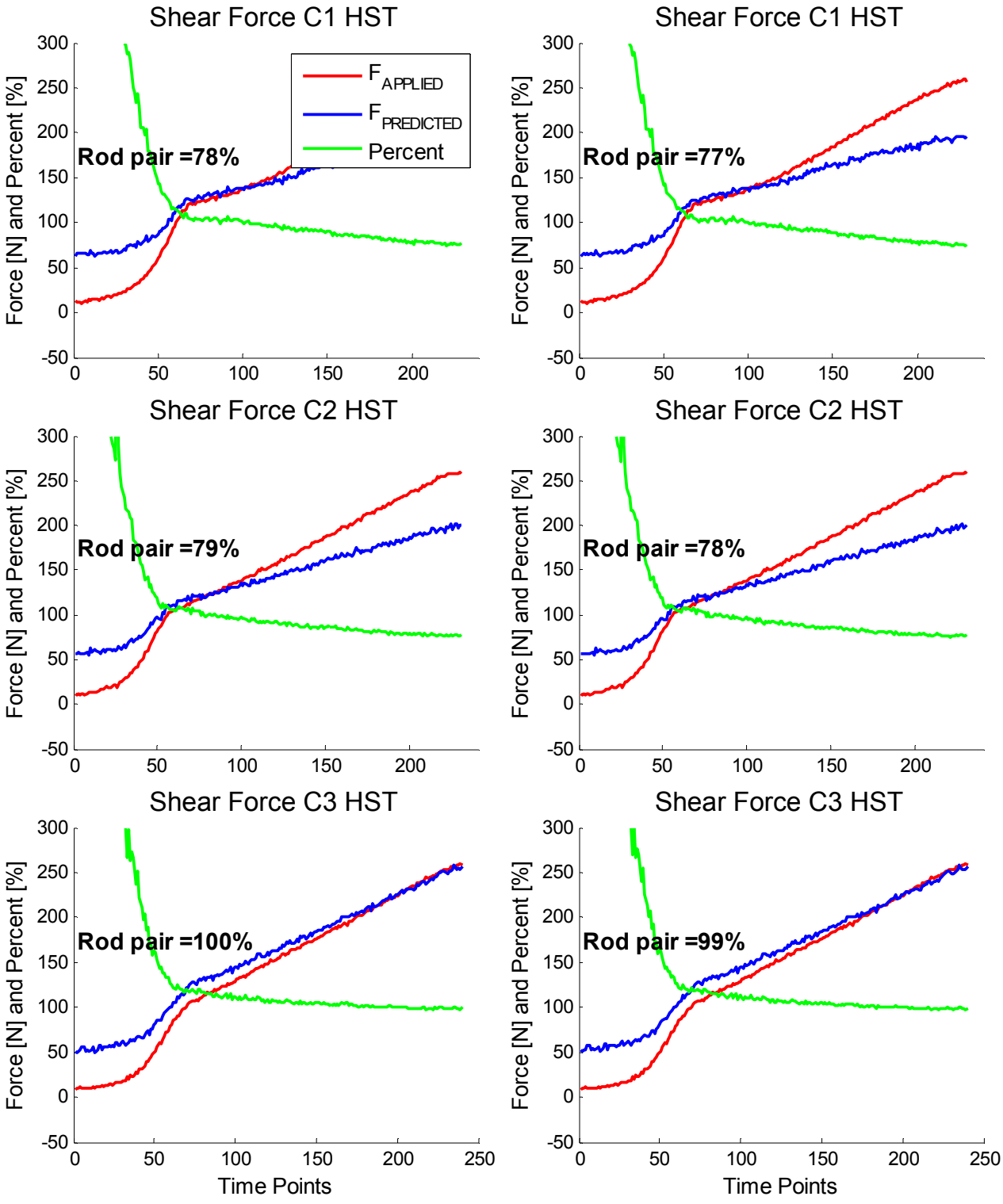
Shear Force C1 HST
Rod pair =78%
Shear Force C1 HST
Rod pair =77%
Shear Force C2 HST
Rod pair =79%
Shear Force C2 HST
Rod pair =78%
Shear Force C3 HST
Rod pair =100%
Shear Force C3 HST
Rod pair =99%
F APPLIED
F PREDICTED
Percent
Force [N] and Percent [%]
Time Points

Specimen 4

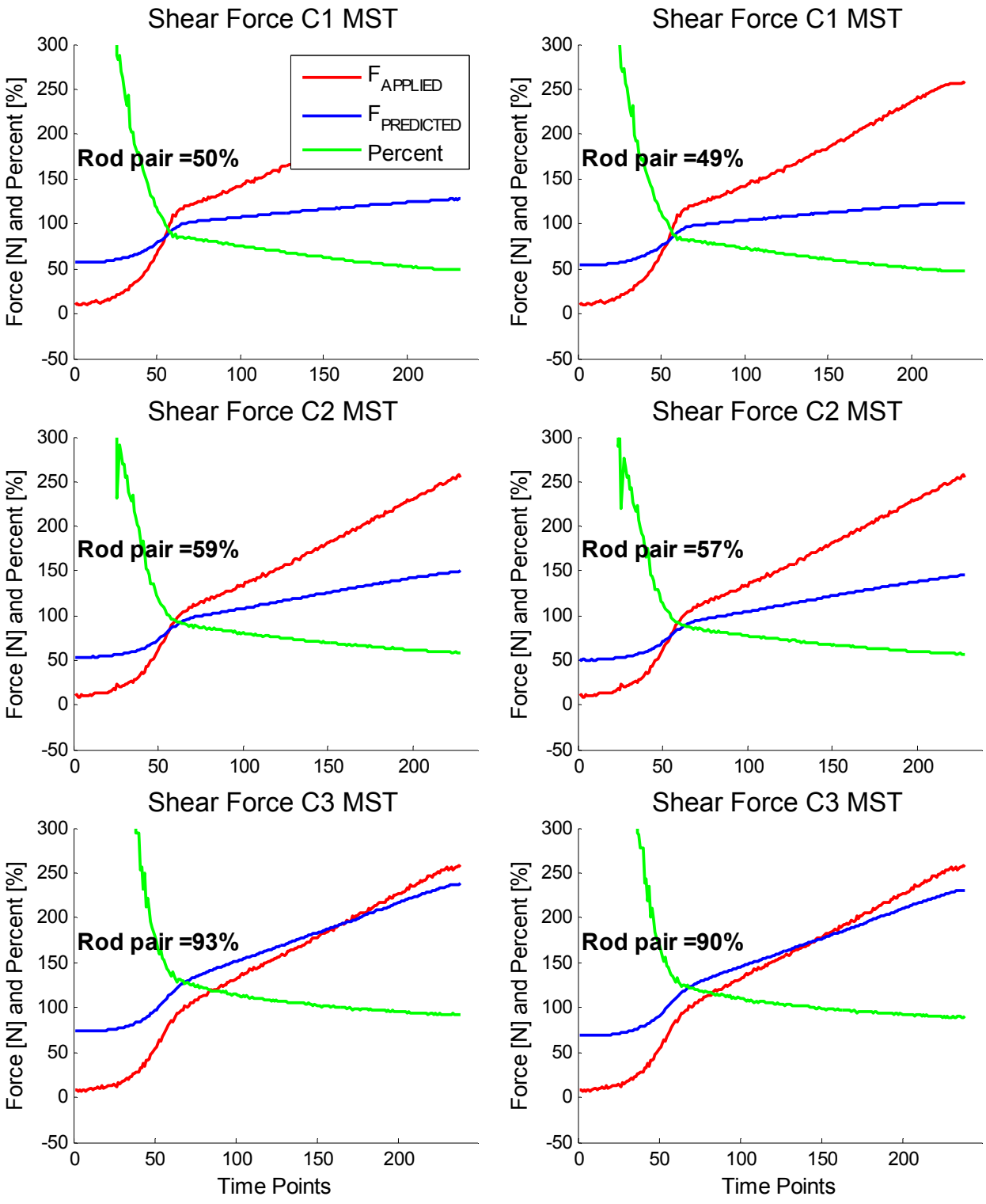
Shear Force C1 MST
Force [N] and Percent [%]
F APPLIED
F PREDICTED
Percent
Rod pair =50%
Shear Force C1 MST
Force [N] and Percent [%]
Rod pair =49%
Shear Force C2 MST
Force [N] and Percent [%]
Rod pair =59%
Shear Force C2 MST
Force [N] and Percent [%]
Rod pair =57%
Shear Force C3 MST
Force [N] and Percent [%]
Rod pair =93%
Time Points
Shear Force C3 MST
Force [N] and Percent [%]
Rod pair =90%
Time Points

Specimen 4

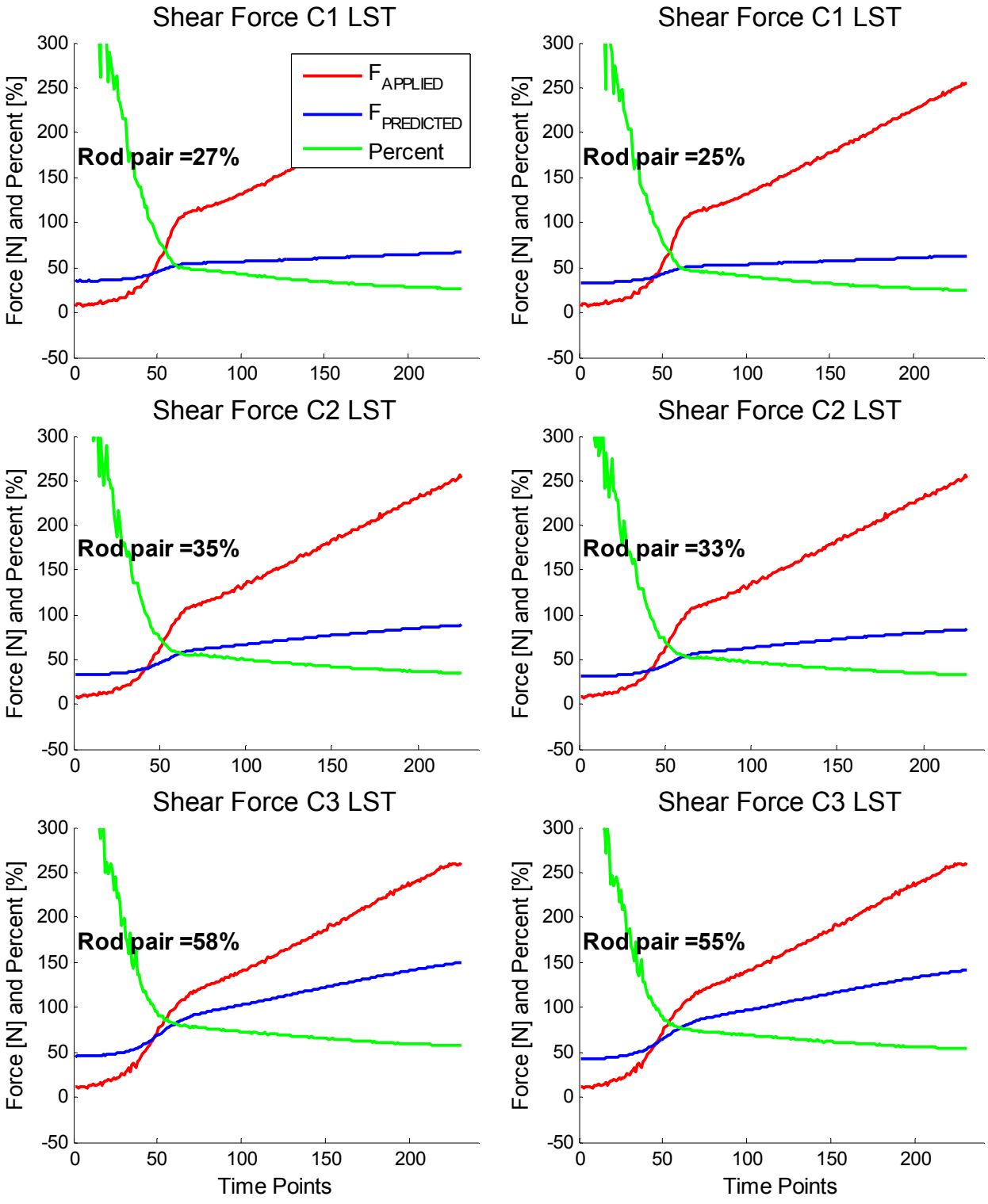
Shear Force C1 LST
Rod pair =27%
Shear Force C1 LST
Rod pair =25%
Shear Force C2 LST
Rod pair =35%
Shear Force C2 LST
Rod pair =33%
Shear Force C3 LST
Rod pair =58%
Shear Force C3 LST
Rod pair =55%
F APPLIED
F PREDICTED
Percent
Force [N] and Percent [%]
Time Points

Specimen 4

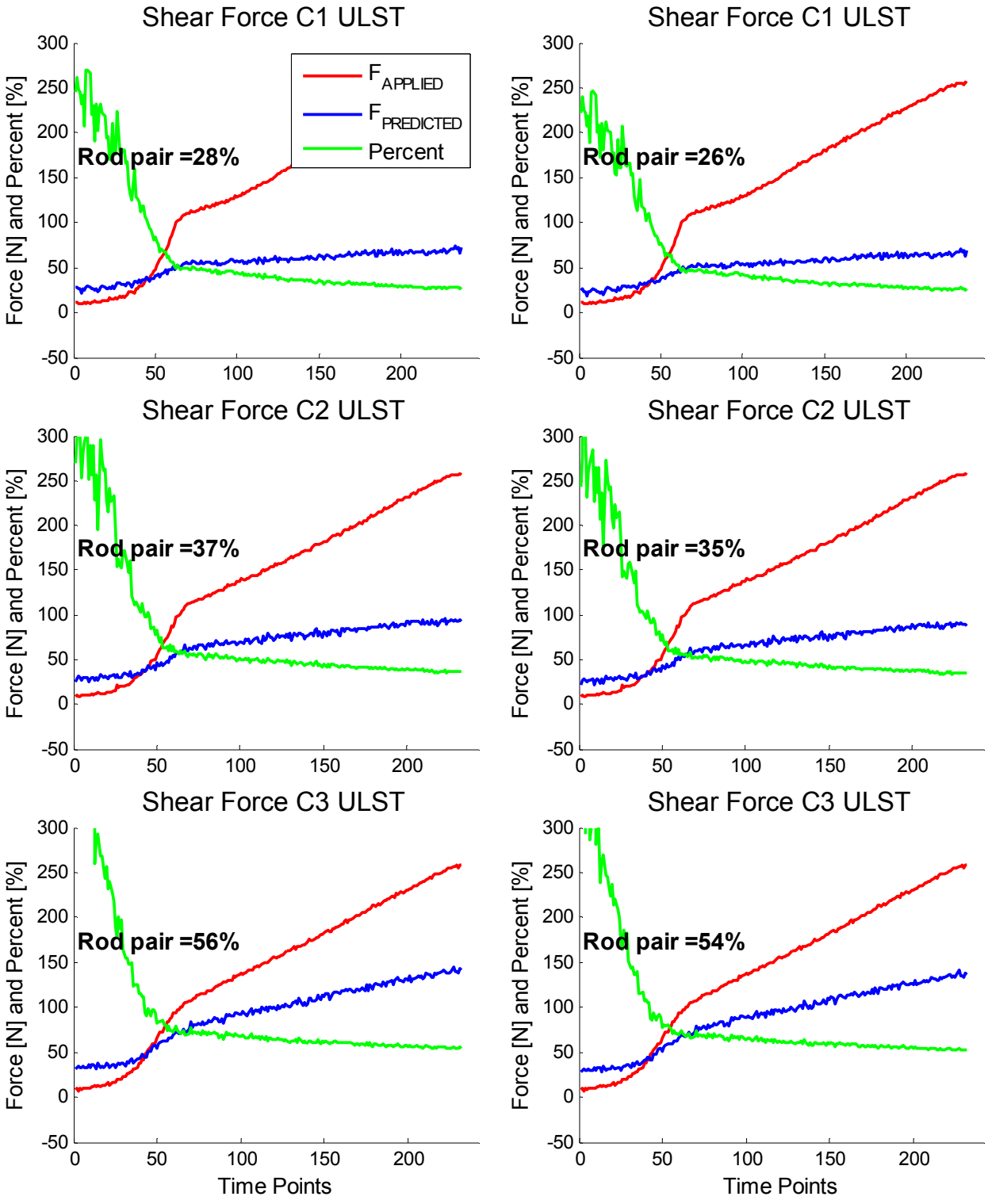
Shear Force C1 ULST
Force [N] and Percent [%]
F APPLIED
F PREDICTED
Percent
Rod pair =28%
Shear Force C1 ULST
Force [N] and Percent [%]
Rod pair =26%
Shear Force C2 ULST
Force [N] and Percent [%]
Rod pair =37%
Shear Force C2 ULST
Force [N] and Percent [%]
Rod pair =35%
Shear Force C3 ULST
Force [N] and Percent [%]
Rod pair =56%
Time Points
Shear Force C3 ULST
Force [N] and Percent [%]
Rod pair =54%
Time Points

Specimen 5

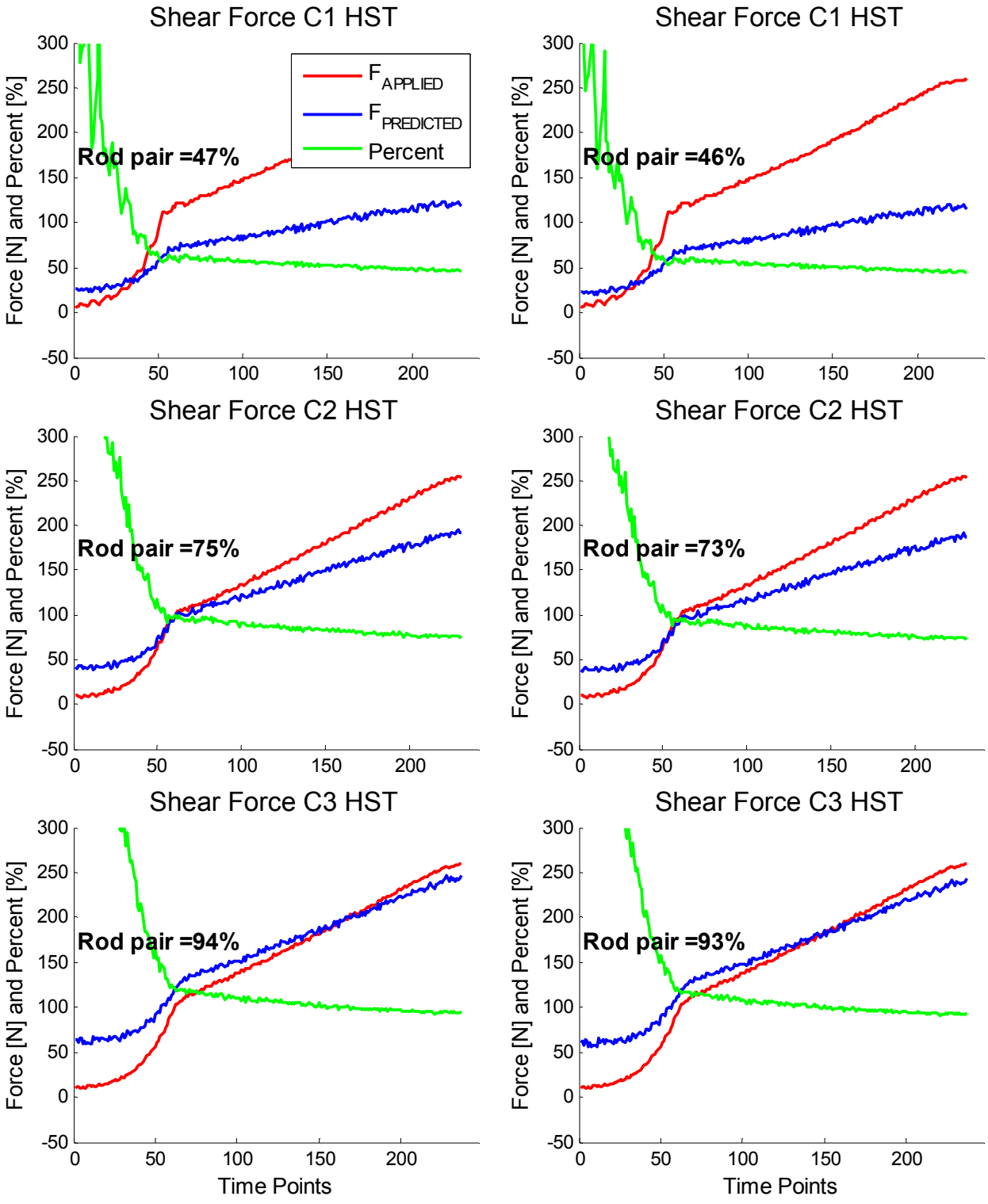
Shear Force C1 HST
Force [N] and Percent [%]
F APPLIED
F PREDICTED
Percent
Rod pair =47%
Shear Force C1 HST
Rod pair =46%
Shear Force C2 HST
Rod pair =75%
Shear Force C2 HST
Rod pair =73%
Shear Force C3 HST
Rod pair =94%
Shear Force C3 HST
Rod pair =93%
Time Points
Time Points

Specimen 5

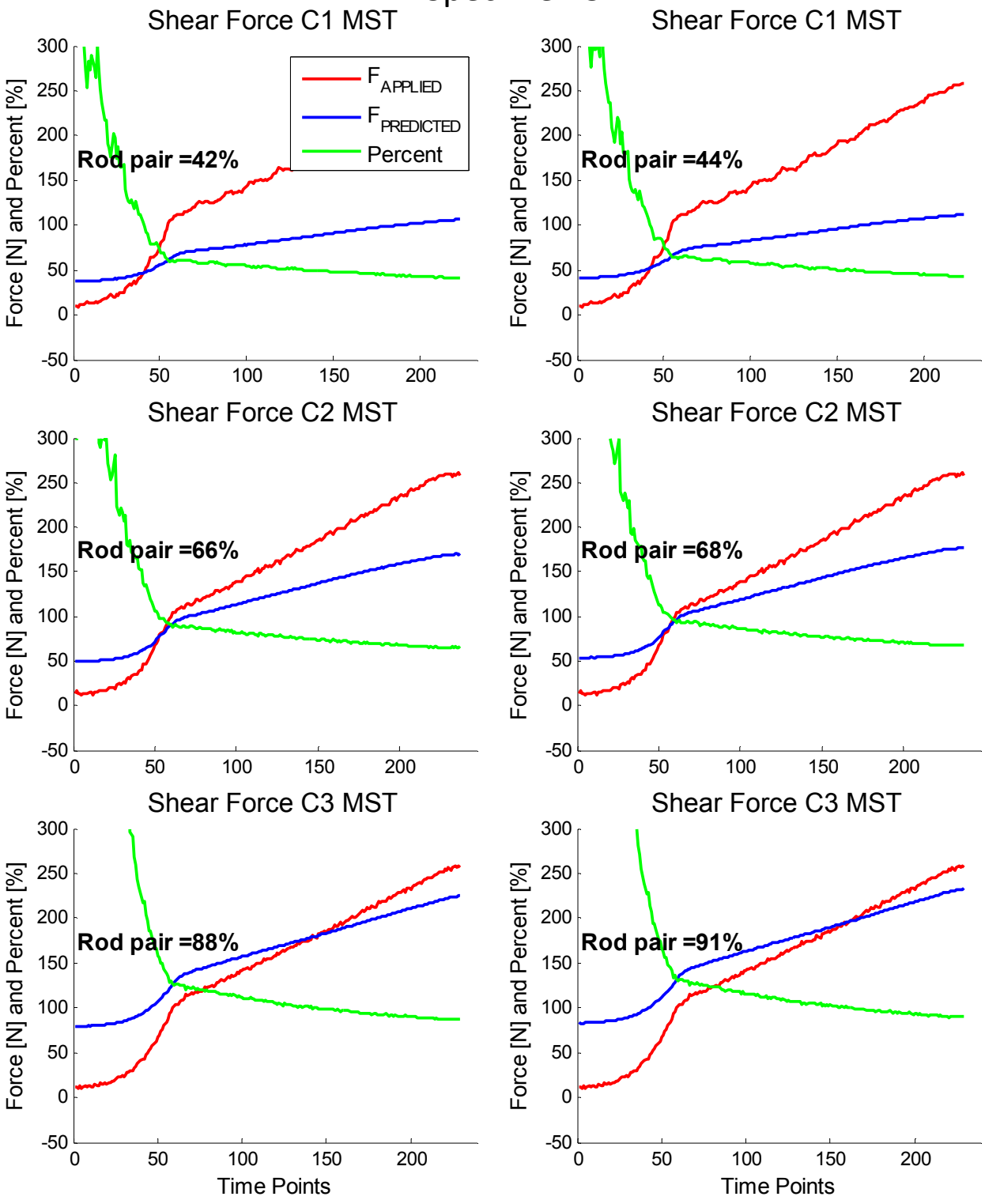
Shear Force C1 MST
Force [N] and Percent [%]
F APPLIED
F PREDICTED
Percent
Rod pair =42%
Shear Force C1 MST
Rod pair =44%
Shear Force C2 MST
Rod pair =66%
Shear Force C2 MST
Rod pair =68%
Shear Force C3 MST
Rod pair =88%
Shear Force C3 MST
Rod pair =91%
Time Points
Time Points

Specimen 5

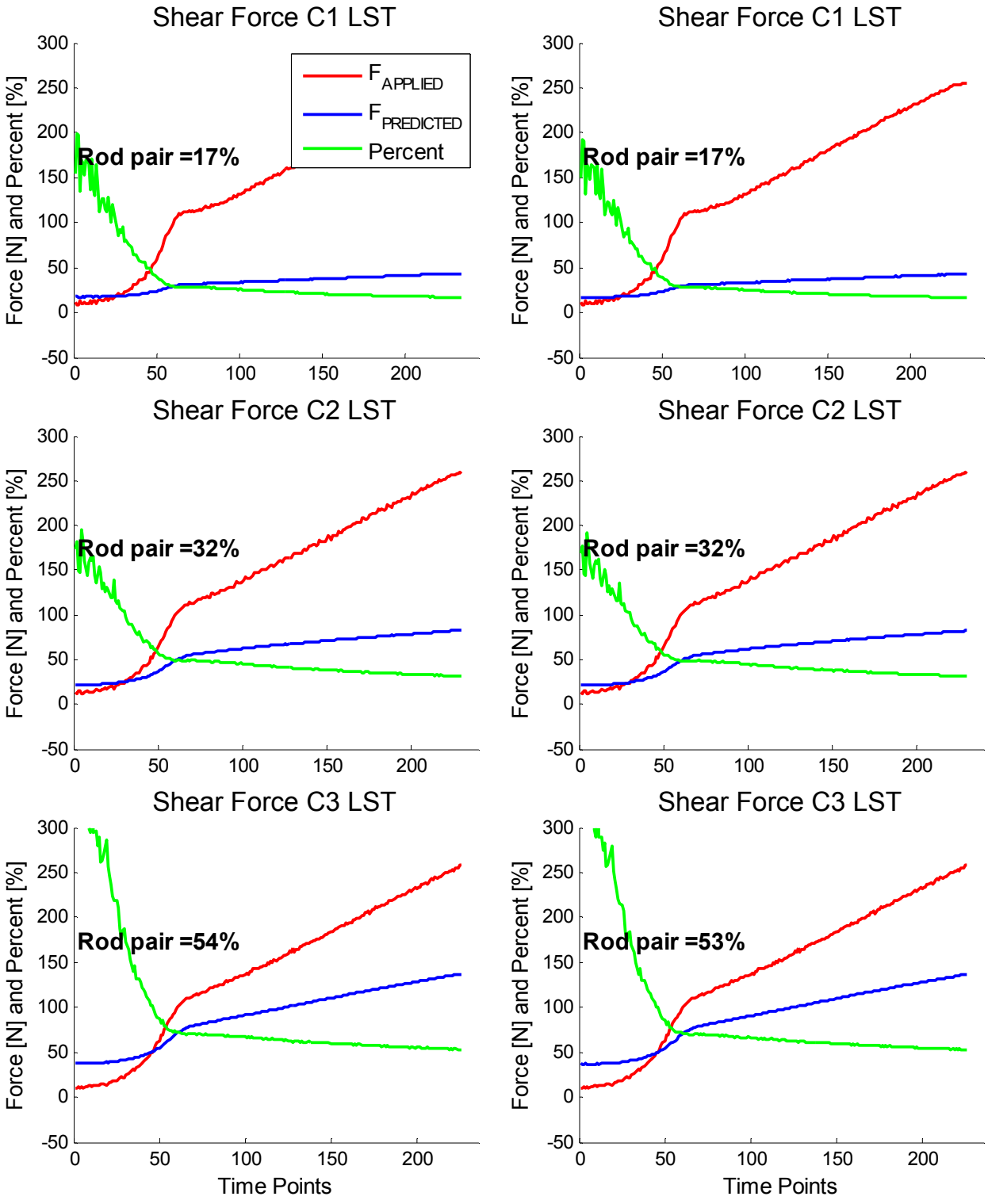
Shear Force C1 LST
Force [N] and Percent [%]
F APPLIED
F PREDICTED
Percent
Rod pair =17%
Shear Force C1 LST
Force [N] and Percent [%]
Rod pair =17%
Shear Force C2 LST
Force [N] and Percent [%]
Rod pair =32%
Shear Force C2 LST
Force [N] and Percent [%]
Rod pair =32%
Shear Force C3 LST
Force [N] and Percent [%]
Rod pair =54%
Time Points
Shear Force C3 LST
Force [N] and Percent [%]
Rod pair =53%
Time Points

Specimen 5

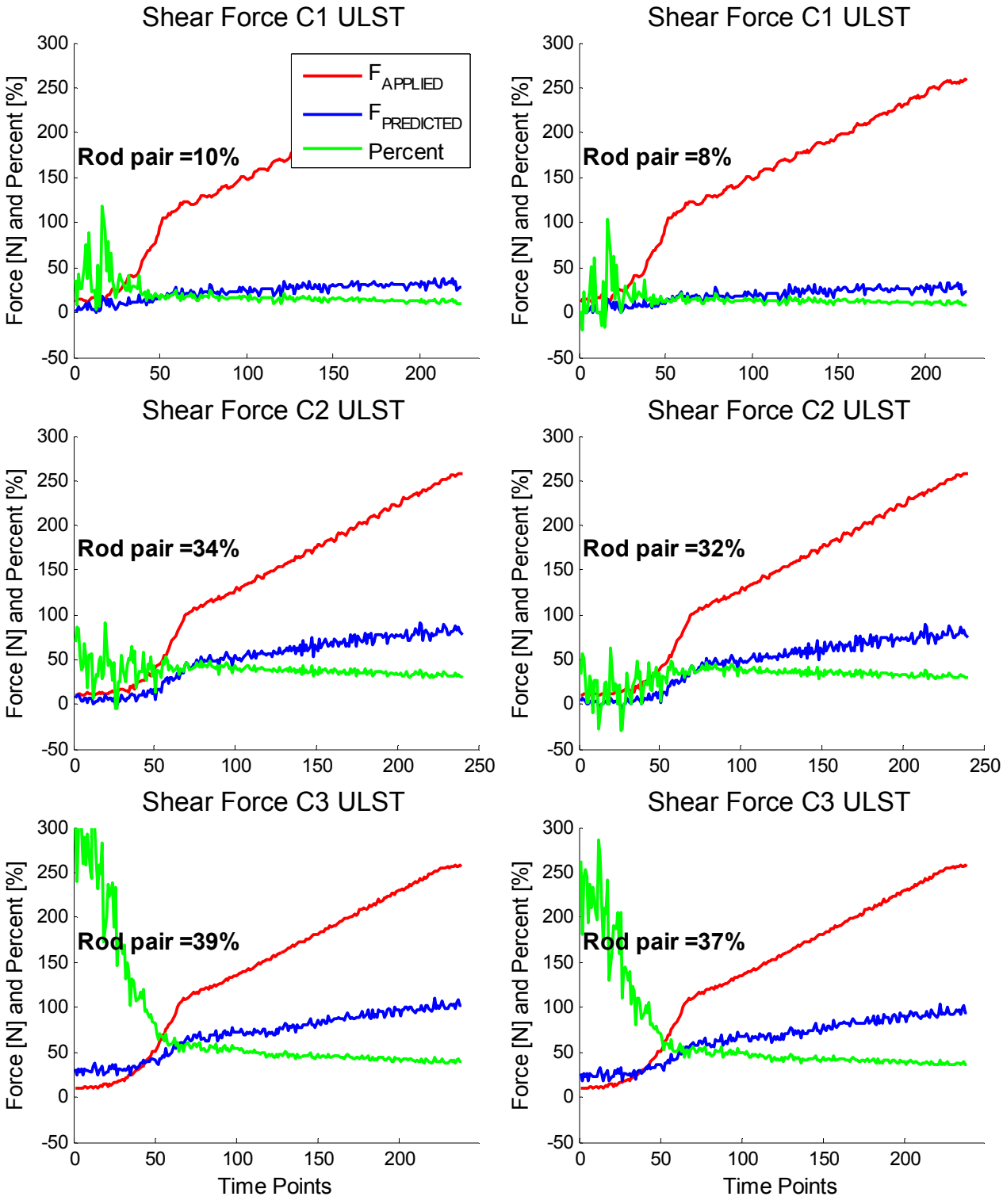
Shear Force C1 ULST
Force [N] and Percent [%]
F APPLIED
F PREDICTED
Percent
Rod pair =10%
Shear Force C1 ULST
Rod pair =8%
Shear Force C2 ULST
Rod pair =34%
Shear Force C2 ULST
Rod pair =32%
Shear Force C3 ULST
Rod pair =39%
Shear Force C3 ULST
Rod pair =37%
Time Points
Time Points

Specimen 6

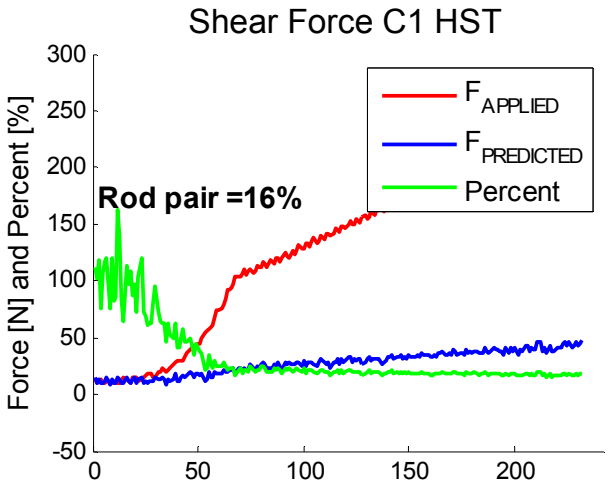
Shear Force C1 HST
F APPLIED
F PREDICTED
Percent
Rod pair =16%
Force [N] and Percent [%]

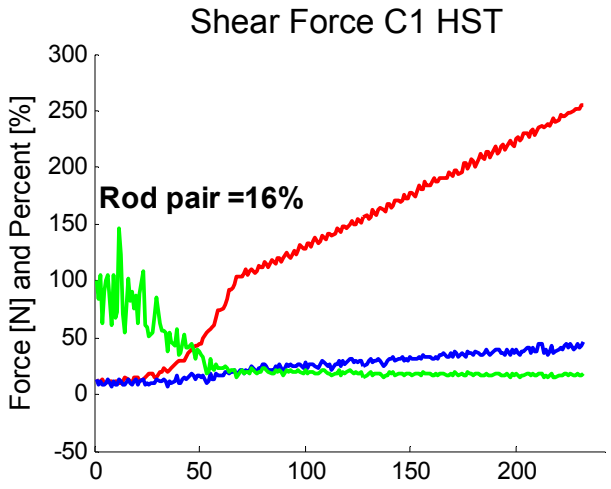
Shear Force C1 HST
Rod pair =16%
Force [N] and Percent [%]

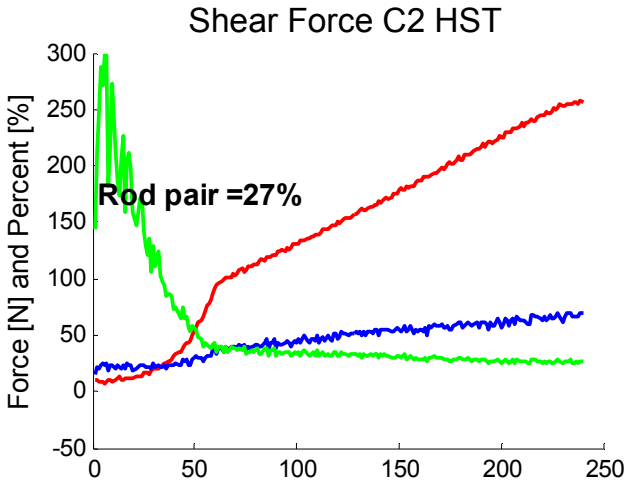
Shear Force C2 HST
Rod pair =27%
Force [N] and Percent [%]

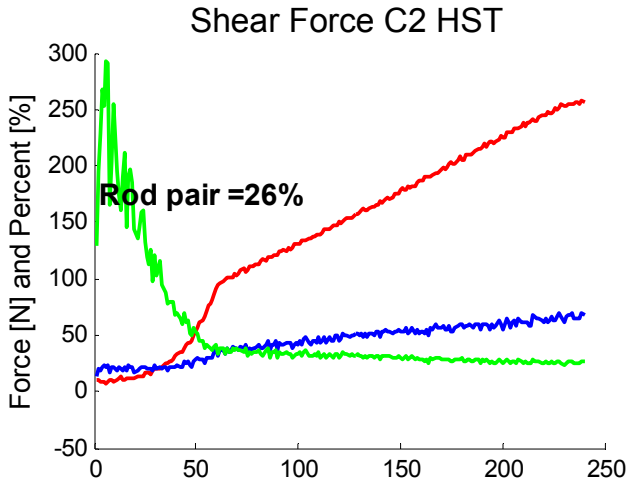
Shear Force C2 HST
Rod pair =26%
Force [N] and Percent [%]

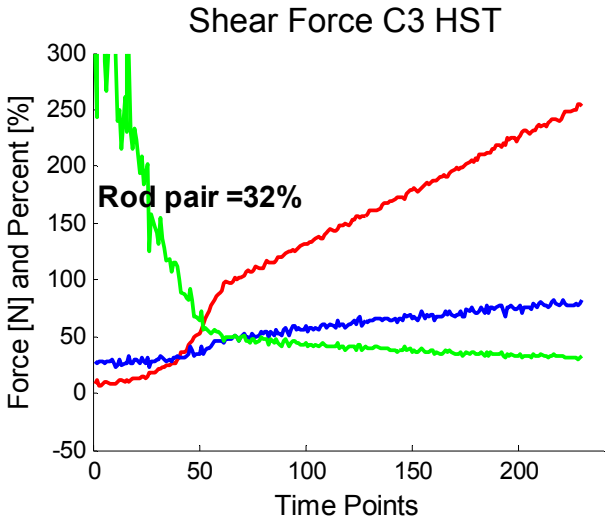
Shear Force C3 HST
Rod pair =32%
Force [N] and Percent [%]
Time Points

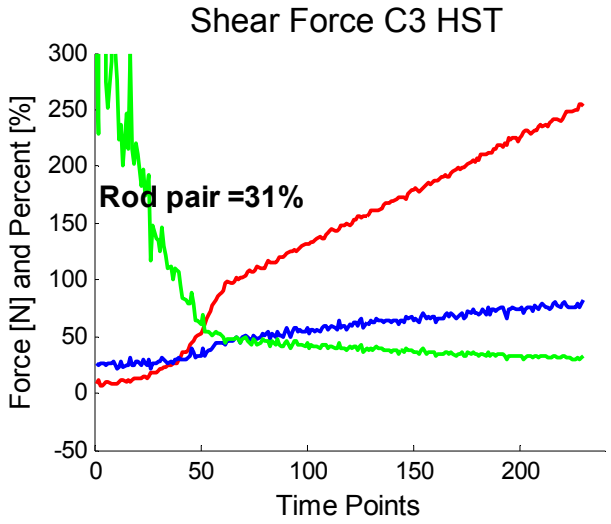
Shear Force C3 HST
Rod pair =31%
Force [N] and Percent [%]
Time Points

Specimen 6

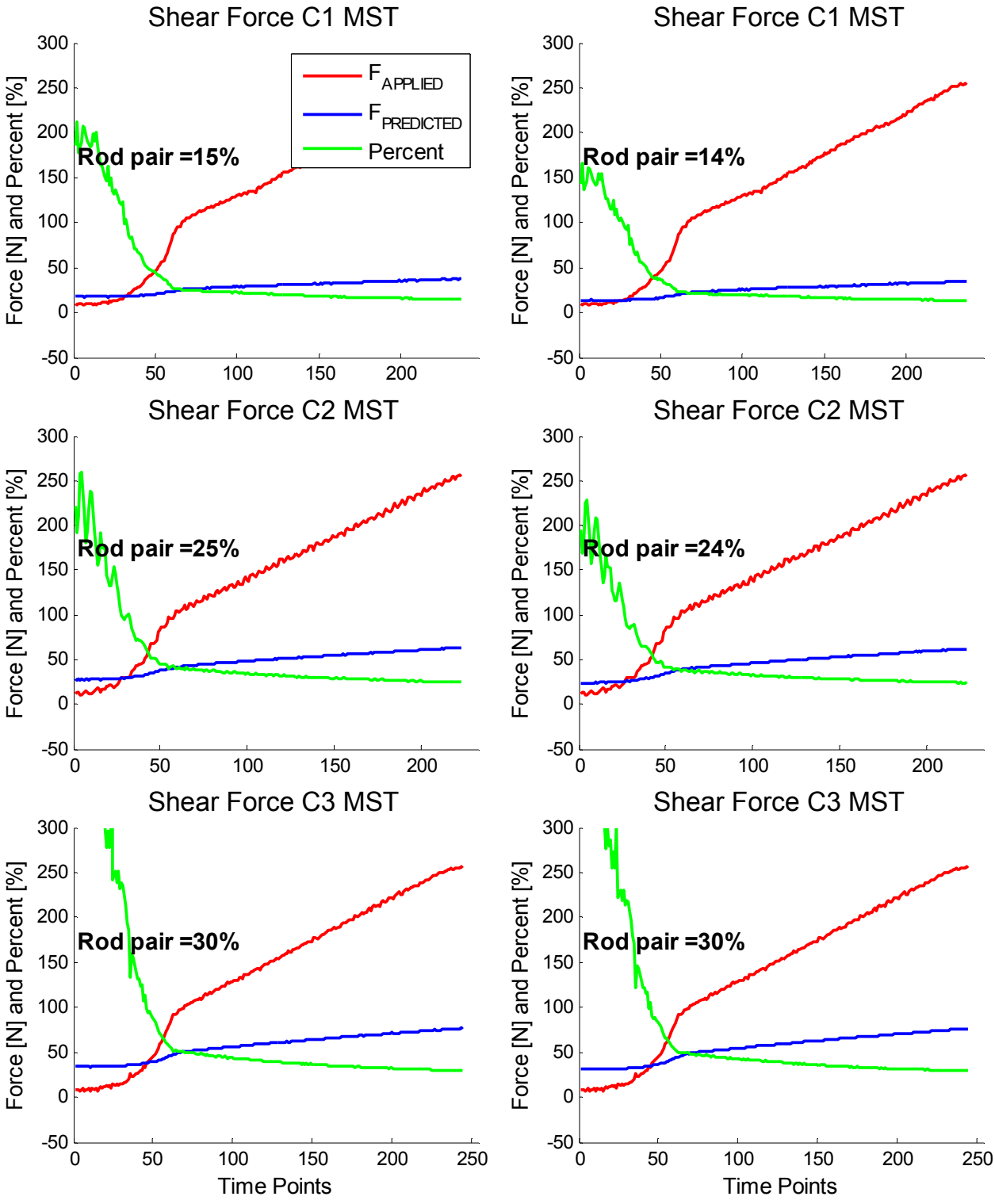
Shear Force C1 MST
Force [N] and Percent [%]
F APPLIED
F PREDICTED
Percent
Rod pair =15%
Shear Force C1 MST
Force [N] and Percent [%]
Rod pair =14%
Shear Force C2 MST
Force [N] and Percent [%]
Rod pair =25%
Shear Force C2 MST
Force [N] and Percent [%]
Rod pair =24%
Shear Force C3 MST
Force [N] and Percent [%]
Rod pair =30%
Time Points
Shear Force C3 MST
Force [N] and Percent [%]
Rod pair =30%
Time Points

Specimen 6

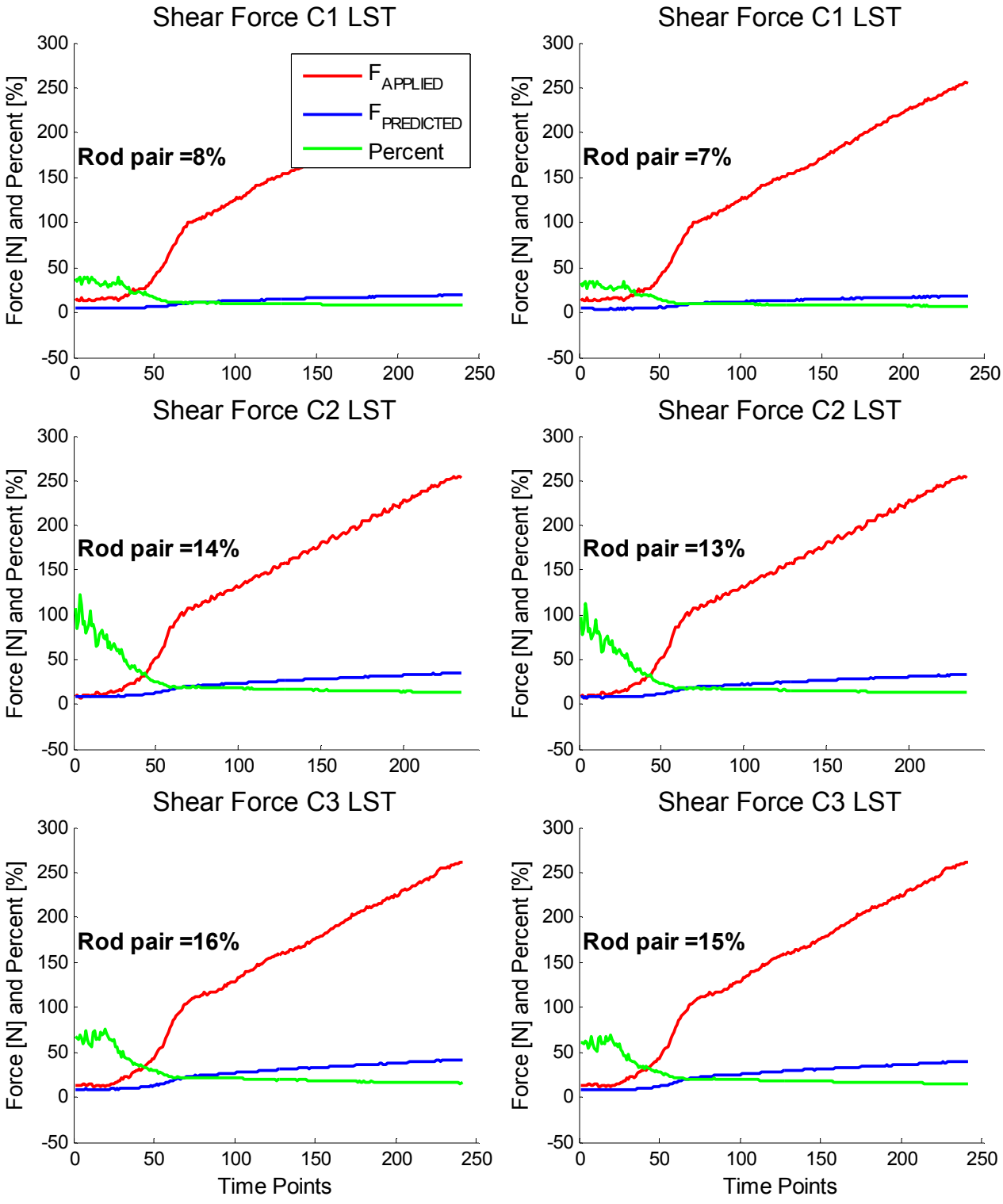
Shear Force C1 LST
Force [N] and Percent [%]
F APPLIED
F PREDICTED
Percent
Rod pair =8%
Shear Force C1 LST
Force [N] and Percent [%]
Rod pair =7%
Shear Force C2 LST
Force [N] and Percent [%]
Rod pair =14%
Shear Force C2 LST
Force [N] and Percent [%]
Rod pair =13%
Shear Force C3 LST
Force [N] and Percent [%]
Rod pair =16%
Time Points
Shear Force C3 LST
Force [N] and Percent [%]
Rod pair =15%
Time Points

Specimen 6

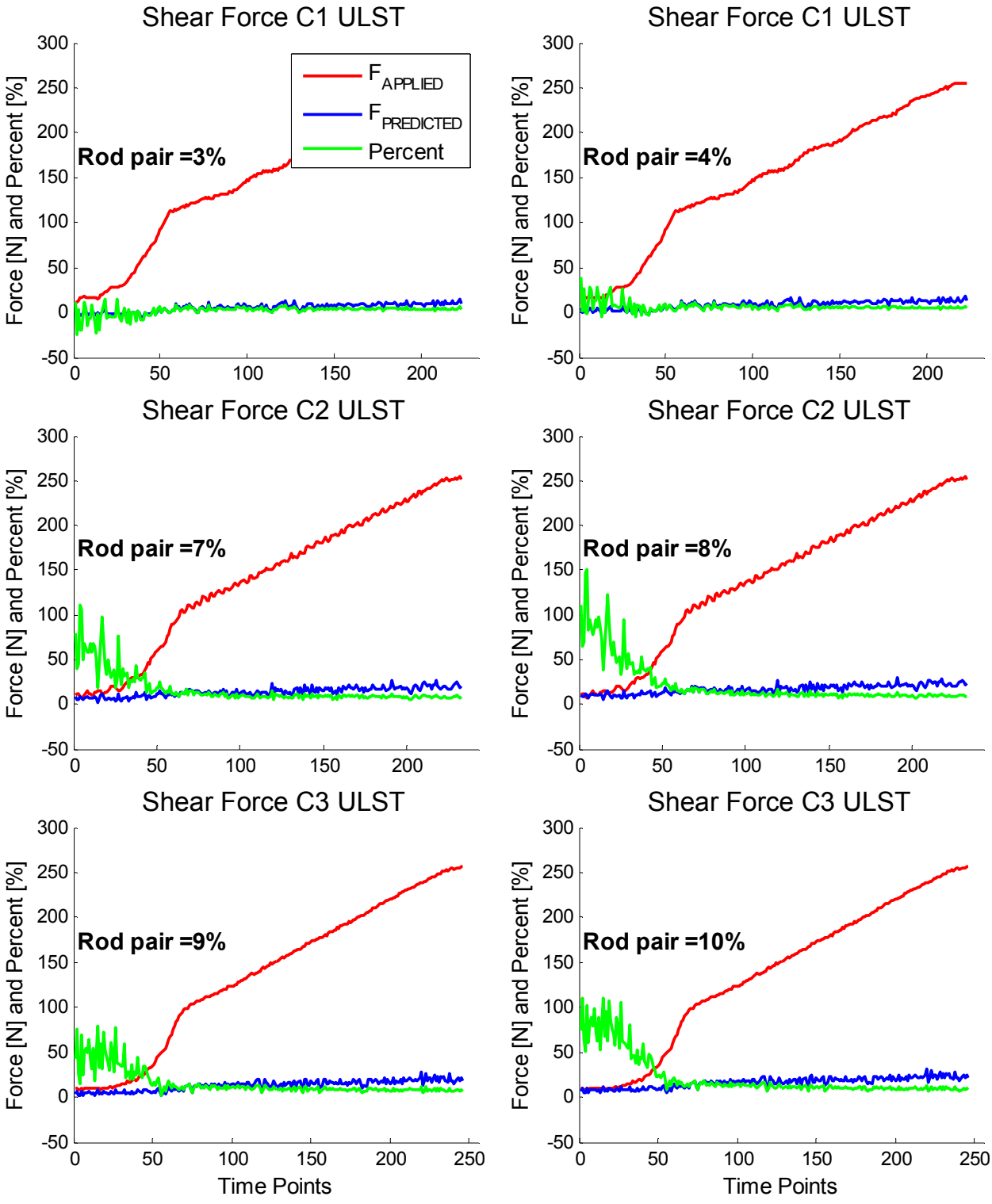
Shear Force C1 ULST
Force [N] and Percent [%]
F APPLIED
F PREDICTED
Percent
Rod pair =3%
Shear Force C1 ULST
Force [N] and Percent [%]
Rod pair =4%
Shear Force C2 ULST
Force [N] and Percent [%]
Rod pair =7%
Shear Force C2 ULST
Force [N] and Percent [%]
Rod pair =8%
Shear Force C3 ULST
Force [N] and Percent [%]
Rod pair =9%
Time Points
Shear Force C3 ULST
Force [N] and Percent [%]
Rod pair =10%
Time Points

Specimen 7

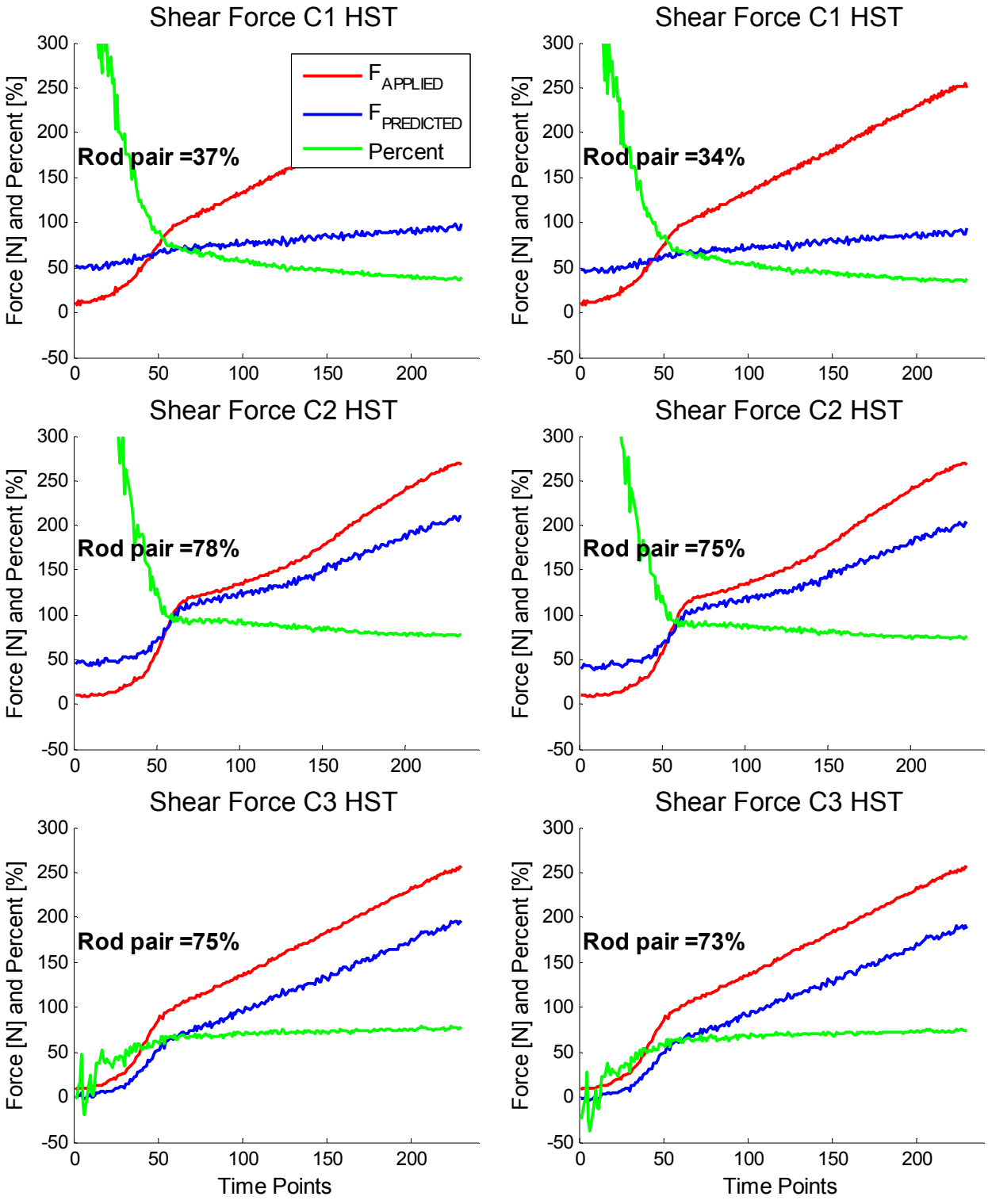
Shear Force C1 HST
Force [N] and Percent [%]
F APPLIED
F PREDICTED
Percent
Rod pair =37%
Shear Force C1 HST
Rod pair =34%
Shear Force C2 HST
Rod pair =78%
Shear Force C2 HST
Rod pair =75%
Shear Force C3 HST
Rod pair =75%
Shear Force C3 HST
Rod pair =73%
Time Points
Time Points

Specimen 7

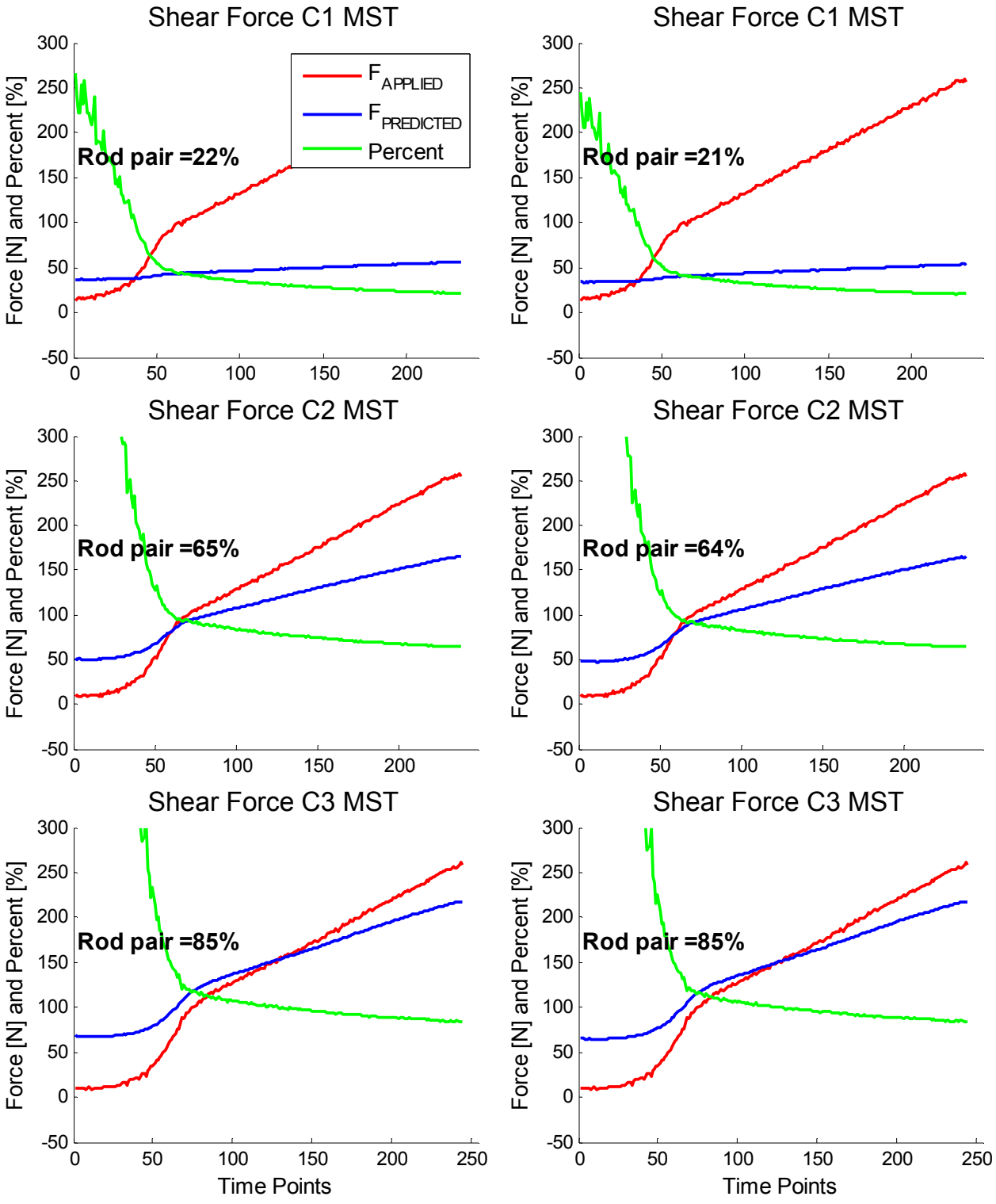
Shear Force C1 MST
Force [N] and Percent [%]
F APPLIED
F PREDICTED
Percent
Rod pair =22%
Shear Force C1 MST
Rod pair =21%
Shear Force C2 MST
Rod pair =65%
Shear Force C2 MST
Rod pair =64%
Shear Force C3 MST
Rod pair =85%
Shear Force C3 MST
Rod pair =85%
Time Points
Time Points

Specimen 7

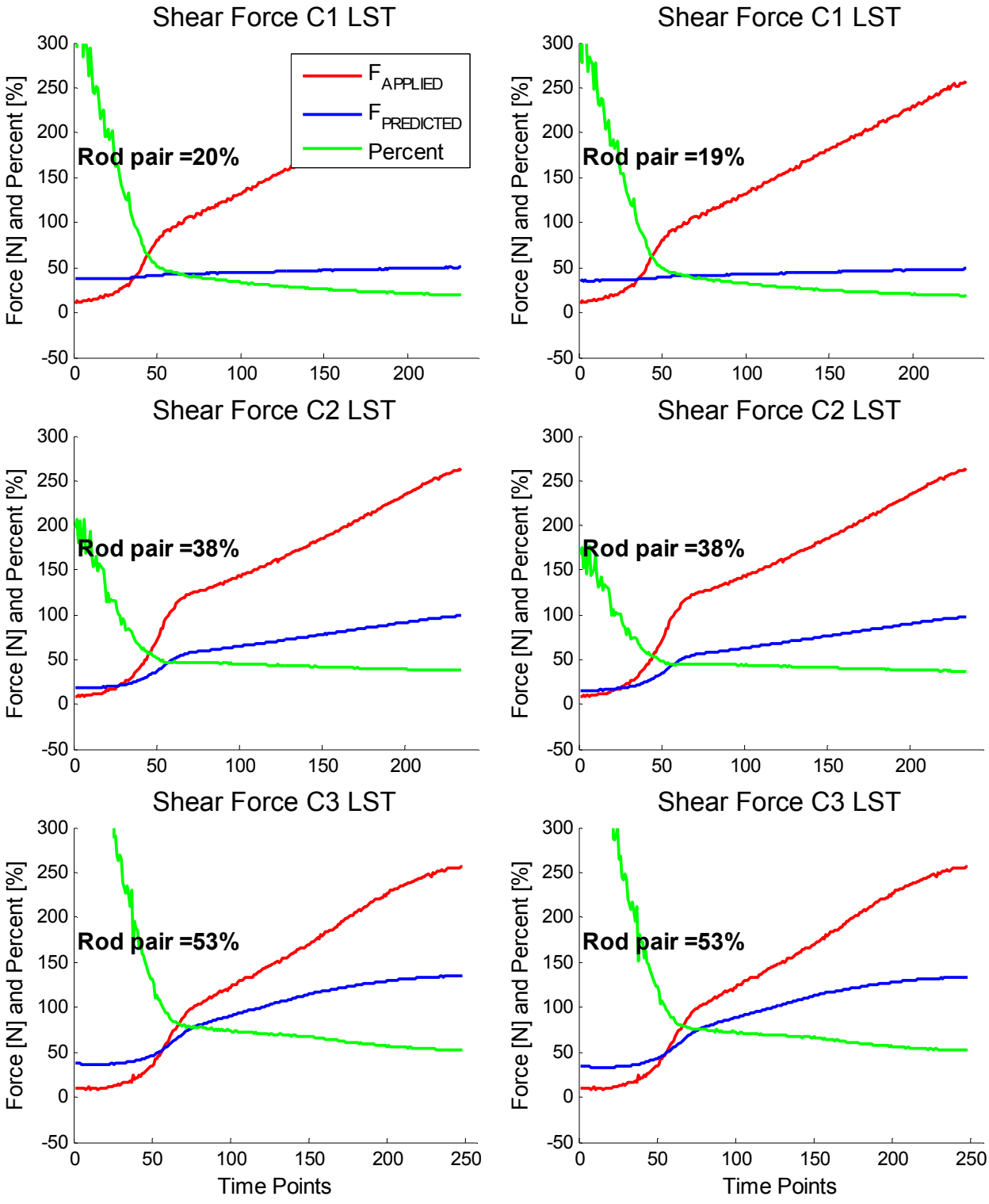
Shear Force C1 LST
Force [N] and Percent [%]
F APPLIED
F PREDICTED
Percent
Rod pair =20%
Shear Force C1 LST
Force [N] and Percent [%]
Rod pair =19%
Shear Force C2 LST
Force [N] and Percent [%]
Rod pair =38%
Shear Force C2 LST
Force [N] and Percent [%]
Rod pair =38%
Shear Force C3 LST
Force [N] and Percent [%]
Rod pair =53%
Time Points
Shear Force C3 LST
Force [N] and Percent [%]
Rod pair =53%
Time Points

Specimen 7

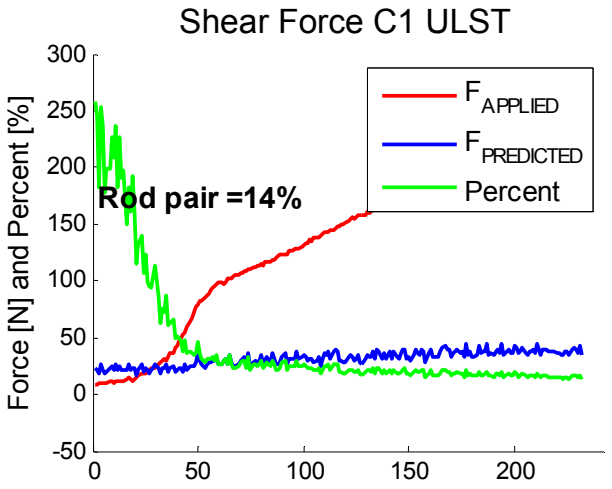
Shear Force C1 ULST
Force [N] and Percent [%]
F APPLIED
F PREDICTED
Percent
Rod pair =14%

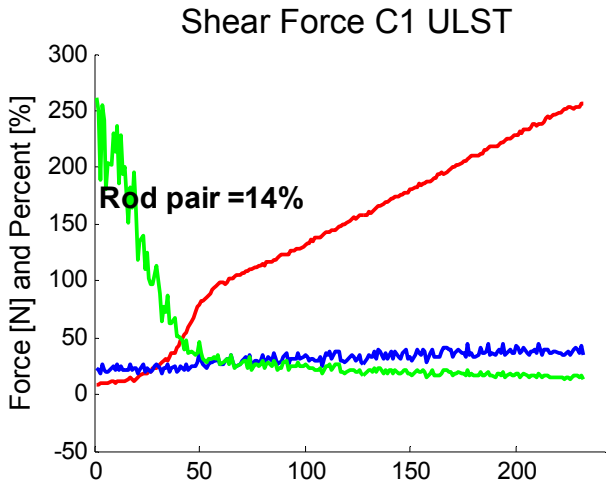
Shear Force C1 ULST
Force [N] and Percent [%]
Rod pair =14%

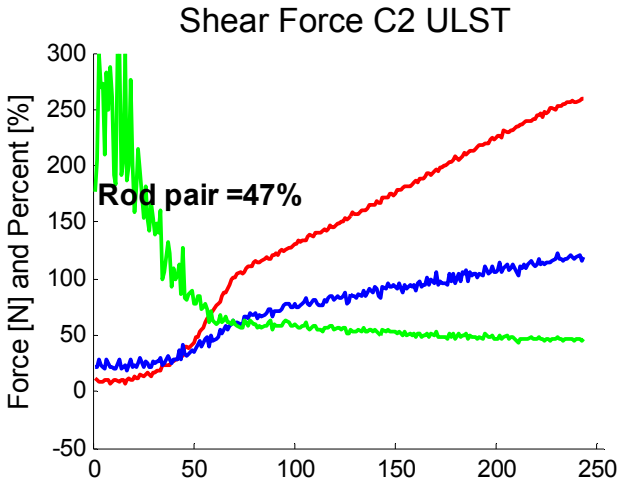
Shear Force C2 ULST
Force [N] and Percent [%]
Rod pair =47%

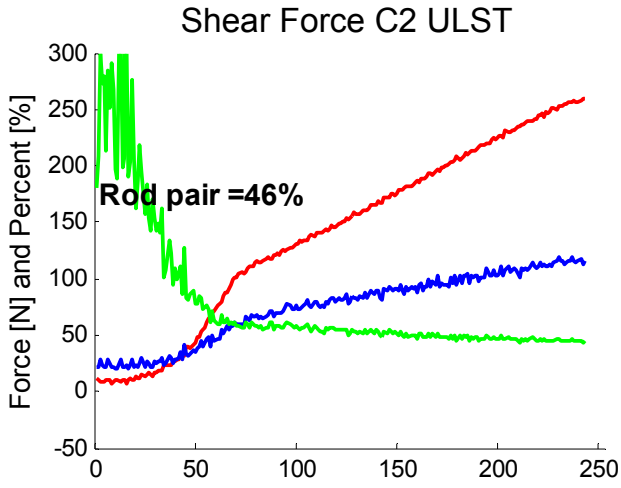
Shear Force C2 ULST
Force [N] and Percent [%]
Rod pair =46%

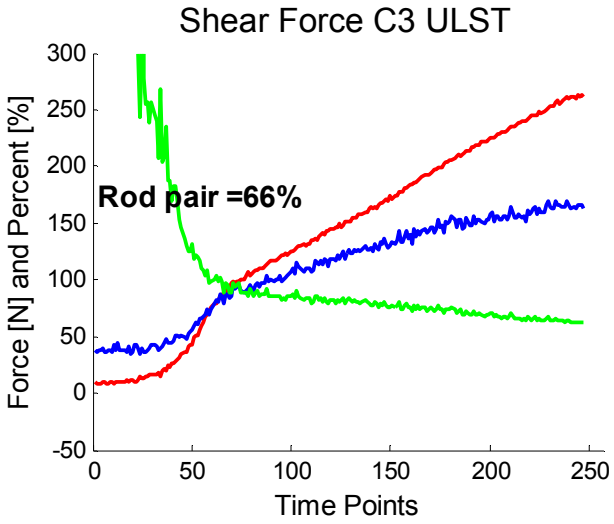
Shear Force C3 ULST
Force [N] and Percent [%]
Rod pair =66%
Time Points

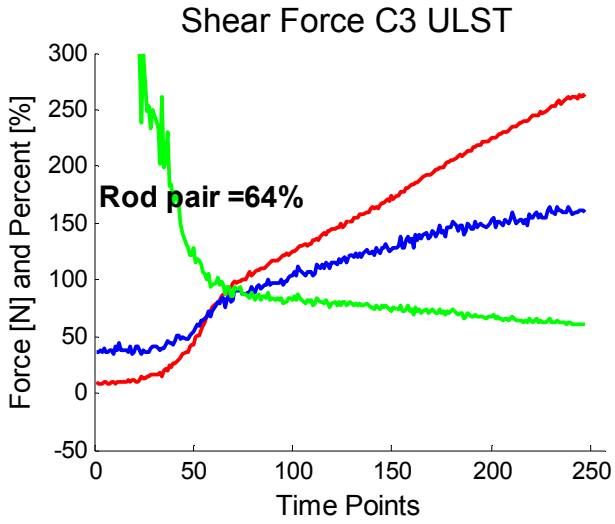
Shear Force C3 ULST
Force [N] and Percent [%]
Rod pair =64%
Time Points

Specimen 8

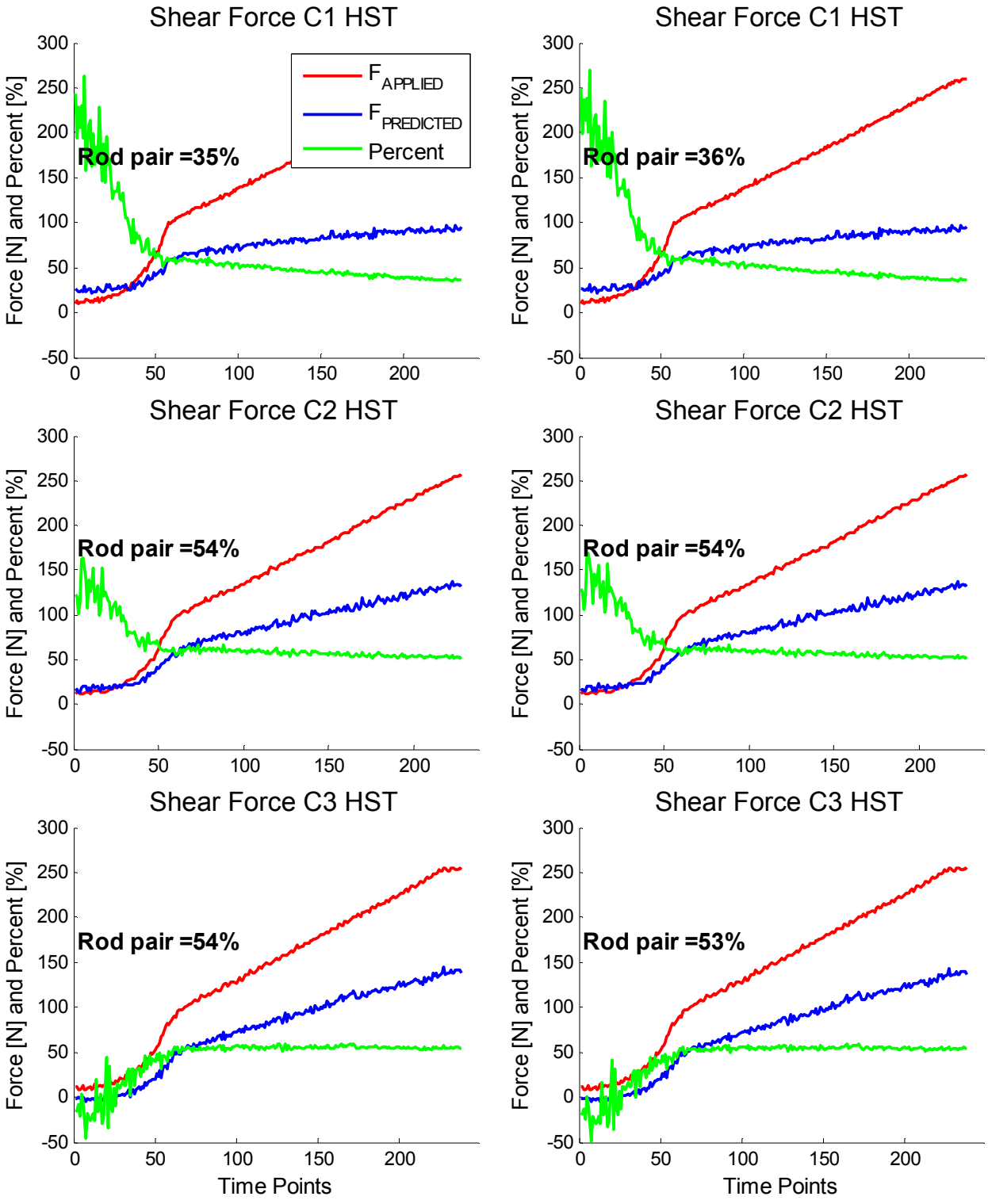
Shear Force C1 HST
Force [N] and Percent [%]
F APPLIED
F PREDICTED
Percent
Rod pair =35%
Shear Force C1 HST
Rod pair =36%
Shear Force C2 HST
Rod pair =54%
Shear Force C2 HST
Rod pair =54%
Shear Force C3 HST
Rod pair =54%
Shear Force C3 HST
Rod pair =53%
Time Points
Time Points

Specimen 8

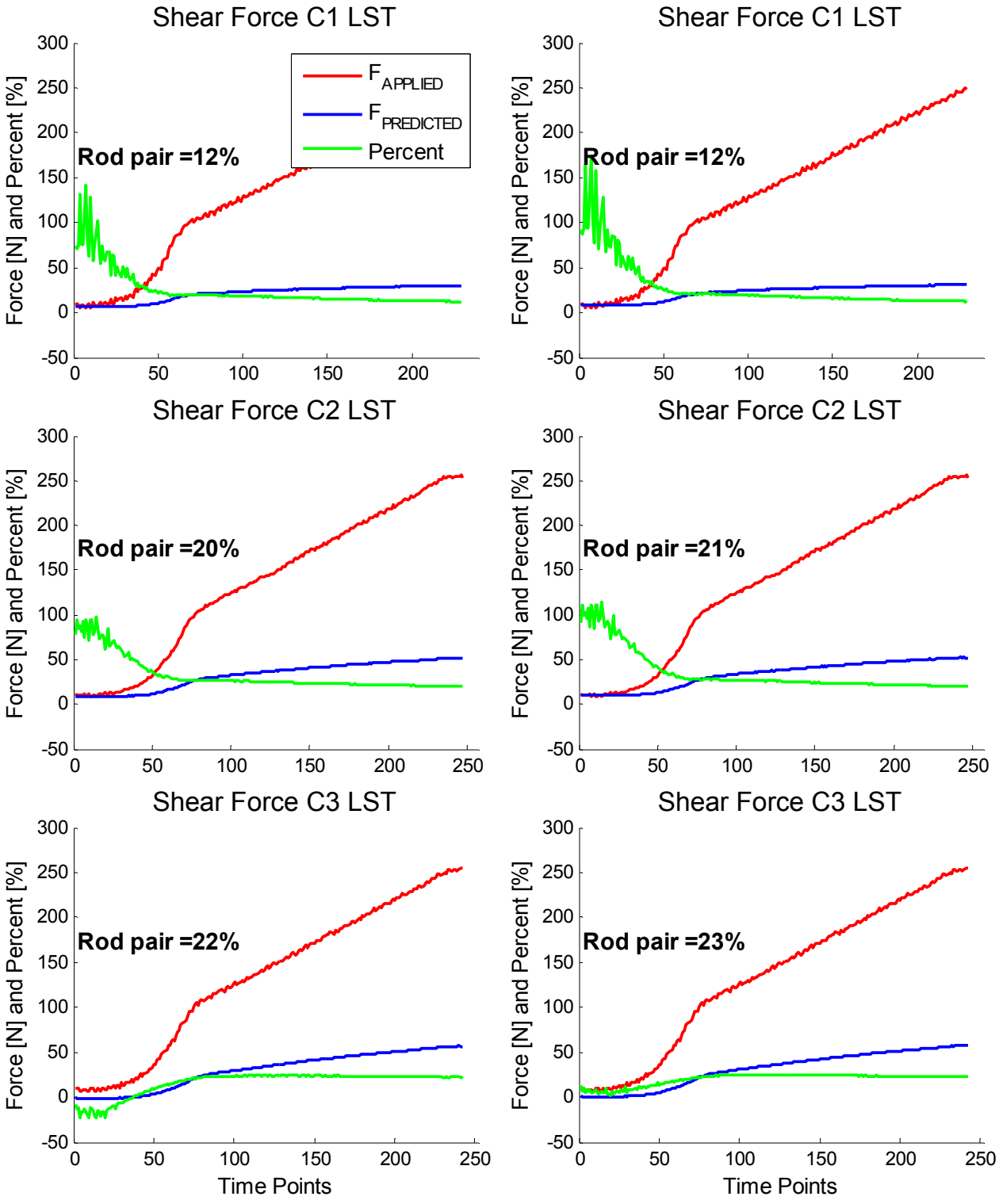
Shear Force C1 LST
Force [N] and Percent [%]
F APPLIED
F PREDICTED
Percent
Rod pair =12%
Shear Force C1 LST
Force [N] and Percent [%]
Rod pair =12%
Shear Force C2 LST
Force [N] and Percent [%]
Rod pair =20%
Shear Force C2 LST
Force [N] and Percent [%]
Rod pair =21%
Shear Force C3 LST
Force [N] and Percent [%]
Rod pair =22%
Time Points
Shear Force C3 LST
Force [N] and Percent [%]
Rod pair =23%
Time Points

Specimen 8

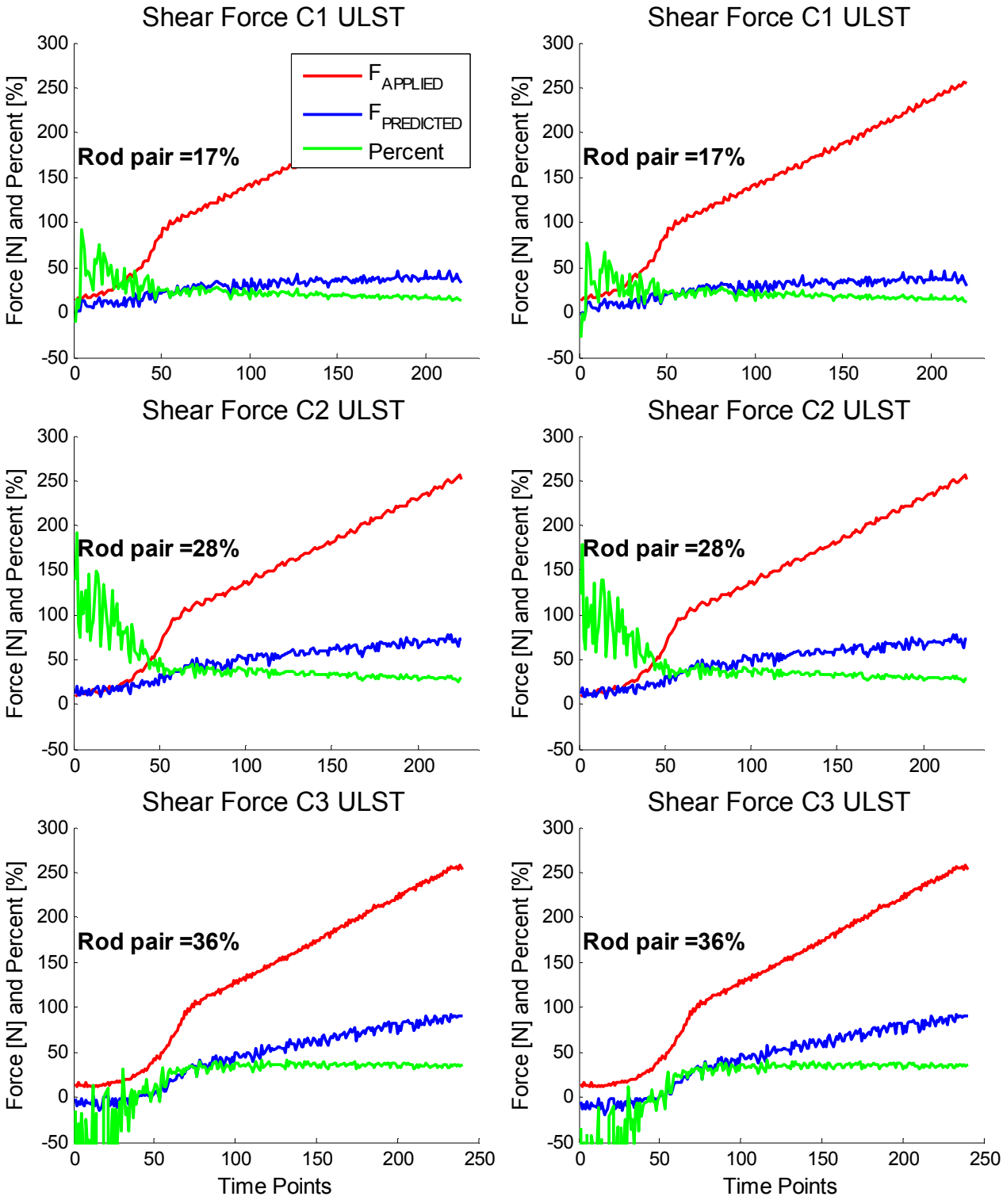
Shear Force C1 ULST
Force [N] and Percent [%]
F APPLIED
F PREDICTED
Percent
Rod pair =17%
Shear Force C1 ULST
Force [N] and Percent [%]
Rod pair =17%
Shear Force C2 ULST
Force [N] and Percent [%]
Rod pair =28%
Shear Force C2 ULST
Force [N] and Percent [%]
Rod pair =28%
Shear Force C3 ULST
Force [N] and Percent [%]
Rod pair =36%
Time Points
Shear Force C3 ULST
Force [N] and Percent [%]
Rod pair =36%
Time Points

Specimen 9

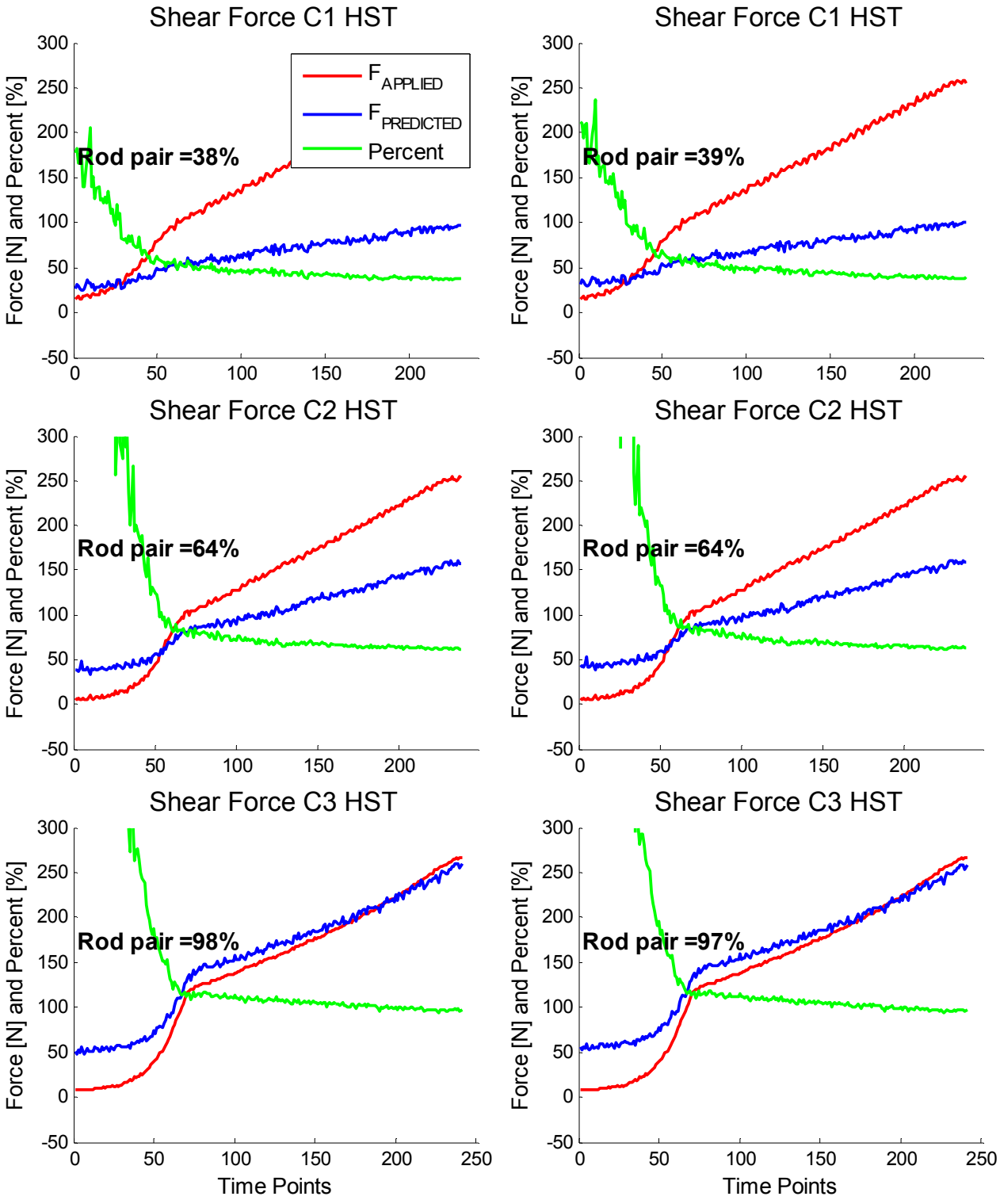
Shear Force C1 HST
Force [N] and Percent [%]
F APPLIED
F PREDICTED
Percent
Rod pair =38%
Shear Force C1 HST
Rod pair =39%
Shear Force C2 HST
Rod pair =64%
Shear Force C2 HST
Rod pair =64%
Shear Force C3 HST
Rod pair =98%
Shear Force C3 HST
Rod pair =97%
Time Points
Time Points

Specimen 9

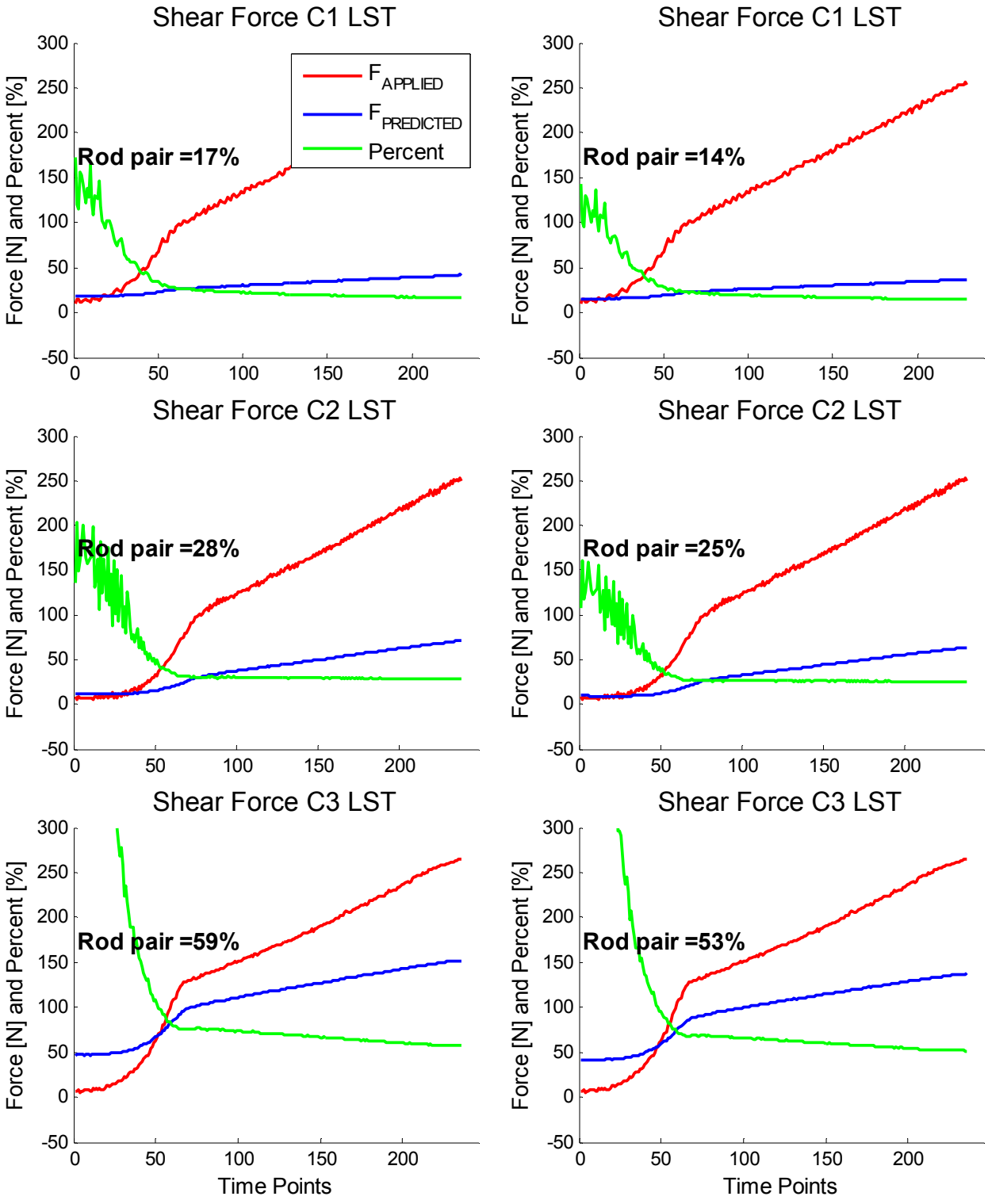
Shear Force C1 LST
Rod pair =17%
Shear Force C1 LST
Rod pair =14%
Shear Force C2 LST
Rod pair =28%
Shear Force C2 LST
Rod pair =25%
Shear Force C3 LST
Rod pair =59%
Shear Force C3 LST
Rod pair =53%
F APPLIED
F PREDICTED
Percent
Force [N] and Percent [%]
Time Points

Specimen 9

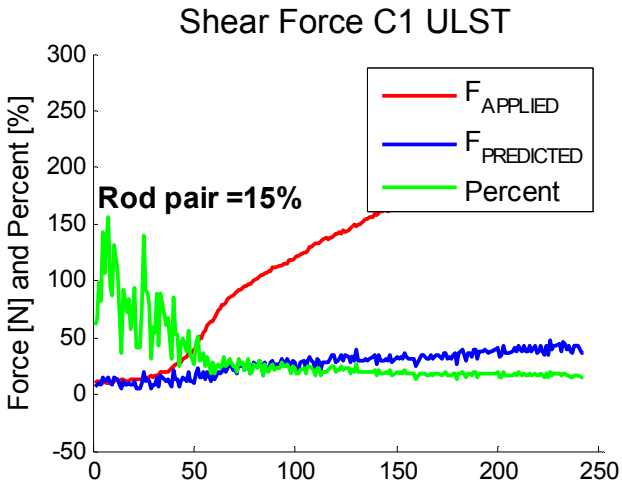
Shear Force C1 ULST
F APPLIED
F PREDICTED
Percent
Rod pair =15%
Force [N] and Percent [%]

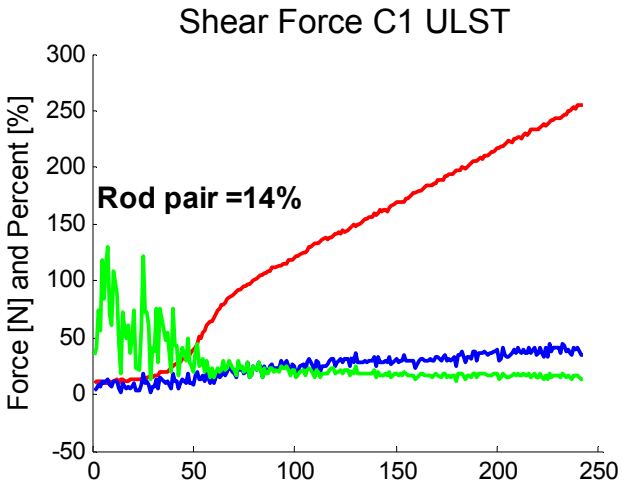
Shear Force C1 ULST
Rod pair =14%
Force [N] and Percent [%]

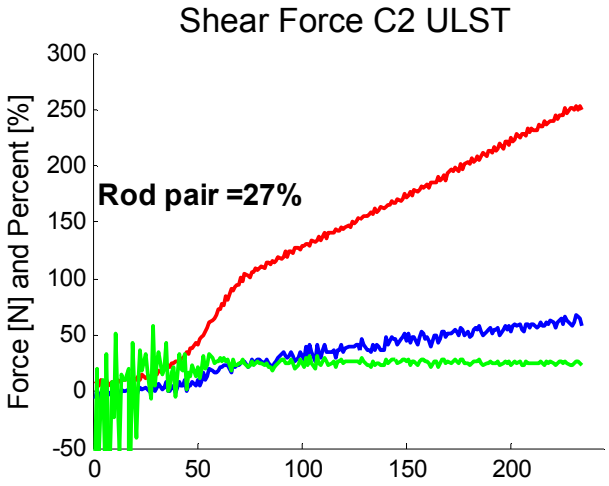
Shear Force C2 ULST
Rod pair =27%
Force [N] and Percent [%]

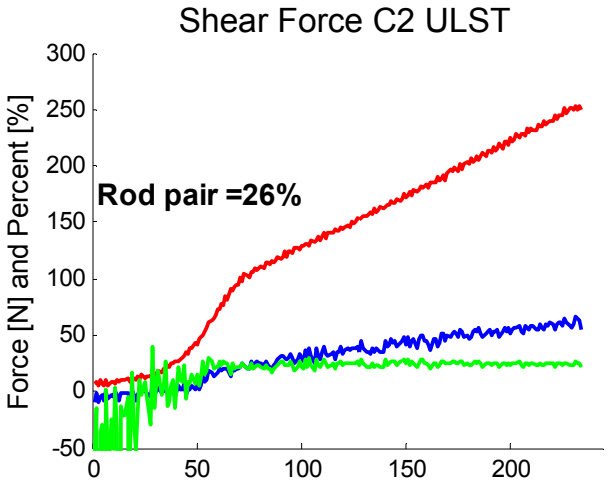
Shear Force C2 ULST
Rod pair =26%
Force [N] and Percent [%]

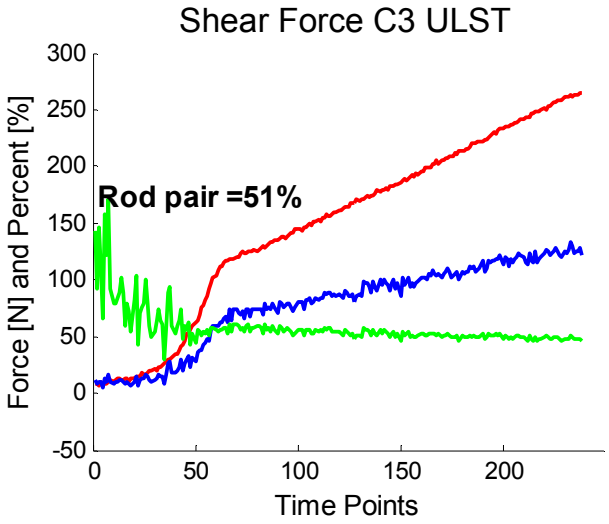
Shear Force C3 ULST
Rod pair =51%
Force [N] and Percent [%]
Time Points

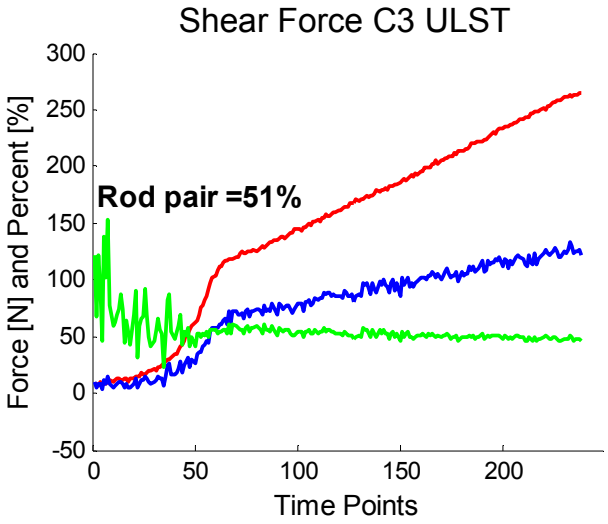
Shear Force C3 ULST
Rod pair =51%
Force [N] and Percent [%]
Time Points

Specimen 10

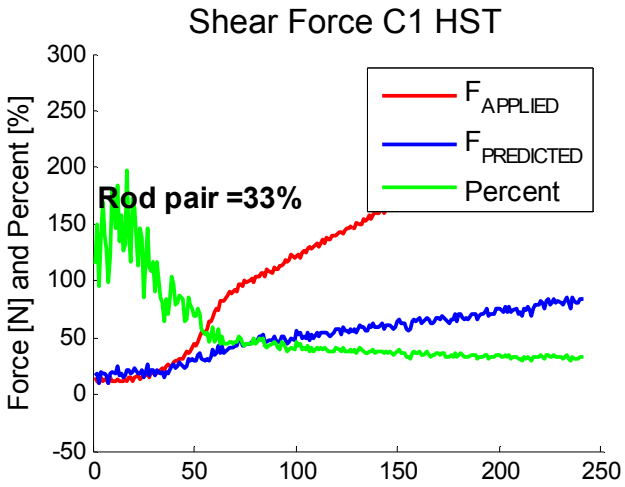
Shear Force C1 HST
F APPLIED
F PREDICTED
Percent
Rod pair =33%
Force [N] and Percent [%]

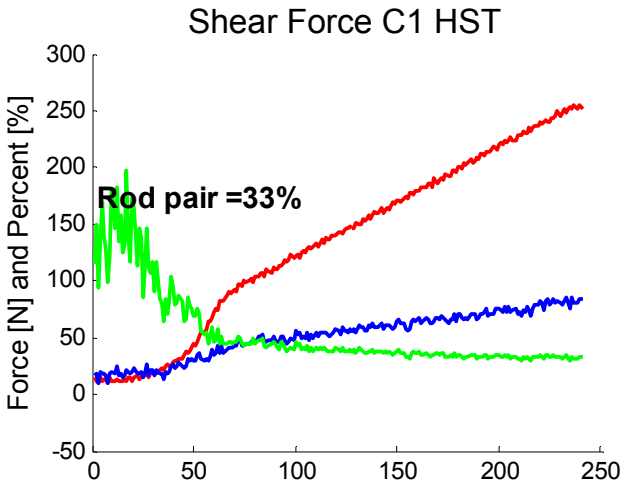
Shear Force C1 HST
Rod pair =33%
Force [N] and Percent [%]

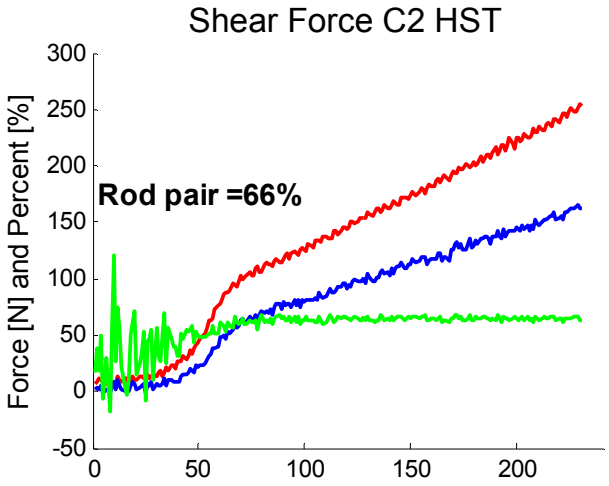
Shear Force C2 HST
Rod pair =66%
Force [N] and Percent [%]

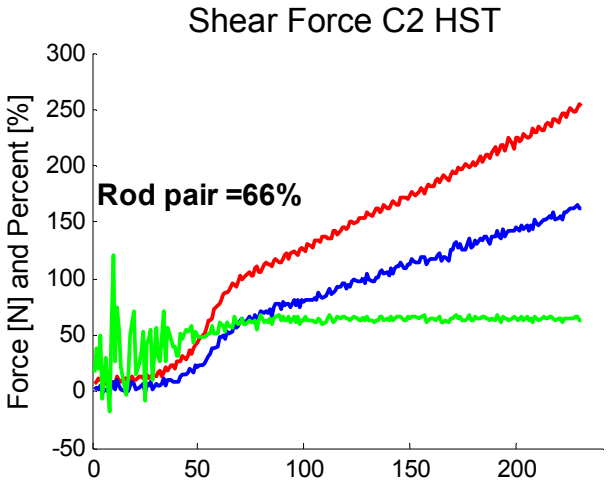
Shear Force C2 HST
Rod pair =66%
Force [N] and Percent [%]

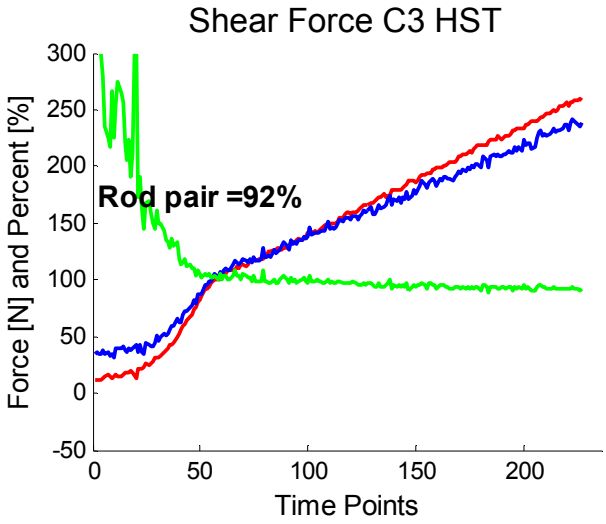
Shear Force C3 HST
Rod pair =92%
Force [N] and Percent [%]
Time Points

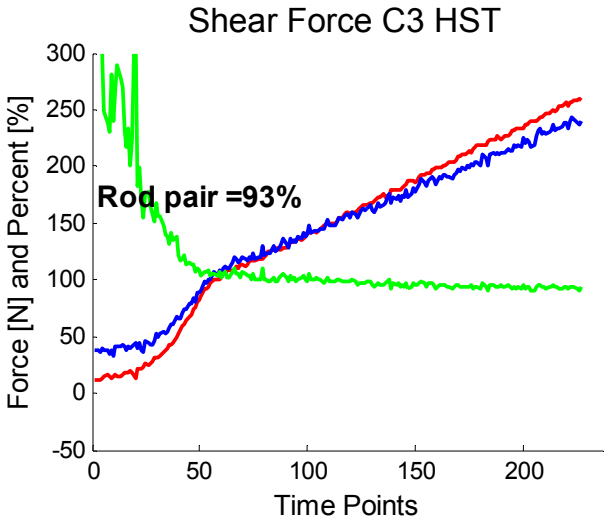
Shear Force C3 HST
Rod pair =93%
Force [N] and Percent [%]
Time Points

Specimen 10

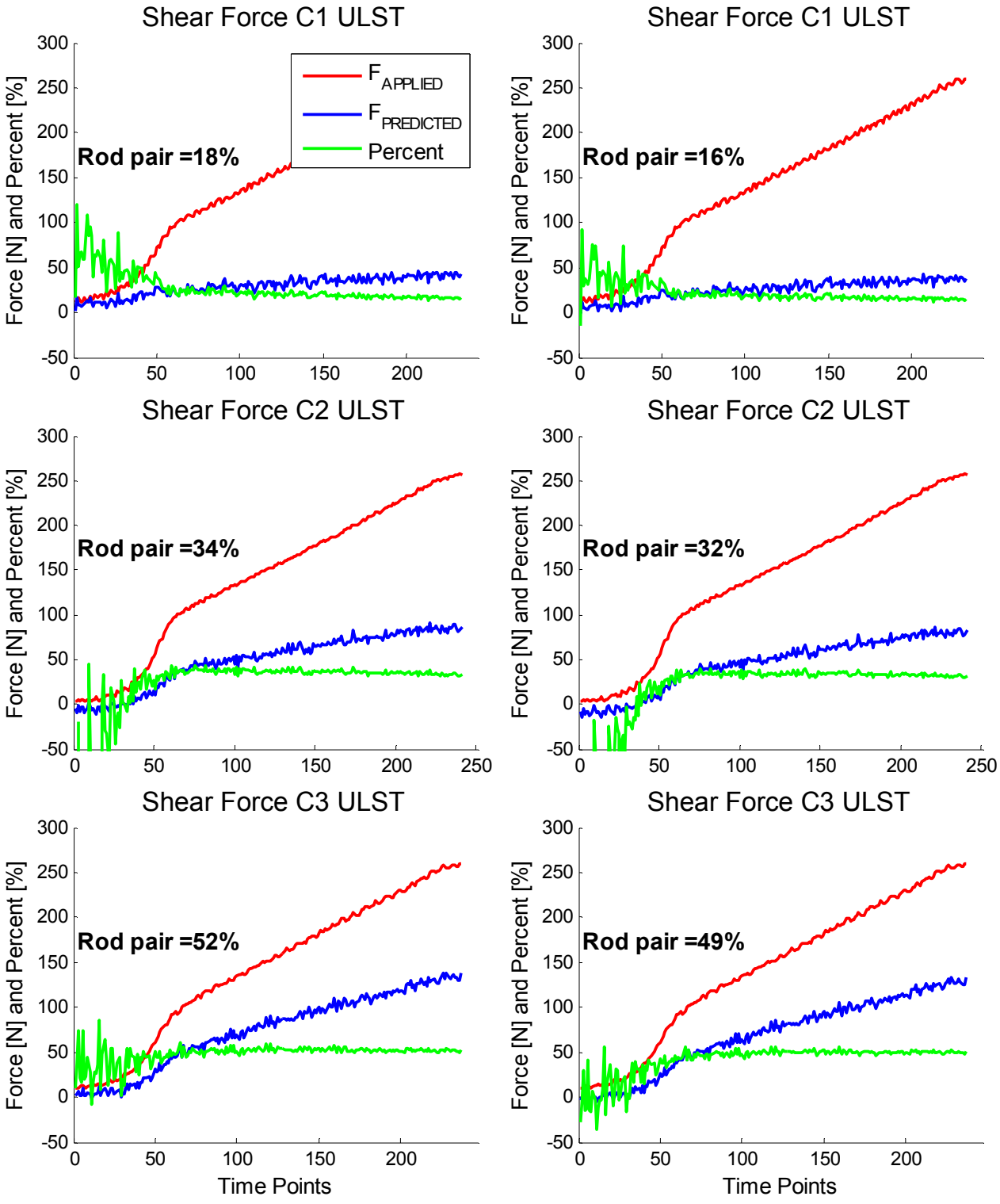
Shear Force C1 ULST
Force [N] and Percent [%]
F APPLIED
F PREDICTED
Percent
Rod pair =18%
Shear Force C1 ULST
Force [N] and Percent [%]
Rod pair =16%
Shear Force C2 ULST
Force [N] and Percent [%]
Rod pair =34%
Shear Force C2 ULST
Force [N] and Percent [%]
Rod pair =32%
Shear Force C3 ULST
Force [N] and Percent [%]
Rod pair =52%
Time Points
Shear Force C3 ULST
Force [N] and Percent [%]
Rod pair =49%
Time Points

Specimen 11

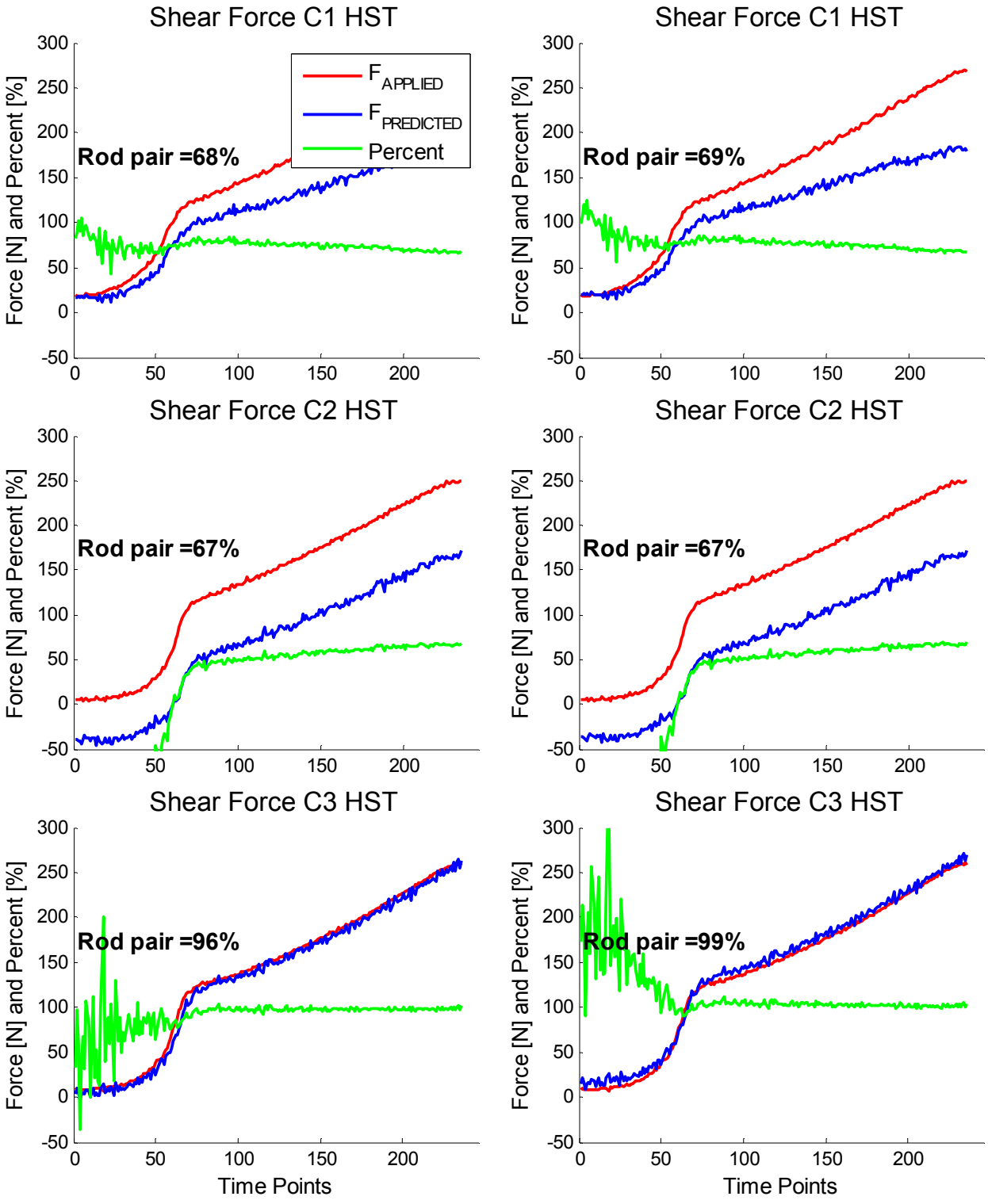
Shear Force C1 HST
Force [N] and Percent [%]
F APPLIED
F PREDICTED
Percent
Rod pair =68%
Shear Force C1 HST
Rod pair =69%
Shear Force C2 HST
Rod pair =67%
Shear Force C2 HST
Rod pair =67%
Shear Force C3 HST
Rod pair =96%
Shear Force C3 HST
Rod pair =99%
Time Points
Time Points

Specimen 11

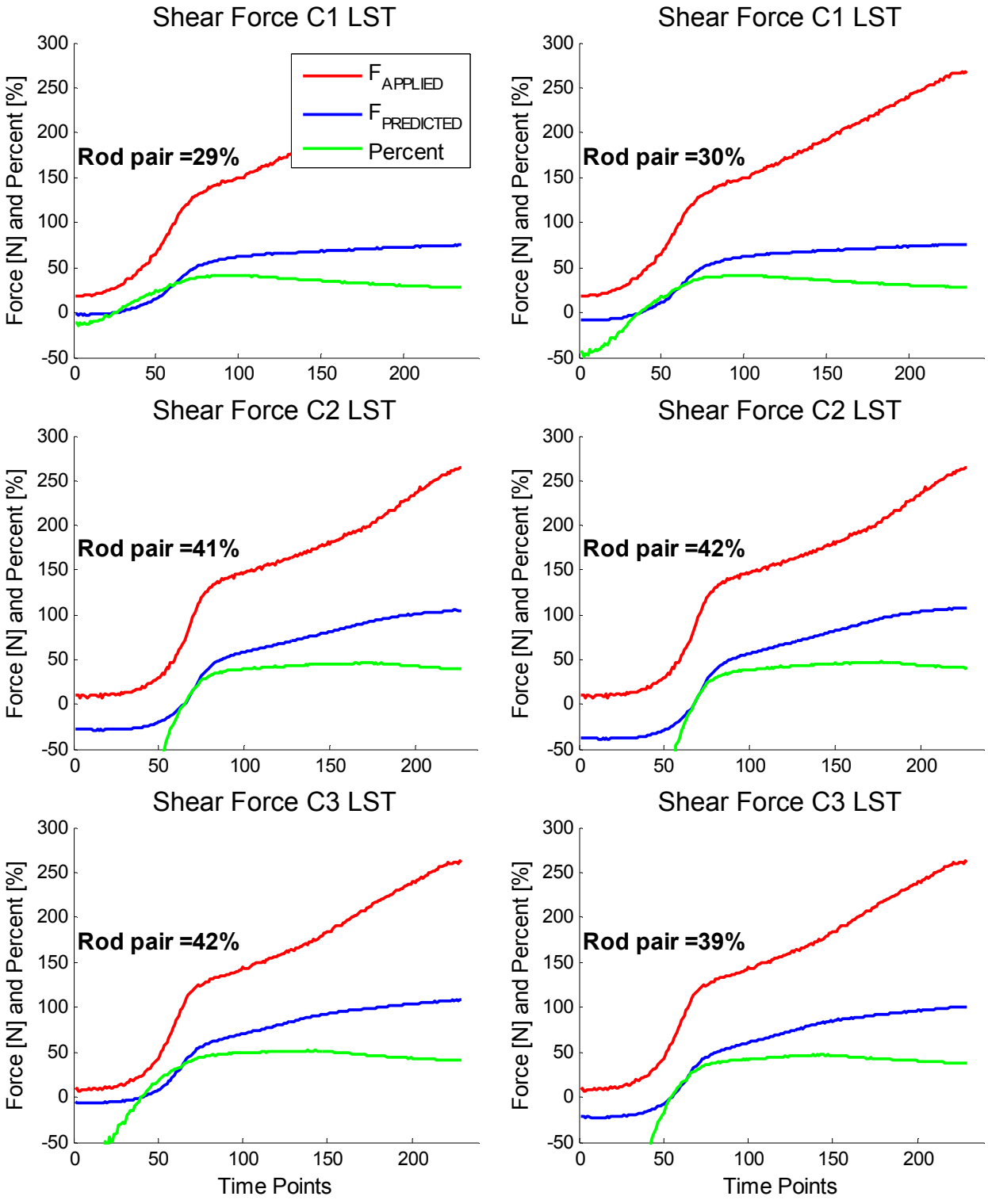
Shear Force C1 LST
Force [N] and Percent [%]
F APPLIED
F PREDICTED
Percent
Rod pair =29%
Shear Force C1 LST
Force [N] and Percent [%]
Rod pair =30%
Shear Force C2 LST
Force [N] and Percent [%]
Rod pair =41%
Shear Force C2 LST
Force [N] and Percent [%]
Rod pair =42%
Shear Force C3 LST
Force [N] and Percent [%]
Rod pair =42%
Time Points
Shear Force C3 LST
Force [N] and Percent [%]
Rod pair =39%
Time Points

Specimen 11

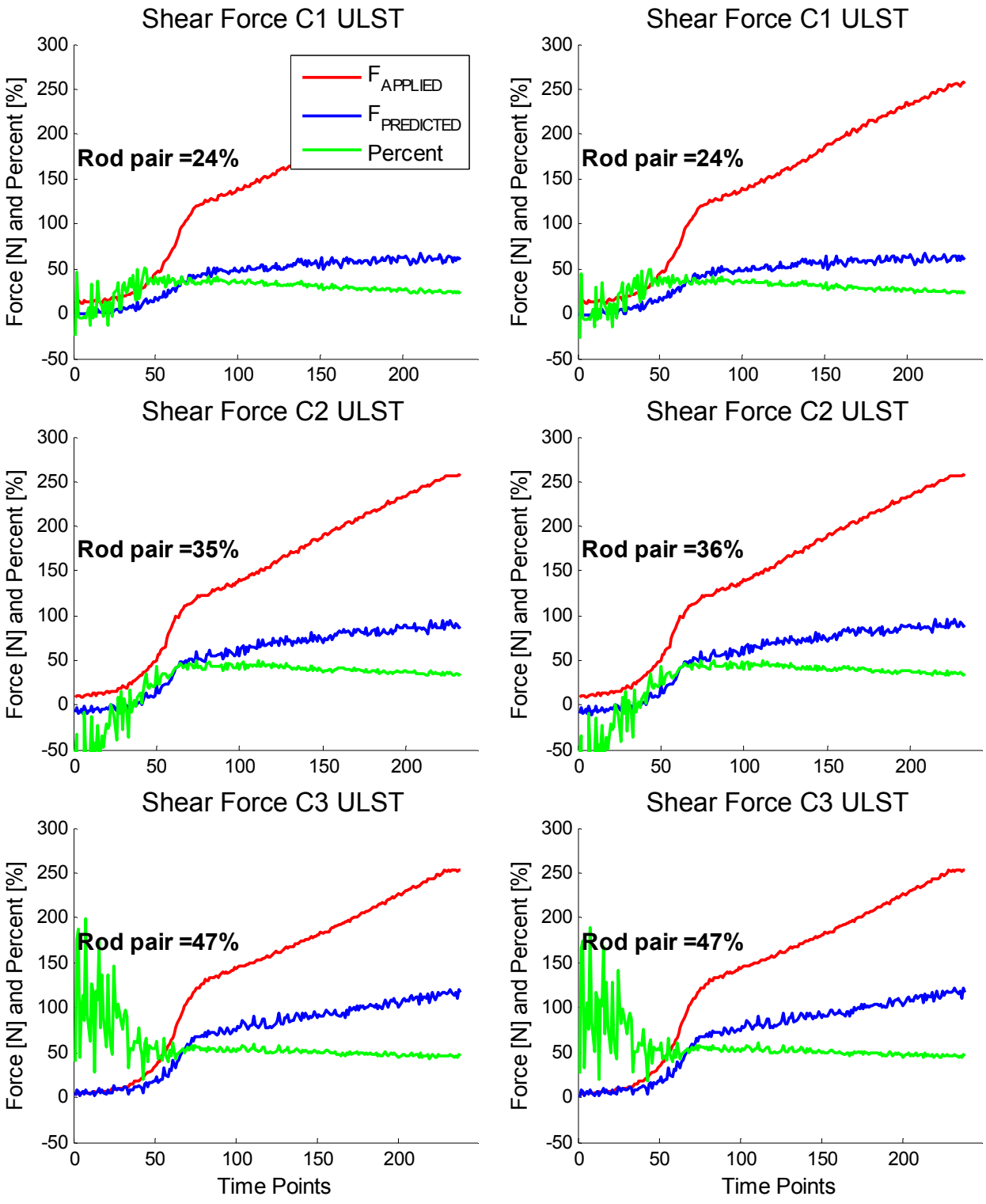
Shear Force C1 ULST
Force [N] and Percent [%]
F APPLIED
F PREDICTED
Percent
Rod pair =24%
Shear Force C1 ULST
Force [N] and Percent [%]
Rod pair =24%
Shear Force C2 ULST
Force [N] and Percent [%]
Rod pair =35%
Shear Force C2 ULST
Force [N] and Percent [%]
Rod pair =36%
Shear Force C3 ULST
Force [N] and Percent [%]
Rod pair =47%
Time Points
Shear Force C3 ULST
Force [N] and Percent [%]
Rod pair =47%
Time Points

Specimen 11 - true

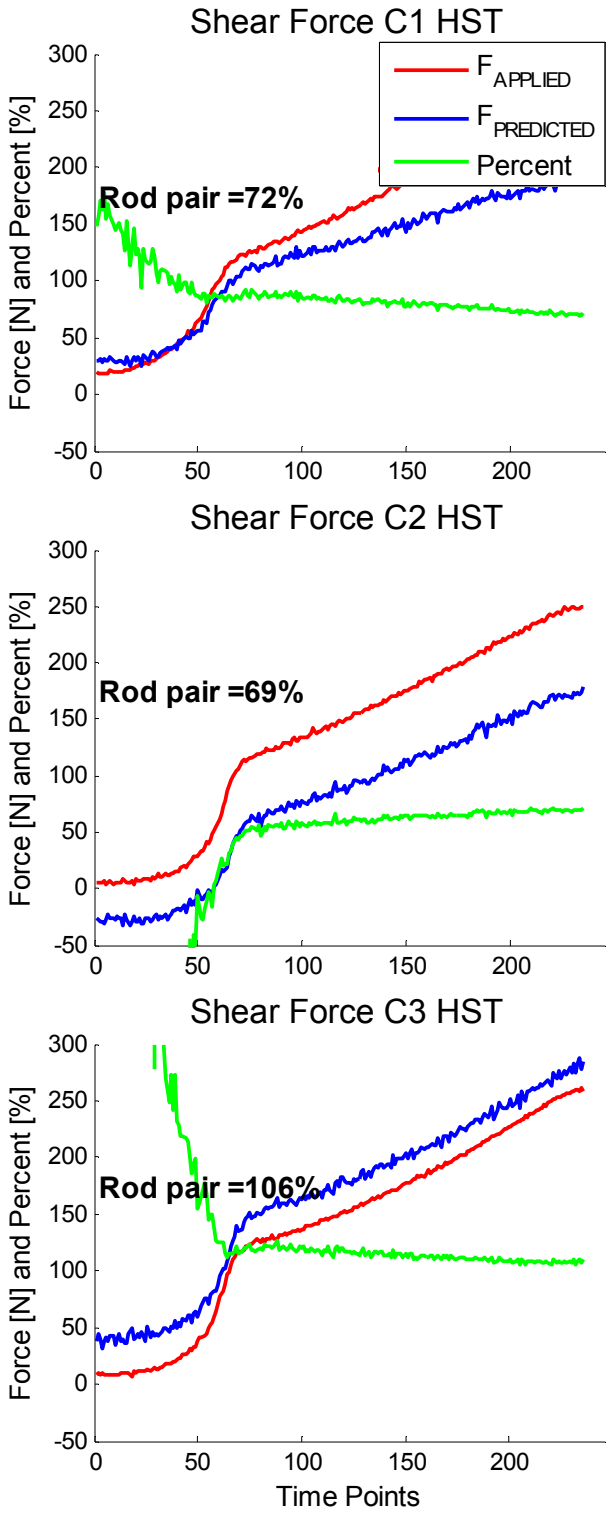

Specimen 11 - true

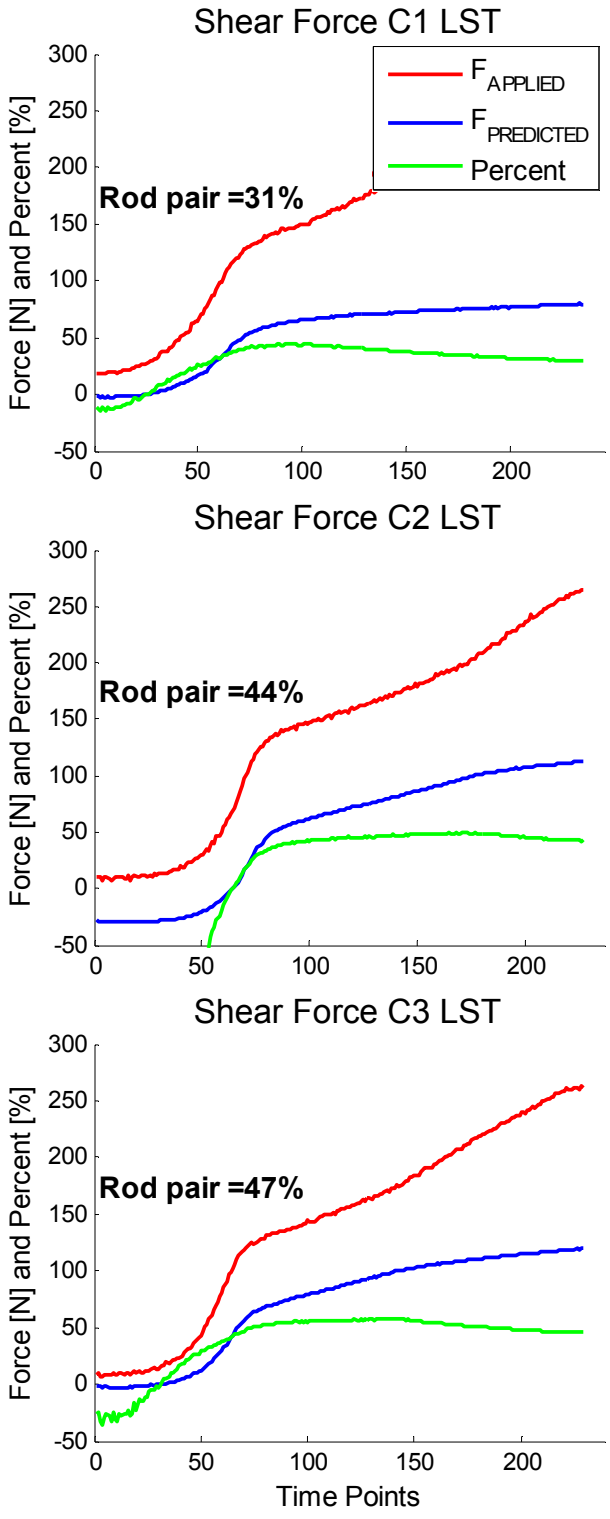

Specimen 11 - true

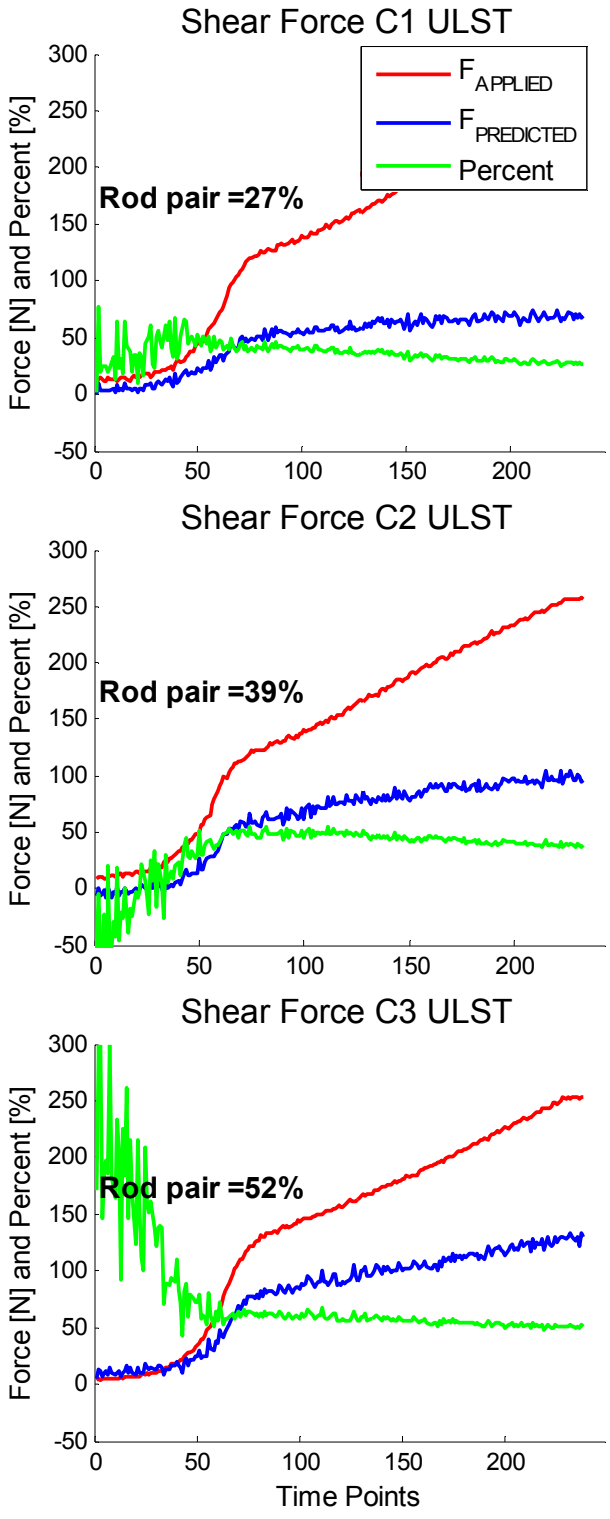

Specimen 12

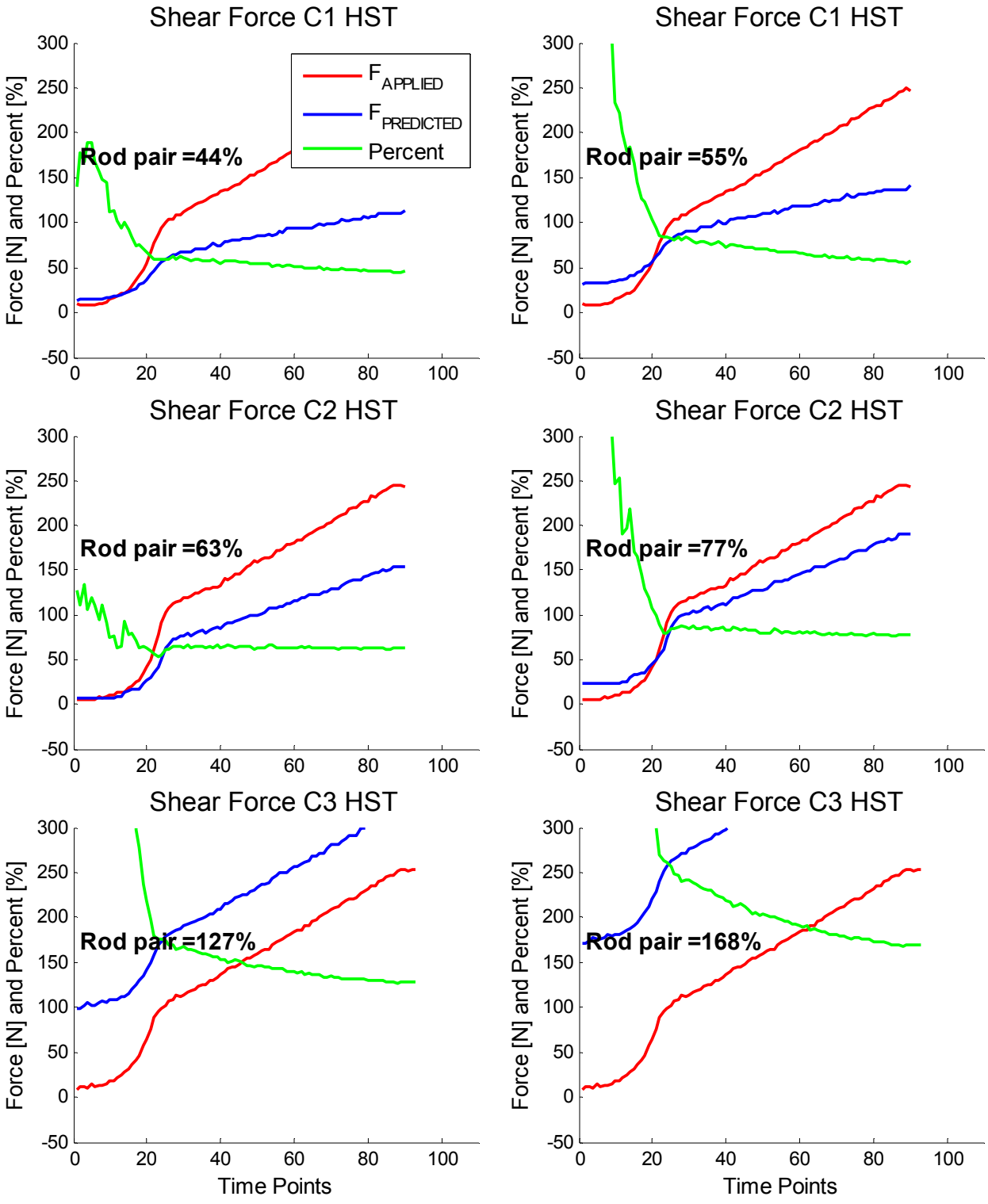
Shear Force C1 HST
Force [N] and Percent [%]
F APPLIED
F PREDICTED
Percent
Rod pair =44%
Shear Force C1 HST
Rod pair =55%
Shear Force C2 HST
Rod pair =63%
Shear Force C2 HST
Rod pair =77%
Shear Force C3 HST
Rod pair =127%
Shear Force C3 HST
Rod pair =168%
Time Points
Time Points

Specimen 12

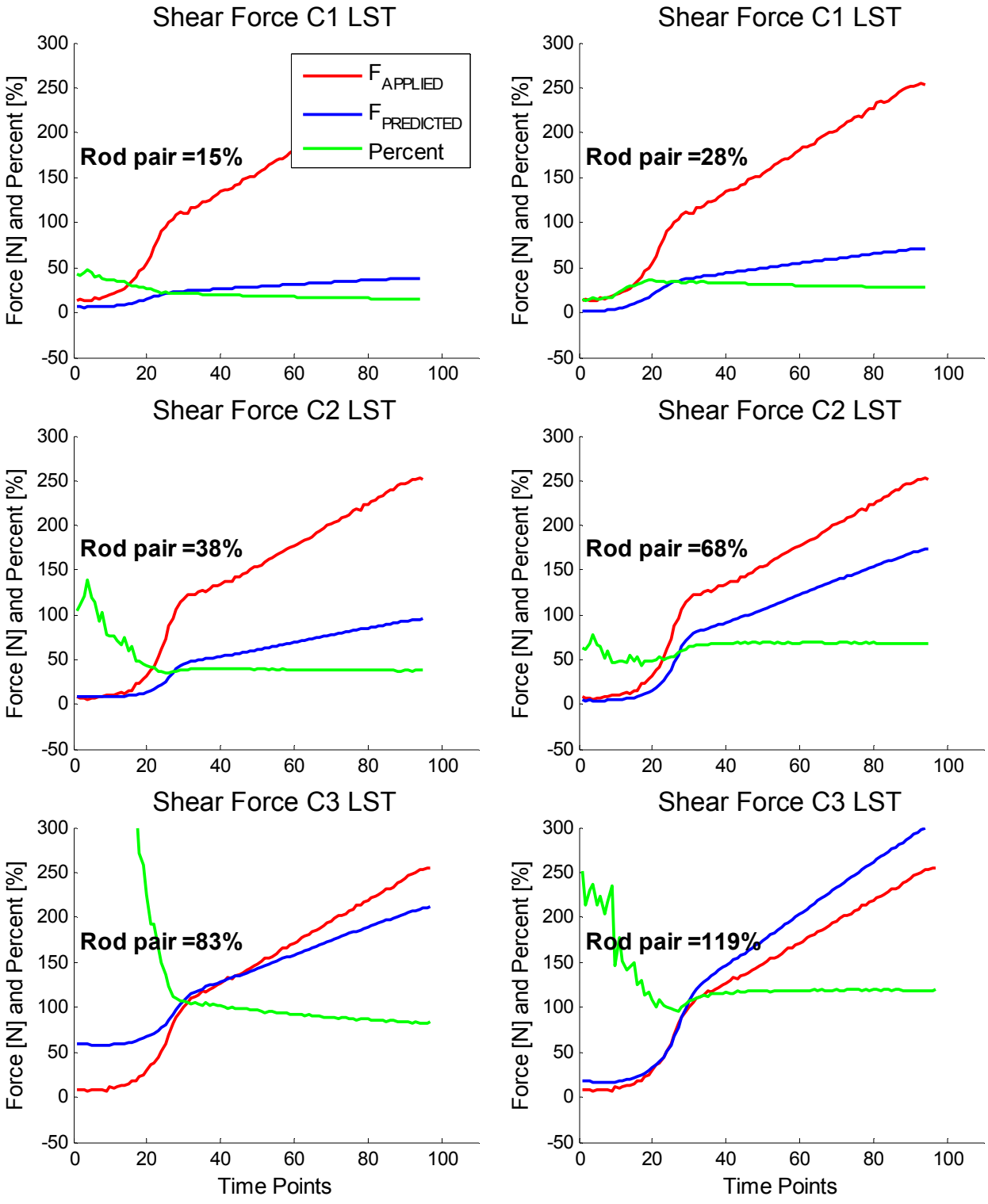
Shear Force C1 LST
Force [N] and Percent [%]
F APPLIED
F PREDICTED
Percent
Rod pair =15%
Shear Force C1 LST
Force [N] and Percent [%]
Rod pair =28%
Shear Force C2 LST
Force [N] and Percent [%]
Rod pair =38%
Shear Force C2 LST
Force [N] and Percent [%]
Rod pair =68%
Shear Force C3 LST
Force [N] and Percent [%]
Rod pair =83%
Time Points
Shear Force C3 LST
Force [N] and Percent [%]
Rod pair =119%
Time Points

Specimen 13

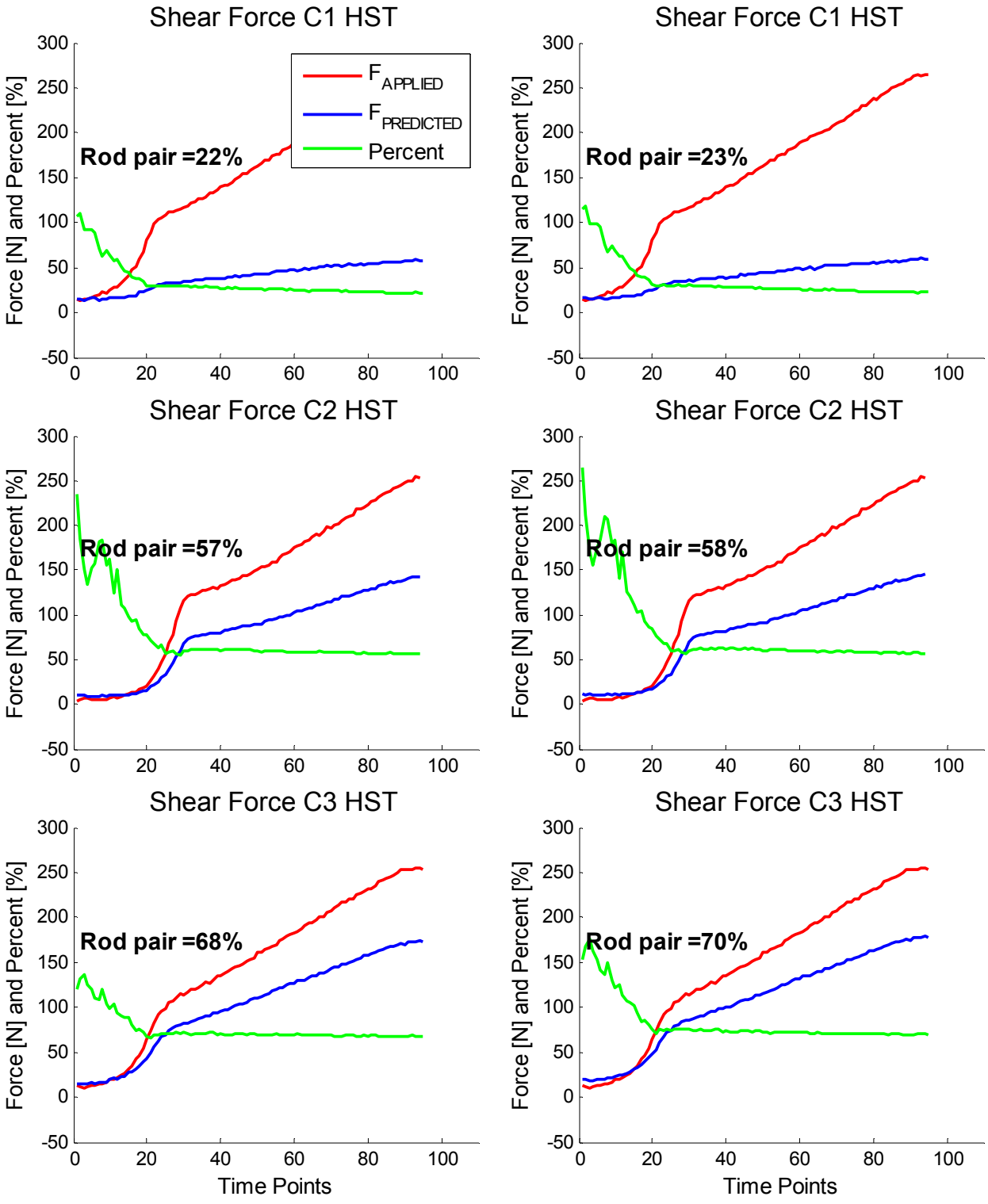
Shear Force C1 HST
Rod pair =22%
Shear Force C1 HST
Rod pair =23%
Shear Force C2 HST
Rod pair =57%
Shear Force C2 HST
Rod pair =58%
Shear Force C3 HST
Rod pair =68%
Shear Force C3 HST
Rod pair =70%
F APPLIED
F PREDICTED
Percent
Force [N] and Percent [%]
Time Points

Specimen 13

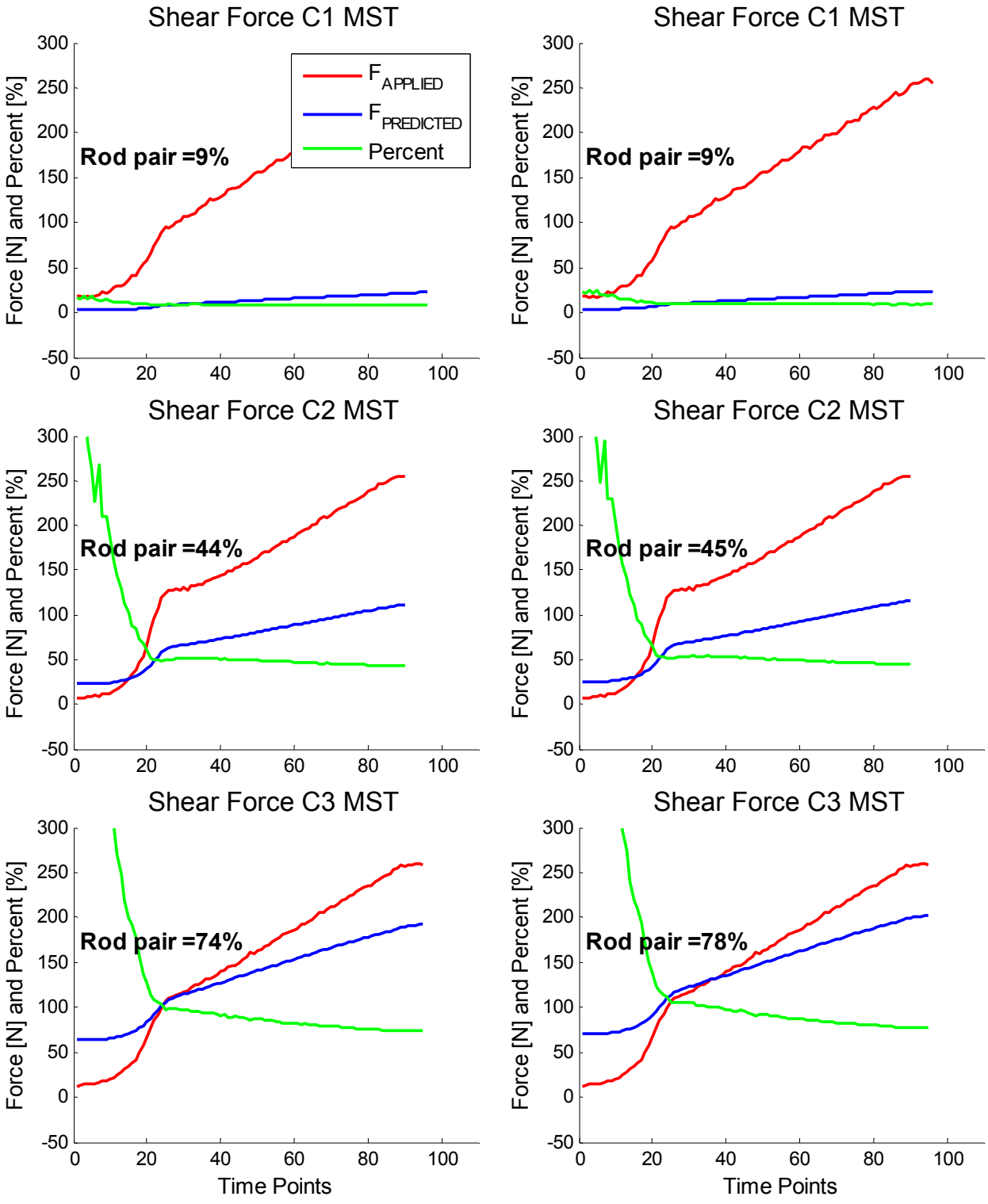
Shear Force C1 MST
Force [N] and Percent [%]
F APPLIED
F PREDICTED
Percent
Rod pair =9%
Shear Force C1 MST
Force [N] and Percent [%]
Rod pair =9%
Shear Force C2 MST
Force [N] and Percent [%]
Rod pair =44%
Shear Force C2 MST
Force [N] and Percent [%]
Rod pair =45%
Shear Force C3 MST
Force [N] and Percent [%]
Rod pair =74%
Time Points
Shear Force C3 MST
Force [N] and Percent [%]
Rod pair =78%
Time Points

Specimen 13

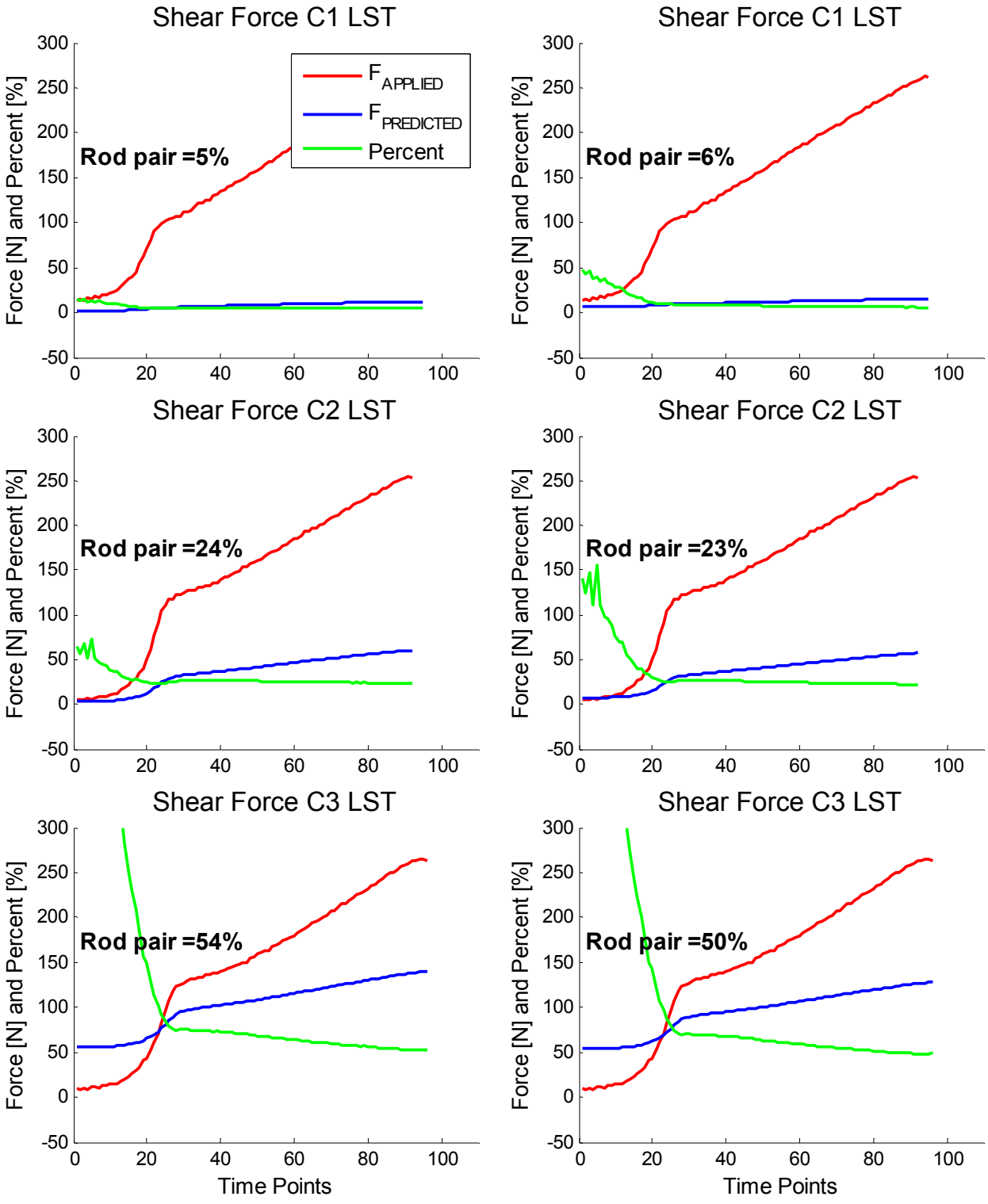
Shear Force C1 LST
Force [N] and Percent [%]
F APPLIED
F PREDICTED
Percent
Rod pair =5%
Shear Force C1 LST
Force [N] and Percent [%]
Rod pair =6%
Shear Force C2 LST
Force [N] and Percent [%]
Rod pair =24%
Shear Force C2 LST
Force [N] and Percent [%]
Rod pair =23%
Shear Force C3 LST
Force [N] and Percent [%]
Rod pair =54%
Time Points
Shear Force C3 LST
Force [N] and Percent [%]
Rod pair =50%
Time Points

Specimen 13

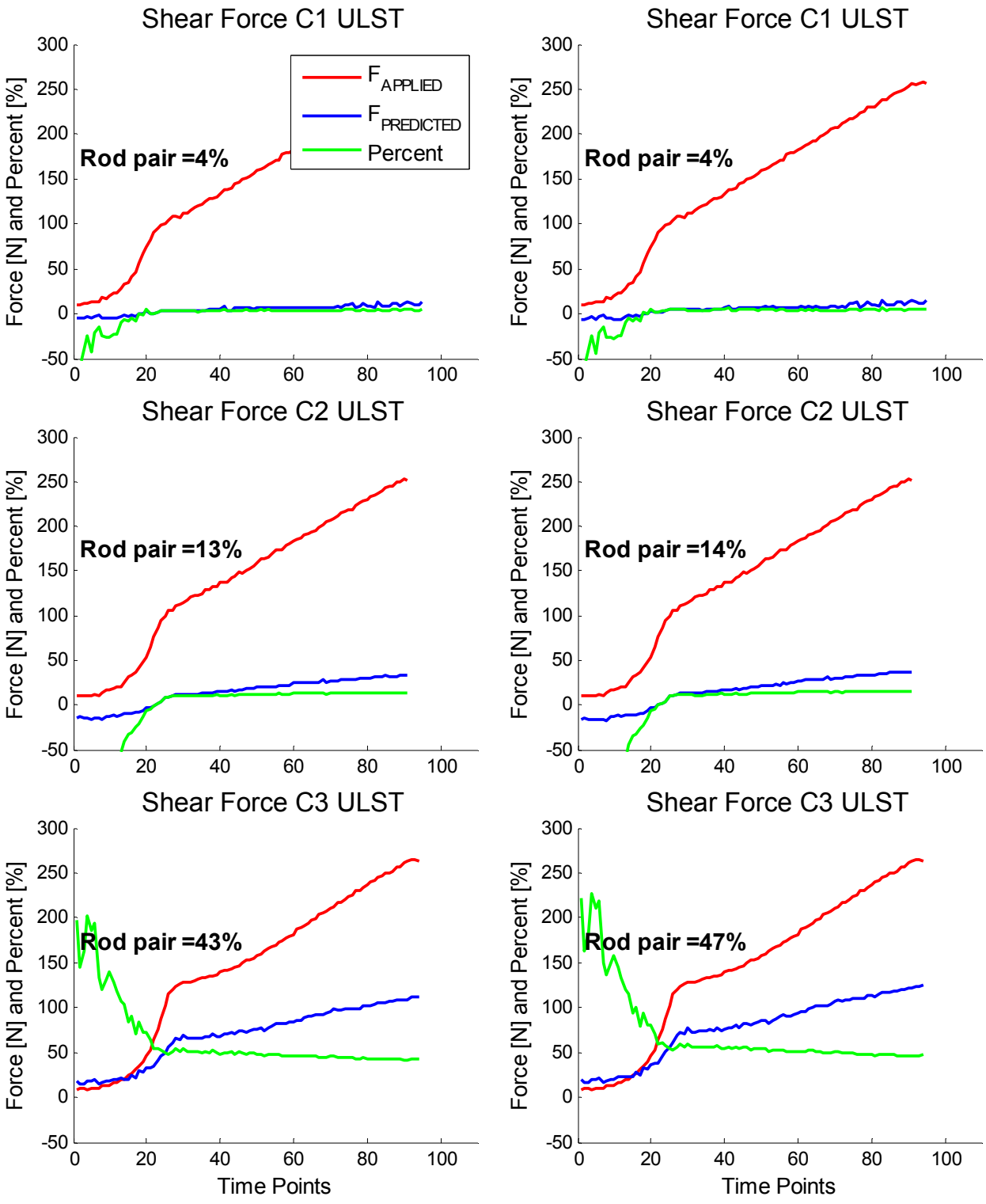
Shear Force C1 ULST
Force [N] and Percent [%]
F APPLIED
F PREDICTED
Percent
Rod pair =4%
Shear Force C1 ULST
Force [N] and Percent [%]
Rod pair =4%
Shear Force C2 ULST
Force [N] and Percent [%]
Rod pair =13%
Shear Force C2 ULST
Force [N] and Percent [%]
Rod pair =14%
Shear Force C3 ULST
Force [N] and Percent [%]
Rod pair =43%
Time Points
Shear Force C3 ULST
Force [N] and Percent [%]
Rod pair =47%
Time Points

Specimen 14

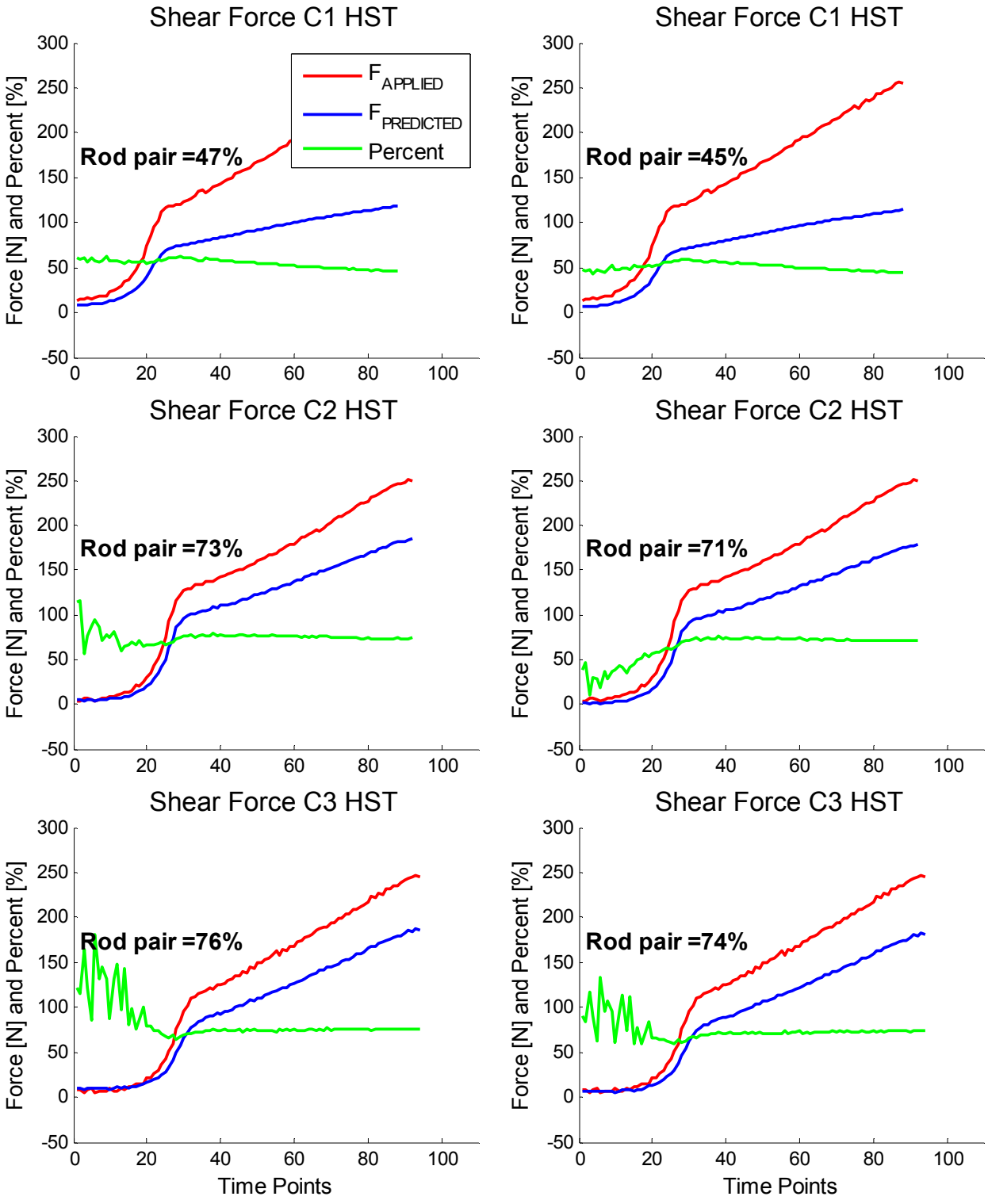
Shear Force C1 HST
Force [N] and Percent [%]
F APPLIED
F PREDICTED
Percent
Rod pair =47%
Shear Force C1 HST
Rod pair =45%
Shear Force C2 HST
Rod pair =73%
Shear Force C2 HST
Rod pair =71%
Shear Force C3 HST
Rod pair =76%
Shear Force C3 HST
Rod pair =74%
Time Points
Time Points

Specimen 14

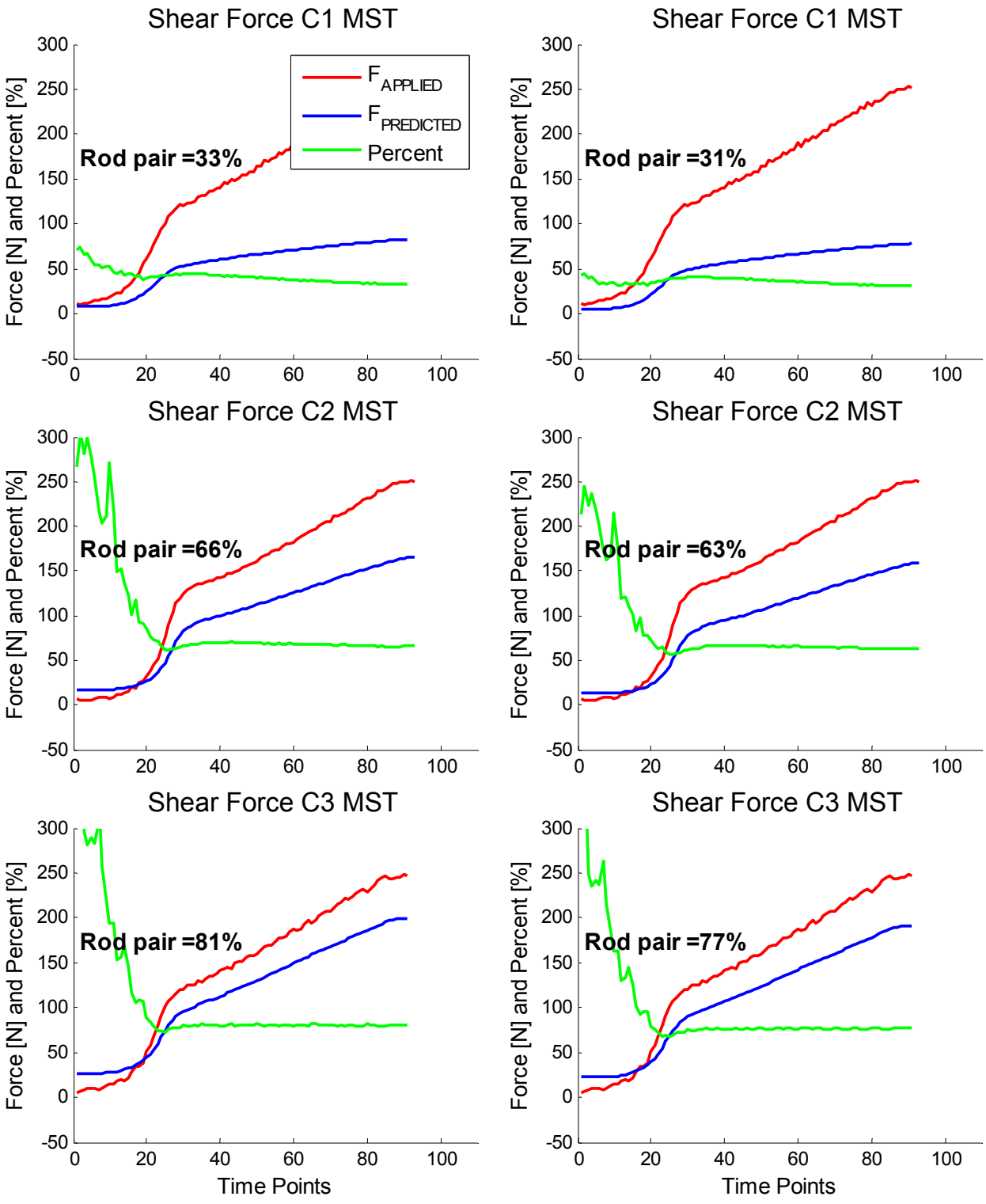
Shear Force C1 MST
Force [N] and Percent [%]
F APPLIED
F PREDICTED
Percent
Rod pair =33%
Shear Force C1 MST
Force [N] and Percent [%]
Rod pair =31%
Shear Force C2 MST
Force [N] and Percent [%]
Rod pair =66%
Shear Force C2 MST
Force [N] and Percent [%]
Rod pair =63%
Shear Force C3 MST
Force [N] and Percent [%]
Rod pair =81%
Time Points
Shear Force C3 MST
Force [N] and Percent [%]
Rod pair =77%
Time Points

Specimen 14

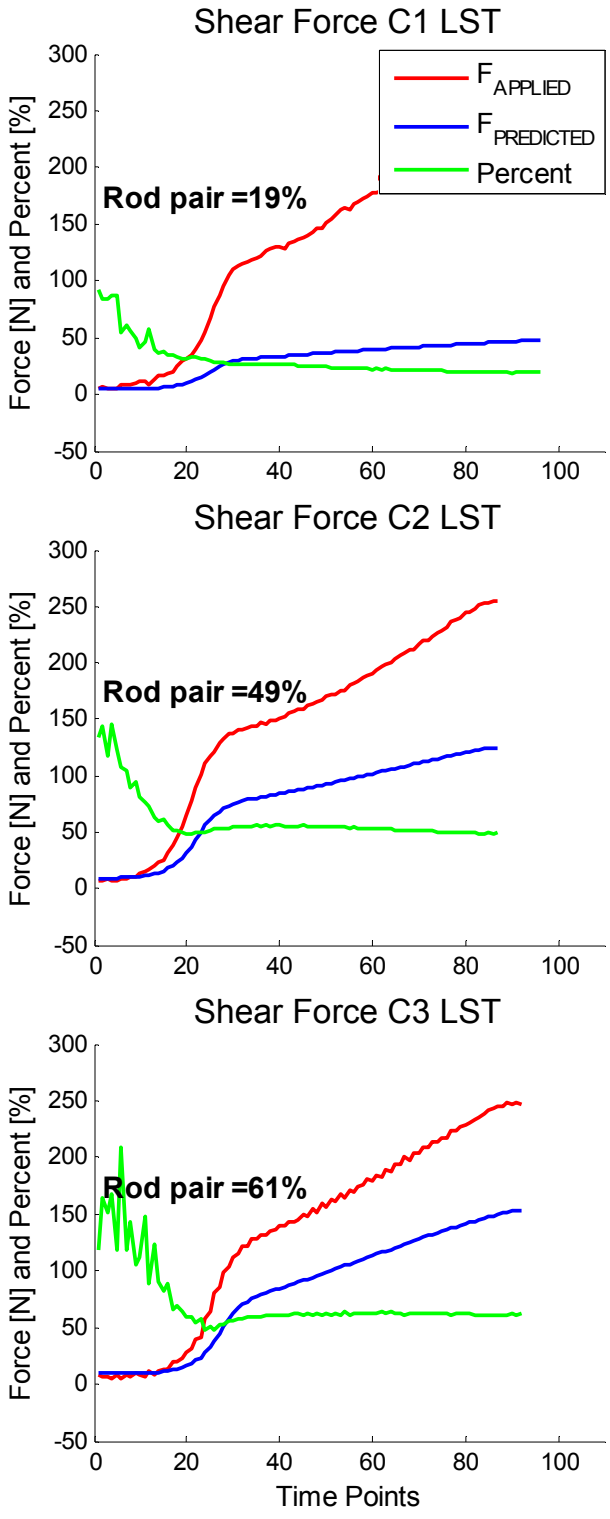
Shear Force C1 LST
F APPLIED
F PREDICTED
Percent
Rod pair =19%
Force [N] and Percent [%]
Shear Force C2 LST
Rod pair =49%
Force [N] and Percent [%]
Shear Force C3 LST
Rod pair =61%
Force [N] and Percent [%]
Time Points

Specimen 14

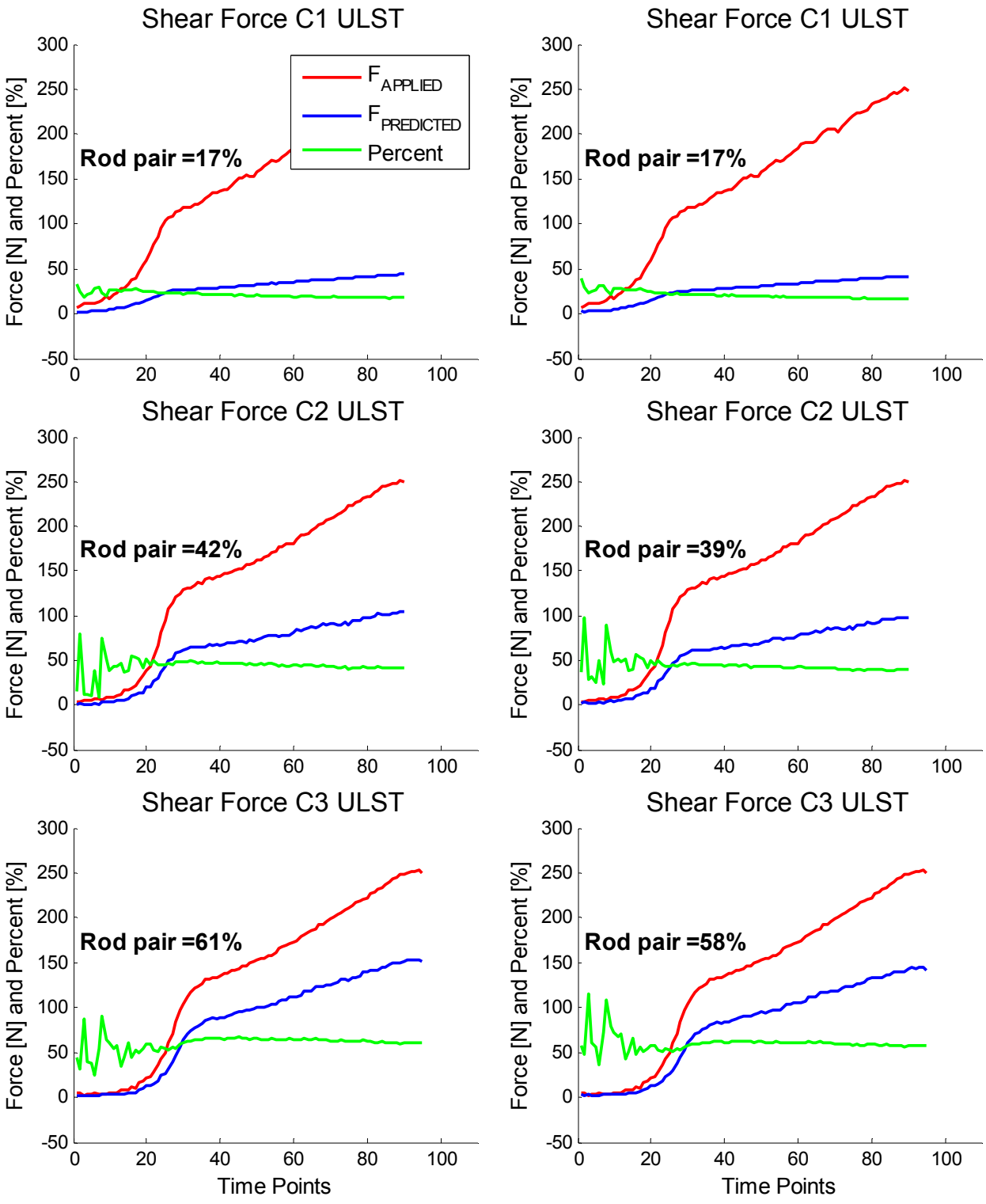
Shear Force C1 ULST
Force [N] and Percent [%]
F APPLIED
F PREDICTED
Percent
Rod pair =17%
Shear Force C1 ULST
Force [N] and Percent [%]
Rod pair =17%
Shear Force C2 ULST
Force [N] and Percent [%]
Rod pair =42%
Shear Force C2 ULST
Force [N] and Percent [%]
Rod pair =39%
Shear Force C3 ULST
Force [N] and Percent [%]
Rod pair =61%
Time Points
Shear Force C3 ULST
Force [N] and Percent [%]
Rod pair =58%
Time Points

Specimen 15

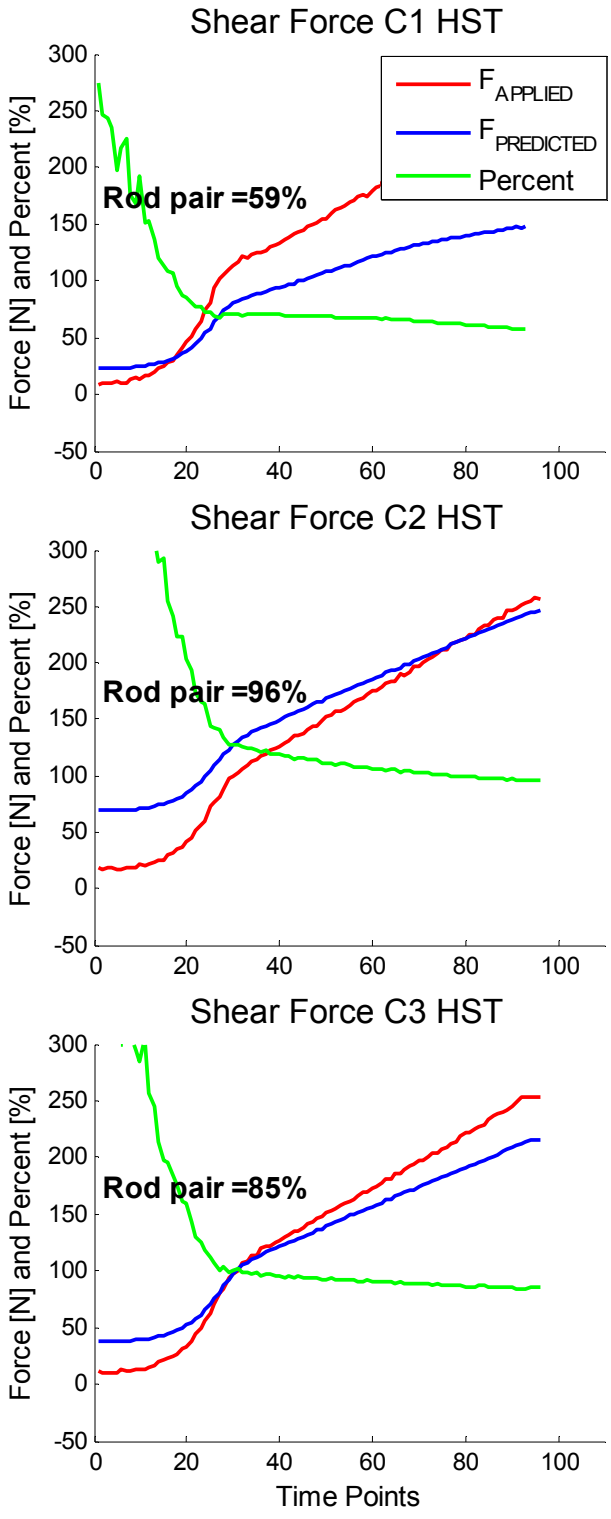
Shear Force C1 HST
F APPLIED
F PREDICTED
Percent
Rod pair =59%
Force [N] and Percent [%]
Shear Force C2 HST
Rod pair =96%
Force [N] and Percent [%]
Shear Force C3 HST
Rod pair =85%
Force [N] and Percent [%]
Time Points

Specimen 15

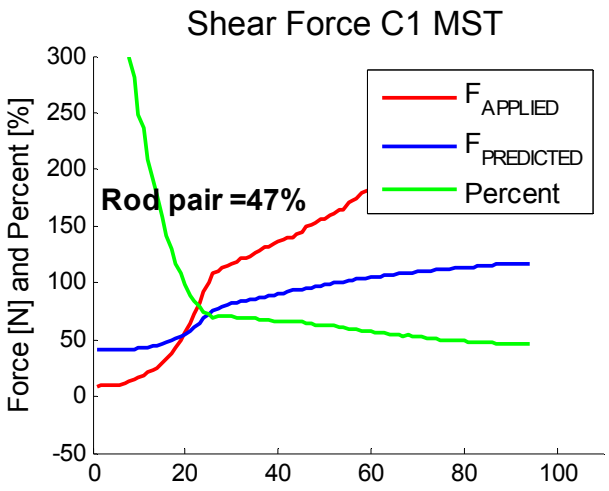
Shear Force C1 MST
Force [N] and Percent [%]
F APPLIED
F PREDICTED
Percent
Rod pair =47%

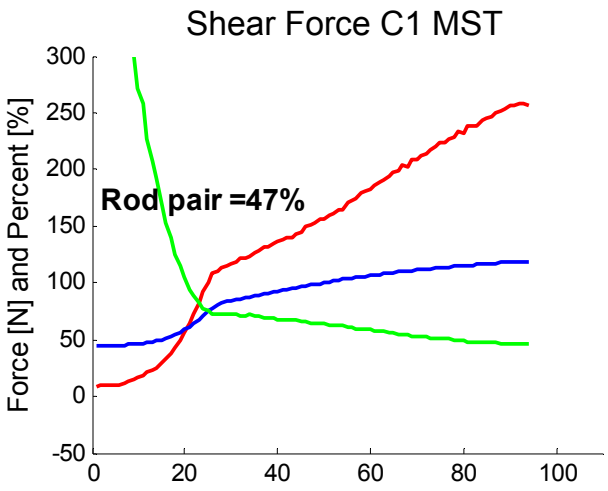
Shear Force C1 MST
Force [N] and Percent [%]
Rod pair =47%

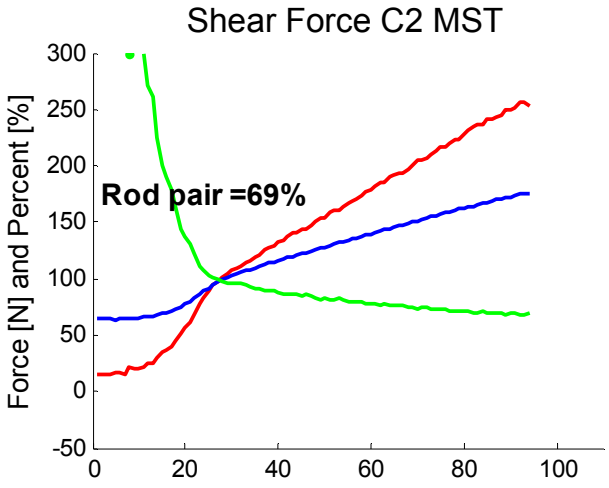
Shear Force C2 MST
Force [N] and Percent [%]
Rod pair =69%

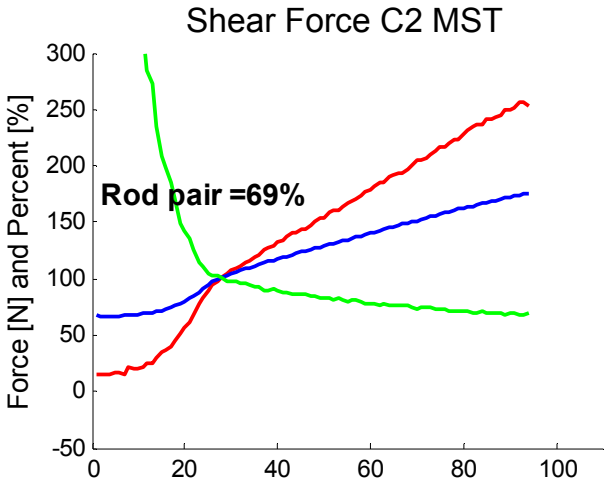
Shear Force C2 MST
Force [N] and Percent [%]
Rod pair =69%

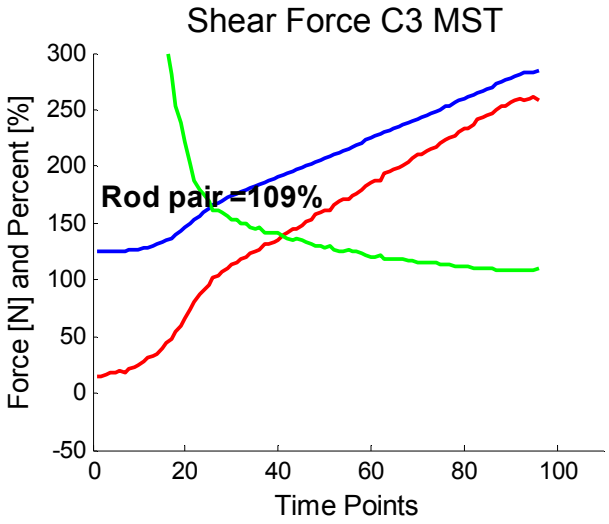
Shear Force C3 MST
Force [N] and Percent [%]
Rod pair =109%
Time Points

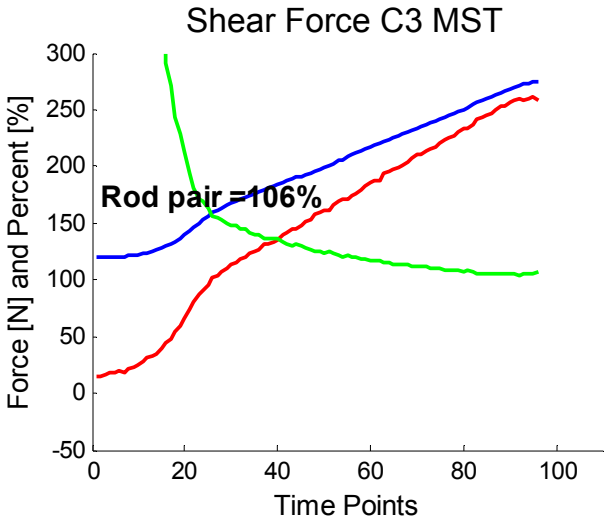
Shear Force C3 MST
Force [N] and Percent [%]
Rod pair =106%
Time Points

Specimen 15

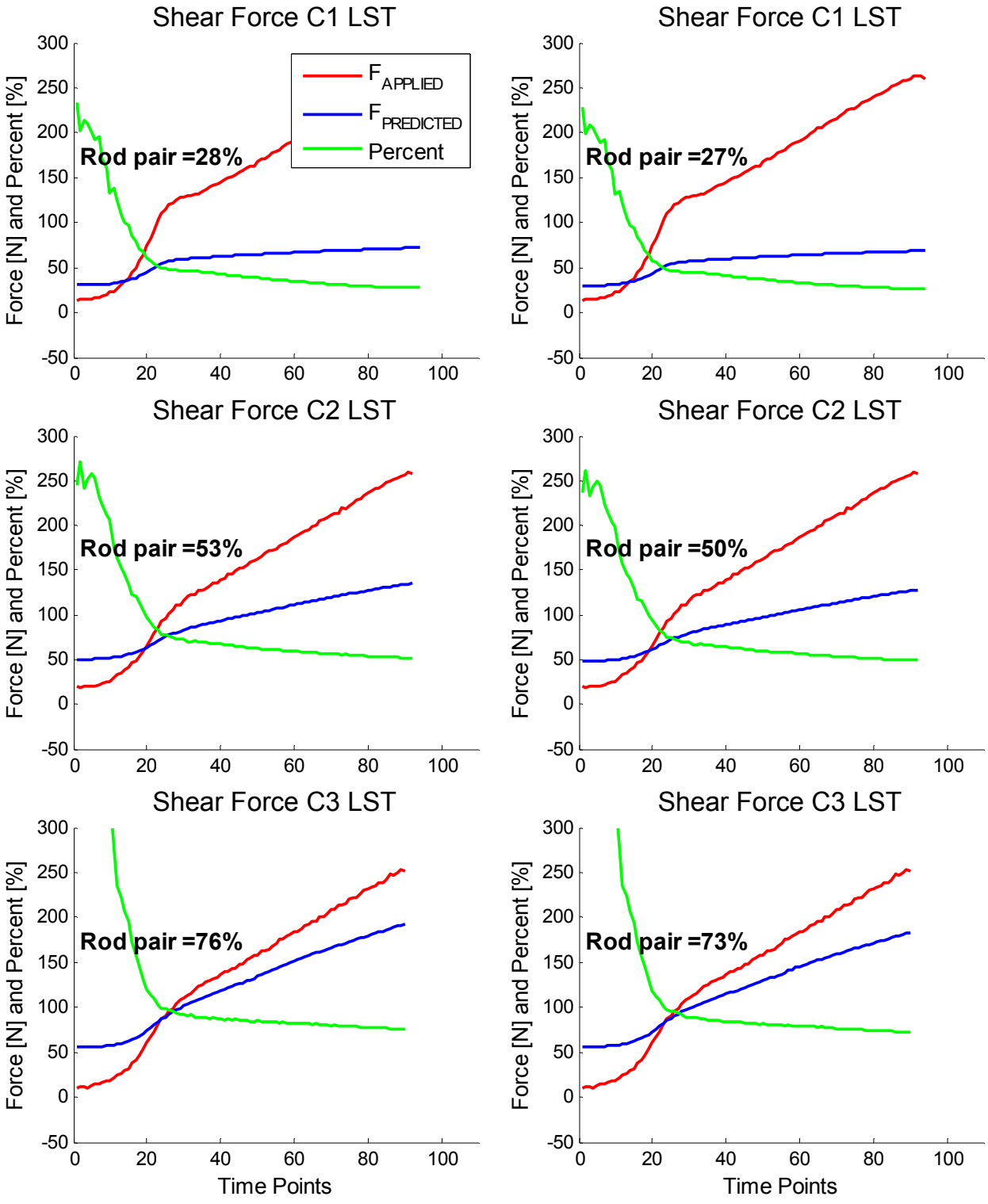
Shear Force C1 LST
Force [N] and Percent [%]
F APPLIED
F PREDICTED
Percent
Rod pair =28%
Shear Force C1 LST
Force [N] and Percent [%]
Rod pair =27%
Shear Force C2 LST
Force [N] and Percent [%]
Rod pair =53%
Shear Force C2 LST
Force [N] and Percent [%]
Rod pair =50%
Shear Force C3 LST
Force [N] and Percent [%]
Rod pair =76%
Time Points
Shear Force C3 LST
Force [N] and Percent [%]
Rod pair =73%
Time Points

Specimen 15

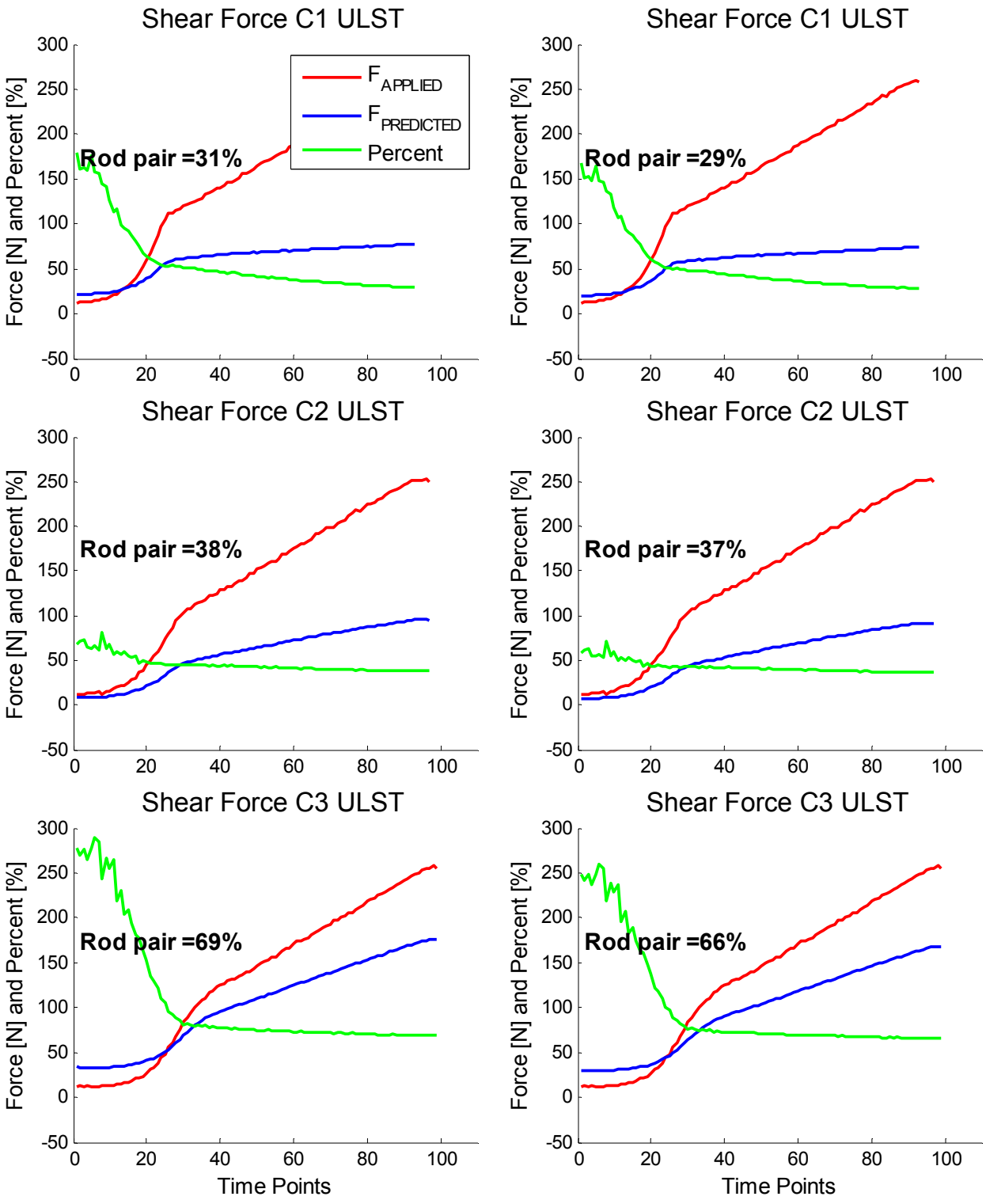
Shear Force C1 ULST
Force [N] and Percent [%]
F APPLIED
F PREDICTED
Percent
Rod pair =31%
Shear Force C1 ULST
Force [N] and Percent [%]
Rod pair =29%
Shear Force C2 ULST
Force [N] and Percent [%]
Rod pair =38%
Shear Force C2 ULST
Force [N] and Percent [%]
Rod pair =37%
Shear Force C3 ULST
Force [N] and Percent [%]
Rod pair =69%
Time Points
Shear Force C3 ULST
Force [N] and Percent [%]
Rod pair =66%
Time Points